Shear Flows of Granular Materials

by

Charles S. Campbell

In Partial Fulfillment of the Requirements

for the Degree of

Doctor of Philosophy

Division of Engineering and Applied Science
California Institute of Technology
Pasadena, California 91125

1982

(submitted May 24, 1982)

ACKNOWLEDGMENTS

I would like to give my deepest thanks to my advisors, Professors Christopher Brennen and Rolf Sabersky whose encouragement and support made me feel less of a student and more of a colleague.

I would also like to thank Bill Newman, Ralph Baca, and especially Ken Sieck for their assistance in performing the experiments; Scott Patton and Tanh Nguyen with whom I had many helpful discussions; Fred MacDonald and Elmer Szombathy for their aid in building the experimental apparatus, and Susan Berkley, Rennie Dudek, Charline MacDonald, Cecilia Lin, Ruth Stratton and Pat Lee for their help in preparing this manuscript.

This work was made possible by the support of the National Science Foundation under grant: CME79-15132 and additional funds provided by the Union Carbide Corporation and Chevron Oil Field Research. The author was also fortunate to receive an R. T. Baker fellowship while at Caltech. These contributions are greatly appreciated.

This thesis marks the culmination of an education. I would like to thank, in addition, many of my past and present teachers: Allan Acosta, Thomas Cecil, Francis Clauser, Noel Corngold, Thomas Dorr, John Feroe, Ronald Gale, Cindy Goldman, James Hutchinson, Philip Kitcher, James Knowles, Frank Marble, David Merriell, Mitchell Miller, Patricia Mooney, Jean Mooskin, Richard Roth, Ronald Scott, Donald Spicer, Eli Sternberg, Morton Tavel, and Theodore Wu. These people made the time spent in learning both exciting and enjoyable.

My warmest love goes to Mia Goldman for her understanding, patience, and quiet encouragement.

Finally I would like to thank my parents and especially my father who first set my heart on a doctorate and in whose memory this thesis is dedicated.

ABSTRACT

Many of the macroscopic and microscopic features of shearing granular materials were observed during the course of this investigation.

The principal results were obtained from a computer simulation of the flows in an inclined chute, and in a Couette shear cell. The simulation followed the exact trajectories of two-dimensional discs through a control volume. Properties of the flow were obtained from temporal averages of the instantaneous particle properties. Macroscopic flow characteristics such as velocity and density profiles are presented. Because the simulation follows the exact mechanics of the particles it was also possible to investigate the statistical nature of granular flows. Towards this purpose velocity distributions, collision angle distributions and pair correlation functions were measured.

The results of the simulation draw a picture of a flowing granular material as a self-excited gas. There appears to be a "temperature" associated with the random motions of the particles, that is a product of gradients in the mean velocity field. An equation of state is proposed, involving this temperature,to describe the behavior of the density within the flow. A phenomenon reminscent of conduction is observed. The particle velocities appear to obey a Maxwellian distribution based on this temperature.

Preliminary experiments were also performed to investigate the flow of glass beads down inclined chutes. It is shown that the flows may be classified as either supercritical or subcritical depending on the local value of the Froude number, and that the classification had a strong influence on the flow properties. In addition, wall friction coefficients were determined.

TABLE OF CONTENTS

TABLE OF CONTENTS (continued)

TABLE OF CONTENTS (continued)

TABLE OF CONTENTS (Continued)

TABLE OF CONTENTS (Continued)

LIST OF FIGURES

Nomenclature

a_m	Maxwellian exponential constant
a_1	constant for u - velocity distribution
a_2	constant for v - velocity distribution
a_3	constant for rotational velocity distribution
a_4	constant for translational velocity distribution
a_5	constant for total velocity distribution
b	channel breadth
c	cohesion
$\underset{\sim}{c}$	instantaneous particle velocity
d	hopper opening
$f(\nu)$, $f_{ij}(\nu)$	density dependence of Bagnold/Savage constitutive law
g	magnitude of gravity vector
$\underset{\sim}{g}$	gravity vector
h	flow depth
$\underset{\sim}{k}$	vector connecting the center of particles at collision
ℓ	general length scale
m	particle mass
$\dot{m}$	mass flow
n	number of particles per unit length/area/volume
p	pressure
p( )	probability distribution
q	general quantity
$\underset{\sim}{r}$, $\underset{\sim}{r}_o$	position vectors

s_1 s_2	particle spacings
u	velocity in flow direction
$\underset{\sim}{u}$	vector velocity
v	velocity normal to flow direction
x	coordinate in flow direction
y	coordinate normal to flow direction
A	flow cross section area
C	mean particle spacing
C_{2-D}	mean particle spacing in two dimensions. $C_{2-D} = (\pi/\nu)^{\frac{1}{2}} R$
C_{3-D}	mean particle spacing $C_{3-D} = (\frac{4}{3}\pi/\nu)^{\frac{1}{3}} R$
Fr	Froude number: $Fr = \bar{u}/\sqrt{gh}$
Fr_g	gate Froude number, $Fr_g = \bar{u}/\sqrt{gHy}$
Fr_d	Froude number based on hopper opening $Fr_d = \bar{u}/\sqrt{gd}$
H	twice the most probable vertical coordinate for a particle
Hy	hydraulic radius: Hy = A/P
K	material constant for the supercritical gate Froude number
L	chute length
N_p	number of particles
N_s	number of sampling periods
P	wetted perimeter
R	particle radius
R_g	ideal gas constant
T	sensible temperature
T_S	principal shear stress
T_N	principal normal stress

S	characteristic velocity scale $S = \frac{2R\left(\frac{du}{dy}\right)}{\sqrt{\langle \underset{\sim}{u}'^2 \rangle}}$
U	normal collision velocity
U_T	upper wall velocity for Couette flows
V	tangential collision velocity
X	velocity distribution variable
X_1	u - velocity distribution variable
X_2	v - velocity distribution variable
X_3	rotational velocity distribution variable
X_4	translational velocity distribution variable
X_5	total velocity distribution variable
α	chute inclination angle
β	is the ratio of the radius of gyration of a particle to the particle radius
γ	profile parameter $\gamma = \int_0^1 \left(\frac{\nu}{\nu_c}\right)\left(\frac{u}{\bar{u}}\right)^2 d\,\frac{y}{h}$
δu, δv	velocity differences
ε	coefficient of restitution
ε_w	wall coefficient of restitution
ε_p	particle coefficient of restitution
ν	solid fraction $\nu = \rho/\rho_p$
ν_M	maximum packing
ν_m	maximum shearable packing
ν_S	maximum square packing
μ	wall friction coefficient
μ_{eff}	effective wall friction coefficient
τ	shear stress
σ_N	normal stress applied to upper plate

ω	particle rotational speed
Ψ	angle through which collision impulse is exerted
ρ	bulk density
ρ_p	density of solid material
θ	collision angle
Γ	profile parameter: $\Gamma = \int_0^1 \int_0^{\frac{y}{h}} \left(\frac{\nu}{\nu_c}\right) d\left(\frac{y}{h}\right)' d\left(\frac{y}{h}\right)$
Φ	internal friction angle
$\chi(\nu)$	density dependence of the equation of state

Superscripts and Subscripts

$(\ )'$	fluctuating quantity
$\overline{(\ )}$	average value derived from mass flow rate
$\langle\ \rangle$	average as defined for computer simulation
$(\ )_c$	critical value
$(\ )_g$	value at gate
i, j, k	indexes
$(\ )_N$	action in normal direction
$(\ )_o$	initial value
$(\ )_p$	value for particle
$(\ )_s$	action in shear direction
$(\ )_w$	value at wall
$(\ )_{3\text{-}D}$	equivalent three dimensional value

Chapter 1

INTRODUCTION

"Granular Materials" is a name given to a packed dispersion of a large number of solid particles. It is required, purely by geometrical constraints, that a packing of arbitrarily shaped particles cannot completely fill a given volume. The space between the particles will be filled with an interstitial fluid, and the particle bulk will be supported across particle contact points.

Many materials like cereal grains occur naturally in granular form. Ores and coal excavated from the earth by large shovels, break into granules as they are forced to conform to the shovel shape. Bulk plastics are generally processed directly into granular form for ease of handling. Large quantities of granular material are moved, stored, and processed daily. It is small wonder that there is a great deal of interest in improving the design of devices to facilitate their transportation and storage.

A granular material has many fluid like properties. The bulk material will conform to the shape of an arbitrary container with a minimum radius of curvature much larger than a particle diameter. Moreover, if a hole much larger than a particle diameter is opened in the container bottom, the local structure in the material next to the opening becomes unstable. The particles will fall or flow out the hole under the influence of gravity.

But granular materials are not fluids and possess many non-fluid

properties. Most evident is that particle packings can withstand a shear force and behave, in the bulk, like an elastic solid.

The differences can be attributed, in part, to the mode at particle interaction. Particles interact directly by colliding or by frictional sliding at points of contact. They may also interact indirectly, transporting momentum in the form of stresses induced in the interstitial fluid. A densely packed granular material; loaded from rest, will behave as a solid until the loading overcomes the resisting frictional forces across particle contact points. At the other extreme, a dilute suspension of particles will retain the Newtonian behavior of the suspending fluid but with an effective viscosity that depends on the particle concentration (see Batchelor [7] page 246).

Other differences arise because of the finite size of the particles. For example a bulk granular material will expand as it is deformed. This was termed "dilatancy" by its discoverer Reynolds [58, 59] who studied granular materials as a macroscopic model of matter on molecular scales. The deformation of a granular solid is accomplished by displacing its constituent particles relative to one another. The material must expand, or dilate in order to allow the particles freedom of motion.

Thus, granular materials exhibit deformation behavior similar to a fluid but still retain many properties that are reflections of their particulate nature. The efficient design of material handling devices would be

greatly improved by an understanding of the material's behavior as a function of its mechanical characteristics.

1.1 Models of Granular Material

Recent concern about granular material flows was motivated by different interests from two different disciplines. The first is the design of material handling devices, primarily hoppers, that must flow without clogging, and are free of internal stagnant regions. (A review may be found in Wieghart [84]). The second is motivated by soil mechanics and a desire to understand the failure behavior of foundations, slopes, and soil surrounding piles during driving. The internal stresses in the former case are many orders of magnitude smaller than in the latter, so it is a bit surprising that the earliest approaches in both cases followed the same physical modeling.

The earliest modeling of a granular material was as a solid. Deformation followed the laws of frictional behavior set down by Coulomb [20]. The Mohr - Coulomb constitutive hypothesis takes the form of a yield condition.

$$|T_s| \leq c + |T_n| \sin \Phi$$

where T_s is the principal shear stress, T_n the mean of the principal normal stresses, c, the cohesion and Φ, the internal friction angle for the material. The law says that the material will maintain its structure as long as the inequality is satisfied, and will yield at points in the material when equality is reached. This expression defines a yield surface. The theory of plasticity may then be applied. As long as Φ is constant this expression predicts that the stresses inside the flowing material will be independent of the strain rate.

Several theories of the plastic flow of granular materials have been proposed, including Shield [74], Jenike and Shield [30], and Spencer et al. [77, 78].

The plasticity model is the most widely used of all the descriptions of granular material. Analytical studies of the flow in hoppers have been performed by Jenike [31], Johanson [34], Savage [66], Sullivan [79, 80], Morrison and Richmond [42], Brennen and Pearce [10], Nguyen [47], Nguyen, Brennen, and Sabersky [46] among others. Reasonably good predictions have been obtained for the flow rates from hoppers with steeply inclined walls.

Plasticity models are unable to describe certain other phenomena. The velocity profiles in inclined chute flows of granular materials, such as those measured by Augenstein and Hogg [1], Savage [68], and Ishida and Shirai [27, 28, 29], may not be described by the Mohr - Coulomb model unless the friction angle is allowed to vary. (Another equation would then be required to describe the evolution of the friction angle. The factors on which the friction angle would depend, and the form of such an equation are not obvious a priori). Also no one has yet been successful in trying to adapt this model to explain the formation and shape of the stagnant funnels that form in hoppers (Nguyen [47]).

Goodman and Cowin [25] have devised a continuum theory for granular materials. The theory has been further refined by Cowin [17] Cowin and Goodman [18], and in a section co-authored by Cowin in Savage [68]. The dilation of the bulk is accounted for by a series of fictitious "equilibrated" forces, that do not have a clear physical interpretation. The theory leaves open the exact form of

the dissipative or dynamic stress tensor. Analyses have been made assuming both linear and non-linear dependence of the stress tensor on the strain rate tensor. Static assemblies and simple flows of granular materials have been solved using this theory by Goodman and Cowin [26], Jenkins [32], Savage [68], Passman et al. [53], and Nunziato et al. [48]. Passman [54] has extended the theory to mixtures of granular materials.

Neither the Goodman and Cowin theory nor the Mohr - Coulomb theory deals with a granular material as a collection of finite sized solid particles. The constitutive nature is hidden within the internal friction angle Φ, and the cohesion c, of the latter and within the equilibrated forces and whatever is chosen as the dissipative stress tensor of the former. The utility of the theories depends on how well and how economically these assumptions model the physical processes occurring at the particle level.

A very simple kinematic theory, valid for extremely slow unidirection granular flows has been proposed and applied by Nedderman et al. [44, 45], which is similar to those proposed by, Mullins [43] and Litwiniszyn [38]. The theory assumes that a particle will move whenever a space is vacated for it to move into. The flow rate is determined by the rate at which voids are propagated through the material. This model is motivated by the material's particulate nature but as the flow is independent of the forces that drive the motion, its usefulness is extremely limited.

Several strain-rate dependent constitutive models that have been proposed, are reviewed by Jenkins and Cowin [33].

The first model that was derived from first principle considera-

tions of particle interactions was proposed by Bagnold [3, 4]. He considered the momentum transferred by collision between layers of evenly spaced particles in a simple shear flow, assuming that each particle takes on the mean velocity appropriate to its position in the velocity field. He found:

$$\tau_s = \rho_p \; R^2 \; f_s \; (\nu)\left(\frac{du}{dy}\right)^2$$

$$\tau_n = \rho_p \; R^2 \; f_N \; (\nu)\left(\frac{du}{dy}\right)^2$$

where τ_s, and τ_n are the shear and normal forces between the layers, $\nu = \rho_{bulk}/\rho_p$ is a dimensionless density; called the "solid fraction", (ν is interpreted as the fraction of a unit volume occupied by solid material), (du/dy) is the local velocity gradient and f_s and f_N are undetermined functions. This model is supported by his experiments on neutrally buoyant wax spheres suspended in a glycerine-alcohol-water solution. More recently these experiments have been repeated, without a suspending liquid by Savage et al. [67, 70, 72].

A more careful calculation leading to the same conclusion was performed by McTigue [40] (motivated by Marble's [39] analysis of fluidized particle interactions). He was able to determine that $f_{s,N}(\nu) \sim \nu^2$. It is clear, however, that these functions should have a singular behavior, (similar to the packing correction found in a Van der Waals equation of state) as the system approaches the maximum possible packing.

Granular materials regarded as an assembly of solid particles are reminiscent of the molecular model of gases. Recently Savage and Jeffrey [71] adapted Enskog's dense gas analysis (see Chapman

and Cowling [14] or Ferziger and Kaper [21]), to derive the complete stress tensor in a simple shearing flow. They were able to include velocity fluctuations in their analysis by assuming that the instantaneous particle velocities obeyed a Maxwell-Boltzmann velocity distribution about their mean values. The stresses were proportional to the square magnitude of fluctuating velocities, and a function of a dimensionless quantity S expressing the relative magnitude of the shear rate to the rms fluctuating velocity:

$$S = \frac{2R\frac{du}{dy}}{\sqrt{\langle \underset{\sim}{u}'^2 \rangle}}$$

where R is the particle radius. As $\langle \underset{\sim}{u}'^2 \rangle = 4R^2 \left(\frac{du}{dy}\right)^2 / S^2$, Savage and Jeffrey were able to recover the $(du/dy)^2$ dependence of Bagnold's constitutive relation. No explicit method to determine S was given although a possible procedure was suggested.

1.2 Interstitial Fluid Effects

In this study, a granular material flow will be defined as the flow of a fluid-particle system in which the effects of the interstitial fluid are negligible. This is the asymptotic state of particle-fluid flows where the majority of momentum is transferred by particle-particle interactions rather than particle-fluid interactions. Intuitively this implies that (1) the fluid viscosity is small, minimizing the effect of viscous drag on the particles, (2) that the solid density, ρ_p, is much larger than the fluid density ρ_f, minimizing buoyancy and added mass effects, and (3) that there are no significant pressure gradients in the interstitial fluid, minimizing fluidizing effects. This suggests that the relative importance of the interstitial fluid will be characterized by three dimensionless quantities, of which only one, ρ_p/ρ_f, is readily apparent.

Bagnold [3] has suggested a parameter governing viscous fluid effects which has been called the "Bagnold number":

$$Ba = \frac{4R^2 \rho_p \frac{du}{dy}}{\left(\left(\frac{\nu_M}{\nu}\right)^{1/3} - 1\right)^{1/2} \eta}$$

where η is the fluid viscosity. Bagnold's experiments suggest that the particle-fluid system behaves as a viscous fluid for $Ba < 40$, and as a fluid free particle system for $Ba > 450$. However it is clear that the Bagnold number may not represent sufficient conditions for granular material flow. In particular, it predicts viscous behavior whenever the velocity gradient is sufficiently small, such as in the contact dominated plug flows discussed in Section 3.1.7, which are clearly not in the viscous dominated regime.

The regime of granular flow within which the interstitial fluid may be neglected has not yet been clearly defined. Based on the albeit incomplete Bagnold number criterion discussed above it probably includes all reasonably fast, non-fluidized, flows of large particles in air. The precise delineation of the granular flow regime will hopefully emerge from further theoretical and experiment studies.

1.3 Topics of the Investigation

Chapter 2 describes a computer model to examine the flow of granular materials at the particle level. Two flow situations are modelled: (1) the flow in an inclined chute and (2) the flow in a Couette shear cell. The computer model, which resembles a molecular dynamics model for gases, allows examination of details that are unobtainable by present experimental methods.

Chapter 3 presents the results obtained from the computer model. Velocity and density profiles are presented for a variety of material properties, inclination angle, shear rates, flow depths, densities, etc. An equation of state is suggested which relates the pressure to the density and the mean-square fluctuating velocities of the particles. The Bagnold/Savage constitutive law is evaluated. In addition the program is used to determine the statistical properties of a granular flow; velocity distribution functions, distributions of collision angle and pair distribution functions are evaluated.

Chapter 4 presents the preliminary results of an experimental study of the flow in inclined chutes. Flow in a chute may be classified as either supercritical or subcritical. Descriptions of both flow types and their effects on the mass flow rates are given. A simple correlation is presented for determining the flow rate from a chute as long as the flow remains supercritical. The coefficient of wall friction for the flow is also determined, and plotted as a function of flow velocity.

Chapter 2

COMPUTER SIMULATION OF GRANULAR MATERIAL FLOWS

2.1 Instrumentation Problems

The greatest problem facing research into the flow of granular materials is the lack of good experimental instrumentaion. There appears to be no completely satisfactory way to measure velocity or density profiles. Profile measurements have been made by four methods: (1) X-ray techniques, (2) interpretation of the mass flow profile, (3) measurement of velocity field at a boundary wall, (4) measurement by probes inserted into the flow.

Lee, Cowin and Templeton [37], and Blair -Fish and Bransby [9], used X-ray techniques to determine deformation patterns in hoppers. Both clearly observed that the material deformation occurred initially along low density rupture zones. No quantitative data was reported although it seems possible to determine the density as a function of the X-ray attenuation.

Ridgway and Rupp [60] and Augenstein and Hogg [1] measured the mass flow rate profile over the depth of inclined chutes. Ridgway and Rupp assumed that the velocity was constant over the depth and determined the density profile. Augenstein and Hogg assumed, that, except for the area right next to the chute bottom, the density was constant across the depth and determined the velocity profile.

It is not clear why both researchers did not derive profiles with roughly the same shape.

Connelly [16] and Nguyen [47] determined velocity profiles in two-dimensional hoppers from motion pictures of colored beads taken through the hopper's front face.

Savage [68] determined the velocity profile next to the side walls of an inclined chute by cross correlating the signals from adjacent fiber optic probes. His profiles showed only a small velocity gradient next to the chute bottom, with the largest gradients occuring near the flow center. Augenstein and Hogg [1] found that the velocity gradient was greatest right next to the chute bottom. It is the opinion of this author, based on observations made during the experiments reported in Chapter 4, that this discrepancy is due to the special conditions near the corner between the chute side wall and bottom. Particles, forced to move along this corner, move noticeably slower than the rest. The velocities measured there need not be indicative of conditions far from the side wall.

Ishida and Shirai [27, 28, 29] developed a velocity probe, that may be directly inserted into the flow, utilizing a fiber optic technique similar to Savage [68]. Their results show an almost linear velocity profile. But again experience dictates that insertion of such a probe will disturb the velocity field far upstream. (The smallest disturbance generated by any probe would be of the order of a particle diameter.)

A review of velocity measurement techniques may be found in Oki, Walawender and Fan [52]. A non-intrusive method for measuring velocity and density profiles independently and far from a boundary

wall is urgently needed. Until this can be accomplished it will be impossible to objectively evaluate theoretical models of granular flow.

2.2 Background

The flow of granular materials can be viewed as a many-body problem much like the molecular picture of matter. In both cases while the behavior of the entire system of particles is hard to predict, the mechanics of two particle interactions are very well understood. Thus granular materials lend themselves to computer simulation by models similar to those applied to gases and liquids. In these models molecules are often approximated as hard spheres, so that they are a better model for granular materials than fluids. If a model can be generated that describes the complete state of the granular system at all times, (the state is described by the instantaneous positions and velocities of the particles), then any information may be found by statistical averaging.

Molecular modeling of fluids is almost as old as the computer. The earliest work was probably done at Los Alamos and reported by Metropolis et al. [41]. Names commonly associated with this work are W. W. Wood at Los Alamos, Alder and Wainwright at Lawrence Livermore and A. H. Rahman at Argonne National Laboratories. Reviews can be found in Barker and Henderson [5], and Wood [86]. Most of these studies can be classified as employing either the "Monte Carlo" or the "Molecular Dynamics" approach.

A Monte Carlo method is one which uses probabilistic techniques to solve a problem. When applied to molecular systems, each state of the system is chosen randomly according to a given probability

distribution. In the method presented by Metropolis et al. [41], each state is chosen from its predecessor by randomly chosen movements of its particles, and either accepted or rejected according to the Maxwellian probability ($\sim \exp(-E/kT)$) that the system will have the final energy E. This type of calculation produces equivalent ensembles of the system and is generally used for calculations of steady, equilibrium properties like the equation of state. A similar technique, used to model unsteady transport phenomena, is described in Bird [8], and is referred to there as "the direct simulation Monte Carlo Method". In this case the particles have velocities which change only at collisions. Whether or not a particle experiences a collision at a given time is determined probabilistically according to the local density. Only the direction and not the magnitude of a particle velocity is changed by the collision. Thus energy is conserved. The direction following a collision is chosen with uniform probability. From this picture a given property is diffused by the transport of particles into different regions of the system. No properties can be transferred by collision because there is really only one particle involved in each collision.

In molecular dynamics calculations, each particle trajectory is determined by the laws of Newtonian mechanics. These trajectories are followed exactly and a collision occurs when two particles touch. This is a much more tedious procedure as each potential collision must be evaluated, but it is more physically appealing because it assumes only the collision mechanism.

Granular materials do not lend themselves to Monte Carlo modeling. At the densities common in granular flow there will

be almost no streaming transport of particle properties and thus the exact collision mechanics will be important. But the greatest difficulty would be the a priori determination of governing statistical distributions. It is not even clear that granular materials may be modelled according to the "Stosszahlansatz" or "molecular chaos assumption" whereby the particles can be considered to be independently distributed in a purely statistical manner without regard to history or other parameters.

2.3 Other Computer Studies of Granular Materials

There has been relatively little use of computer modeling as a research tool for granular materials. Rogers and Gardner [64] used a Monte-Carlo method to simulate the flow of powder through rotating cylinders, but they did not directly consider particle interactions. Yoshida, Masuda, and Inoya [87] modeled the flow of fluidized particles in a turbulent carrier but considered only the motion due to fluid forces on the particles and not particle-particle collisions. Powell [56] studied the static packings of spheres in beds built by placing spheres of randomly distributed size into randomly chosen locations.

The only computer model which considers in detail the particulate nature of granular materials and the interactions of particles is described in Cundall and Strack [19]. The model was designed with soil and rock mechanics problems in mind. The stresses are large and the bulk is allowed to deform only slightly. Under these conditions the individual particles will deform. Cundall and Strack assumed that for small deformations, the particles behaved

like linear springs across the contact points. They solved the time dependent problem over small time steps using a finite difference technique, attributed to Cundall and called the "Discrete Element Method". The program was used to predict the stress patterns developed in two dimensional discs that were compressed and slightly sheared between rigid boundary walls. The model could be equally well applied to large deformations encountered in granular flow problems (provided that enough computer time is available to follow the flow over a large number of small time increments.) In an earlier report, Cundall [19] used a similar simulation scheme to investigate large deformation gravity flows such as rockfalls and hopper flows. This was one of the earliest attempts to simulate granular material flows.

2.4 Description of the Model

The stresses encountered in material handling devices will be much smaller than would be found in soil mechanics problems. Significant particle deformations will be unlikely. Interstitial fluid effects are assumed to be negligible. There are assumed to be no other range forces between particles. Particle interactions will have a short duration compared to the time between interactions, and may be approximated as instantaneous collisions. Two collisions cannot occur simultaneously so only two-particle or binary collisions need be considered. Between collisions the particles follow their kinematic trajectories and their positions and velocities are simple functions of time. Trajectories change only at collisions. Thus it is practical to update time in the program from collision to collision. The incremental time steps are as long as the interval between

collisions (instead of being much smaller than the collision time as required for Cundall and Strack's model). Large deformations of the bulk may be observed at much reduced computational expense.

The program therefore proceeds as follows:

(see the flow chart in Figure 2.1)

1) The next collision to occur is determined.
2) The particle positions and velocities are updated to the time at which the collision is to occur.
3) The collision result is determined. (Note that only the trajectories of the two particles involved in the collision will be altered).
4) This procedure is repeated for a specified number of collisions. At each collision after that time the properties of the flow are sampled and averaged.
5) After another specified number of collisions the simulation is stopped and the results printed out.

There is nothing in the above description that limits the situations that may be modelled or, for that matter, is particular to flowing granular materials as opposed to a molecular model of gases.

Essentially what differentiates a granular material from a gas is that the collisions are inelastic. The system is continually losing energy. The energy must be resupplied from an external source such as the acceleration, of the particles, due to gravity, or by collisions with a moving boundary.

A granular material subject to a shear flow will show continuous bulk deformation. Suppose one were to cut a cubic slice out of the flow, and follow the particles in that slice. The volume containing

just those particles will soon lose its cubical shape. Furthermore, the particles originally in the cube will be interacting mostly with particles from outside the cube. For computational efficiency it is desirable to keep the number of particles as small as possible. One would like to consider only the particles inside the cube, but still allow them to undergo shearing motions. This is accomplished by employing a "periodic boundary condition" in the direction of flow.

Consider a control volume filled with particles. Suppose that an infinite region is built up by placing exact replicas of the control volume side by side in the direction of flow. This is referred to as a periodic boundary condition because the control volume, particle positions, and velocities, are repeated every control volume width. In effect, as a particle passes through a periodic boundary of the control volume, it reenters the opposite boundary with exactly the same position along the boundary and at the velocity with which it left.

The disadvantage of this set-up is that there can be no spatial variations in the direction of flow. The flow may accelerate or decelerate but this is experienced as a temporal change for the entire flow region. In a sense it's as if one were following a Lagrangian fluid element which experienced spatial variations in the flow field as temporal changes.

The periodic boundary condition limits the types of flows that may be modelled. One could not for example model the flow in the converging throat of a hopper using a periodic boundary condition because there are essential changes in the direction of flow.

Also one could not expect to see the effect of a "choked"chute, discussed in Sections 4.4, 4.5, as choking is related to the flow near the chute exit.

Although they are not the only class of applicable flows, unidirectional flows seem to lend themselves to this type of modelling. The two situations modelled are the flow in an inclined chute, and the flow in a Couette flow shear cell. "Snapshots" from both may be seen in Figures 2.2, 2.3 .

In the chute program the control volume is bounded on the bottom by a rigid wall, simulating the chute bottom, on the vertical sides by periodic boundaries, and is unbounded on the top. The inclination is simulated by inclining a body force vector at an angle, α, with respect to the chute bottom. For the Couette flow program, the body force is zero, and the top of the control volume is closed with a solid wall in motion relative to the bottom, in the direction of flow.

In both cases, only the flow of two-dimensional discs, of equal size and mass, was examined. There is nothing inherent in the model that prevents examination of three-dimensional spheres, except that a much larger number of spheres would be required to fill the third dimension. This would greatly increase the computer costs. Direct quantitative comparison with real 3-D flows is somewhat difficult (some particular problems will be indicated later), and a logical next step will be to extend the model to the flow of three-dimensional spheres. Nevertheless, the two-dimensional model will exhibit many of the features of its three-dimensional counterparts, and will yield insights into the nature of the particle mechanics.

2.5 Convergence of the Simulation

The periodic boundary condition eliminates all spatial gradients in the direction of flow. Even though a temporal change of properties inside the control volume may be interpreted as the effect of spatial gradients on a Lagrangian element, the simulation can, strictly speaking, only model flows that likewise experience no changes in the flow direction. This is satisfied a priori for Couette flows, but implies that only uniform (constant depth, non-accelerating) chute flows may be modelled. Such flows have no temporal or spatial evolution. Consequently the simulation is an accurate representation only if its properties do not change with time. A system that has attained steady conditions is referred to as "converged".

The total kinetic energy is chosen as an indicator of convergence because it may be instantaneously determined. If the energy is constant the flow is not accelerating or decelerating, and in all probability most other properties are steady. Representative plots of the total kinetic energy in converged state, for both chute and Couette flows are shown in Figure 2.4. In both cases the energy is fluctuating within about 20% of its mean value but there is no apparent change in the mean state.

Fluctuations of this nature are characteristic of small thermodynamic systems in equilibrium with large systems. These fluctuations may be treated statistically, and are given an extensive treatment in Landau and Lifshitz [36]. In the present case the fluctuations are due to the fact that energy is not conserved in the

simulation due to the inelasticity of collisions. Energy is added to the system by the action of gravity, in the chute program or by collisions with the moving wall, in the Couette flow program. A steady state is achieved when the rate of energy added more or less equals the rate of energy dissipated. Fluctuations occur when there are imbalances in this energy flux over a short time period. They make the judgment of convergence necessarily subjective.

The fluctuations will disappear only as the number of particles goes to infinity. But if the averaging time is much longer than the fluctuation time, the fluctuations should have very little effect on the measured quantities.

2.6 Dimensional Analysis

The model describes the flow on the microscopic level of individual particle mechanics, (as opposed to the macroscopic level of a deforming continuum). It is appropriate then to scale the parameters and variables of the problem by quantities characteristic of the particles. The particle radius R, is chosen as a characteristic length, and the particle mass m as the characteristic mass, (producing as a characteristic density $m/\pi R^2$)

If gravity is present, as in the chute flow simulation, a convenient time scale is $\sqrt{R/g}$. This is derived from the non-dimensionalization of the equations for the individual particle trajectories. Dimensionless velocities will have the form of Froude numbers: $u/\sqrt{gR}$, and dimensionless stresses will have the form $\tau/\left(\frac{mg}{\pi R}\right)$.

However, if gravity is not present, as in the Couette flow simulation, the trajectory equations are linear and the time scale is imposed through the boundary conditions. A time scale enters the problem only from the upper wall velocity, U_T. U_T must be the velocity scale of the problem making R/U_T the corresponding time scale. Stresses are then non dimensionalized in the form $\tau/(mU_T^2/R^2)$.

Even though quantities are non-dimensionalized in the above manner for the computer simulation, it is clear that the basic problem of a Couette flow of granular material does not scale with a characteristic time R/U_T. It will be shown in Section 3.2 that the appropriate time scale is H/U_T. This may be seen from simple heuristic considerations. U_T is an external quantity that only directly affects the particles that collide with the moving boundary. The only velocity, that directly affects every particle, is the relative velocity of its neighbors. On the average, this is related to the product of the local velocity gradient and some appropriate length scale. In terms of easily accessible quantities this may be approximated as RU_T/H. The corresponding characteristic time is then H/U_T .

2.7 Structure of Program

The programs are built of a main program and many subprograms. Five subprograms are integral parts of the model. The rest are used in the data analysis. The individual programs are described below:

1) Main program coordinates the various subprograms and performs the data sampling and analysis. After each collision the state of the simulation is stored on a magnetic tape for further analysis at a later time.

2) Collup is the collision assessment routine. It computes all possible collisions for a particle and stores them in a collision list using the routine Insrt.

3) Insrt - creates and maintains the collision list. (See Section 2.10) It has three entry points.

   i) Insrt - inserts a collision into the collision list.

   ii) Next - produces the next collision to occur from the list.

   iii) Init - Initializes the collision list.

4) Remove - Removes all collisions for a given particle from the collision list.

5) Partcl - Computes the result of a collision between two particles.

6) Wallcl - Computes the result of a collision with a wall.

2.8 Initial State

The initial positions and velocities of the particles are externally generated and given to the program as initial data. A typical configuration is shown in Figure 2.5. The number of particles horizontally n_H, and vertically n_v as well as an average particle spacing C are specified. The generating program places the particles into positions slightly perturbed from an evenly spaced square lattice. The width of the control volume is chosen to be $n_H C$ and the height for the Couette flow simulation $n_v C$. The system then has a uniform initial density $\nu = \pi R^2/C^2$

Most of the simulations were started with a configuration n_H = 4 particles wide and n_v = 10 particles high with an initial

spacing of 2.4 R, yielding a control volume 24 R high and 9.6 R wide with initial solid fraction $\nu \simeq 0.55$. This particular configuration was arbitrarily chosen. Doubling the width of the control volume (by doubling the number of particles horizontally) produced insignificant changes in the results, so while in some cases n_V was varied, $n_H = 4$ was used for most of the computations.

In the chute flow program all the particles are initially given roughly the same velocity. In the Couette flow program the velocities are chosen to roughly fit into a velocity profile that varies linearly from zero at the stationary wall, to U_T at the moving boundary. In both cases the velocities are randomly perturbed from the mean by small amounts.

As the program runs, all traces of the initial state quickly disappear. The system develops velocity and density profiles that are quite different from the starting values and changing the the initial state seems to have very little effect on the final results.

2.9 Collision Assessment

The position of a particle in the program is determined by the position of its center. Hence a collision occurs whenever the centers of two particles are a diameter apart.

Between collisions a particle moves along its kinematic trajectory. Thus until it collides with another particle the position $\underset{\sim}{x}_i$ of a particle that at t = o was at $\underset{\sim}{x}_{io}$ is given, at time t, by

$$\underset{\sim}{x}_i = \underset{\sim}{x}_{io} + \underset{\sim}{u}t + \frac{1}{2}gt^2$$

where $\underset{\sim}{g}$ is the gravity vector which may be zero. A collision between two particles (i) and (j) occurs when: $||\underset{\sim}{x}_i - \underset{\sim}{x}_j|| = 2R$

or when:

$$\left(\underset{\sim}{x}_i - \underset{\sim}{x}_j\right)^2 = 4R^2 = \left(\underset{\sim}{x}_{io} - \underset{\sim}{x}_{jo}\right)^2 + 2\left(\underset{\sim}{x}_i - \underset{\sim}{x}_j\right)\cdot\left(\underset{\sim}{u}_i - \underset{\sim}{u}_j\right)t + \left(\underset{\sim}{u}_i - \underset{\sim}{u}_j\right)^2 t^2$$

This is a scalar quadratic equation to solve for the time at which a collision is to occur. Note that this equation is independent of gravity because both particles are accelerated at the same rate. (Gravity does however appear in assessing collisions with solid boundaries or pseudo collisions with the periodic boundaries.)

The collision assessment is further complicated by the periodic boundary condition. Figure 2.6 shows the control volume from the Couette flow program and the periodic images immediately upstream and downstream. Because a particle has a finite radius it is possible for a particle whose center is in the main frame to collide with another particle whose center is in the upstream or downstream frames. In Figure 2.6 collisions of this type can be seen between particles 32, and 35, 15 and 21, 15 and 26, 7 and 5, 25 and 18, and 14 and 3.

To account for the periodic images collisions are not only assessed between particles inside the control volume but also with their images mapped into the upstream and downstream frames. The upstream frame is denoted -1, the main frame 0, and the downstream frame +1, corresponding to the number of control volume widths added to map it into its periodic image.

Then the four quantities that characterize a collision are the

indexes of the two particles involved, the frame in which the target particle will be during the collision, and the time at which the collision is to occur.

2.10 Collision List

To find the next collision, The number of potential collisions which need to be evaluated is of order N_p^2. Each evaluation involves solving a quadratic equation for the collision time, and comparing the roots. This is a formidable task and must be performed after each collision. But, when a collision occurs, only the trajectories and potential collisions of the two particles involved, will change. Potential collisions for most of the particles will be unchanged and most of the $O(N_p^2)$ evaluations will be repetitive.

This redundancy can be eliminated by storing the future collisions in a collision list. After each collision only the future collisions of the two particles involved need be reevaluated and only $O(N_p)$ equations need be solved.

It is not necessary to store all potential collisions in the list. But it is not sufficient to store only the next collision for each particle. This can be illustrated by the following example: Suppose that the next collision of a particle i will be with particle j, but j is scheduled to collide with another particle, k, first. After j's collision, its trajectory has changed so that i's first collision will be with some other particle. If only i's collision with j was stored in the list, all i's collisions would need to be evaluated along with j's. The same would be true for all particles that would have collided first with j or k.

This problem is solved by storing all collisions until a particle hits either a solid wall or a periodic boundary. These collisions will stay in the list regardless of what happens to other particles. Experience has shown that three or four collisions will be stored on the average for each particle. (This quantity will depend on the control volume size, and the number of particles, and the flow conditions.)

2.10.1 General Description

The routines which maintain the collision list are required to perform two functions. The list must be sorted in order of occurrence so that the next collision may be easily found and each potential collision added to the list must be placed so as to keep the list ordered. Secondly, after a collision between two particles all potential collisions that involve either of the particles must be removed from the list.

The simplest way to go about this would be to store the collision information physically in the computer memory, in the order of occurrence. Thus if a collision needs to be added to the center of the list all the information for potential collisions that will occur later must be moved to make room for it, and when the collision is removed from the list all that information must be moved back again to fill the vacated space. In general the collision list for N_p particles was $3N_p - 5N_p$ collisions long, implying that on average every particle has 3 - 5 collisions stored in the list. A great deal of computer time would be spent in just moving information about the memory, most of which would never be used.

These computer costs can be avoided at the expense of some memory storage. A collision may be placed anywhere in the physical computer memory, as long as information about the collision order is stored with it. This extra information is in the form of "pointers". The pointers give the location in physical memory of the next collision in the list. The information for the second collision may be found in the list element at the location specified by the pointer attached to the first collision, the third collision is specified by the pointer attached to the second, and so on. The list may be followed by stepping from one element to the next following the pointers.

It is critical to maintain the structure of this type of list. If a single pointer is misplaced the rest of the list is lost. As described, this structure is inadequate for the simulation. There is not enough information attached to each element to reconnect the list after an element is added or removed from the center.

This difficulty is avoided by using a "double linked list". Two pointers are associated with each element, one pointing to the next element in the list (a "forward pointer") and the other pointing to the previous element in ths list, (a "backward pointer"). An element A may then be removed from the center of the list by placing its backward pointer in the backward pointer of the element pointed to by A's forward pointer, and by placing A's forward pointer in the forward pointer of the element pointed to by A's backward pointer. A collision may be added to the list by following the reverse procedure. This is shown schematically in Figure 2.7.

Three double linked lists are associated with each collision. The first connects the collisions in the order in which they will occur. The other lists contain all the collisions involving a single particle. One list is needed for each particle involved in the collision. That which is called the collision list will actually contain many lists, one for each particle, and one to keep all the collisions in the proper temporal sequence.

2.10.2 Details of the Data Structure

The data structure used in the program is shown in Figure 2.8. Most of the information is contained in a large integer array called ICOLL. Each row of ICOLL is nine elements long and stores the information for one potential collision. The first three elements are the two particles involved in the collision and the frame in which the target particle (j) is to be at the time of the collision. The time at which the collision is to occur is in the same row of a Double Precision array appropriately titled TIME.

The other six elements in each row of the array are pointers attaching the collision information to three lists: the list of collisions, ordered as to the time of occurrence, and the two lists of all collisions involving each of the particles.

The fourth and fifth elements in the row give the index of the rows in which the information is stored for the collisions that will occur directly before and after. These constitute the backward and forward pointers in the collision time list. Two pointers external to ICOLL: ISHORT, and ILONG, contain the indexes of the rows containing the collision information for the collisions which

will occur at the shortest and longest time. The list of collisions, in the order which they will occur, from the shortest to the longest, starts with the first element indexed by ISHORT. The next entry in the list is always found in the forward time pointer of the last entry. In this way the list is followed along. At the end of the chain (the largest time) there will be a zero in the forward pointer, which indicates the end of the list. One can go the other way by starting with ILONG and following the backward pointers.

The proper location of a new collision, in the order of occurrence list, is found by starting at ILONG and following the chain until another collision is found that will occur in a shorter time. The new collision is placed in the list just behind the other.

The lists containing all collisions for the particles i, j involved in the collision are linked by pointers in the sixth through ninth columns. The main difference between these and the time list is that order of the elements is not important. These are organized as LIFO (Last In First Out) lists which means essentially that the first element appearing in each list was the last to be added to it. The list for the i^{th} particle is pointed to by the i^{th} element in an integer array NPOINT. If the particle index appears in the first column of ICOLL, the pointers to its list are contained in the sixth and seventh columns, and if its index appears in the second column, the pointers are in the eighth and ninth columns. A problem arises because, for a given particle, the pointers may be found in different columns for different entries in the list. That the list is to be continued in the eighth and ninth columns is

indicated by adding two-hundred thousand to the value in the pointer.

A single linked LIFO list, pointed to by the pointer IFREE, keeps track of all rows in the ICOLL that are free to be filled with new collisions. The pointer to each successive entry in the list can be found in the ninth column of the present entry; all other columns are unimportant. There is no need for forward and backward pointers in this list because no entries will ever be removed from the list's center.

2.11 Collision Solutions

There are three types of collisions encountered in this program: (1) particle-particle collisions, (2) particle-wall collisions, and (3) "collisions" with the periodic boundaries.

A collision with a periodic boundary occurs when a particle's center crosses into the downstream periodic image of the control volume. This must be accompanied by another particle entering from the upstream periodic image with exactly the same velocity and relative position as the one that left. The solution of a collision with a periodic boundary is obtained by just moving the center of the particle one control volume width upstream.

Particle-particle and particle-wall collisions are both assumed to be inelastic. This is realized in the program by assuming that the ratio of the approach to the recoil velocities in the center of mass frame is given by a coefficient of restitution, ε, which is specified as an input parameter for the program. Different coefficients of restitution, ε_p, and, ε_w, may be specified for particle and wall collisions respectively.

The particles are assumed to be fully rough in the sense that on departure there is zero relative velocity in the direction tangential

to the particle's surface. This assumption implies that the friction at the particle surface is always large enough to bring the relative velocity of the particles to a halt.

Both of these conditions result in energy dissipation. The energy dissipated by the no-slip condition is equal to the work that friction would do in bringing the relative tangential velocities of the particles to a halt.

2.11.1 Particle-Wall Collisions

Consider the collision between a particle moving with horizontal velocity U_o, verticle velocity V_o, and with rotation ω_o, and a solid wall. The collision will impact the wall with an impulse per unit mass, J that is applied at some angle γ with respect to the vertical (see Figure 2.9a,b). The governing equations are then:

$$U = U_o - J \sin \psi$$

$$V = V_o + J \cos \psi$$

$$\omega = \omega_o \mp \frac{J \sin \psi}{\beta}$$

where β is the ratio of radius of gyration of the particle to the particle radius ($\beta = .5$, the value for a cylinder, is used in all our simulations.) U, V, and ω are the final velocities of the particle. The negative sign is chosen for a lower wall collision and the positive sign is chosen for a collision with the upper moving boundary.

The effects of the coefficient of restitution and the no-slip conditions may be written respectively as:

$$V = -\varepsilon_w V_o$$

$$U - U_T \pm \omega = 0 \quad .$$

This yields five equations for the five unknowns: U, V, ω, J, and γ. Then:

$$U = \frac{U_o}{(1+\beta)} + \frac{U_T \pm \omega_o}{(1+1/\beta)}$$

and

$$\omega = \frac{\beta}{1+\beta}\,\omega_o \mp \frac{U_o - U_T}{1+\beta} \quad .$$

So for a collision with a stationary wall:

$$U = \frac{U_o}{1+\beta} - \frac{\omega_o}{1+1/\beta}$$

$$V = -\varepsilon_w V_o$$

$$\omega = \frac{\beta}{1+\beta}\omega_o - \frac{U_o}{1+\beta}$$

and for a collision with the upper, moving wall

$$U = \frac{U_o}{1+\beta} + \frac{U_T + \omega_o}{(1+1/\beta)}$$

$$V = -\varepsilon_w V_o$$

$$\omega = \frac{\beta}{1+\beta}\,\omega_o + \frac{U_o - U_T}{(1+\beta)}$$

2.11.2 Particle-Particle Collisions

Consider now the collision between two particles A, and B, in the center of mass coordinate system. The particles approach each other

with velocity of magnitude U_o along the vector $\underset{\sim}{k}$ connecting their centers and V_o tangential to $\underset{\sim}{k}$. The collision results in an impulse J inclined at an angle ψ with respect to $\underset{\sim}{k}$ (see Figure 2.9c). The equations governing the collision are:

$$U = U_o - J\cos\psi \;\; ; \;\; \omega_A = \omega_{A_o} + \frac{J\sin\psi}{\beta}$$

$$V = V_o - J\sin\psi \;\; ; \;\; \omega_B = \omega_{B_o} + \frac{J\sin\psi}{\beta} \quad .$$

The effect of the coefficient of restitution may be written as:

$$U = -\varepsilon_p U_o$$

and the no-slip condition as:

$$\omega_A + \omega_B - 2V = 0 \quad .$$

The solution is:

$$U = -\varepsilon_p U_o$$

$$V = V_o - \frac{\omega_{A_o} + \omega_{B_o} - 2V_o}{2(1+1/\beta)}$$

$$\omega_A = \omega_{A_o} + \frac{\omega_{A_o} + \omega_{B_o} - 2V_o}{2(1+\beta)}$$

$$\omega_B = \omega_{B_o} + \frac{\omega_{A_o} + \omega_{B_o} - 2V_o}{2(1+\beta)}$$

2.12 Coefficients of Restitution

The coefficients of restitution, ε_w, for wall collisions, and ε_p, for particle-particle collisions, are the only material properties that are used in the program. They represent the energy balance in the collision solution and reflect the degree to which energy is dissipated in a collision. For most of the simulations they were taken to be $\varepsilon_w = 0.8$, $\varepsilon_p = 0.6$. The coefficient of restitution for polystyrene beads bounced off aluminum plates was observed experimentally and found to be about 0.7. It was felt that the wall coefficient should be somewhat larger due to the error introduced into the measurements by the non-sphericity of the particles, hence the value 0.8 was chosen. As particles were much softer than the wall the particle-particle coefficient of restitution would probably be somewhat less and was taken to be $\varepsilon_p = 0.6$.

Actually coefficients of restitution are not material constants but vary with impact velocity as well as other parameters. Measurements of coefficients of restitution are given by Goldsmith [23], Raman [57], and Barnes [6]. Some are shown in Figure 2.10. For almost all materials the coefficient of restitution ε seems to approach one (elastic collision) as the impact velocity goes to zero. The coefficient of restitution always decreases with impact velocity. The ε's generally decrease very rapidly from unity at small impact velocities; the decline becomes less rapid and ε appears to be approaching an asymptotic value for extremely violent collisions.

This rapid decrease in the coefficent of restitution could produce a stabilizing effect on granular systems. The impact velocities of the particles will always be of the order of the velocity gradient

multiplied by a particle diameter and will generally be small. The coefficient of restitution will then ordinarily be in this rapidly decreasing region and a small change in velocity will bring about a large change in ε and a subsequent change in the rate of energy dissipation. If the flow slows the impact velocities will be smaller yielding a smaller rate of energy dissipation which would tend to accelerate the flow. Similarly an accelerating flow would tend to increase the rate of energy dissipation, retarding the flow. For this reason an exponentially decreasing coefficent of restitution was used to aid the convergence of some chute simulations. (See Section 3.1)

As the coefficient of restitution reflects the energy dissipated by the plastic deformation of the particles, one would expect that ε would depend on the deformation history of the particle, as well as temperature and anything else that might affect the plastic properties of the material. Raman [57] notes, for example, that the surfaces of his test spheres had to be cleaned and highly polished before testing to assure consistent results. A constant coefficient of restitution is then not the most realistic material property but is the most convenient to use in the format chosen for the simulation.

2.13 Averaging

Up to this point our simulation appears as a black box. It describes the behavior of the system, but no useful information has been obtained from it. The simulation describes the complete state of the system at any time. But one is not really interested in the instantaneous state of the system, but in the time averages of its properties. For example, to perform an experiment on a chute flow of glass beads,

say to measure the velocity profile, requires averaging the velocities of many particles passing through a point.

As shown in Figure 2.11 , the control volume is divided into strips and at each collision properties of the particles inside every strip are averaged. The result is the distribution of properties in the direction normal to the direction of flow. The periodic boundary condition has eliminated the possibility of time averaged spatial variations along the flow direction.

A strip width of about one particle diameter was found to be optimum. A particle's diameter is a characteristic microscopic length scale and significant variations in the velocity and density profiles are observed between adjacent strips. The strips are narrow enough to show detail, yet wide enough to contain several particle centers at each sampling time.

While a particle center may be inside a given strip a large portion of the particle may reside in an adjacent strip. Thus the percentage of a property possessed by a particle that is attributed to a strip is weighted by the percentage of the particle's volume that is contained within the strip. Let $\langle f_i \rangle$ denote the average value of some property f in strip i. For the j^{th} sample the particle k will have an instantaneous value of f denoted by f_{jk}. Let A_{ijk} be the area of particle k in strip i for sample j. (See Figure (2.11.) Then

$$\langle f_i \rangle = \sum_{j=1}^{N_s} \frac{\sum_{k=1}^{N_p} A_{ijk} f_{jk}}{\sum_{k=1}^{N_p} A_{ijk}}$$

where N_p is the number of particles in the control volume, and N_s is the number of samples taken. Most properties are determined in this way.

The ideal samples would be taken from a set of equivalent "ensembles". The simulation is set up to provide the ensembles as time evolutions of a converged system. The sampling period must be chosen with some care to provide an accurate representation of the phenomena. Properties are averaged over many thousands of collisions to avoid transients. Unless otherwise stated, all the data presented here were derived from converged systems.

2.14 Special Problems

Certain problems presented themselves in the creation of this simulation that deserve special mention. These problems all arose from expected physical phenomena that tested the limitations of the assumptions upon which the model was built.

2.14.1 Roundoff errors

Computing the time at which a collision is to occur requires solving a quadratic equation by: $(1/2a)(-b \pm (b^2 - 4ac)^{1/2}))$. Problems arise when $-b$ and $(b^2 - 4ac)^{1/2}$ have close to the same magnitude if $b^2 >> |4ac|$. When the difference is taken there may then be a significant loss of precision in the answer. This would mean that the two particles overlap slightly or are not yet in contact at the time specified for the collision. Greater error is introduced because the particle's position is updated, often several times, between the time a collision is assessed and when it finally occurs; each updating becomes another source of error.

The final error in the particle positions, at the time a collision occurs, is still probably several orders of magnitude less than a particle's radius, hardly noticeable except to the computer. The problems arise only in certain seemingly unlikely chains of events; but even unlikely events are likely to occur in a hundred thousand collisions.

Suppose that particle A collides with particle B, but due to the roundoff error is overlapping it slightly at the collision time. A's trajectory is altered so that while it is still overlapping B it collides with a third particle C. The collision with C sends A back towards B. However, the collision assessment routine looks for the time when A and B will be a particle diameter apart. As A and B overlap already this will not occur until A has passed completely through B. Occasionally particles would be found overlapping as much as a particle radius.

The solution to this problem was rather heuristic. After a collision the particles are moved so that their edges are a hundred-thousandth of a particle radius apart. The collision assessment routine will always check for slight overlaps between particles and call an immediate collision if one is found. In addition the collision assessment is performed with double precision accuracy. This eliminated particle overlaps.

2.14.2 Rolling Particles

If one were to throw a soccer ball down a street, it would bounce a few times and eventually end up rolling along the street. This common event cannot be modeled by this simulation without a special provision.

Consider a particle that collides with the lower wall with a very small impact velocity. It will recoil only a short distance and will very quickly collide with the wall again. Each successive collision will decrease its recoil velocity further,(by the action of the coefficient of restitution) until the time between collisions becomes effectively zero. As the program time is updated at each collision, time would cease to advance, particles would not move, and the simulation would for all intents and purposes stop as the computer assesses an endless string of instantaneous collisions.

Like the soccer ball, the particle is trying to roll along the bottom wall. However the simulation as so far described, does not allow that type of interaction. The problem is solved by tagging the particles that are rolling so that no further wall collisions will be assessed for it. The particle ceases to roll when it collides with another particle.

When a particle is rolling it is no longer in the same inertial frame as a free falling particle. The collision assessment equation becomes quartic which further complicates the roundoff error problems.

2.14.3 Moving Couette Flow Boundaries

In the first generation of the Couette flow program, the solid boundaries between which the particles are trapped were kept a fixed distance apart. With no gravity the particles eventually drifted away from both walls and moved like a solid plug down the center of the channel, with only occasional wall interactions. Energy is added to a Couette flow by the moving boundary and must be dissipated by the straining of the material. For a Couette flow of granular material,

energy is added to the system only by the few particles that collide with the moving boundary. These particles pass the energy on by collisions with the rest of the material. The subsequent collisions drive the particles back to the moving boundary to gather further energy. The rate at which energy is transferred to the system is governed in part by the collision rate with the moving boundary.

If the flow is N particles deep then there will be $O(N)$ particle-particle collisions for each wall collision. As each collision dissipates energy, a delicate balance would be required to keep the energy of the system constant. If the energy of the bulk decreases, the forcefulness with which particles are driven against the moving boundary is diminished reducing the collision rate and the rate of energy transfer to the bulk. Less and less contact will be made with the walls until the material moves almost like a plug between the walls.

Both Bagnold [3] and Savage et al. [67, 70, 72] have performed rheological experiments with granular materials in Couette flow devices. Bagnold studied wax spheres suspended in a glycerine-water-alcohol mixture. The fluid then acts as a carrier of shear forces between the particles and the boundary making direct contact unnecessary. The spacing between the walls was not fixed in Savage's shear cell. Instead the spacing adjusted itself until the pressure exerted on the walls by the particles balanced an externally applied force. Sufficient contact between the particles and the boundary was thus insured.

It was Savage's device that was finally used as the physical model for the simulation. A normal force is specified as an input parameter to the program. The force exerted on the walls by the

particles, is compared to the inputted value every N_p collisions (where N_p is the total number of particles in the control volume) and the solid boundaries are set in motion in the direction normal to the flow. The velocities of the walls are assumed to be constant in the period between comparisons. This greatly enhances the efficiency of the program as the complete collision list must be recomputed each time the wall velocity is changed.

The density of the system cannot be explicity specified. Instead it is determined implicitly as a function of the normal force and the wall velocity.

The moving walls created another problem that was not immediately apparent. If the applied normal force was large the particles would be forced into a high density configuration. But if the width of the control volume is kept constant while the solid walls are moving, there will be densities, or at least, configurations of particles corresponding to a given density that will be unrealizable. The first simulation run at high density was very slow in converging. After some time, it became apparent that the converging solid boundaries were trying to force the particles into a configuration they could not reach due to the fixed width of the control volume.

For example, consider the configuration used for the initial state of the system, (see Figure 2.5). The particles are arranged randomly inside a square lattice. The lattice spacing determines the density of the configuration. For a density ν the spacing would be roughly $(\pi/\nu)^{\frac{1}{2}}$ R. A lattice N spaces wide can only fit into a control volume of width $N(\pi/\nu)^{\frac{1}{2}}$ R. If the density is to change while the width remains fixed during the course of the simulation,

then a square lattice configuration cannot be maintained.

One solution would be to choose a control volume that is wide enough so that the error in the configuration imposed by a changing density is small. This would entail using many more particles to fill the control volume and would greatly reduce the program's efficiency.

Another solution is to simultaneously vary the width so that the ratio of height to width remains constant. The material is then compressed at the same rate by the changing control volume thickness as it is by the converging solid boundaries. The particles in the upstream and downstream periodic images will approach at the same speed as the boundaries, simulating the compression due to density changes in the upstream and downstream periodic images.

Clearly the square lattice configuration will always fit into this control volume, but one cannot be certain that other configurations are not artificially excluded. This is therefore a somewhat less appealing solution to the problem than using a very wide control volume. However, it is used in this model because it does not require additional particles and added computer expenses. (It will be shown later that the square lattice is not a bad model for the local particle configuration in a high density shear flow.)

2.15 Animation of the Simulation

An animated film has been made from the simulation. The instantaneous state of the system, at each collision, is recorded on magnetic tape. A program was written to interpolate the state of

the system, between collisions, to produce "frames" that are evenly spaced in time. Each frame is drawn on a Tektronix graphics terminal and photographed with a Bolex H16M motion picture camera.

The filmed sequences were derived from three different inclination angles of the chute flow simulation, and three different densities of the Couette flow simulation. With explanatory titles, the total length of the film is about five minutes.

2.16 Summary of the Simulation

A computer simulation of the flow of granular materials in inclined chutes, and in a Couette flow shear cell, has been described. The simulation follows the exact trajectories of two-dimensional discs through a control volume. The particles interact by colliding with one another. The collisions are assumed to occur instaneously. The interstitial fluid is assumed to have a negligible effect on the particle motion; between collisions the particles follow their simple kinematic trajectories.

In the flow direction the control volume is bounded by periodic boundaries. This isolates the specific particles in the simulation, but has the unfortunate effect of eliminating all gradients in the direction of flow and imposes the requirement that the system must assume a steady (converged) state to be a valid model for real flows.

In a converged state the energy of the system must be nearly constant; the work performed by gravity or by the moving wall must be dissipated inside the granular mass by inelastic collisions. The inelasticity is represented in the simulation by a coefficient

of restitution relating the approach to recoil velocities of the particles in the center of mass and by making the surface of the particles fully rough so that there will be no relative tangential motion between the particles after the collision. The coefficients of restitution were assumed to be constants for most of the simulations. In a few runs, that appeared to have convergence difficulties, the coefficient of restitution was allowed to vary according to the impact velocity.

Measurements are performed on the system by time averaging the properties of the particles that lie in strips parallel to the flow. (The periodic boundary condition assures that there can be no time averaged variation of properties in the flow direction).

Very few assumptions are made about the behavior of the flow. Once started the particles behave purely mechanistically, in their trajectories and collisions. By far the greatest restriction is imposed by the periodic boundary condition, not because it directly influences the flow dynamics but because it limits the type of flows that may be modeled.

The greatest asset of this model is its versatility. The model describes the complete state of a granular system, and from that information, everything about the flow may be derived. The model will provide insight into these flows that cannot be obtained from experiments at the present time.

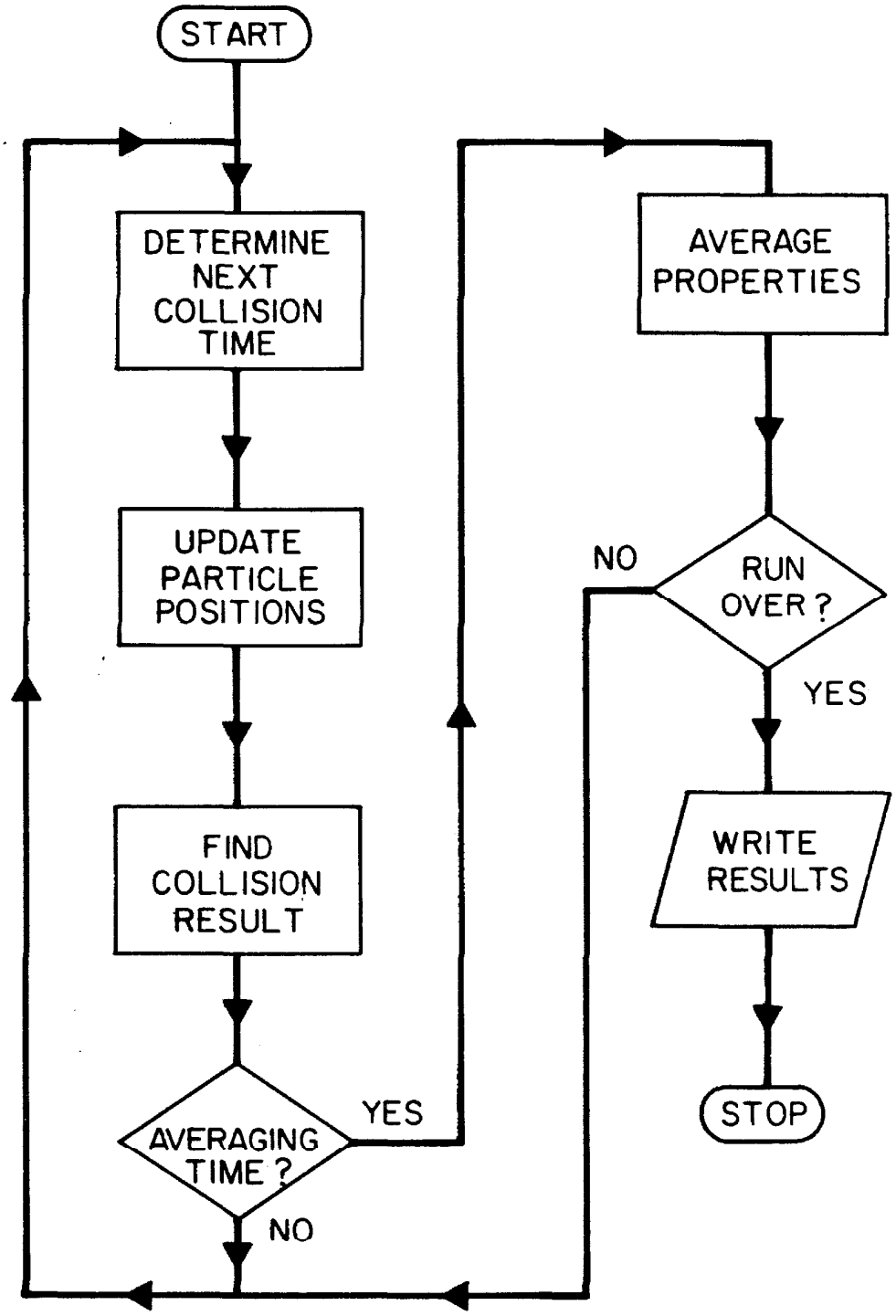

Figure 2.1 Flowchart of the simulation structure.

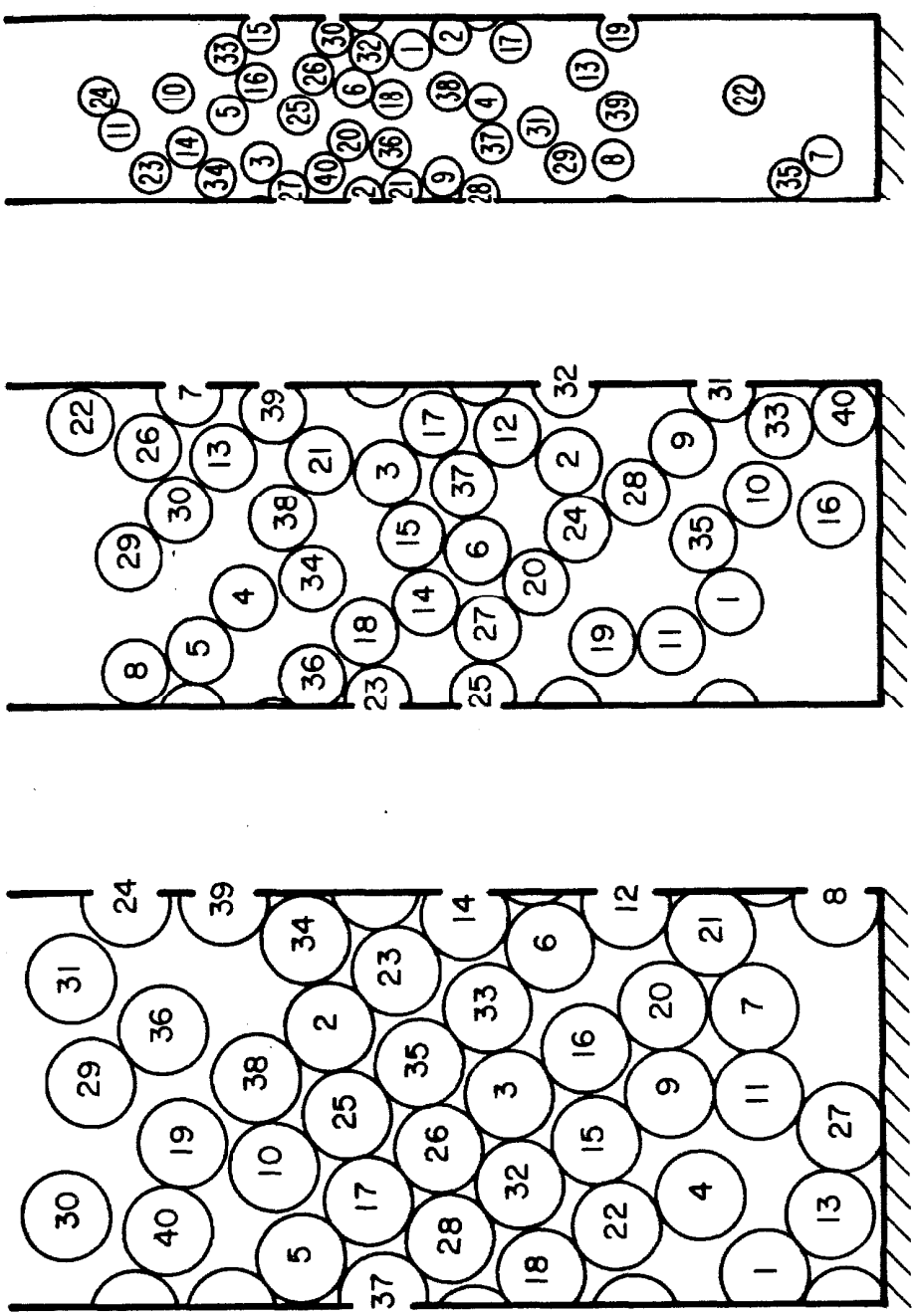

Figure 2.2 Snapshots from the inclined chute simulation. (a) $\alpha = 20^{\circ}$, (b) $\alpha = 30^{\circ}$, and (c) $\alpha = 40^{\circ}$ (angle measured relative to horizontal).

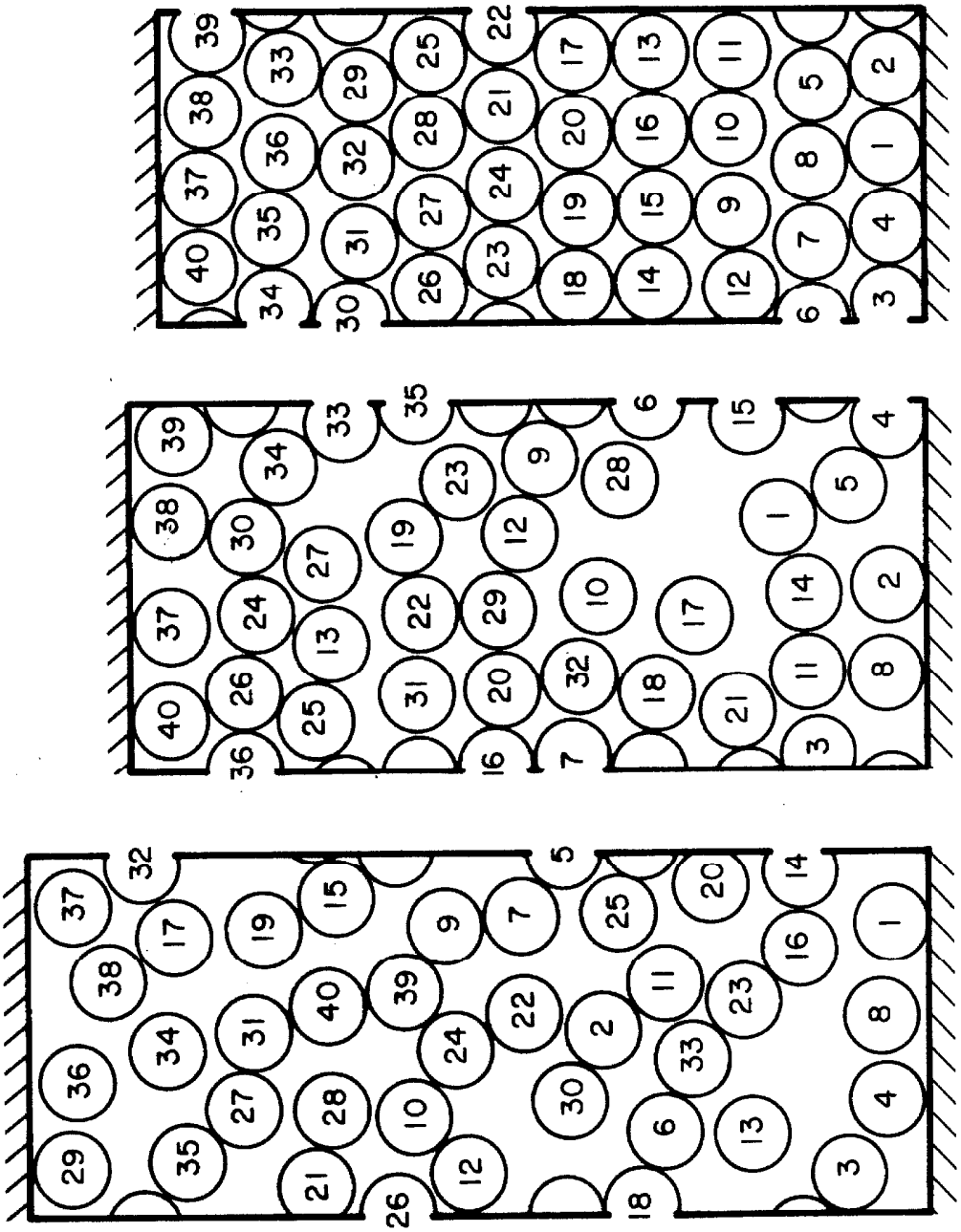

(a) (b) (c)

Figure 2.3 Snapshots from the couette flow simulation. (a) $\nu = .56$, (b) $\nu = .63$, (c) $\nu = .76$.

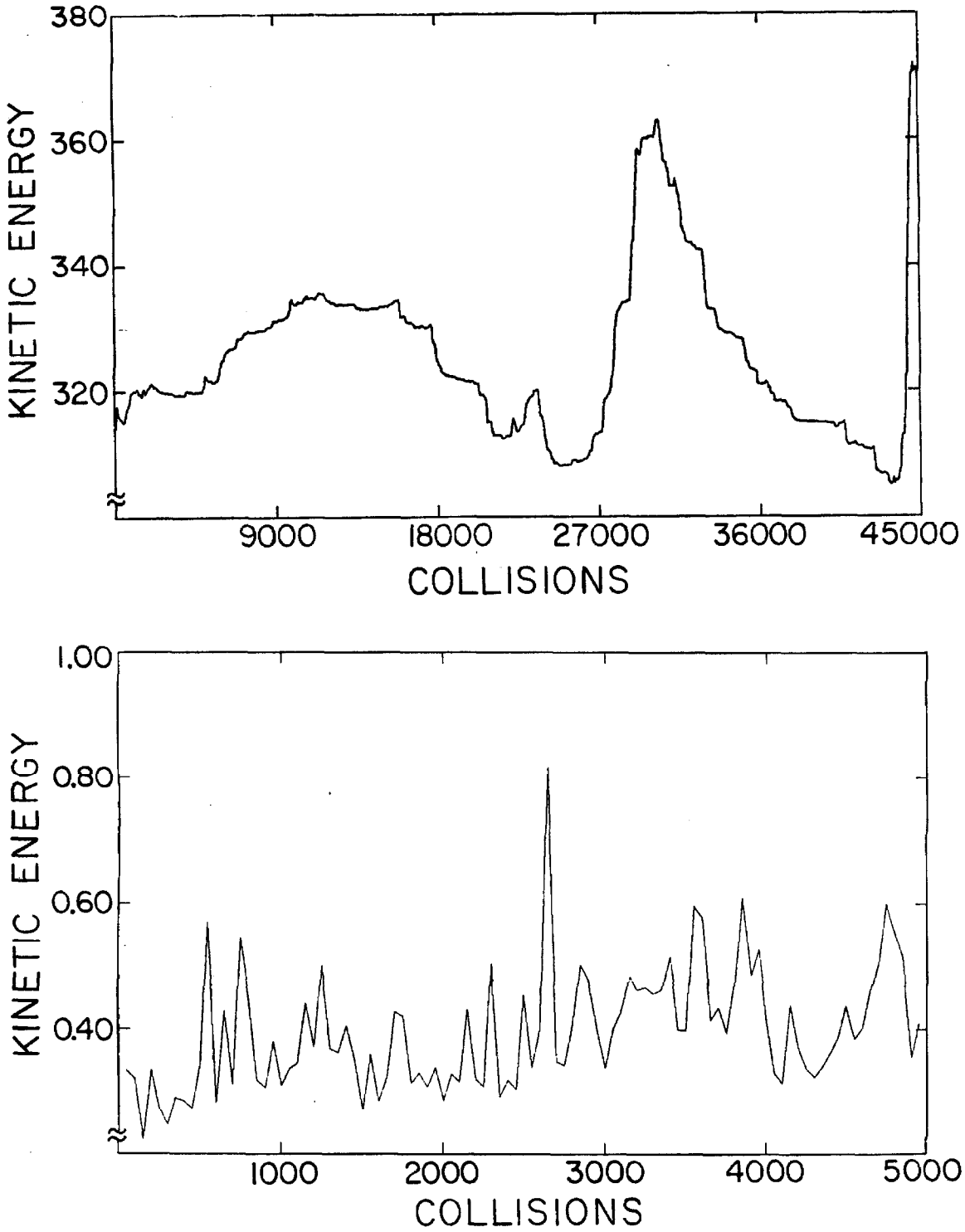

Figure 2.4 Dimensionless kinetic energy history (per particle) of converged simulations top: chute flow ($\alpha = 30°$) bottom: Couette flow (R/H=0.1).

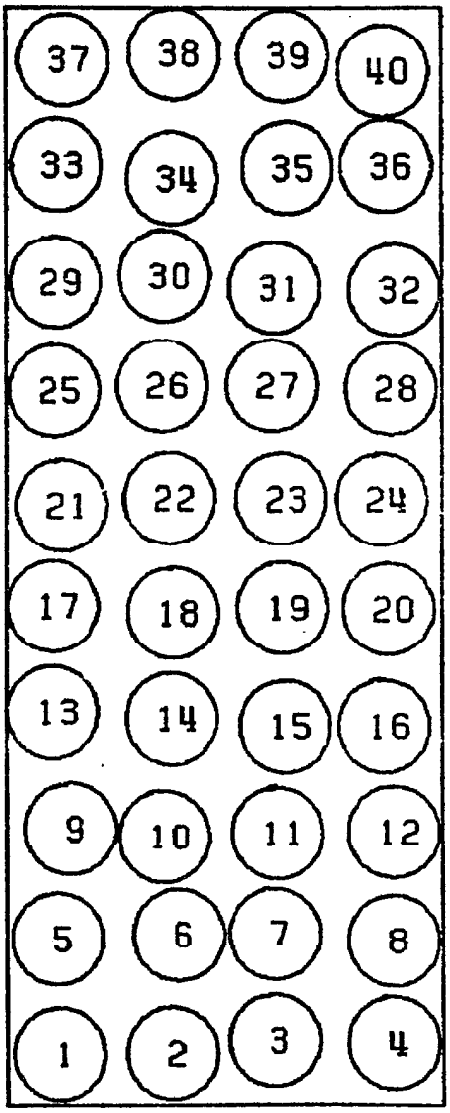

Figure 2.5 Typical initial configuration of 40 particles, configured 10 x 4.

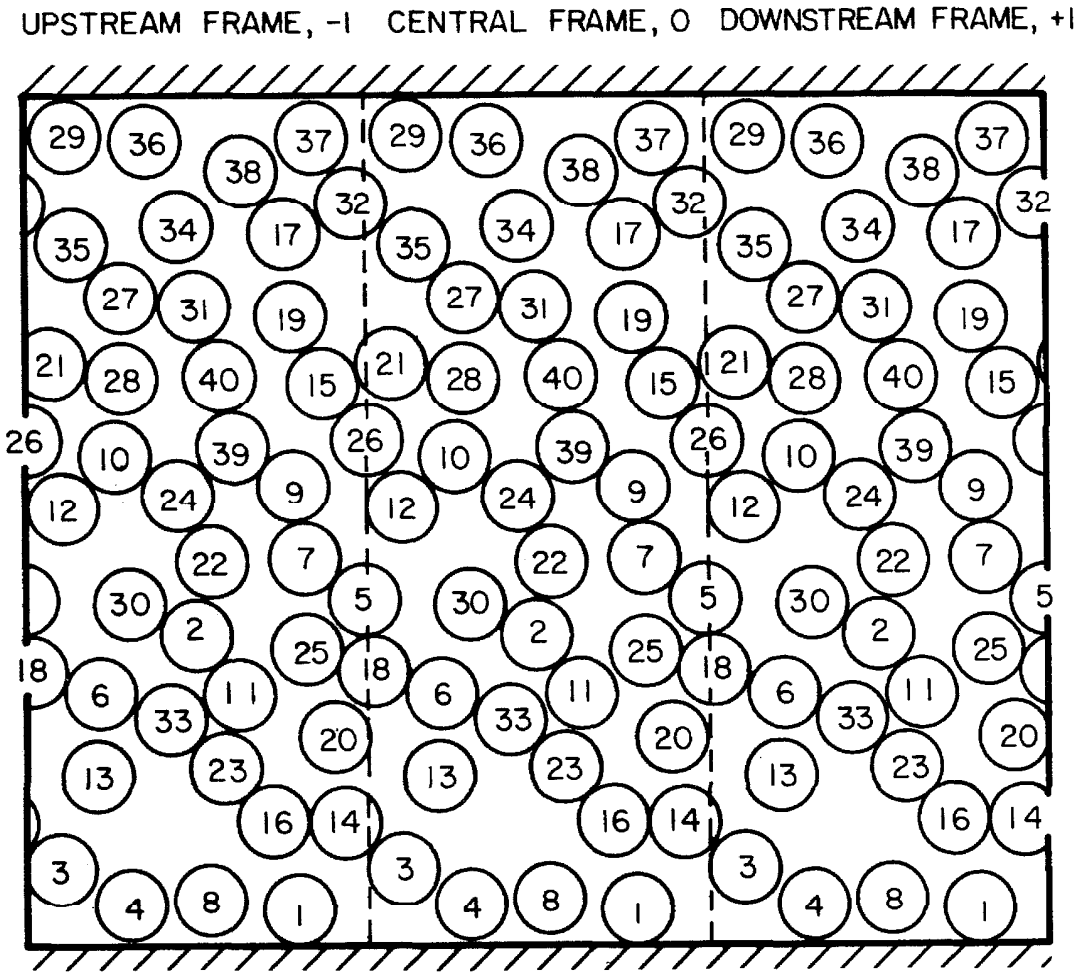

Figure 2.6 The principle control volume (o) and its upstream (-1), and downstream (+1), periodic images.

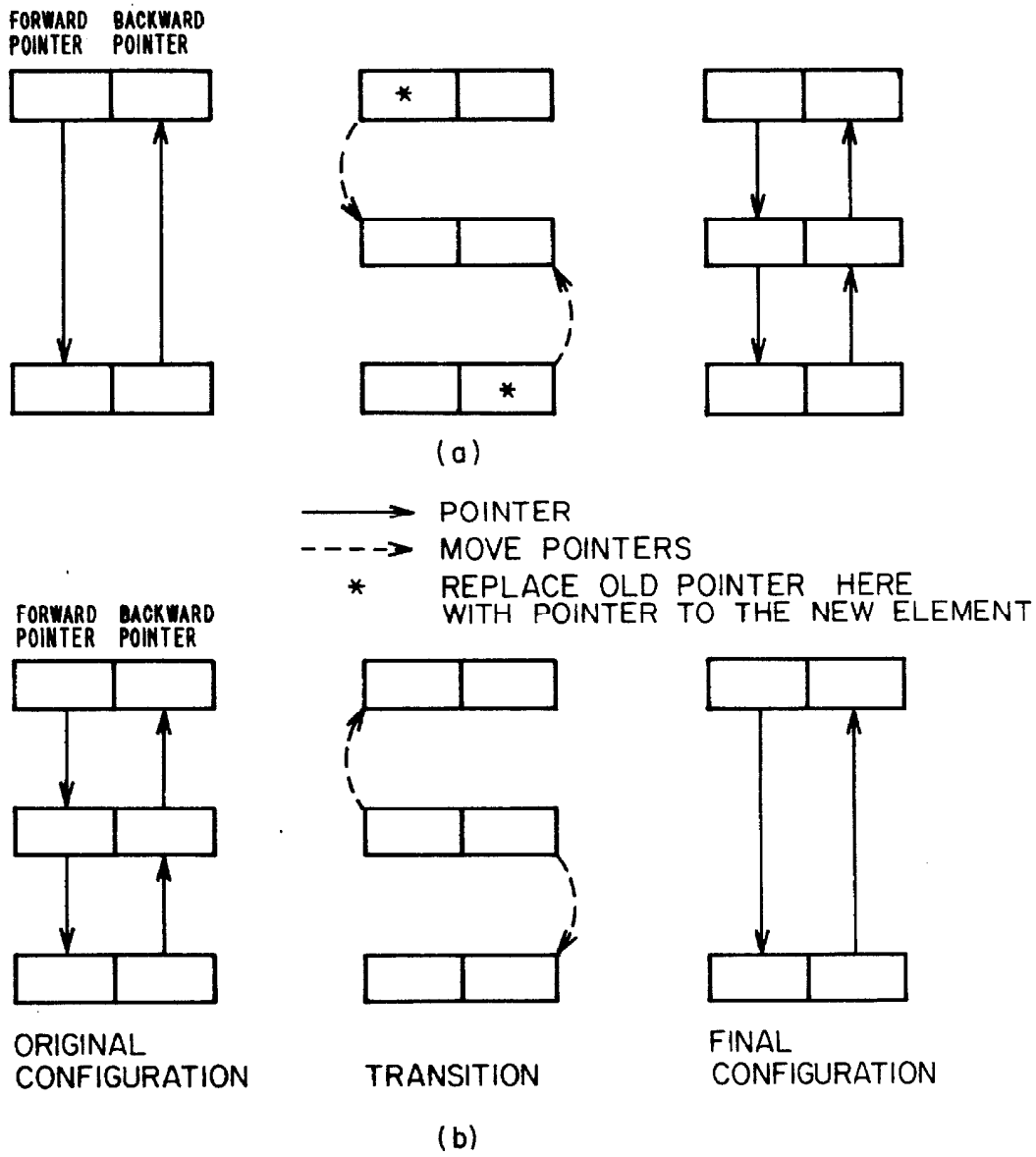

Figure 2.7 Insertion (a), and removal (b), of an element from a double-linked list.

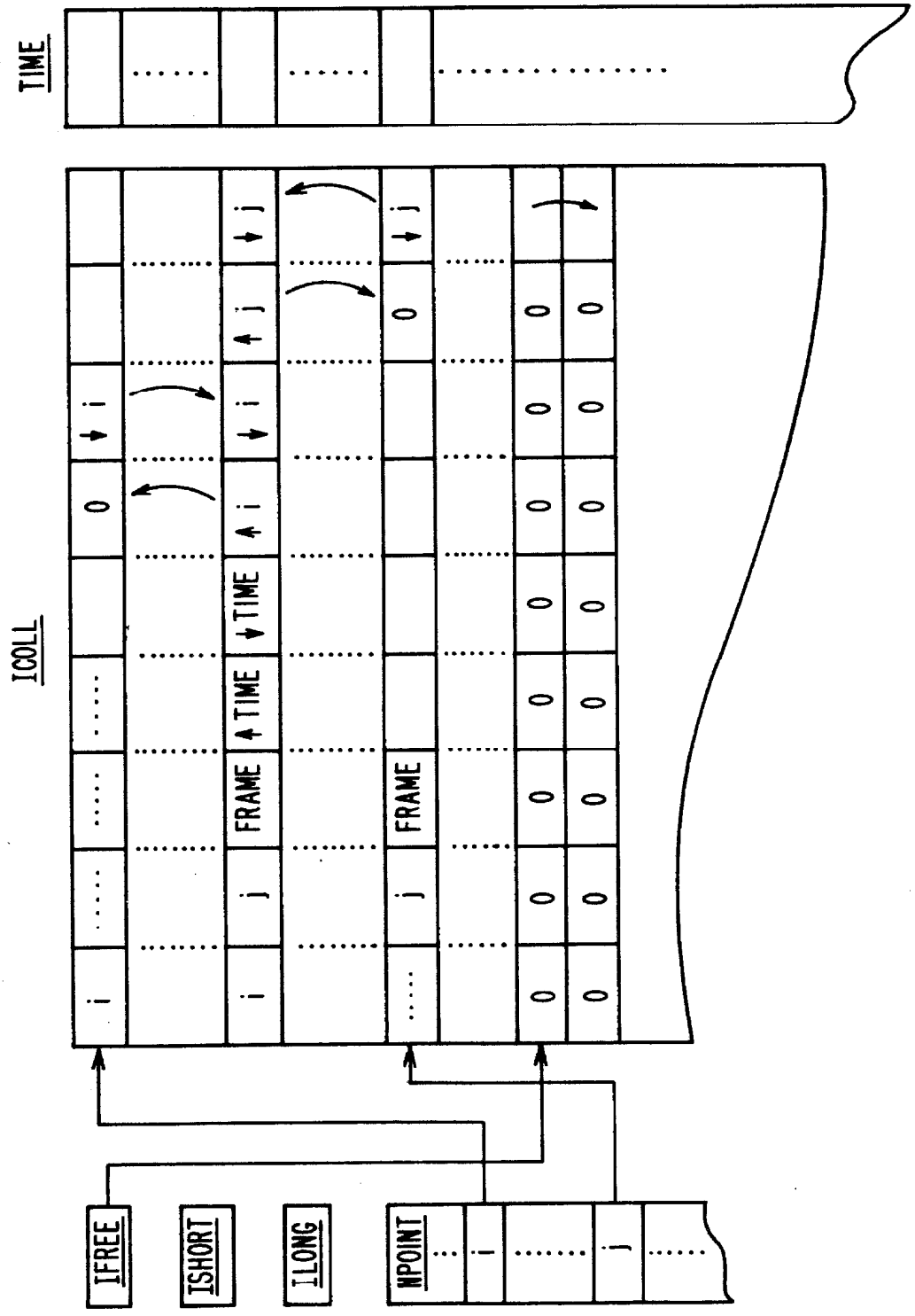

Figure 2.8 Structure of the collision list. ↑ backward pointer, ↓ forward pointer.

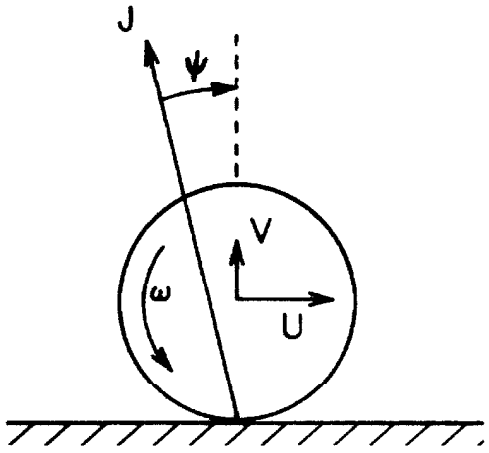

(a)

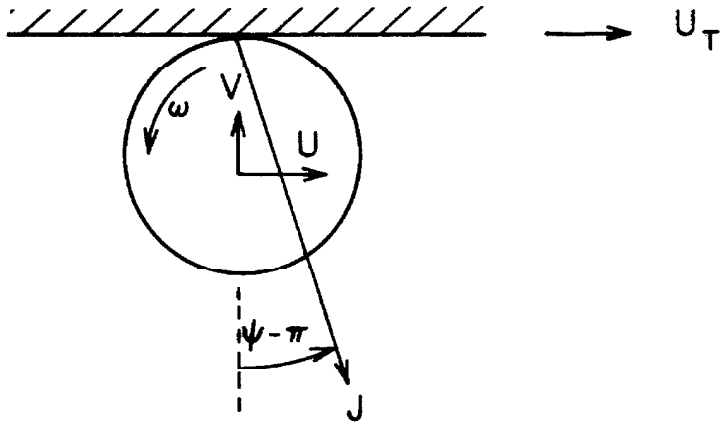

(b)

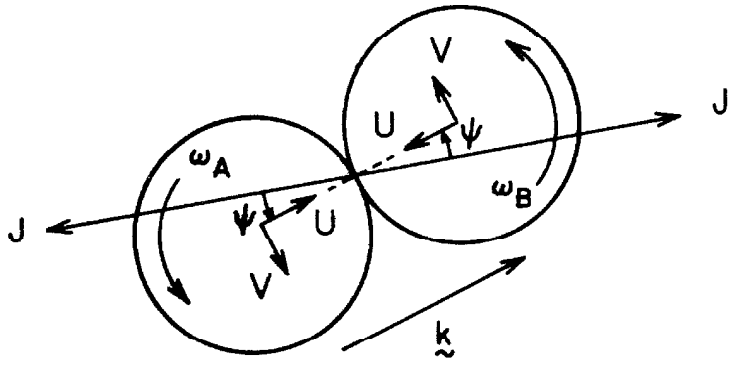

(c)

Figure 2.9 Collision diagrams.
(a) Stationary lower boundary collision. (b) Moving upper boundary collision, (c) Particle-particle collision.

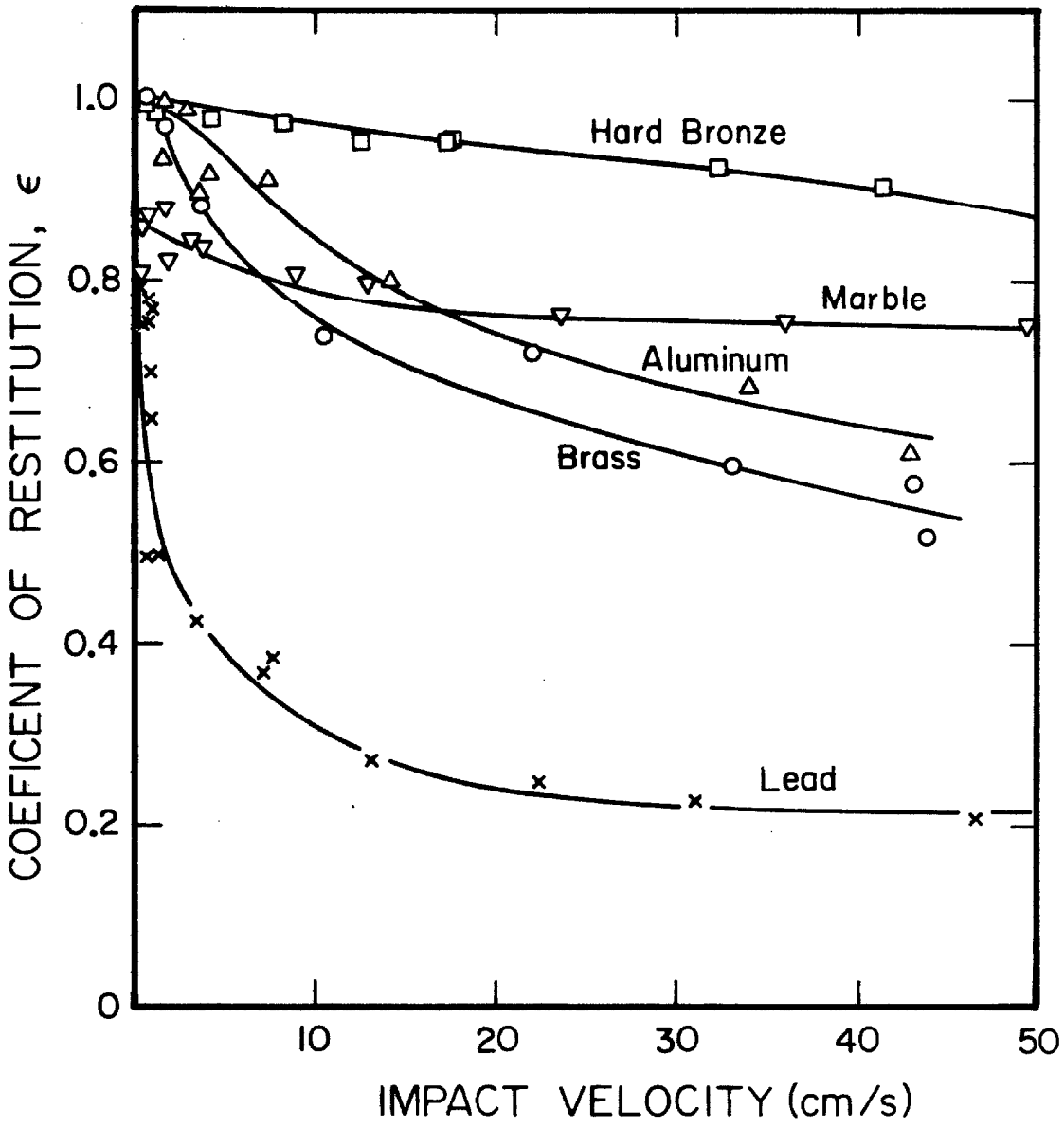

Figure 2.10 Variation of the coefficient of restitution with impact velocity for collisions between spheres of various materials. These data were taken from Rahman [57], and Goldsmith [23].

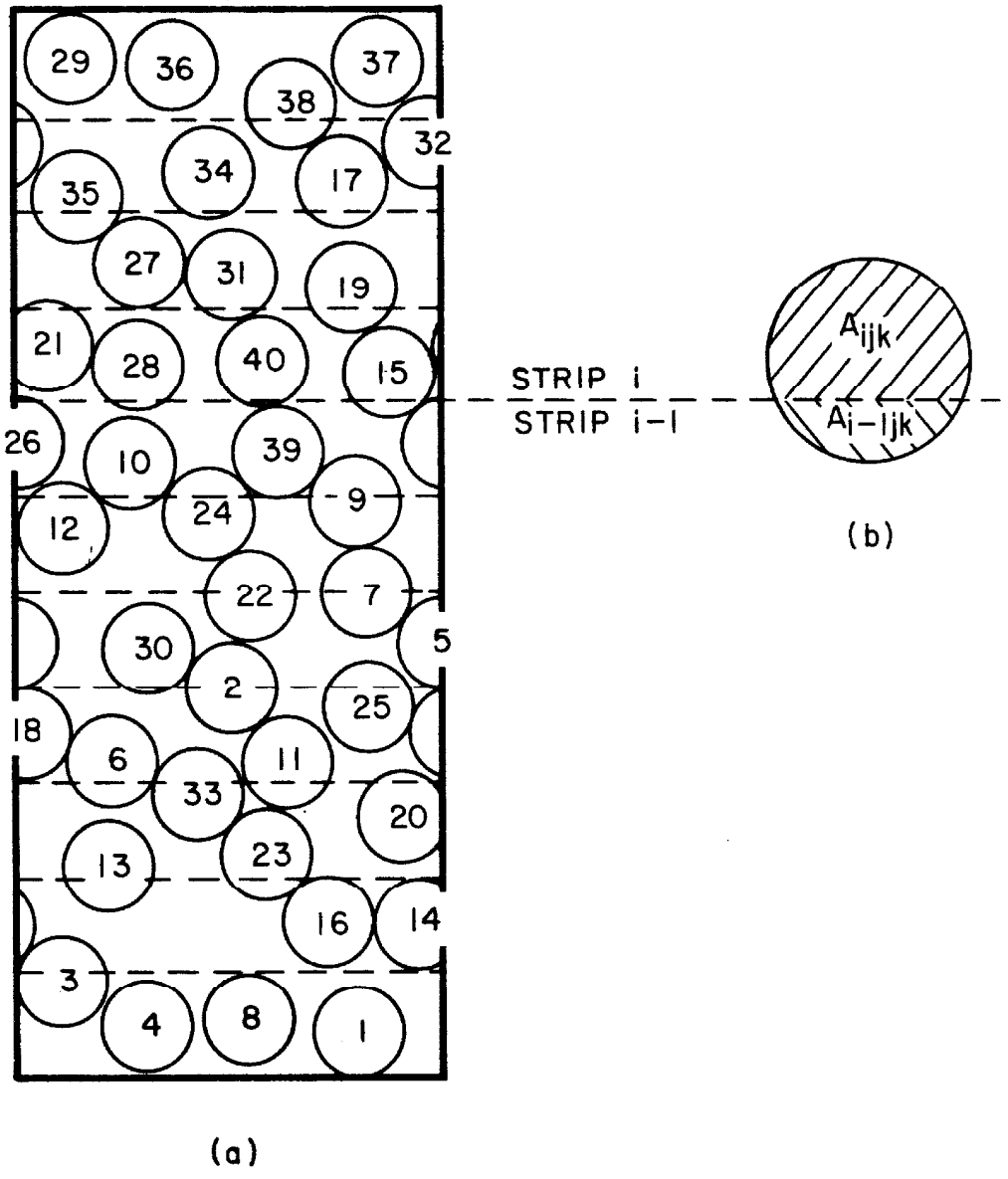

Figure 2.11 (a) Division of the control volume into strips for averaging. (b) Division of a particle between adjacent strips.

Chapter 3

SIMULATION RESULTS

3.1 Chute Velocity and Density Profiles

In Figure 3.1 is a typical velocity profile, taken from the chute flow program. It is the converged state of 40 particles (originally configured in a 10 x 4 square lattice) for a channel inclination of 30°.

In this plot the velocities have been scaled by dividing by the maximum velocity. The vertical coordinate has been scaled by dividing by H, an approximation to the flow depth. When examined on the scale of a particle diameter, the flow will have no distinct free surface. H is chosen to be twice the mass mean height, or twice the most probable vertical position of a particle. It can be seen in Figure 3.1 that the density has fallen to a low value at Y/H = 1. Hence H is a reasonable measure of the flow's depth.

From Figure 3.2 it can be seen that the main features of normalized velocity profiles are similar for the three inclinations, 20°, 30°, and 40°. In all cases there is slip at the wall with a magnitude of about 40% of the maximum velocity. The flow shears through most of its depth, but the shear rate is greatest next to the wall wall.

These velocity profiles agree qualitatively with those of Augenstein and Hogg [1], and contradict those measured by Savage [68]. Comparing the results must be done with considerable care. Not only is there the problem of comparing two-dimensional calculation with the

real three-dimensional problem, but appropriate coefficients of restitution and the proper interaction with the wall is unknown.

Augenstein and Hogg's [1] measurements were made on thin ($\simeq 10$ particle diameters thick) flows of sand on chutes with three different surface properties. In addition to measuring the velocity profile on a smooth stainless steel surface, they also investigated the flow on walls roughened by gluing on particles of either the same sand used for the test material, or a sand with a smaller size than the test material. A profile for each surface condition is reproduced in Figure 3.3 along with one of the computer results that has a similar maximum velocity and height. The flow of sand on the smooth wall chute appears to be almost a plug flow, with only about a 20% velocity variation over its depth. On the other hand, if the chute is roughened with the same material used in the test, the velocity approaches zero at the chute wall, simulating a no-slip condition. In this case the gaps between the particles glued to the surface will be of roughly the same size as the flowing particles, forcing the flowing particles next to the wall to become temporarily trapped. However, if the wall is roughened with smaller particles, the gaps will be smaller and the particles will be less likely to become trapped, allowing slip at the wall. Presumably, as the roughening particles become smaller, the profile will more closely approximate that on a smooth surface.

It appears that the velocity profile in a chute depends, to a large degree, on the surface characteristics of the chute bottom. The wall condition used in the program seems to provide somewhat more drag

on the flowing particles than a smooth wall, and somewhat less drag than the wall roughened with small particles. In the simulation it is assumed that the surface of the particle and the surface of the chute are "fully rough" in the sense that there will be no relative tangential velocity between the two surfaces immediately following a collision. (The coefficient of restitution, which affects only the motion of the particle perpendicular to the wall, will only affect the drag imposed on the flow indirectly by the way it affects the motion of particles in the neighborhood of the wall.) The particle then transforms its initial relative tangential motion into rotational motion and will tend to roll down the wall and not halt its forward motion. It is not clear how this would relate to sand particles which have an irregular surface and are incapable of rolling, but it appears to be one of many reasonable boundary conditions.

Except for the finite slip at the wall, these velocity profiles are similar to those one would measure in a shallow water channel. On the other hand, the density profile shown in Figure 3.1 is quite surprising.

In the bulk, a granular material is compressible even if its constituent particles are not. The bulk density is varied by changing the number of particles per unit volume; thus it is convenient to express the density dimensionlessly as the solid fraction ν.

The two-dimensional ν, measured by the simulation is a ratio of the area covered by a particle to the total area. In three dimensions

ν_{3-D} is the ratio of the volume occupied by a particle to the total volume. The numerical values of ν and ν_{3-D} are quite different. However, for comparison purposes, corresponding two and three-dimensional values of the solid fraction may be derived from the characteristic particle spacing, C, associated with each.

$$C_{2-D} = \left(\frac{\pi}{\nu_{2-D}}\right)^{1/2} R$$

$$C_{3-D} = \left(\frac{4/3\ \pi}{\nu_{3-D}}\right)^{1/3} R$$

Equating C_{2-D} and C_{3-D}, we get the correspondence:

$$\nu_{3-D} = \frac{4}{3\pi^{1/2}}\ \nu^{3/2}$$

This relation may be used to obtain an approximate value of ν for comparison with experimental results. In general, it will probably predict values of ν_{3-D} that are too small, because the 3-D flow has greater freedom in packing configurations.

For purposes of discussion, the flow of granular materials may be compared to that of other compressible fluids. The density of an isothermal atmosphere, in a gravitational field, would be highest on the planet's surface, and decrease to zero infinitely far away. But the density profile in Figure 3.1 exhibits the highest density in the center of the flow and a low density zone right next to the chute wall, as well as the expected reduction on the free surface. This is the same phenomenon observed experimentally by Ridgway and Rupp [60]

and by Savage [69]. It is the opposite behavior to that predicted by Nunziato et al. [48] based on the theory of Goodman and Cowin [25]. (The author has been informed, however, that an error existed in Nunziato's calculations [49].)

Note that the low density region near the wall in Figure 3.1 corresponds closely with the high shear zone in the velocity profile. This is the first step in understanding this phenomenon. The connection will be examined closely in the next section.

3.1.1 The Concept of Granular Temperature and the Equation of State

A flowing granular material has properties similar to a turbulent fluid in the sense that it is unlikely that any particle will ever be moving with exactly the time averaged mean velocity. A particle's velocity may, in general, be decomposed into the sum of the local time averaged mean velocity $\langle \underset{\sim}{u} \rangle$ and the unsteady instantaneous perturbation $\underset{\sim}{u}'$: $\underset{\sim}{u} = \langle \underset{\sim}{u} \rangle + \underset{\sim}{u}'$. By definition, $\underset{\sim}{u}'$ will have zero time average. The unsteady velocities are a byproduct of every collision. Consider, for example, the collision (shown in Figure 3.4) between two particles whose initial velocities were both in the same direction. The perturbations to the initial velocities, Δu, Δv, produced by the collision will have a total magnitude $((\Delta u)^2 + (\Delta v)^2)^{1/2}$ and a relative magnitude $|\Delta u/\Delta v|$ that depend only on the initial relative velocity dU and on the collision angle θ. One would expect that the largest magnitudes of the perturbed velocities would occur in regions with the largest velocity gradients in which the relative velocity at collision is augmented by the differences in mean velocity within the flow field.

This is clearly shown in the temperature plot in Figure 3.1.

The perturbation velocities must, by definition, have a zero time average, but their rms magnitude may be easily determined from the simulation in much the same way as one determines the magnitude of turbulent fluctuating velocities. Taking the time average of the unsteady velocities, one finds:

$$\langle \underset{\sim}{u}'^2 \rangle = \langle \underset{\sim}{u}^2 \rangle - \langle \underset{\sim}{u} \rangle^2$$

$\langle \underset{\sim}{u}'^2 \rangle$ is the mean square magnitude of the unsteady velocities. From a kinetic theory point of view, the perturbation velocities would have as their analog the random motions of the molecules that are governed by the temperature of the gas. In both molecular gas dynamics and granular material flows, pressure and other macroscopic forces are the result of the impulses exerted by the impact of particles, which are proportional to the magnitude of the random velocities.

From here on, the term "temperature" will be used to reflect the total energy contained in the random motion of a granular material: $(\frac{1}{2}m\,(\langle u'^2 \rangle + \langle v'^2 \rangle + \beta\langle \omega'^2 \rangle)$ and the term "translational temperature" to refer to that contained in the unsteady linear velocities: $(\frac{1}{2}m\,(\langle u'^2 \rangle + \langle v'^2 \rangle)$. In this sense flowing granular materials may be likened to self-excited gases. The "temperature" in a granular material flow comes about as a result of the velocity profile. (The analogy between the random particle motions and the molecular temperature has been used previously by Ogawa[50,51] and Kahatani [35]). In the flows modeled, temperature is not added to the system from an external source. If there were no velocity

gradients, there would be no temperature. Intuitively the generation of granular temperature is similar to the generation of sensible temperature by viscous dissipation. It is the change of energy carried by the mean motion into energy contained in the random motion of particles or, alternatively, the change of kinetic energy into thermal energy. When $2R\nabla\underset{\sim}{u}$ is of the same order as $\sqrt{<\underset{\sim}{u}'^2>}$, then a significant part of the particle velocities at impact may be attributed to the differences in the mean velocities of the particles. There is a characteristic quantity $S = 2R(du/dy)/\sqrt{<\underset{\sim}{u}'^2>}$ which was originally defined by Savage and Jeffrey [71], and will generally be of order 1. S is a Mach number. Granular temperature is generated when S is significant. Similarly, viscous dissipation is important in gas dynamics only for significant Mach numbers.

Continuing with the ideal gas analogy, the density is low near the wall despite the large pressure because the temperature is high. (Note that the temperature profile in Figure 3.1c is almost a mirror image of the density profile. Where the density is highest, the temperature is lowest and vice versa.) The equation of state for an ideal gas is

$$p = \rho R_G T$$

Proceeding formally, the expected form of an equation of state for granular materials is:

$$p = \rho_p \chi(\nu)(<u'^2> + <v'^2>)$$

where $\chi(\nu)$ is some function of the density. The standard ideal gas

law ($\chi(\nu) \sim \nu$) applies only at low densities. $\chi(\nu)$ represents a correction term, similar to that which appears in the Van der Waals equation of state, and accounts for the reduction in the free volume due to the presence of other molecules. The Van der Waals equation of state has a singular behavior when the free volume goes to zero ($\nu \to 1$). For incompressible, two-dimensional discs, it is impossible to have a density greater than $\nu = .91$ and a singular behavior is expected there.

The pressure may be assumed to be isotropic so that the pressure at a point in steady state may be defined to be the weight of material above it. In Figure 3.5 is shown a plot of $\chi(\nu)$, calculated from values of p, γ, and $(\langle u'^2 \rangle + \langle v'^2 \rangle)$. It exhibits the expected behavior: $\chi \to 0$ as $\nu \to 0$ and the singular behavior at large ν. This gives strong support for a granular equation of state of the proposed form.

3.1.2 Comparison with Ridgway and Rupp

Ridgway and Rupp [60] present the only published density profiles of granular flow in chutes. Some doubt must be cast upon their data due to their assumption that the velocity was constant across the depth (even though Augenstein and Hogg's [1] velocity profiles show only a small variation for smooth channels).

Their raw data, the mass flow rate profiles, were reconstructed and compared with the simulation results. In nondimensionalizing their data, it is assumed that the specific gravity of the sand particles was about 2.65. This value was characteristic for the sands used by Pearce [55]. The density from the simulation was converted from 2-D to 3-D by the formula described in Section 3.1.1. The resulting

profiles, shown in Figure 3.6, show very good agreement. This demonstrates that density variations,such as those obtained in the computer simulation,do occur in practice.

3.1.3 Effect of Chute Angle

In Figure 3.4 are shown density distributions for three chute inclinations and the corresponding velocity profiles. All the profiles have the expected shape and exhibit the low density region near the wall, but the maximum density decreases with angle. This is due to large velocity gradients at higher angles, leading to correspondingly higher temperatures and lower densities through the depth.

3.1.4 Evolution of the Velocity and Density Profiles

Figures 3.7, 3.8, and 3.9 show the evolution of the velocity and density profiles towards steady state for α = 20°, 30°, and 40°, respectively. The initial state is the same for all three simulations. Each case will respond so as to equalize the dissipation rate to the work performed on the system by gravity.

Both the 20° and the 30° simulations immediately start to slow down from the initial state and settle into more density packed states. This indicates that the initial velocity was too great, and not that the flow in a real chute would be expected to decelerate. After having settled into what is presumably a more natural configuration, the 30° simulation begins to accelerate again until it reaches a final velocity that is close to the initial velocity. Note that the first velocity profiles shown for both those angles show a region with a constant plug flow velocity profile near the free surface. This

is left over from the initial state and indicates that knowledge of the chute bottom has not yet been conveyed to the free surface.

The 40° simulation has not converged by the final state shown, and gives no indication that it ever will. The system has accelerated continuously since its initial state. As it accelerates, the low density region near the chute bottom increases its thickness until there are only a few particles that ever touch the wall (see the snapshot in Figure 2.2c). In this region the "temperature" is so high that these few particles can support the mass of particles above them. The bulk glides along in a relatively undisturbed configuration. When the flow has evolved to the final state shown here, it accelerates with practically no resistance from the chute bottom. The low density region acts as a sort of lubricating layer. It has been suggested by Campbell [12] that such a mechanism may account for the small friction that is encountered in certain types of landslides.

The evolution of the 40° simulation is similar to that given by Ridgway and Rupp (also for 40°). Direct comparison is difficult once again. Not only are there the inherent problems in comparing 2-D flows with 3-D but a real chute flow must become shallower as it accelerates to satisfy the conservation of mass.

3.1.5 Effect of the Flow's Depth

Figure 3.10 shows the velocity and density distributions for three depths of flow at a chute inclination of 30°. Flows of different

depths were obtained by varying the number of particles in the control volume. Initial configurations of 5, 10, and 13 rows of 4 particles were examined. (They will be designated as 5 x 4, 10 x 4, and 13 x 4, respectively.)

As the flow becomes deeper, the maximum density approaches a limiting value which is first attained here in the 10 x 4 configuration. The 13 x 4 simulation does not reach any significantly greater density but instead the region of maximum density becomes thicker.

Exactly the same phenomenon was experimentally observed by Ridgway and Rupp for a chute angle of 40°, although their flow is somewhat shallower than ours. It is also interesting to note that the maximum density they obtain corresponds in two dimensions to $\nu \simeq .62$, which is close to the maximum value obtained by the simulation.

The thickness of the low density zone near the wall is greater for the 10 x 4 simulation, where the limiting packing is first attained, than for the 5 x 4 case. But as the depth is further increased to the 13 x 4 case, the zone becomes thinner, compressed by the material above it. Note also that the velocity profile in the 13x4 case appears to be almost linear and does not show the characteristic high shear zone next to the chute bottom.

While the low density zone next to the chute bottom is clearly of greater interest, it is useful here to examine the low density region near the free surface. Almost all researchers who have examined the flow of granular materials in chutes, including the author, have noted the existence of a thin haze of "saltated" particles above the

free surface of the flow at large inclination angles. This makes the exact determination of the flow depth difficult. Saltation is probably affected by aerodynamic forces on the particles which are absent from our simulation. Note, however, that it would be extremely difficult to pinpoint the free surface of the 5 x 4 flow, as it takes about half its depth (12R) for the density to decay from its maximum value to zero. By comparison, the 10 x 4 simulation requires 6R, and the 13 x 4 simulation requires 2R. The saltated nature of the 5 x 4 simulation is probably due to a high granular temperature near the free surface which is dissipated within the mass of the deeper flows. It is possible that this is a granular contribution to saltation.

It turned out to be very difficult to attain convergence in flows of various depths. Originally, when the program was run with constant coefficients of restitution, the 5 x 4 simulation would continually accelerate and showed no sign of converging. Due to the lower density that resulted from the small number of particles, collisions would occur too infrequently to allow the coefficients of restitution to dissipate the energy added to the system by gravity. Attaining a steady state thus appears to be a function of the flow depth, as well as the coefficient of restitution and the inclination angle. To aid convergence, an exponentially decaying coefficient of restitution $\varepsilon_p = \varepsilon_w = \exp(-3\delta v/\sqrt{gR})$ was introduced where $\delta v/\sqrt{gR}$ was the impact velocity. This resulted in a value of about 0.6 for the average impact velocity of the 10 x 4 chute flow simulation for $\varepsilon_w = 0.8$, $\varepsilon_p = 0.6$. So if the velocity of the simulated flow increased, increasing the violence of the particle collisions, the

dissipation rate would increase, slowing the flow. Similarly, if the flow slowed, the dissipation rate would decrease, speeding the flow. In this way convergence was reached for all three flows.

3.1.6 Effect of Coefficients of Restitution

In Figures 3.11 and 3.12 are shown the velocity and density profiles for various values of ε_p and ε_w.

Varying the particle coefficient of restitution has very little effect on the shape of the velocity profiles shown in Figure 3.11. (The data for $\varepsilon_p = 0.8$ are of questionable validity, since the simulation never properly converged.)

Much more interesting are the corresponding density profiles in Figure 3.11. As the coefficient of restitution is changed, the flow becomes more tightly or loosely packed depending on the dissipation rate of granular temperature. Thus, for $\varepsilon_p = 0.1$, the flow is very tightly packed flow, while for $\varepsilon_p = 0.8$ the flow is very loose.

Varying the wall coefficient of restitution as shown in Figure 3.12 seems to have very little effect on the flow. The velocity is slightly greater for the larger ε_w, but this is probably due to the lower density in the vicinity of the wall. ε_w will only affect the local dissipation rate of granular temperature. Reducing ε_w will thus bring about slightly larger densities near the wall, but seems to have only a small effect on the rest of the flow.

3.1.7 Plug Flows

Unlike the normal notion of a continuum, the local density of a granular material will impose limitations on the velocity field. For

incompressible discs, the largest attainable packing corresponds to $\nu_m = \frac{\pi}{2\sqrt{3}} = .91$. This will occur only when the particles are arranged so that the local space is filled by equilateral triangles connecting the particle centers, as shown in Figure 3.13a. Such a configuration however, may not be deformed without decreasing its density. This makes it impossible for the material to assume such a density and maintain a local velocity gradient. Any region that attains this density must necessarily move as a solid plug.

The largest locally constant density which allows a shearing motion would be $\nu_s = \frac{\pi}{4} \simeq .78$, and this corresponds to the particle centers arranged in a square (or a parallelogram) packing as shown in Figure 3.13c. This allows particle layers to move freely over one another.

It is possible to set up a shearing motion in the particles at even higher density. The flow would look something like that in Figure 3.13b. Here the particles' paths exactly follow the contour of the particles in the layer below. The local packing is constantly varying between the square and triangular configurations. The time average of the density would be about $\nu_m = \pi/(\sqrt{3} + 2\pi/3) \simeq .822$. This could only occur if the shear rate were very small, since only particles with zero inertia (zero mass or zero velocity) could respond instantly to follow the particle contours.

These limits place an upper bound on the density at which a bulk of two-dimensional incompressible particles may be sheared. (Note that the limits will be different for 3-dimensional particles.) One may wish to think of this transition as the condensation of the

granular material from a "liquid" (which may be sheared) to a "solid."

In any case, these should be considered as very idealized limits because it is possible for the material to pack itself into unshearable configurations that correspond to smaller values of ν than these. (An example of an unshearable configuration with a lower ν is the square packing shown in Figure 3.13c rotated through 45°.)

This may be clearly seen in the converged state of our 20° simulation, where the density does exceed this limit for a region in the center of the flow (see Figure 3.14). The velocity gradient drops to zero in this region, and in fact is zero for all densities greater than $\nu = \pi/4$. This region moves like a plug. In the snapshot, taken from this flow in Figure 2.2a, one will see instances where the local packing has assumed the high density triangular structures.

It was argued earlier that granular temperature resulted from a velocity gradient. Note that the temperature is nonzero in the region where the velocity gradient vanishes. Note also that there is a noticeable gradient of temperature into this region. This suggests that temperature is not simply a product of the local velocity field but may also be conducted. From the equation of state shown in Figure 3.5, it can be seen that if the temperature becomes high enough, it would reduce the density to the point where this zone may be sheared.

It is possible that exploring concepts like these may lead to an understanding of the formation of the stagnant zones that characterize funnel flows in hoppers, and occasionally form on chute bottoms.

3.2 Couette Flow Velocity and Density Profiles

The Couette flow profiles in general are much less interesting than those from the chute flow simulations. Simulations were run with two wall boundary conditions. The first was the same as that used in the chute flow program, which assumes that there would be zero relative tangential slip between the particle surface and wall upon departure. The second assumed that the particle's center would adopt the velocity of the wall after collision, modeling a "no-slip" condition. The latter case was studied for comparison to Savage and Sayed's [68,70, 72] studies of the rheological properties of a granular material sheared in a Couette flow device with roughened walls.

Velocity and density profiles for the first or standard wall conditions and for three different normal forces are shown in Figure 3.15. (The normal force is the quantity against which the total normal force applied to the walls is periodically compared. The movement of the walls is based on the result of this comparison.) In all cases the wall velocity is the same and the spacing between the plates is varied. For all profiles there is slip at either wall amounting to about 20% of the upper wall's velocity. Thus the shear rate across the particle bed is at most 60% of the ratio of wall velocity to wall spacing. At the lower densities (lower normal forces) most of the shearing occurs in a small region next to each wall. In these cases the bulk of the material moves down the center as a plug. It is not quite clear why these high shear zones come about (especially in the light of the simulation with a "no-slip" wall condition), but it is probably peculiar to this wall condition. The

moving wall has only a tangential component of velocity relative to the particle at all times. A large component of the energy added to the particle in a collision with the wall is added as rotational energy.

In Figure 3.16 are shown profiles for the second or "no-slip" boundary condition at three different normal forces. In all cases, the wall spacing is changed to keep the shear rate a constant. The velocity profiles all vary linearly from zero at the bottom wall to the upper wall's velocity. Furthermore, the density is practically uniform across the flow.

In the absence of a gravitational field, the pressure will be constant across the depth of a Couette flow. From the equation of state proposed in Section 3.1.1, a uniform density and pressure indicates that the temperature should also be uniform. As expected, the variation of temperature shown in Figure 3.16 is small across the depth, compared to the chute flow profile shown in Figure 3.1.

The absolute magnitude of the temperature in Figure 3.16 decreases with density. It may be speculated that the large collision rate at high densities results in a greater dissipation of the energy contained in the random motions.

Figure 3.17 illustrates the effect of shear rate (represented dimensionlessly in the simulation's scaling by R/H) on the flow properties. It was argued in section 2.6 that the natural time scaling of a Couette flow was the inverse shear rate, H/U_T. To test this hypothesis the applied normal stress was varied accordingly as $\sigma_n = (0.567)(R/H)^2$. It can be seen in Figure 3.17 that under these conditions the density and scaled temperature are independent of the

shear rate, indicating that the proposed scaling is correct.

Figure 3.17 indicates that the temperature is directly proportional to the square of the velocity gradient. The proportionality may not be valid for flows that do not have uniform temperature fields that may experience the effects of conduction. Such an occurrence has already been noted for the 20° chute simulation in Section 3.1.7.

Figures 3.18 and 3.19 illustrate the partition of the total temperature into its three components for four densities.

At low densities the energy contained in the fluctuating velocity component in the direction of flow $(\frac{<u'^2>}{U_T^2})$, is a few times greater than that contained in the normal component $(\frac{<v'^2>}{U_T^2})$ or in the rotational component $\beta<\omega'^2>/ U_T^2$. The latter two components are of roughly the same order of magnitude. As the density is increased, the three components become roughly equal, until at the highest density the rotational component has a large magnitude relative to the linear component, even though the absolute magnitude is smaller here than in the lower density plots. (Each plot has a different temperature scale.)

There is no clear explanation for the non-equipartition of energy in the fluctuating velocities.

The large relative magnitude of the $<u'^2>/U_T^2$ component at low may be due to convection of the mean velocity within the velocity gradient. At low densities, a particle will travel a relatively long distance between collisions, and carry with it the mean velocity corresponding to its former position. In a time average, this mean velocity difference will appear as a fluctuating velocity. At high densities,

this mechanism would be nullified as the particles can move only slightly between collisions. This would explain why the two linear fluctuating velocity components are of the same order of magnitude in Figure 3.19b.

The linear fluctuating components will be dissipated by both the coefficient of restitution and the interaction between the rough particle surfaces. The rotational component will only be dissipated by the latter. The large relative magnitude of the rotational components at high densities (high collision rates) may be accounted for by this less efficient dissipation mechanism.

3.3 The Bagnold/Savage Constitutive Law

It was mentioned in the introduction that Bagnold [3] presented the first constitutive law for a granular material that took into account its particulate nature. Translated from Bagnold's notation into the notation used in this paper, the proposed constitutive law would have the form (for simple shearing flows)

$$\tau_{ij} = \rho_p \, f_{ij}(\nu) \, R^2 \, \left(\frac{du}{dy}\right)^2$$

where $f_{ij}(\nu)$ is some unspecified dimensionless tensor valued function of the density, and du/dy is the local velocity gradient.

Clearly there are limits on the situations to which this law is applicable. For example, it can give no insight into the stresses inside a region of plug flow where $du/dy \equiv 0$. A case where that occurred and yet the stress was nonzero, was found in the 20° simulation discussed earlier in Section 3.1.7. This suggests that the

Bagnold/Savage law is applicable only to situations with moderate or high shear rates.

The physical reasoning that Bagnold used to support this constitutive law was as follows: Consider the collisions between two planes of particles moving in a velocity gradient as shown in Figure 3.20. Ignore for now any perturbations to the structure or velocities. Let the spacing between the layers be s_1 and the spacing between particles in each layer be s_2. Then the momentum transferred in each collision in the normal direction is proportional to $m\delta u$, where m is the particle mass and δu the velocity at collision.

$$\tau_{ij} \sim m\delta u = m\left(\frac{du}{dy}\right) s_1$$

The frequency of collision is proportional to the velocity difference divided by the particle spacing, $\delta u/s_2$ and further multiplied by the square of the number of particles per unit area of each plane $(1/s_2)^2$. Hence the frequency of collision is proportional to

$$\frac{\delta u}{s_2^3} = \left(\frac{du}{dy}\right) \frac{s_1}{s_2^3}$$

Hence the stress tensor may be written as

$$\tau_{ij} \sim m \frac{s_1^2}{s_2^3} \left(\frac{du}{dy}\right)^2$$

Now s_1/R and s_2/R may be assumed to be functions of the density. Expressing the particle mass as $m = \rho_p \frac{4}{3}\pi R^3$ and absorbing all constants into f, this may be written as

$$\tau_{ij} = \rho_p f_{ij}(\nu) R^2 (\frac{du}{dy})^2$$

Some insight may be derived by comparing this derivation to that for the viscosity of a gas as derived from simple kinetic theory arguments. It is generally assumed that the random velocities due to the gas temperature will be of much greater magnitude than the mean velocity differences over a mean free path. Thus, the rate of momentum transport is governed by the magnitude of the random velocity which is proportional to the square root of temperature. In Bagnold's model of granular material the rate of momentum transport is determined by the collision rate, which in turn is proportional to the velocity gradient. Hence the second factor of du/dy, which introduces the nonlinearity into this constitutive law, essentially replaces the $\sqrt{T}$ found in the viscosity coefficient of a Newtonian fluid. This reasoning is supported by Figure 3.17 which shows that the granular temperature is proportional to the square of the velocity gradient. (In this case the temperature is constant everywhere in the velocity field, eliminating conduction effects.) One may view a granular material as a self-excited Newtonian fluid, where the transport rate is determined by the velocity profile and not by the externally imposed temperature.

3.3.1 The Function $f(\nu)$

The functional dependence on density, $f(\nu)$, in the Bagnold/Savage constitutive relation is unknown. One might guess, especially from the above remarks, that it may be related to the radial distribution function that fills a similar role in the statistical mechanics

of dense gases and liquids. This analogy was used by Savage and Jeffrey [71].

Asymptotic limits for f may be estimated.

For small ν, collisions would be rare. Thus the stresses will be zero no matter what the velocity field. Hence as $\nu \to 0$, $f(\nu) \to 0$.

It has been noted previously that the maximum density that can allow a velocity gradient in a granular material composed of incompressible particles is: $\nu = \pi/(\sqrt{3} + 2\pi/3)$. For any greater density it would require an infinite stress to impose a velocity gradient. Thus one can assume that $f(\nu) \to \infty$ as $\nu \to \pi / (\sqrt{3} + 2\pi/3)$.

To determine $f(\nu)$ from the computer simulation, the stresses must first be determined. Using the basic form of the momentum equation,

$$\rho u_{,t} + \nabla \cdot \underset{\sim}{\tau} = \rho \underset{\sim}{g}$$

where $\underset{\sim}{\tau}$ is the stress tensor and $\underset{\sim}{g}$ is the gravity vector. The only nonzero components of $\nabla \cdot \underset{\sim}{\tau}$ will be $\frac{\partial}{\partial y} \tau_{xy}$ and $\frac{\partial}{\partial y} \tau_{yy}$ as the periodic boundary condition assures that $\frac{\partial}{\partial x} \equiv 0$.

The density dependence for the shear and normal components of stress will be examined. The functions will be denoted $f_s(\nu)$ and $f_N(\nu)$, respectively. The stresses are defined by

$$\tau_s = \tau_{xy} = \rho_p \nu \int_y^H (g \sin \theta - \rho u_{,t}) \, dy + \tau_s(H)$$

and

$$\tau_N = \tau_{yy} = \rho_p \nu \int_y^H (g \cos 0 - v_{,t}) \, dy + \tau_N(H)$$

where $u_{,t}$ and $v_{,t}$ are determined by measuring the difference in total

momentum in a strip at the beginning and end of the averaging period. (This is generally only a small correction.) The integration is performed numerically between the strips using the trapezoidal rule. Velocity gradients were taken to be the derivatives of cubic spline fits to the velocity profile.

Plots of $f(\nu)$ versus ν are given in Figures 3.21 and 3.22. The points were obtained from the chute flow simulations at three different inclination angles and from several Couette flow simulations. There is a lot of scatter in the data, but it is clear that the functions agree with the asymptotic limits proposed above.

In Figures 3.22 and 3.23 is shown the comparison of our data with the Couette flow experiments of Bagnold [3] and Savage and Sayed [70]. (The data for both cases were taken from Savage and Jeffrey [71].) Here again, the densities from the simulation have been converted to their three-dimensional equivalents (as proposed in Section 3.1).

The agreement between the data is fair. The simulation generally predicts values of $f(\nu)$ larger than those measured experimentally.

The main value of this comparison is to show that the predicted values of the proper magnitude. There are just too many apparent difficulties involved in making a direct comparison. First, as noted previously in Section 3.1, the conversion from ν to $\nu_{3\text{-}D}$ predicts values that are probably too small. Proper coefficients of restitution for Savage and Bagnold's particles are unknown. Bagnold's material was suspended in a fluid carrier which will exert an

indeterminate influence on the particle interactions. However, Savage and Bagnold could not have known whether (1) there was slip at the walls of their devices, or (2) their material was shearing completely. This latter objection was raised by Savage and Jeffrey [71] with regard to Bagnold's data. Indeed it is unlikely that Bagnold could get material to shear at a density greater than $\nu_{3-D} = \pi/6 \simeq .52$, which corresponds to the maximum cubical packing. Instead, the material either slipped at the walls or sheared over only a small portion of its depth. In either case the measured values of $f(\nu)$ would appear to be smaller than the actual values.

The Bagnold/Savage constitutive law seems to be on a firm footing. Although there is a great deal of scatter in our data, it seems to behave in a consistent and coherent manner that is in accord with the expected behavior. But this is the extent to which it can be evaluated by the simulation.

The Bagnold/Savage constitutive law for normal stress

$$\tau_N = \rho_p \, f_N(\nu) \, R^2 (\frac{du}{dy})^2$$

may be considered as an alternative form of the equation of state

$$p = \rho_p \, \chi(\nu)(\langle u'^2 \rangle + \langle v'^2 \rangle)$$

that was proposed in Section 3.1.1. They are analogous as long as $p \simeq \tau_N$. The comparison is especially appealing because the temperature is in some way a product of the velocity gradient and in the absence of conduction it has been shown (see Section 3.2) that

$(\langle u'^2 \rangle + \langle v' \rangle^2) \sim (\frac{du}{dy})^2$. However, there is a great deal more scatter in the data for $f_N(\nu)$ than for $\chi(\nu)$. This indicates that the $(du/dy)^2$ in the Bagnold/Savage law appears as a surrogate for the temperature. Their model may only be applicable to flows such as the Couette flow upon which their experiments were performed, that are free from the effects of conduction.

A model based on temperature has the added appeal that it is applicable to densities beyond which shearing is possible. It is likely that such a model could have universal validity.

3.4 Statistical Properties of Granular Material Flows

The results presented so far indicate that flowing granular materials possess many of the same features as the molecular models of matter. A great body of work has been developed describing transport phenomena on a molecular level from which macroscopic conservation laws such as the Navier-Stokes equations have been derived (see [14,21]). Great progress would be made if this body of work could be adapted to granular materials.

The fundamental assumption in molecular transport phenomena is that the molecules are statistically distributed independently. Procedures have been established to derive the macroscopic conservation laws, once these probability distributions are known. The determination of these distributions is easily done by simulation, and may not be accomplished by other means.

Savage and Jeffrey [71] were the first to try and adapt the molecular theory of transport phenomena to the flow of granular

materials. As a basic statistical theory of granular flows has not been developed, they were forced to assume that a granular material possessed many of the properties of gases. They assumed that the particles followed a Maxwell-Boltzmann velocity distribution, and used the radial distribution function of Carnahan and Starling [13] to describe the relative positions of particles.

While it is intuitively appealing to equate granular materials considered on particle scales with fluids considered on molecular scales, there are still many seemingly irreconcilable differences between them. Generally the statistical analyses of gases occur at or near equilibrium conditions, or conditions where the energy of the system is locally constant. This requires that the velocity gradient be small, so that no energy is added to the system by viscous dissipation, and that the particle interactions be elastic so that no energy is lost in the collisions. Granular materials are quite the opposite. The collisions are inelastic so that there must be a large velocity gradient to supply the energy lost in the collisions.

If there is to be equilibrium in a granular material flow, then there must be a constant influx of energy in through the velocity gradient and out into thermal energy, via the inelastic collisions. The Couette flow simulation with the no-slip wall condition comes very close to an equilibrium state, and will be used as a sample from which most of the statistical information about granular flows is obtained.

3.4.1 Distribution of Particle Velocities

The velocities of molecules in a gas at equilibrium will be arranged in a Maxwellian probability distribution, i.e., the probability

that a given molecule will have a velocity in the range $d\underset{\sim}{u}$ about $\underset{\sim}{u}$ is:

$$\|d\underset{\sim}{u}\| \; \frac{4(\underset{\sim}{u}-\langle\underset{\sim}{u}\rangle)^2}{\sqrt{\pi}(\frac{2}{3}\langle u'^2\rangle)^{3/2}} \; \exp[-(\underset{\sim}{u}-\langle\underset{\sim}{u}\rangle)^2 / \tfrac{2}{3}\langle u'^2\rangle]$$

where $\langle\underset{\sim}{u}\rangle$ is the average velocity and $\langle u'^2\rangle$ is the rms value of the fluctuating velocity $u' = |\underset{\sim}{u}-\langle\underset{\sim}{u}\rangle|$. This was the velocity distribution used by Savage and Jeffrey [71].

Because the computer model is based on the exact particle mechanics instead of on a Monte Carlo approach (in which one would have to make judgments based on probability distributions that were determined a priori), the simulation may be used to measure the distribution of particle velocities.

At each collision, during the averaging period, the state of the system is recorded on a magnetic tape. The tape is rewound after the average values of the velocities and fluctuating velocities have been determined. Then, the instantaneous state of the system is read from the tape at each collision and the quantity:

$$X = \frac{\underset{\sim}{c}_i - \langle\underset{\sim}{u}\rangle_j}{\langle\underset{\sim}{u}'^2\rangle_j}$$

is computed. Here $\underset{\sim}{c}_i$ is the instantaneous velocity of particle i, and $\langle\underset{\sim}{u}\rangle_j$ and $\langle\underset{\sim}{u}'^2\rangle_j$ are the average velocity and mean square fluctuating velocities, respectively, in the strip j in which particle i resides. The number of particles with values of X between 0.1(I-1) and 0.1I are counted in the I^{th} slot of a fifty-element array (covering a range of X between 0 and 5). The total in each slot is

normalized by dividing by the total number of particles counted. The number one would then find in the I^{th} slot is the probability that a particle will have a value of X between 0.1(I-1) and 0.1I. In terms of a probability distribution P(X) this quantity would correspond to P(X) dX for X = 0.1(I - 0.5) and dX = 0.1. Hence it is further necessary to divide the value in each slot by dX = 0.1 to obtain the probability distribution.

Distributions were measured for all three velocity components, u, v, and ω, as well as all the combinations of all components and the combination of just the linear components u,v. The source of most of the distributions will be the Couette flow program with the no-slip wall condition.

The five sampled variables for the individual velocity components are:

$$X_1 = \frac{|u - \langle u \rangle|}{\sqrt{\langle u'^2 \rangle}}$$

$$X_2 = \frac{|v - \langle v \rangle|}{\sqrt{\langle v'^2 \rangle}}$$

$$X_3 = \frac{|\omega - \langle \omega \rangle|}{\sqrt{\langle \omega'^2 \rangle}}$$

For the combinations of the linear velocity components:

$$X_4 = \left(\frac{(u - \langle u' \rangle)^2 + (v - \langle v \rangle)^2}{\langle u'^2 \rangle + \langle v'^2 \rangle} \right)^{1/2}$$

and for all the velocity components:

$$X_5 = \left(\frac{(u - \langle u \rangle)^2 + (v - \langle v \rangle)^2 + \beta(\omega - \langle \omega \rangle)^2}{\langle u'^2 \rangle + \langle v'^2 \rangle + \beta \langle \omega'^2 \rangle} \right)^{1/2}$$

The sampled variables each represent the ratio of the instantaneous energy contained in the fluctuating velocity, to its mean value. Thus, the rotational component must be scaled by β in X_5 to convert it into an equivalent kinetic energy.

The distributions are shown in Figures 3.25 through 3.29. Four distributions of each type are shown compared to a Maxwell-Boltzmann distribution.

All of the distributions have the basic shape of a Maxwellian. For a single velocity component a Maxwellian has the form:

$$P_i(X_i) = \sqrt{\frac{a_i}{\pi}} \; e^{-a_i X_i^2} \qquad i = 1,2,3$$

for two velocity components,

$$P_4(X_4) = 2a_4 X_4 \; e^{-a_4 X_4^2}$$

and for all three velocity components,

$$P_5(X_5) = 4\sqrt{\frac{a_5^3}{\pi}} \; X_5^2 \; e^{-a_5 X_5^2}$$

To be consistent, the average value of each square fluctuating velocity $\langle q'^2 \rangle$ should be the average value of $(q - \langle q \rangle)^2$. X has the form

$$X = \frac{|q - \langle q \rangle|}{\sqrt{\langle q'^2 \rangle}}$$

Therefore,

$$|q - \langle q \rangle| = \sqrt{\langle q'^2 \rangle}\, X$$

For consistency it is required that

$$\langle q'^2 \rangle = \langle q'^2 \rangle \int_0^\infty X^2\, P(X)\, dX$$

or

$$1 = \int_0^\infty X^2\, P(X)\, dX$$

This requires

$$a_1 = a_2 = a_3 = \frac{1}{2}$$

$$a_4 = 1$$

$$a_5 = \frac{3}{2}$$

These values would yield the standard Maxwellian velocity distributions. Most of the distributions shown require a somewhat different value of a_i. The distributions for the individual, total and combined components of linear velocity come very close to being Maxwellian, but the distribution of rotational velocities exhibits a strong deviation from Maxwellian.

The deviations can almost be accounted for by changing the value of a_i from the Maxwellian values a_{mi}, given above. Then the consistency conditions may no longer be satisfied. The corrected values for a_i could be determined by making curve fits to the measured distributions. It appears that the magnitude of the deviation, a_i/a_{mi}, depends strongly on the characteristic quantity S, introduced in Savage and Jeffrey [71]:

$$S = \frac{2R \frac{du}{dy}}{\sqrt{\langle \underset{\sim}{u}'^2 \rangle}}$$

and is more or less independent of the coefficients of restitution and all other flow properties. For small values of S the translational velocity distributions are essentially Maxwellian, but they deviate noticeably for larger values of S. Except for the rotational distributions, all the a_i's increase with S. (The sole exception to this rule is the u velocity distribution for $\nu = .75$, $S = 1.87$ which shows a large narrow peak just below $X_1 = 1$, but otherwise exhibits this generalized Maxwellian behavior).

S may be looked upon as a scale of the system's deviation from equilibrium. For small values of $S, \sqrt{\langle \underset{\sim}{u}'^2 \rangle} >> 2R \frac{du}{dx}$, and the material will behave like a gas. In particular, the magnitude of the impact velocity between particles will depend mostly on $\underset{\sim}{u}'$ and will not be enhanced by the gradient of mean velocities. For $S >> 1$ exactly the opposite is true. Hence S is indicative of the relative importance of the velocity gradient on the motion of particles at the microscale. To determine the exact nature of the dependence of a_i/a_{mi} on S would require extensive analysis which would probably involve deriving and solving an equation similar to the Boltzmann equation.

For less ideal circumstances than Couette flow with a no-slip wall condition, the distributions will not be as well behaved. For comparison, several velocity distributions generated by the chute flow simulation are shown in Figure 3.30. Chute flows exhibit large variations in S, density, and temperature within the control volume. Nevertheless, the velocity distributions could be represented by a generalized

Maxwellian form.

In summary, it appears that Savage and Jeffrey's [71] assumption of a Maxwellian velocity distribution is a reasonable approximation.

3.4.2 Distribution of Collision Angle

There is an angle θ that is characteristic of each collision between two particles. The angle θ shall be defined as shown in Figure 3.31a. The range of θ is then $0 \leq \theta \leq 180°$. The datum, $\theta = 0$, is arbitrary and for convenience is chosen to be in the direction of flow.

The angle θ will affect the angle of the impulse applied by the collision. These impulses, when averaged over a plane with time, will determine the continuum stress tensor. Thus one would expect that θ will affect the relative magnitude of the components of the stress tensor. In particular, θ will have some relationship to the friction angle. Bagnold [3], in the derivation of his constitutive law, assumed that all collisions would occur at the same angle, and found that that angle equalled the friction angle of his material. It is thus important to know whether there is anisotropy in the collision distribution which would result in preferred values for θ .

The distribution of collisions must be isotropic in a low density uniform gas. However, if there is a velocity gradient imposed on the gas, anisotropy will develop.

The collision angle distribution may be measured in much the same way as we determined the velocity distribution. The region $0 \leq \theta \leq 180°$ is divided into 50 regions. The number of collisions that occur in each region are counted and the result is stored in the

appropriate element of an array. The totals in each region are normalized by dividing by the total number of collisions and by the region width.

The collision distributions for various values of the density, with the shear rate held fixed, are shown in Figure 3.32. At low densities ($\nu = .35$) they form a smooth curve indicating a preference for values of θ in the range $90° \leq \theta \leq 180°$. With increasing density a peak develops about $\theta = 90°$. The peak grows until, at highest densities ($\nu \simeq .75$), the distribution becomes just two peaks, around $\theta = 90°$ and $\theta = 0°$ $(180°)$.

In Figure 3.33 is shown a typical collision distribution from the chute flow simulation. A great variation in density occurs in a chute flow and the distribution is a mix of the distributions for many densities.

Collisions occur when particle surfaces touch. This is only possible if there is a component of their relative velocity drawing the particles together. If there is a mean velocity gradient in the flow, the relative velocity of two particles will be augmented by the mean velocity differences due to the position of their centers in the velocity field. Consider a test particle at some position in the velocity field, as shown in Figure 3.31b. Locally, the mean relative velocity will create a preference for collisions in the second and fourth quadrants of the disc. This corresponds to the preferred values of the collision angle falling in the range $90° \leq \theta \leq 180°$.

The pair distribution function of Savage and Jeffrey [71] was based on this idea. They assumed that the particles obeyed a

Maxwellian distribution of velocity about the local value of mean velocity. Then, by integrating over all possible velocities, they found the probability distribution for a collision to occur at θ to be (after converting their result to two dimensions and renormalizing)

$$P(\theta) = \frac{1}{\pi} \operatorname{erfc}[2^{-1/2} S \cos\theta \sin\theta]$$

where

$$S = \frac{2R \frac{du}{dy}}{\langle v'^2 \rangle}$$

and erfc is the complementary error function:

$$\operatorname{erfc}(\eta) = \int_{\eta}^{\infty} e^{-\eta'^2} \, d\eta'$$

This should predict the collision distribution at low densities before the peak at $\theta = 90°$ develops. It is difficult to generate low density flows with different values of S. It was possible to obtain two, for $S \simeq .90$ and $S \simeq .45$, by changing the coefficient of restitution. These are shown in Figure 3.34.

Savage and Jeffrey predict the same form of the collision distribution, but the predicted magnitude of the deviation from isotropy is too low. The anisotropy is a function of the magnitude of S. The deviation of the velocity distribution from Maxwellian would partially, but not entirely, account for the discrepancy. By changing the length scale in S from R to C (where C is the mean particle spacing: $C = R(\pi/\nu)^{1/2}$), good agreement with the measured curves is obtained. This may be interpreted physically as indicating that a particle carries

its distribution with it from the point of its last collision. (The last collision for each particle would have occurred at a distance of about C. Thus the total separation of the particles at their last collisions would be about 2C.) A similar idea was suggested in Section 3.2 to explain the large relative magnitude of the fluctuating component in the flow direction at low densities. However, this would cloud somewhat the interpretation of the velocity distribution.

In any case, Savage and Jeffrey's distribution is only applicable to densities that are too low to be commonly found in granular material flows.

At higher densities a peak develops in the collision angle distribution about $\theta = 90°$. When the particle packing becomes dense enough, structures or preferred particle positions develop in the flow. As the density becomes large, the distances that a particle may move before colliding become extremely short. The only structure,that allows shearing motion at high densities, involves layers oriented perpendicular to the direction of the velocity gradient (or along stream lines). All the particles in a given layer have roughly the same velocity, but the mean velocity of neighboring layers varies according to the velocity field. The layers may only be seen in snapshots for very high densities, as in Figure 2.3c. The development of the layers will be examined in greater detail in the next section.

The effect of the layering on the collision distribution will be to exclude certain collision angles. Consider the test particle shown in Figure 3.3lc. The particles in the same layer will block collisions with the test particle by particles from neighboring layers

except in a small region about $\theta = 90°$. At the same time, the particles within each layer are free to collide with each other in a small region about $\theta = 0$ (or 180°). This is the source of the two peaks in the collision distribution at high density.

Savage et al. [67,70,72] found that the friction angle, or the ratio of shear to normal forces τ_s/τ_N in their Couette shear cell, decreased with density. It is likely that this is due to the formation of the $\theta = 90°$ peak in the collision distribution. This is indicated by Bagnold's [3] analysis which yields a zero friction angle for $\theta = \pi/2$.

3.4.3 Structure in a Granular Shear Flow

Structure, in a statistical sense, may be described by a probability distribution $p(\underset{\sim}{r}|\underset{\sim}{r}_o)$ which is the probability of finding a particle at $\underset{\sim}{r}$ given that there is a particle at $\underset{\sim}{r}_o$.

Structure arises because of the influence of a particle on the positions of others. At the simplest level, it is impossible to have two equal sized particles less than a particle diameter apart. Even more complicated structural properties will appear if the particles exert long range, such as gravitational and electromagnetic forces on one another. Clearly a gas of point particles, which have zero size and no long range force, will have no structure, and $p(\underset{\sim}{r}|\underset{\sim}{r}_o) = n = \text{const.}$, where n is just the number of particles per unit volume.

Except for extremely ordered systems like crystals, one would expect a particle's influence to be limited in range. Hence it can be assumed that

$$\lim_{\|\underset{\sim}{r}-\underset{\sim}{r}_o\| \to \infty} p(\underset{\sim}{r}|\underset{\sim}{r}_o) = n(\underset{\sim}{r})$$

where $n(\underset{\sim}{r})$ is the local value at n about $\underset{\sim}{r}$.

In a gas at equilibrium, isotropy implies that the probability distribution $p(\underset{\sim}{r}|\underset{\sim}{r}_o)$ must be spherically symmetric about $\underset{\sim}{r}_o$. The distribution could then be denoted p(r) where $r = \|\underset{\sim}{r}-\underset{\sim}{r}_o\|$ may be interpreted as the probability that two molecules will be separated by a distance r.

Apply a velocity gradient to the material and the spherical symmetry breaks down. A particle that at time t was at a distance r will be at $(r + \frac{rd\ V_r}{dr}\ dt)$ at $t + dt$. This would smear out the distribution, because both points on the particle path must have the same probability. In a shearing material there may be structure along stream lines. Thus, given a particle, there is a probability of finding another at a distance along or in the near vicinity of, say within a particle diameter of, the same stream line. There may also be structure in the direction normal to the stream lines. Given a particle on one stream line, there may be preferred stream lines on which to find other particles, although there can be no preference as to the positions of the particles along those other stream lines.

This does not imply the existence of layers for other than granular flows. It only puts limitations on the information that can be obtained from $p(\underset{\sim}{r}|\underset{\sim}{r}_o)$.

Structure is determined in much the same way as the velocity and collision distributions. First, a test particle is chosen. To eliminate as much as possible any influence of the flow boundaries, any particle

whose center lies within a diameter of the midpoint between the walls is chosen as a test particle. The interval [0,8R] was broken into 50 slices, each of which is assigned to an array element. At each sampling time the number of particles that fall into each slice is counted, and the answer placed in the appropriate element of the array. The totals are normalized by dividing by the number of samples taken and the size of the sampling region, yielding the probability distributions. The Couette flow simulation with the no-slip wall condition is again chosen to provide samples. In all cases, the same material properties ($\varepsilon_w = 0.8$, $\varepsilon_p = 0.6$) and the same shear rate were used.

Two distributions were assessed: The "normal distribution" is the probability of finding any particle in the control volume with a position in the direction normal to the flow direction, which is a certain distance from the test particle. The "parallel" distribution" is the probability of finding a particle, at a given distance from the test particle, in the direction parallel to the flow, whose normal position did not differ by more than a particle diameter from that of the test particle. (A particle diameter is a first approximation to the thickness of a layer.)

The normal distribution will illustrate the formation of layers within the flow, and the parallel distribution will illustrate the development of structure within the layer.

Five examples of each distribution, covering the range $.35 \leq \nu \leq .75$, are shown in Figures 3.35 through 3.39. Note that, as expected, all of the distributions for small densities asymptote to the expected value at $n = \nu/\pi R^2$.

There is a peak at a spacing of about 2R in all of the correlations. This represents the direct influence of the test particle. The peak is formed by those particles that approach, collide with, and recoil from the test particle. These particles pass through roughly the same region twice, and are thus counted twice. The double counting forms the peak.

Note that in many of the parallel distributions a large peak is formed close to a spacing of 8R. This is the periodic image of the peak at 2R. The periodic boundary condition imposes an order on the flow, in the sense that there is a 100% probability that there will be another particle at the same position exactly one control volume width on either side of the test particle.

As the density increases, more peaks develop. These are caused by the particles that collide with those that formed the first peak. The peaks grow with density until they are roughly equal in size, indicating the existence of well formed layers.

Layers oriented parallel to the boundaries are probably peculiar to unidirectional flows. The layers are required by kinematically reasoning that, to maintain a shear flow at high densities, the particles must align themselves in the direction parallel to the flow direction. This idea may be generalized to more complicated flows, and it may be supposed that similar structures will form along stream lines.

In passing, it should be noted that

$$S = \frac{2R(\frac{du}{dy})}{\sqrt{<\underset{\sim}{u}'^2>}}$$

can be interpreted as a kind of order parameter. 2R(du/dy) is indicative of the relative velocity of neighboring layers, and $\sqrt{<\underset{\sim}{u}'^2>}$ is indicative of the particle velocity normal to the layers. $\sqrt{<\underset{\sim}{u}'^2>}/(du/dy)$ is then a scale of how far a particle may travel outside its layer before a collision with a particle in the neighboring layer forces it back. Flows with large S should have sharp well defined layers, and flows with small S should have a more diffuse structure. In Figure 3.41 it is shown that as the density increases, and the structure becomes more distinct, S is also increasing. S may then assume different values for the same shear rate at different densities, while S is roughly a constant for a given material at a given density and any shear rate.

3.5 Conclusions

A great variety of data was obtained from the computer simulation. Macroscopic phenomena such as velocity and density profiles and scaling parameters were derived. On the other hand, the simulation was an invaluable tool for examining microscopic behavior, such as velocity distributions, collision distributions, and the pair correlation that indicated the presence of considerable structure within the flow.

There is a strong similarity between the chute flow velocity profiles generated by the simulation and those measured experimentally by Augenstein and Hogg [1]. Both shear completely across the depth and exhibit a region of particularly high shear next to the chute

bottom. The simulation profiles slip at the wall with about 40% of the maximum velocity. Comparison with Augenstein and Hogg's [1] measurements suggest that the degree of slip and the character of the velocity profile in the neighborhood of the wall are greatly affected by the mechanism of particle wall interaction.

The Couette flow simulation was run with two different wall conditions. The first is the same one as was used for the chute flow: on departure, after a collision, the relative velocity between the chute and the particle surface is zero. The second, or "no-slip" condition dictated that the particle center assume the same linear velocity as the wall. Velocity profiles from the simulations employing the second condition were linear. With the first wall condition there were zones of high shear next to each wall with almost a plug flow between. Again, the wall condition has a strong effect on the profile shape.

The chute density profiles agree with those measured by Ridgway and Rupp [60]. Their most intriguing aspect is that the density reaches a maximum in the center of flow with regions of low density near the free surface and near the chute wall. The location of the low density region at the wall corresponds almost exactly with the high shear zone in the velocity profile. The density profile exhibited the same type of behavior in the high shear zone next to the walls of the Couette flow simulation with the first wall condition. However, the density is constant for the Couette flow with the second wall condition, which has a constant velocity gradient.

These observations led to defining a "temperature" to govern the

density of a granular flow. Drawing an analogy with the molecular theory of gases, the temperature is defined as the mean square fluctuating velocity of the particles $\langle \underset{\sim}{u}'^2 \rangle$. Continuing the analogy with a gas, an equation of state was heuristically proposed of the form

$$p = \rho_p \chi(\nu) \langle \underset{\sim}{u}'^2 \rangle$$

Measurements of $\chi(\nu)$ from many flow situations indicate that it is a well-defined function.

Temperature is generated as a byproduct of collisions between particles, and will depend to some degree on the gradient in the velocity field. There are indications that the temperature may be conducted and dissipated. Stagnant regions appear when the density becomes too large to allow the material to shear. It is possible that understanding conductivity will lead to prediction of the formation and shape of stagnant wedges in chutes and hoppers. Attempts to measure the conductivity by applying a balance on the fluctuating energy within a strip were unsuccessful.

The fluctuating energy is not equipartitioned into its three components $\langle u'^2 \rangle$, $\langle v'^2 \rangle$, and $\beta \langle \omega'^2 \rangle$. How the energy is distributed depends on the density. The effect of the non-equipartition on the flow is unknown, but it is possible that it leads to normal stress difference effects.

It was shown that the Couette flow simulation has an intrinsic time-scale equal to the reciprocal of the velocity gradient. In particular, the temperature is proportional to the square of the velocity gradient in the case where a uniform temperature eliminates

all conduction effects.

The Bagnold/Savage constitutive law was examined and was shown to have some validity. Values of the density dependence for the shear and normal directions $f_{s,N}$, were obtained and were found to behave as expected, although there was a great deal of scatter in the data. Favorable comparison was made with experimentally determined values for $f(\nu)$. Some doubt was thrown on the strict validity of this model, by comparison with the previously proposed equation of state. It was suggested that the scatter in the data was a result of replacing the temperature by the square of the velocity gradient, an approximation that only appears to be valid in the absence of conduction.

The simulation allowed a unique opportunity to examine the statistical properties of granular flow. The instantaneous particle velocities were found to nearly obey a Maxwell-Boltzmann distribution about their mean velocities. The deviation from the Maxwellian form appeared to depend on the flow's departure from equilibrium as measured by quantity

$$S = \frac{2R\,\frac{du}{dy}}{\sqrt{\langle \underset{\sim}{u}'^2 \rangle}}$$

Distributions measured by the chute flow simulation showed a large deviation from Maxwellian that is probably a result of conduction.

A strong anisotropy was found in the collision angle distribution. At low densities the anisotropy was of the form predicted by Savage and Jeffrey [71]. At higher densities, peaks began to form in the distribution about $\theta = 0°$ and $90°$, until the distribution consisted of just these two peaks. This anisotropy explains the

experimental results of Savage et al. [67,70,72]: that the ratio of shear to normal forces is a decreasing function of density.

The formation of the peaks in the collision distribution is a result of the development of structure within the flow. The only configuration that allows a shearing motion at a high density consists of layers of particles oriented in the direction of flow. The development of these layers and the development of structure within the layer has been clearly demonstrated by the measured probabilities of finding particles a given distance from a test particle in directions normal and parallel to the flow.

These results indicate that a flowing granular material behaves like a self-excited gas. The constituent particles undergo random, temperature-like motions, but this temperature is a byproduct of the velocity field. This suggests that in a future model of granular flow there will be an energy equation describing the production, dissipation, and conduction of temperature coupled with the equations of motion.

Adaptation of the molecular theory of transport phenomena appears to be a promising approach toward developing a mathematical theory of granular flow. Preliminary calculations of this type were performed by Savage and Jeffrey [71] to derive a stress tensor. Unfortunately, they had to heuristically adopt much of the statistical properties of gases for granular flows. In particular, they could not include the collision anisotropy that results from the formation of layers in the flow. Once the statistical behavior of granular flow has been

established, it is a relatively simple matter to derive the complete transport equations.

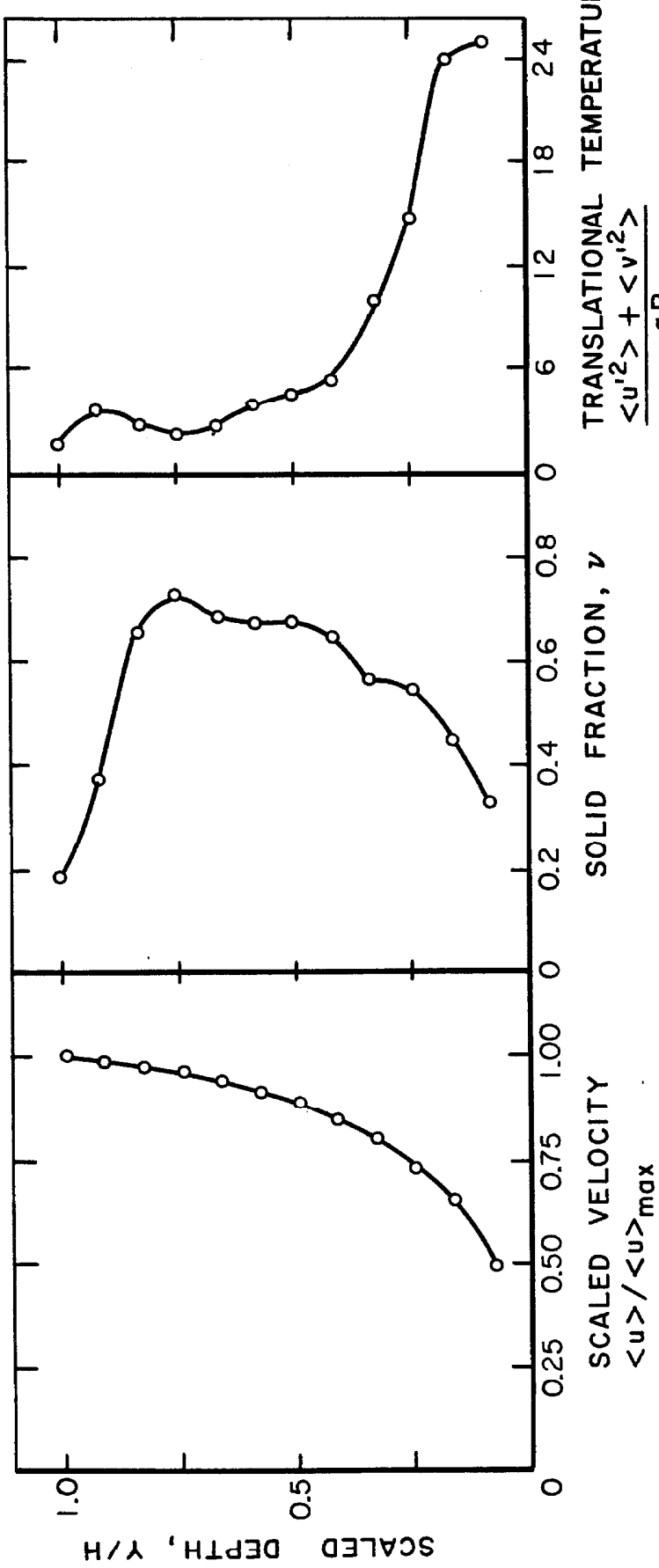

Figure 3.1 Typical velocity, density, and temperature profiles for inclined chute flow. $\alpha = 30^{o}$, $\varepsilon_w = 0.8$, $\varepsilon_p = 0.6$, 10 x 4 particles.

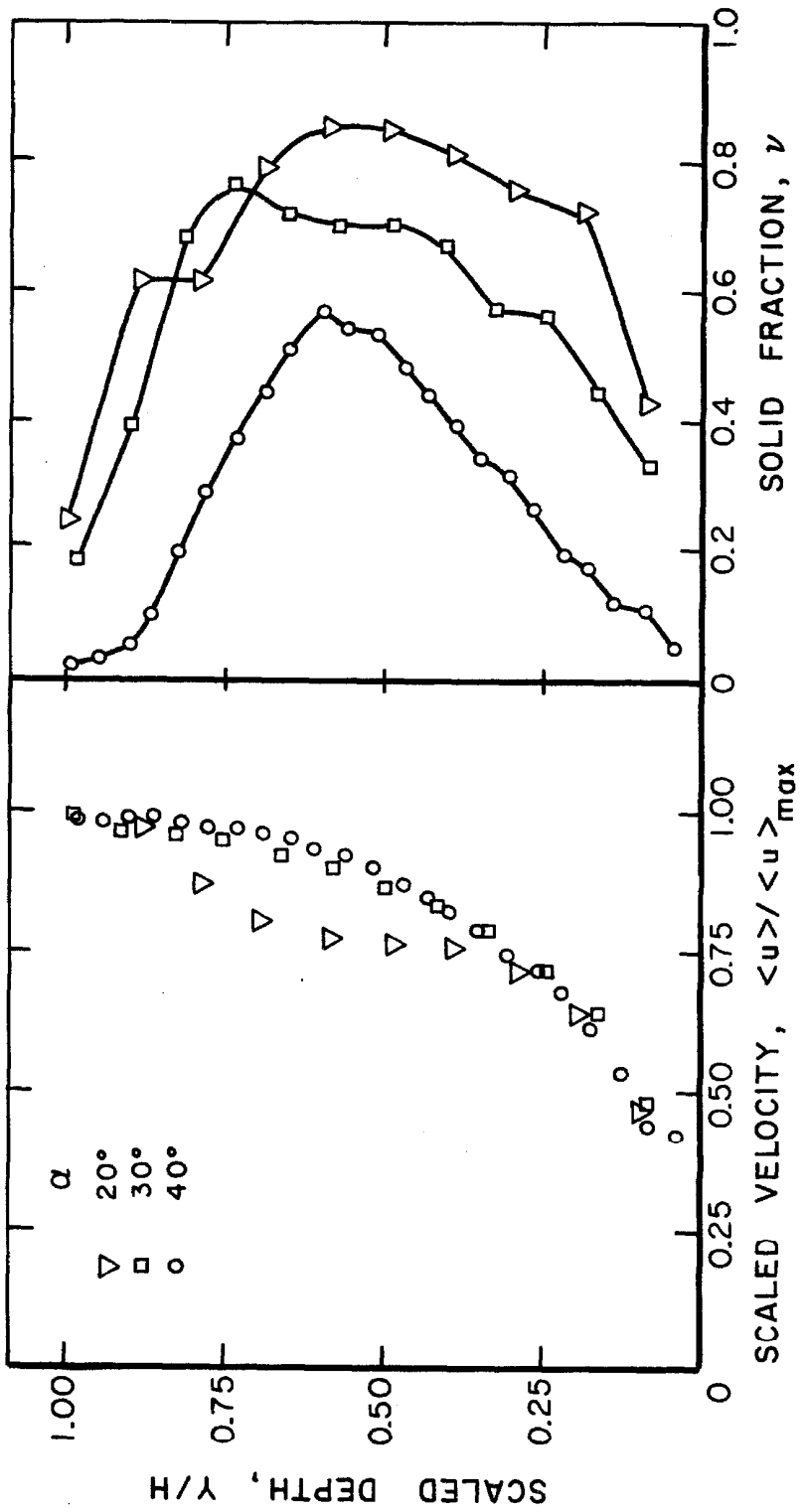

Figure 3.2 Velocity and density profiles for chutes inclined at $\alpha = 20^{o}$, 30^{o}, and 40^{o}. $\varepsilon_w = 0.8$, $\varepsilon_p = 0.6$, 10 x 4 particles.

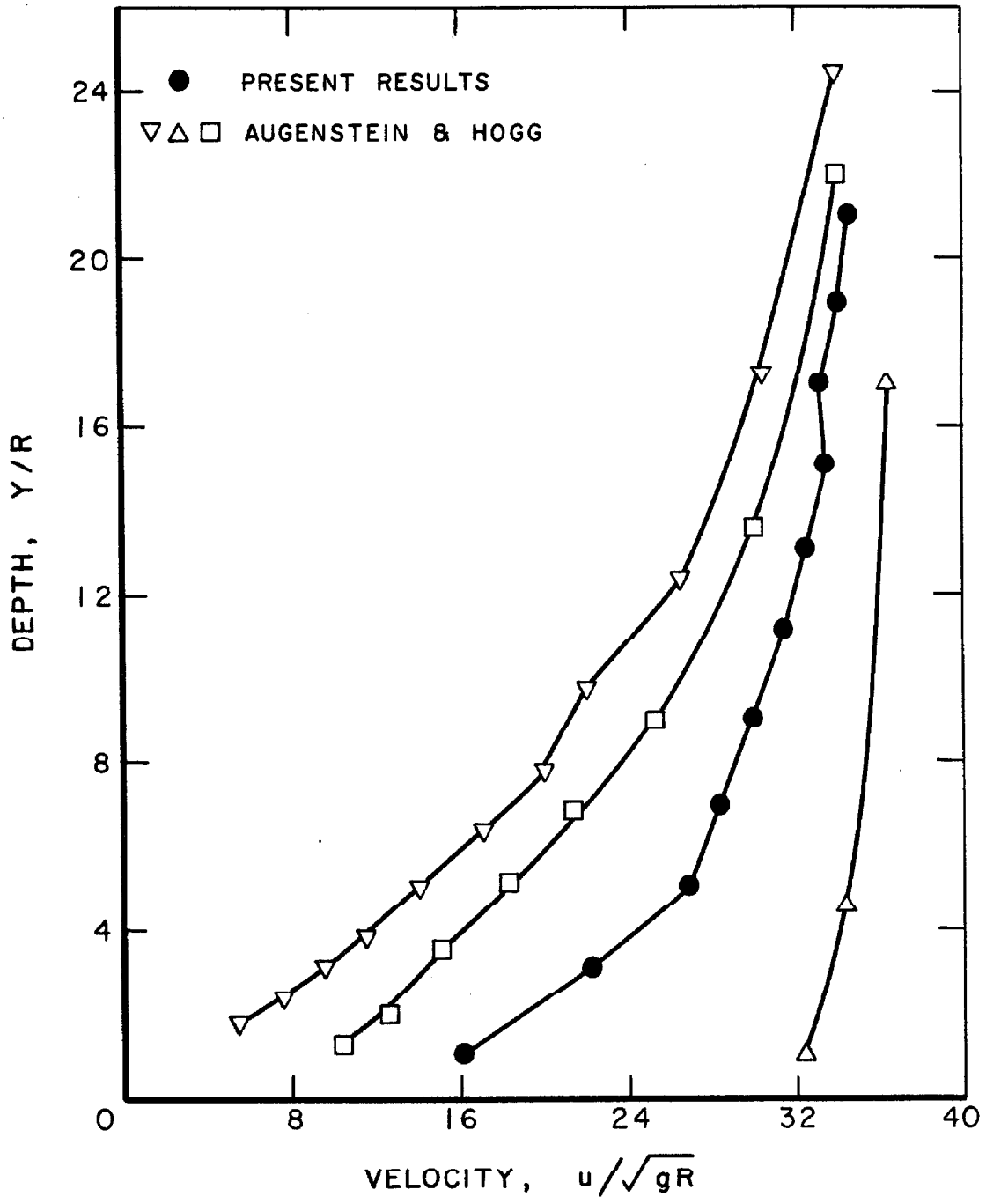

Figure 3.3 Comparison of a simulation generated velocity profile ● ($\alpha = 40^{o}$, 5 x 4 particles, $\varepsilon_w = 0.8$, $\varepsilon_p = 0.6$) with profiles measured by Augenstein and Hogg [1], Δ 35 x 48 mesh sand on stainless steel, ∇ 35 x 48 sand on surface roughened with 35 x 48 sand, □ 28 x 35 sand on 65 x100 sand surface.

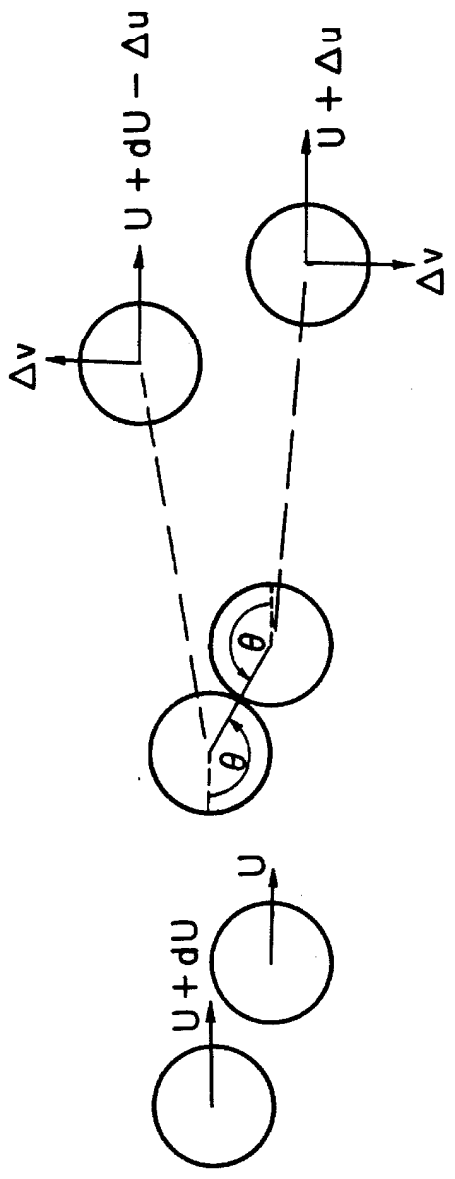

Figure 3.4 Generation of perturbation velocities Δu and Δv by a collision.

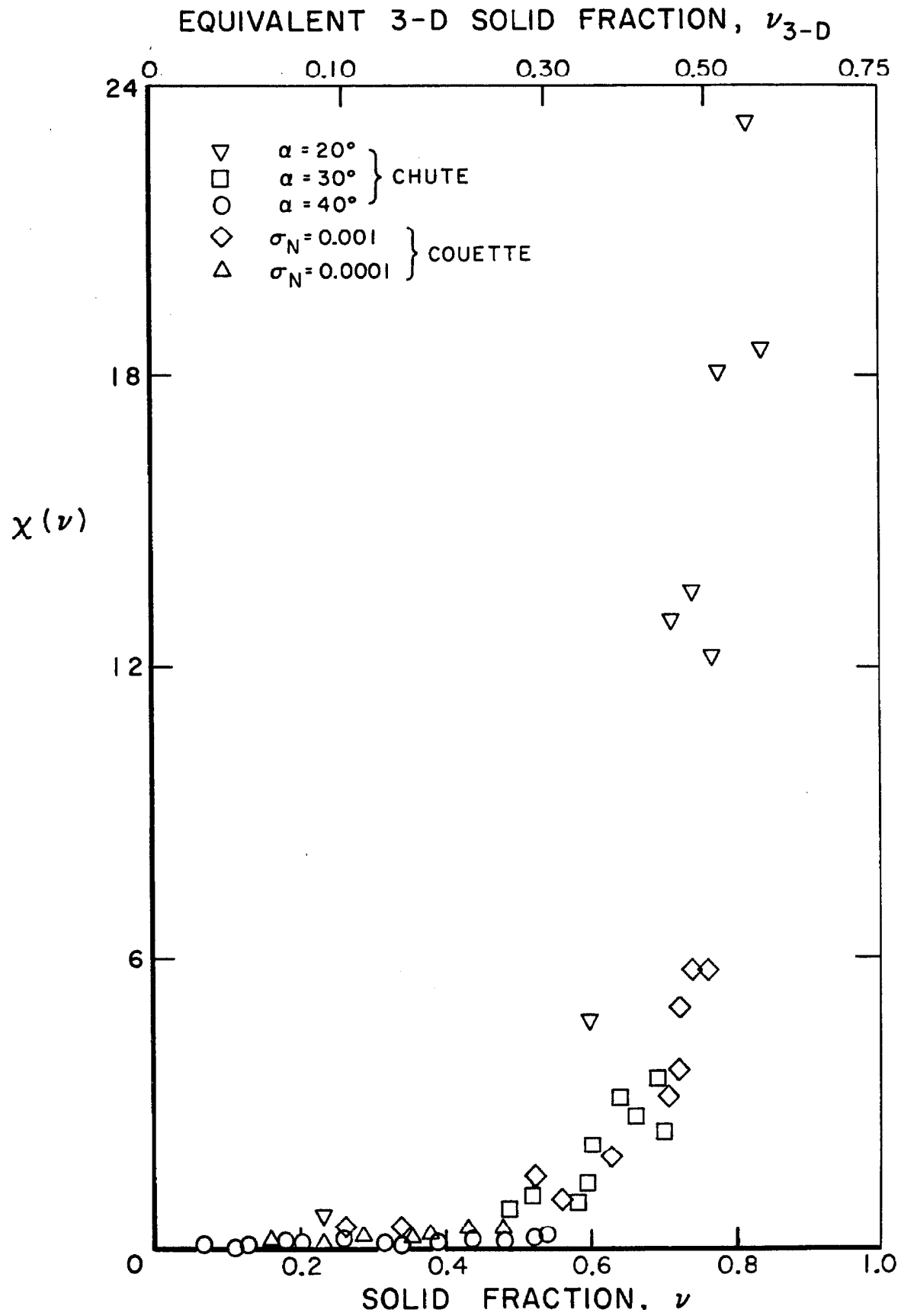

Figure 3.5 Density dependence of the equation at state.

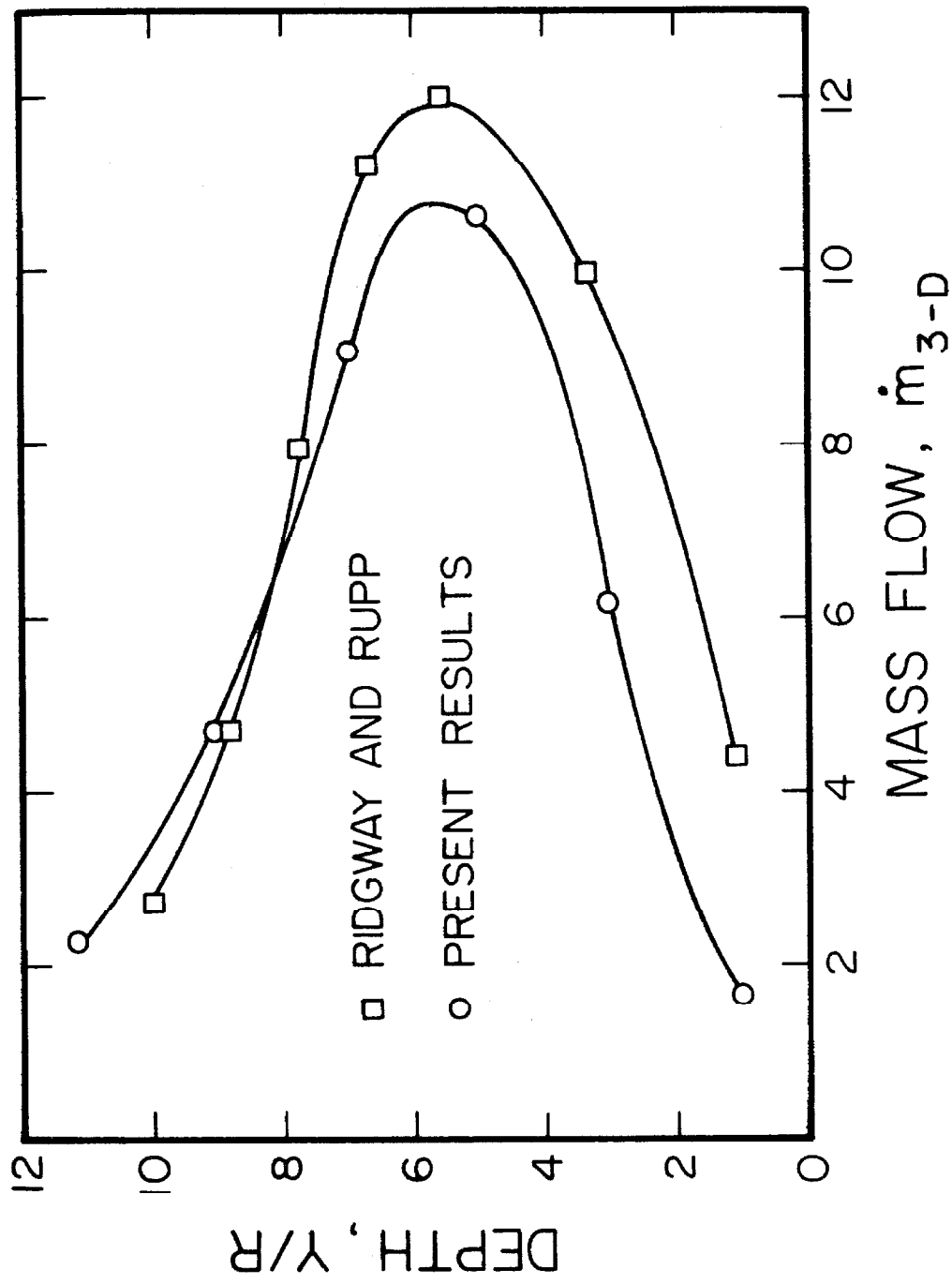

Figure 3.6 Comparison of simulation generated equivalent 3-D mass flow profile, (4 x 4 particles, $\alpha = 40^{o}$, variable coefficients of restitution) with the measurements of Ridgway and Rupp [60].

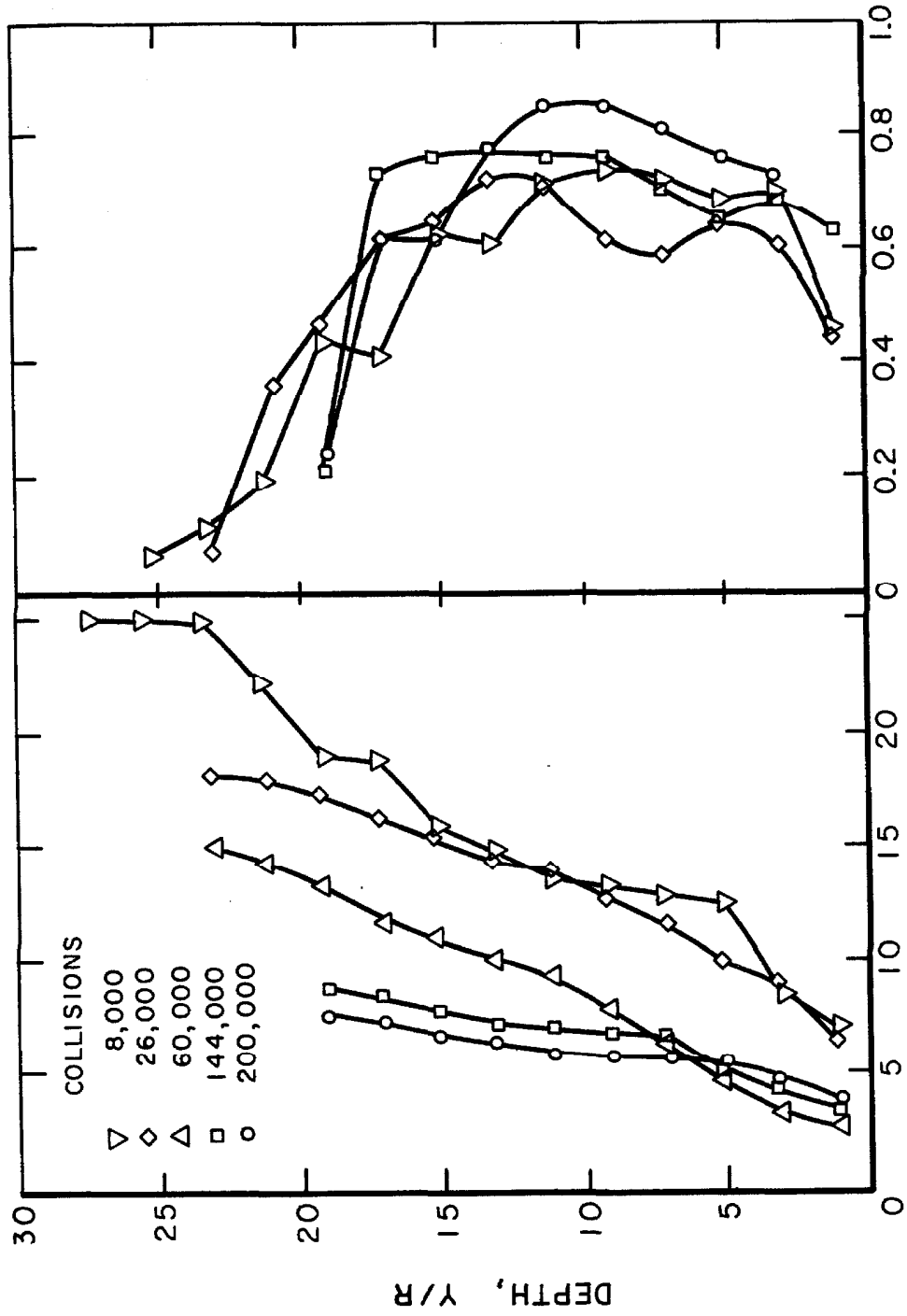

Figure 3.7 Evolution of the 20° chute simulation. 10 x 4 particles, $\varepsilon_w = 0.8$, $\varepsilon_p = 0.6$.

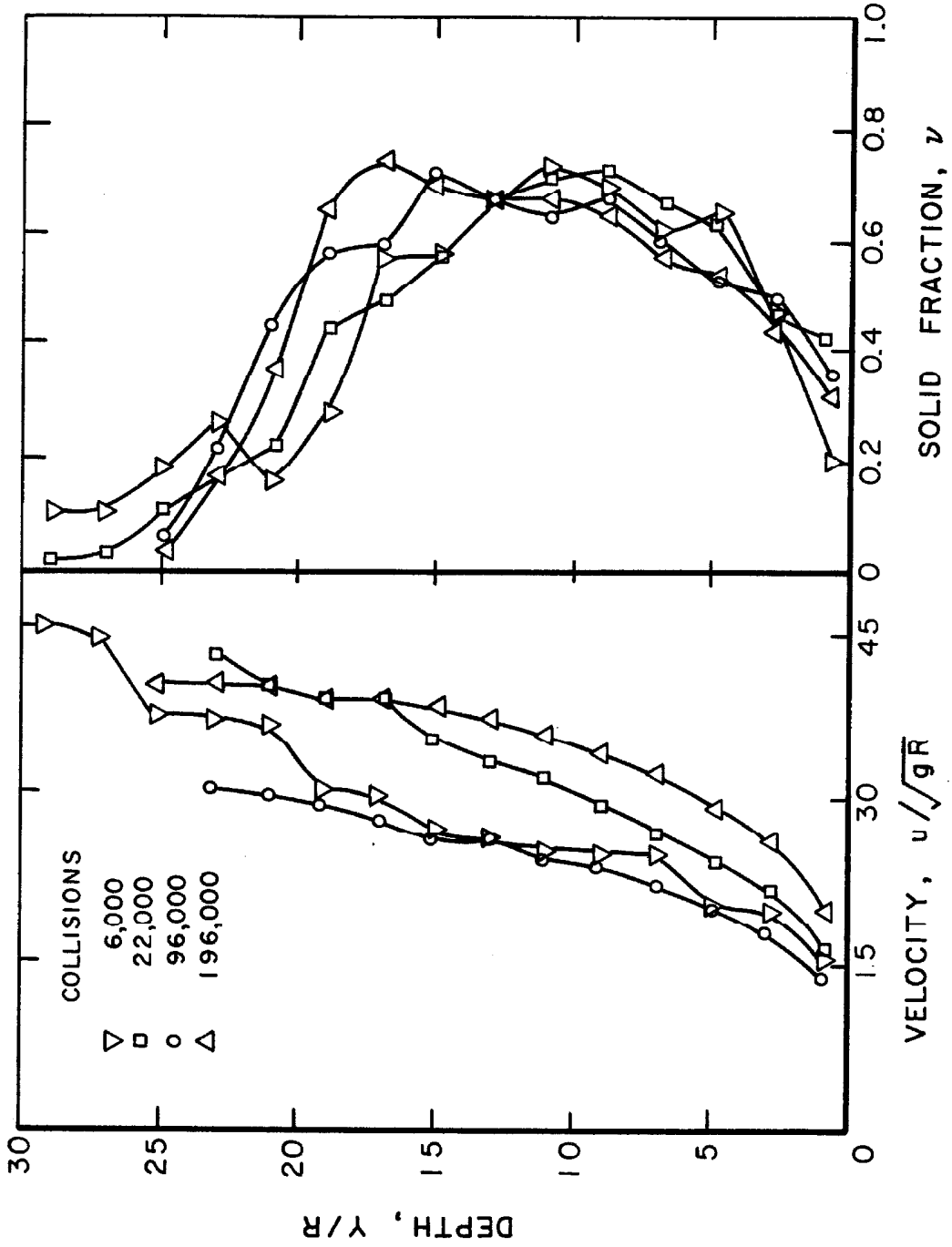

Figure 3.8 Evolution of the 30° chute simulation. 10 x 4 particles $\varepsilon_w = 0.8$, $\varepsilon_p = 0.6$.

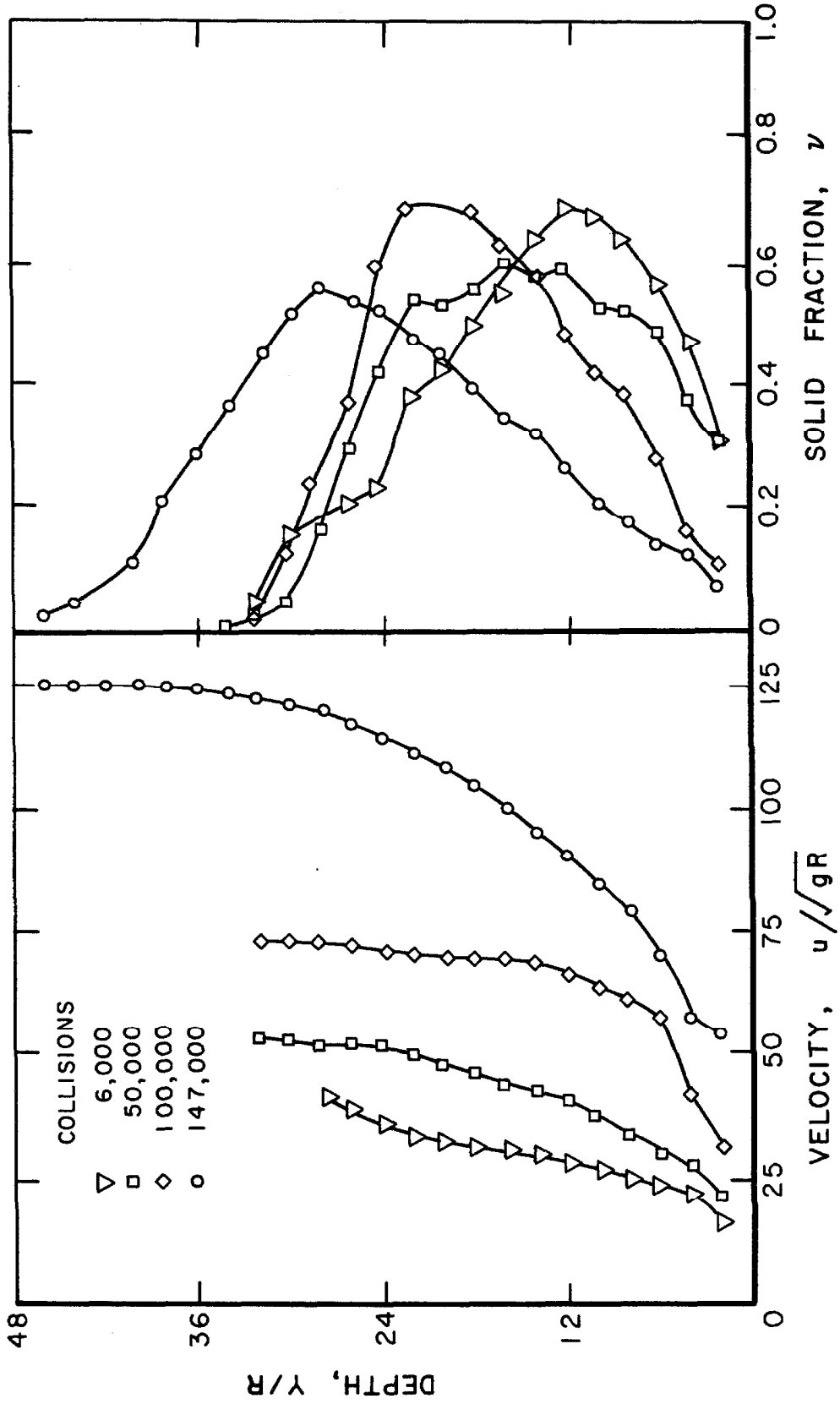

Figure 3.9 Evolution of the 40° chute simulation. 10 x 4 particles, $\varepsilon_w = 0.8$, $\varepsilon_p = 0.6$.

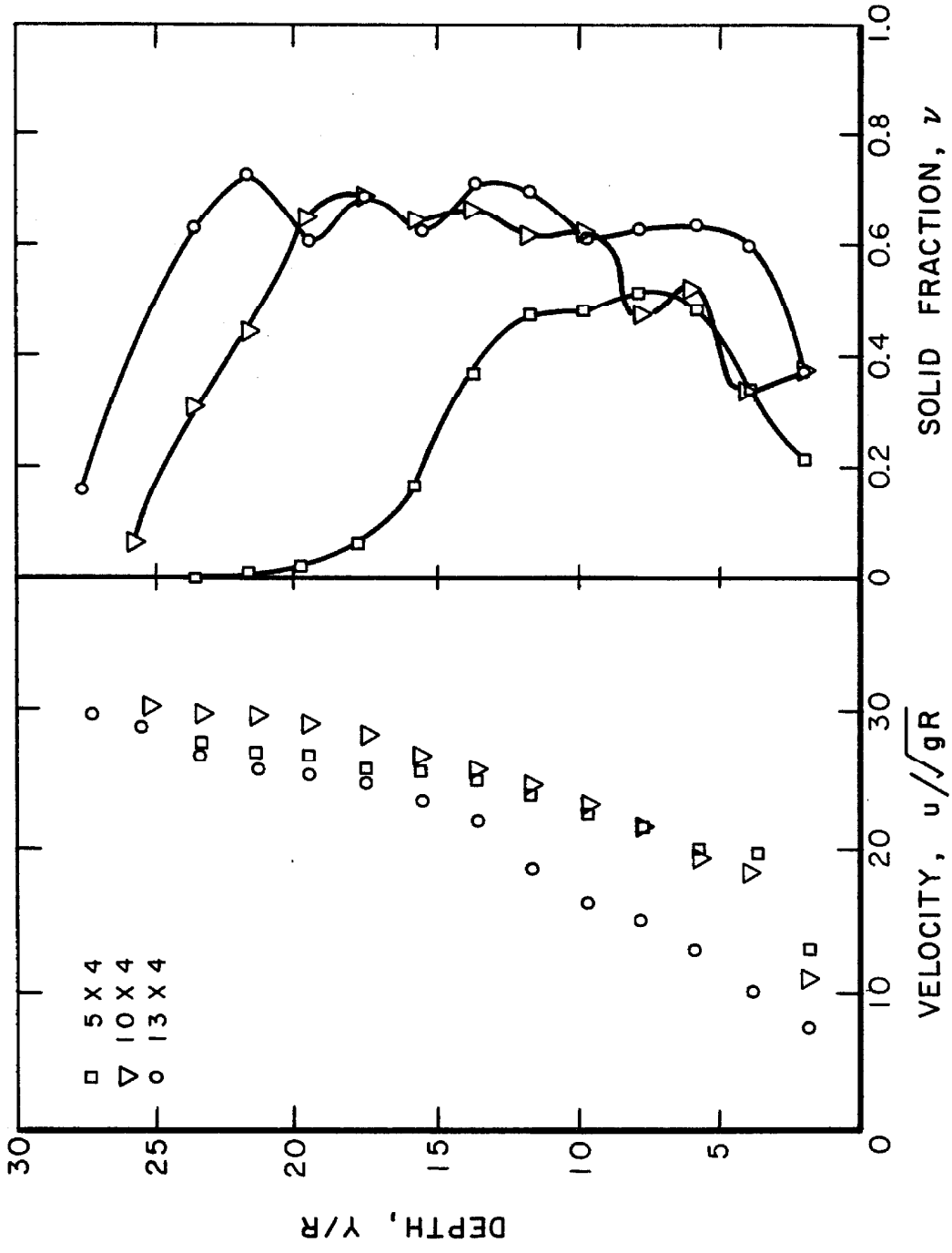

Figure 3.10 Effect of the flow depth on the chute flow profiles. variable coefficients of restitution.

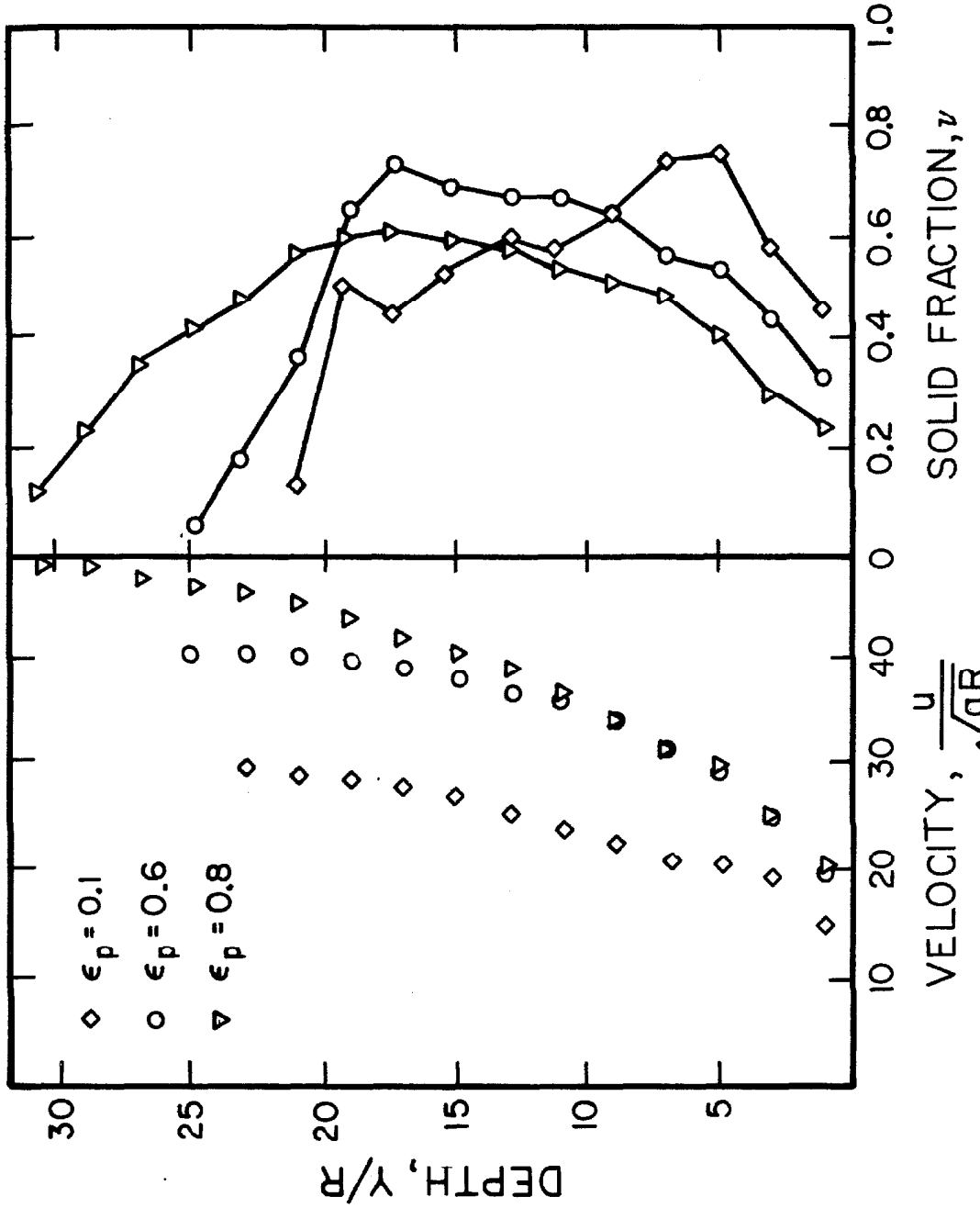

Figure 3.11 Effect of the particle coefficient of restitution on chute flow profiles. $\alpha = 30^{o}$, 10 x 4 particles. $\epsilon_w = 0.8$.

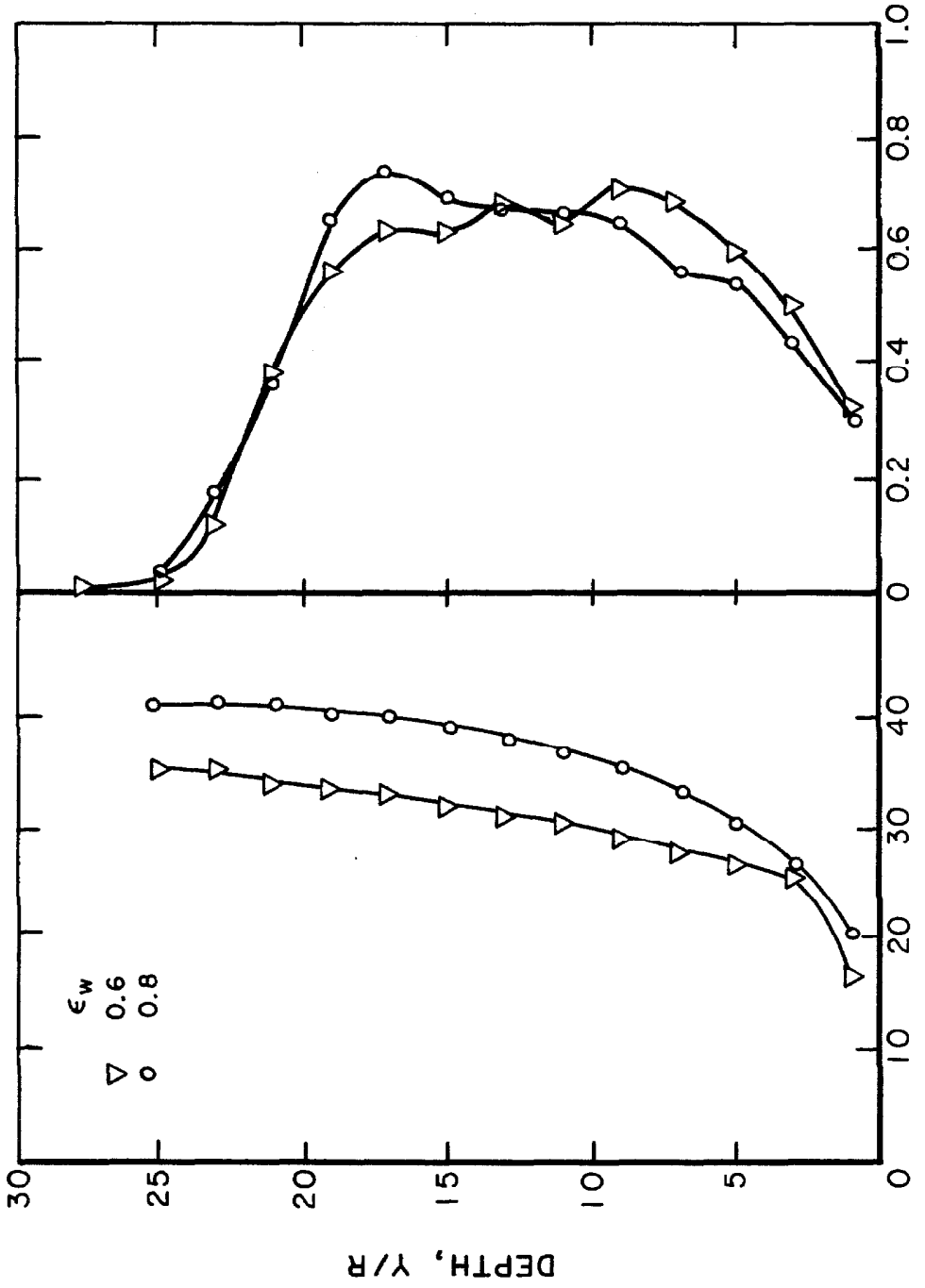

Figure 3.12 Effect of the wall coefficient of restitution on chute flow profiles. $\alpha = 30^{o}$, 10 x 4 particles, $\epsilon_p = 0.6$.

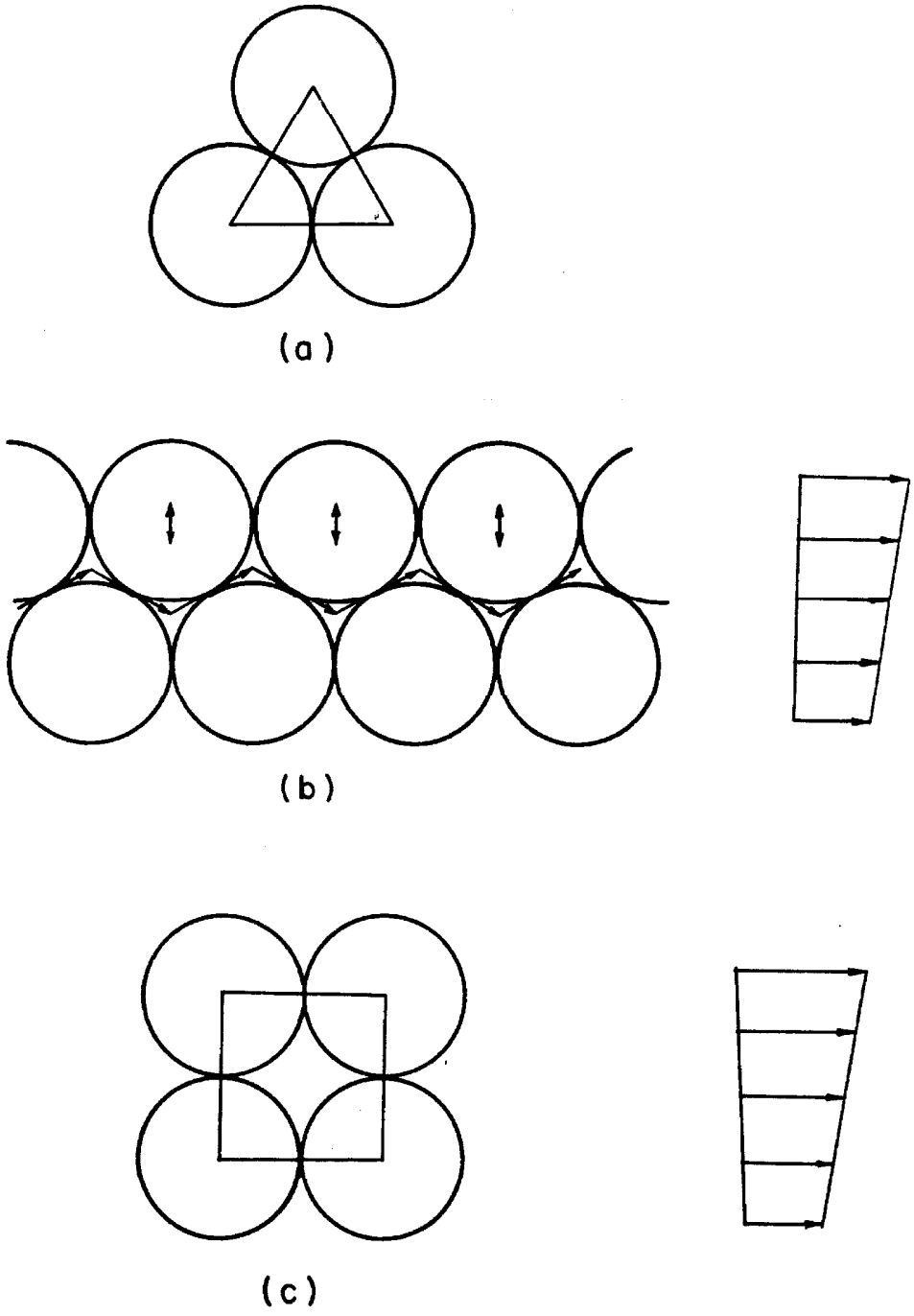

Figure 3.13 Limiting values of the solid fraction, (a) maximum packing $\nu_M = \pi/2\sqrt{3} = 0.91$, (b) maximum shearable packing, $\nu_m = \pi/(\sqrt{3} + 2\pi/3) = .822$, (c) maximum square packing $\nu_s = \pi/4 = 0.78$.

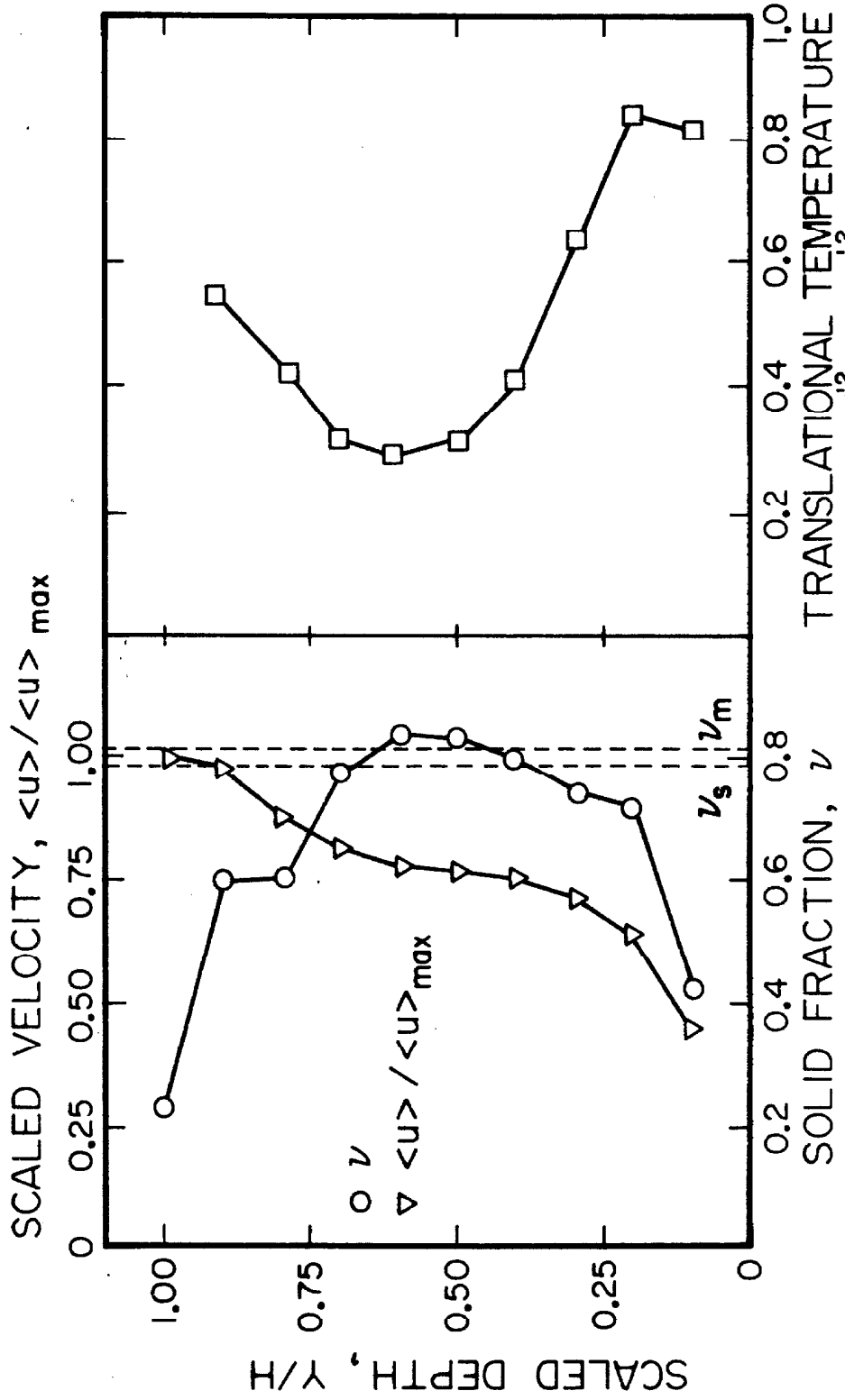

Figure 3.14 Velocity density, and temperature profiles for the $\alpha = 20^{o}$, chute simulation showing a plug flow region and conduction of temperature 10 x 4 particles, $\varepsilon_w = 0.8$, $\varepsilon_p = 0.6$.

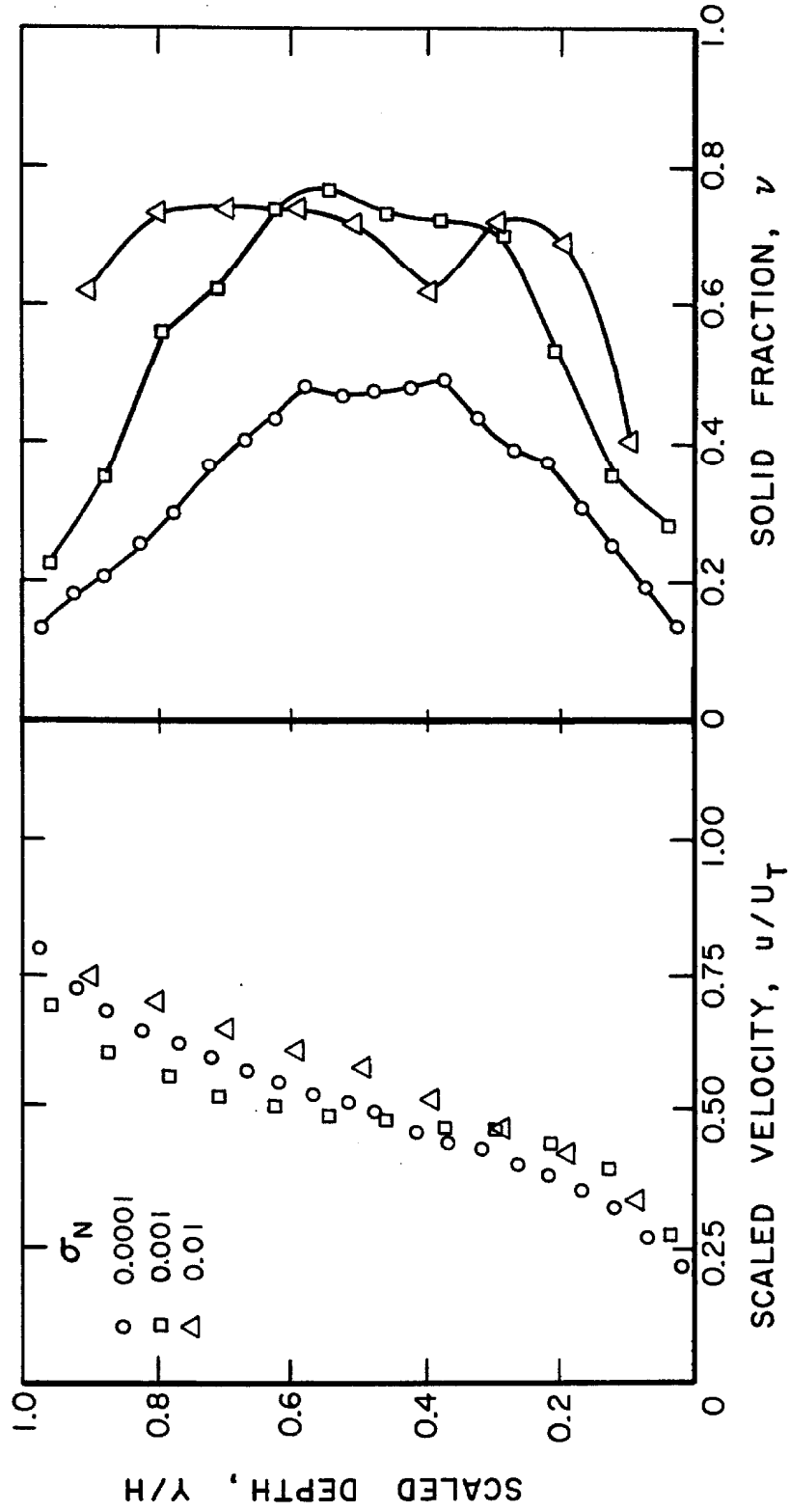

Figure 3.15 Velocity and density profiles for the Couette simulation with the first (rough particle and wall surfaces) wall collision condition. 10 x 4 particles, $\varepsilon_w = 0.8$, $\varepsilon_p = 0.6$.

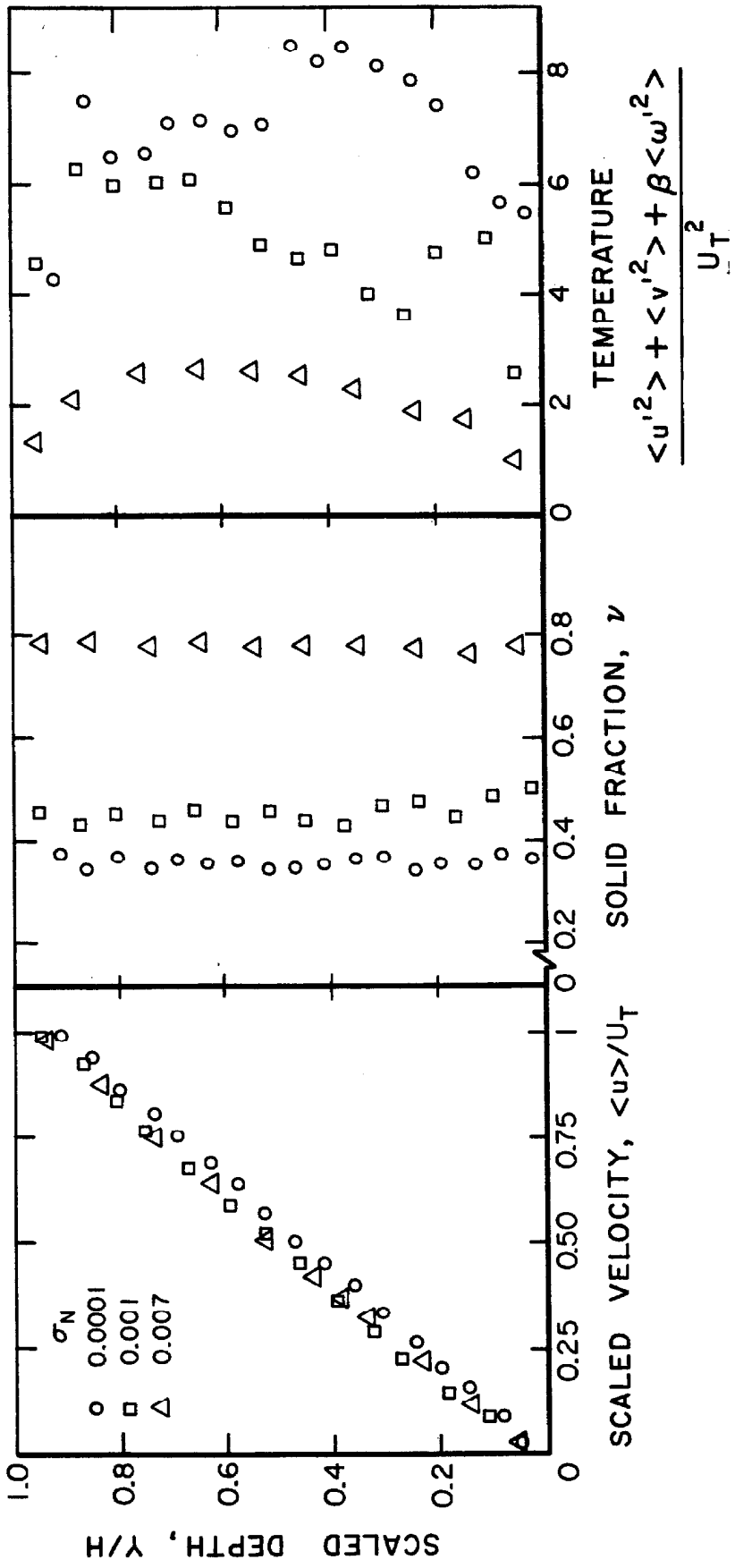

Figure 3.16 Velocity, density, and temperature distributions for the Couette simulation with the second (no-slip) wall collision condition. 10 x 4 particles, $\varepsilon_w = 0.8$, $\varepsilon_p = 0.6$.

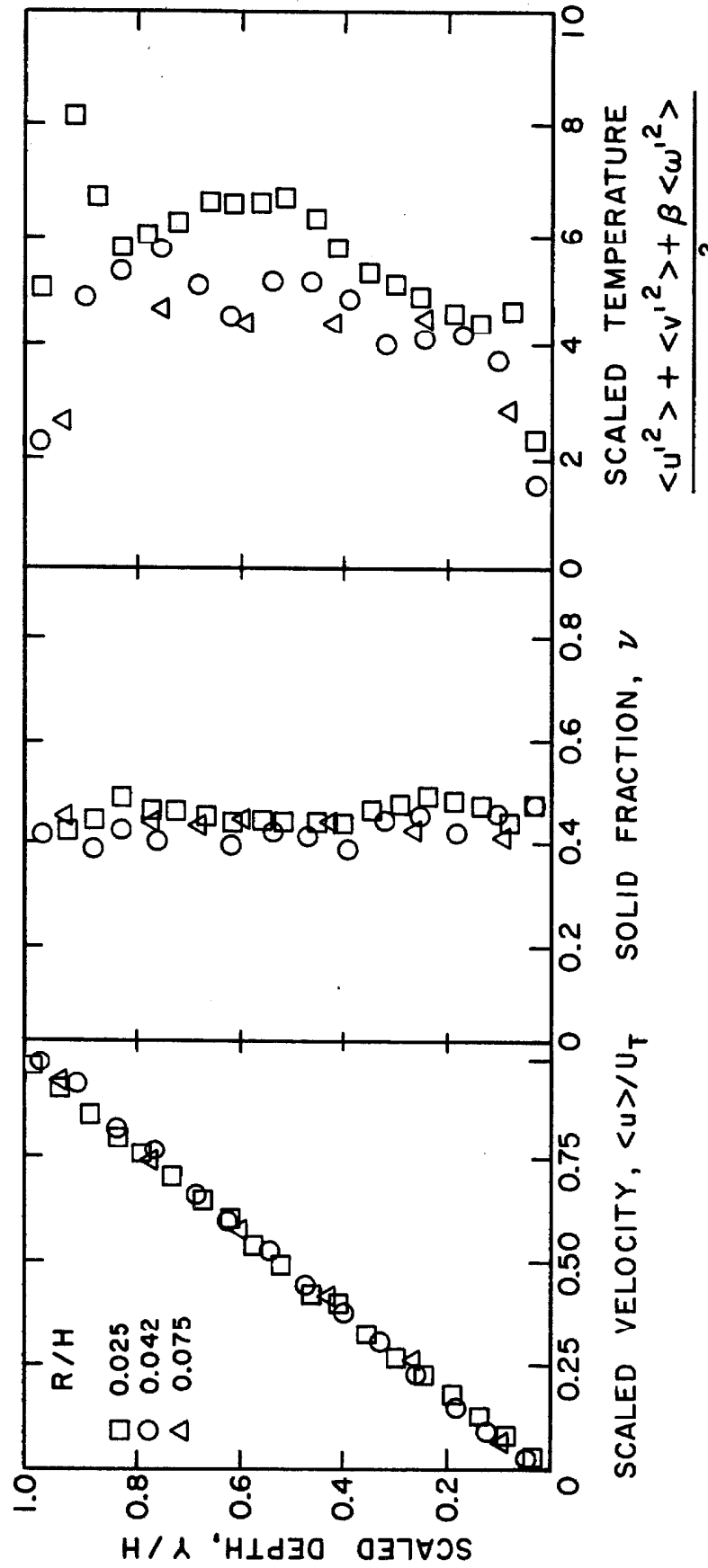

Figure 3.17 Effect of shear rate on the velocity, density, and temperature distributions, $\sigma_p^2 = .567(R/H)^2$, 10 x 4 particles, $\varepsilon_w = 0.8$, $\varepsilon_p = 0.6$.

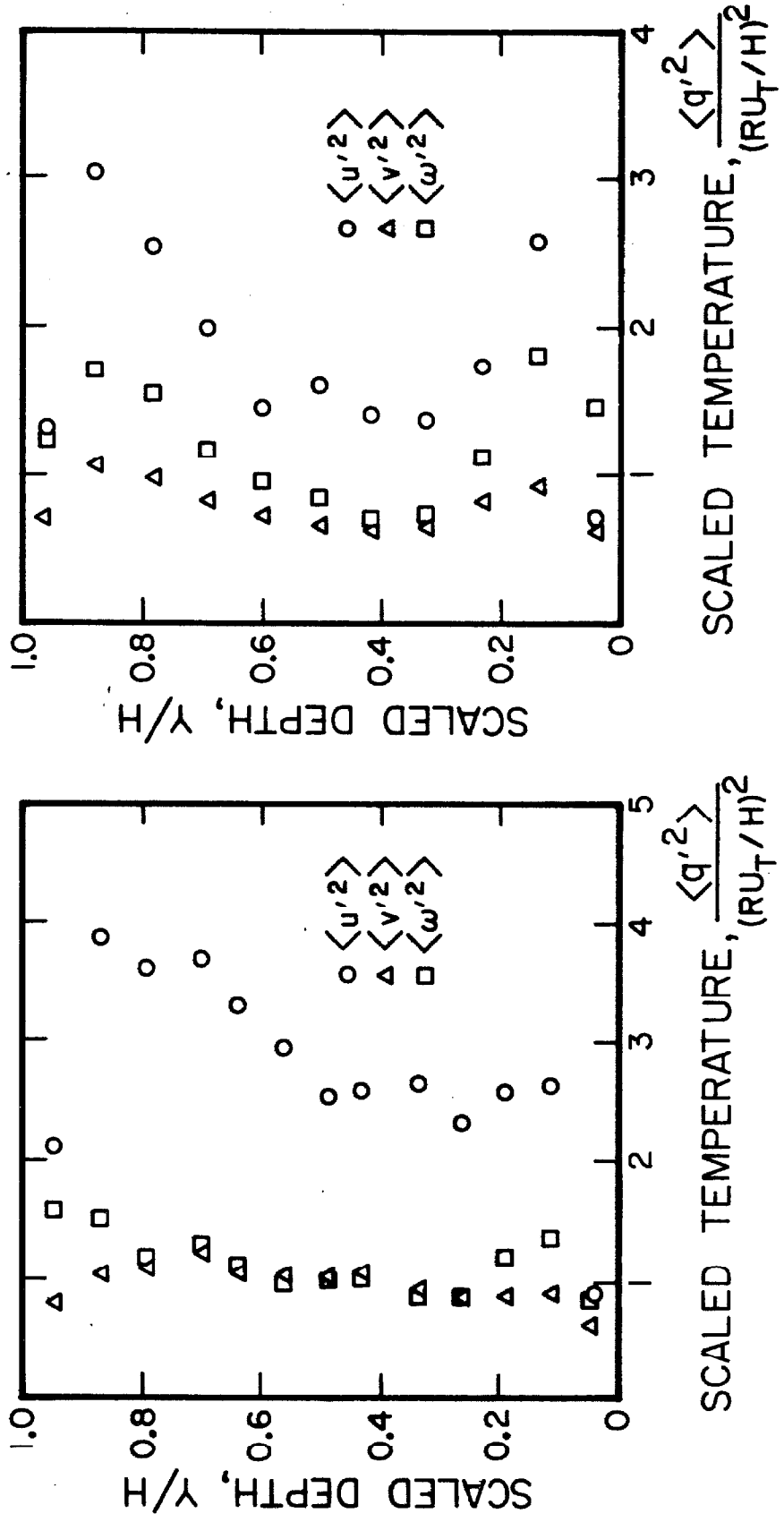

Figure 3.18 Partition of the temperature into its three components, from the Couette simulation with the no-slip wall condition. (a) ν = .45, (b) ν = .55, 10 x 4 particles, ε_w = 0.8, ε_p = 0.6.

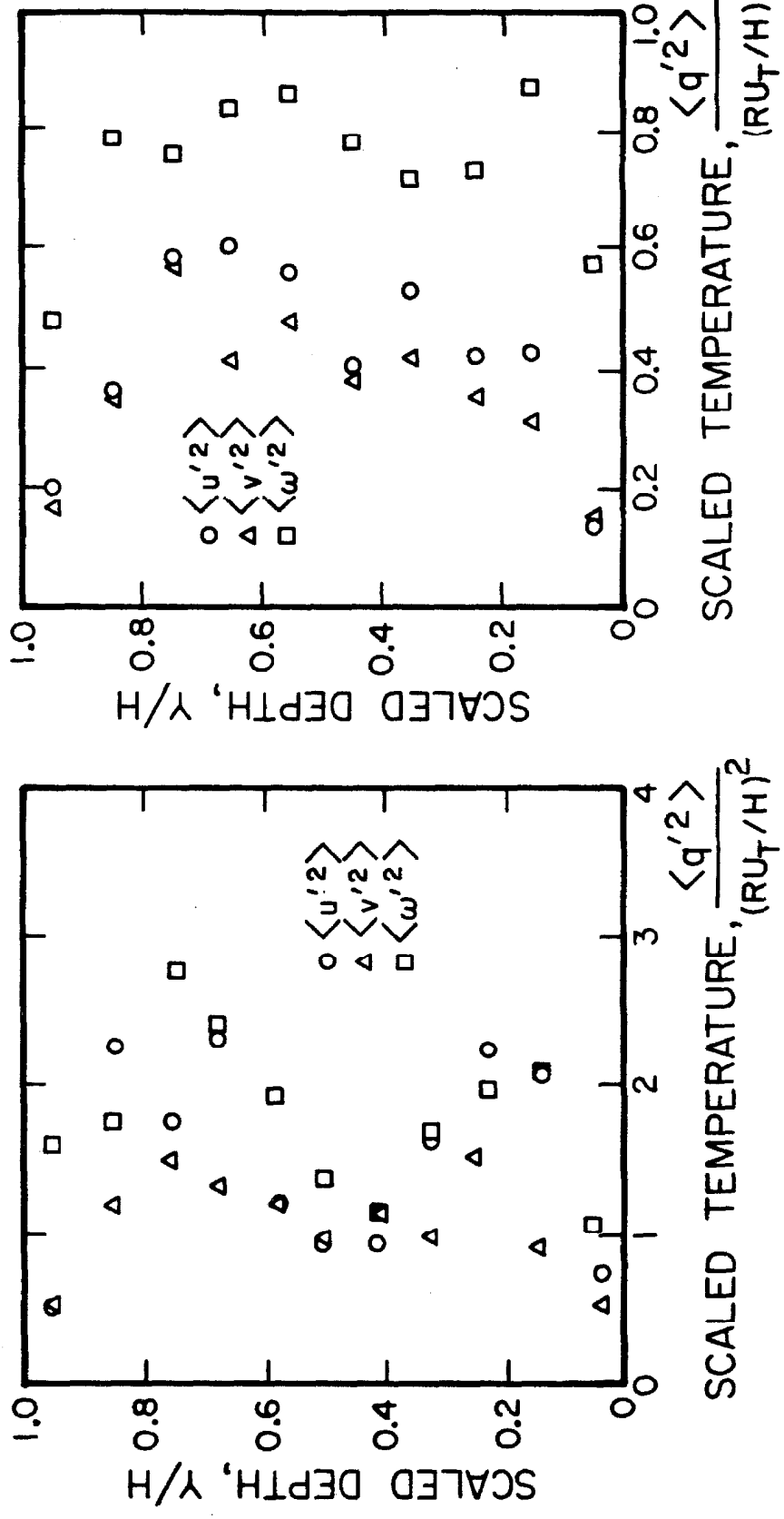

Figure 3.19 Partition of the temperature into its three components, from the Couette simulation with the no-slip wall condition.
left: $\nu = .65$, right: $\nu = .75$, 10×4 particles, $\varepsilon_w = 0.8$, $\varepsilon_p = 0.6$.

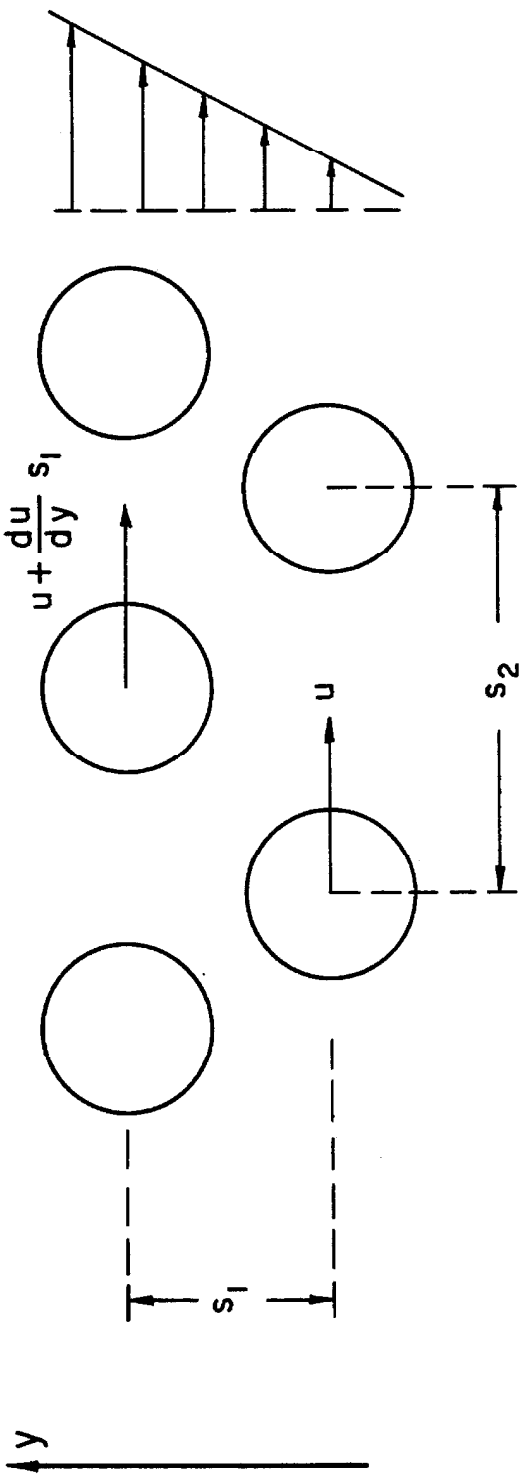

Figure 3.20 Illustration for the derivation of the Bagnold/Savage constitutive law.

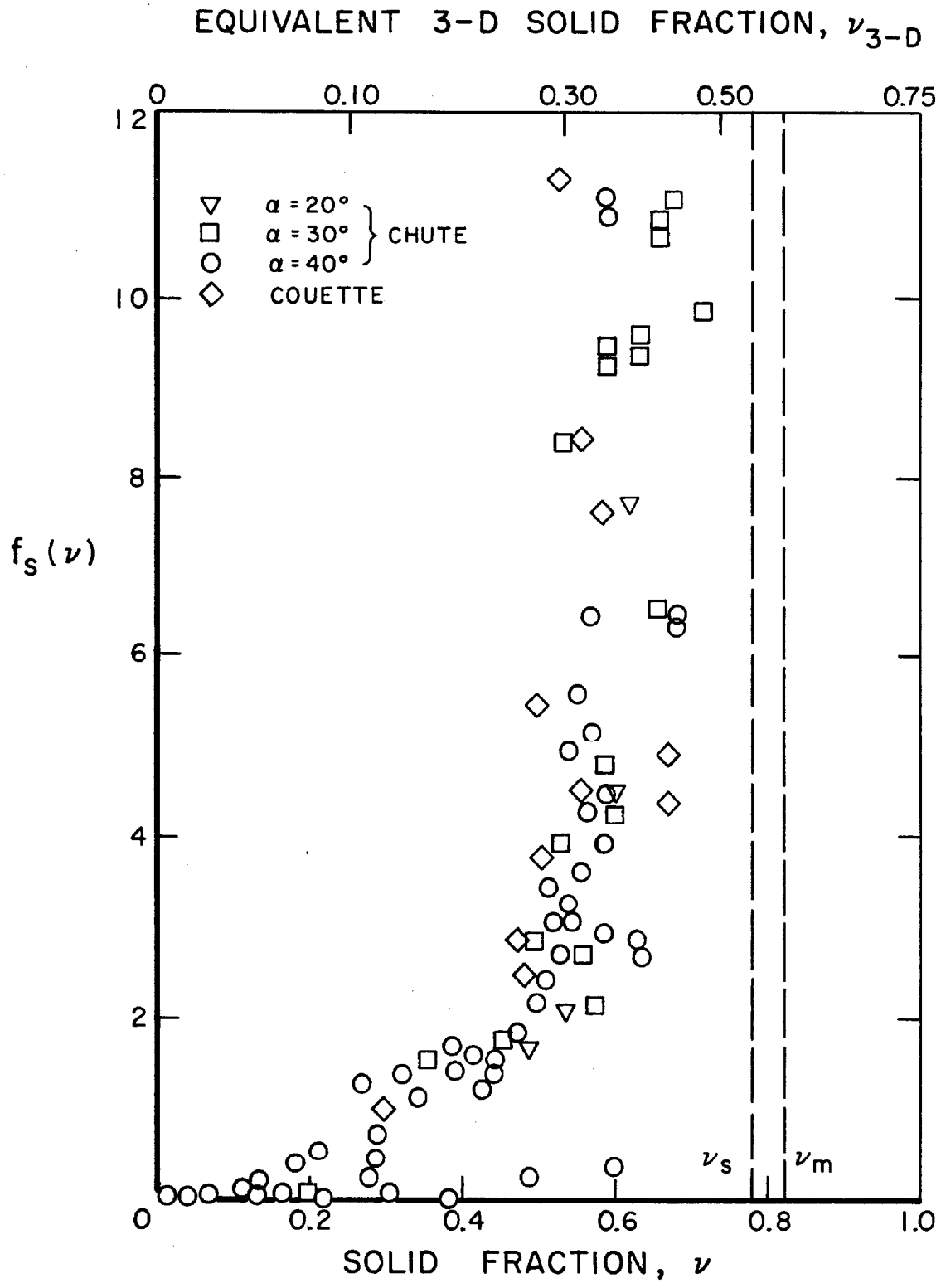

Figure 3.21 Shear stress density dependence of the Bagnold/Savage constitutive law, $f_s(\nu)$, $\varepsilon_w = 0.8$, $\varepsilon_p = 0.6$.

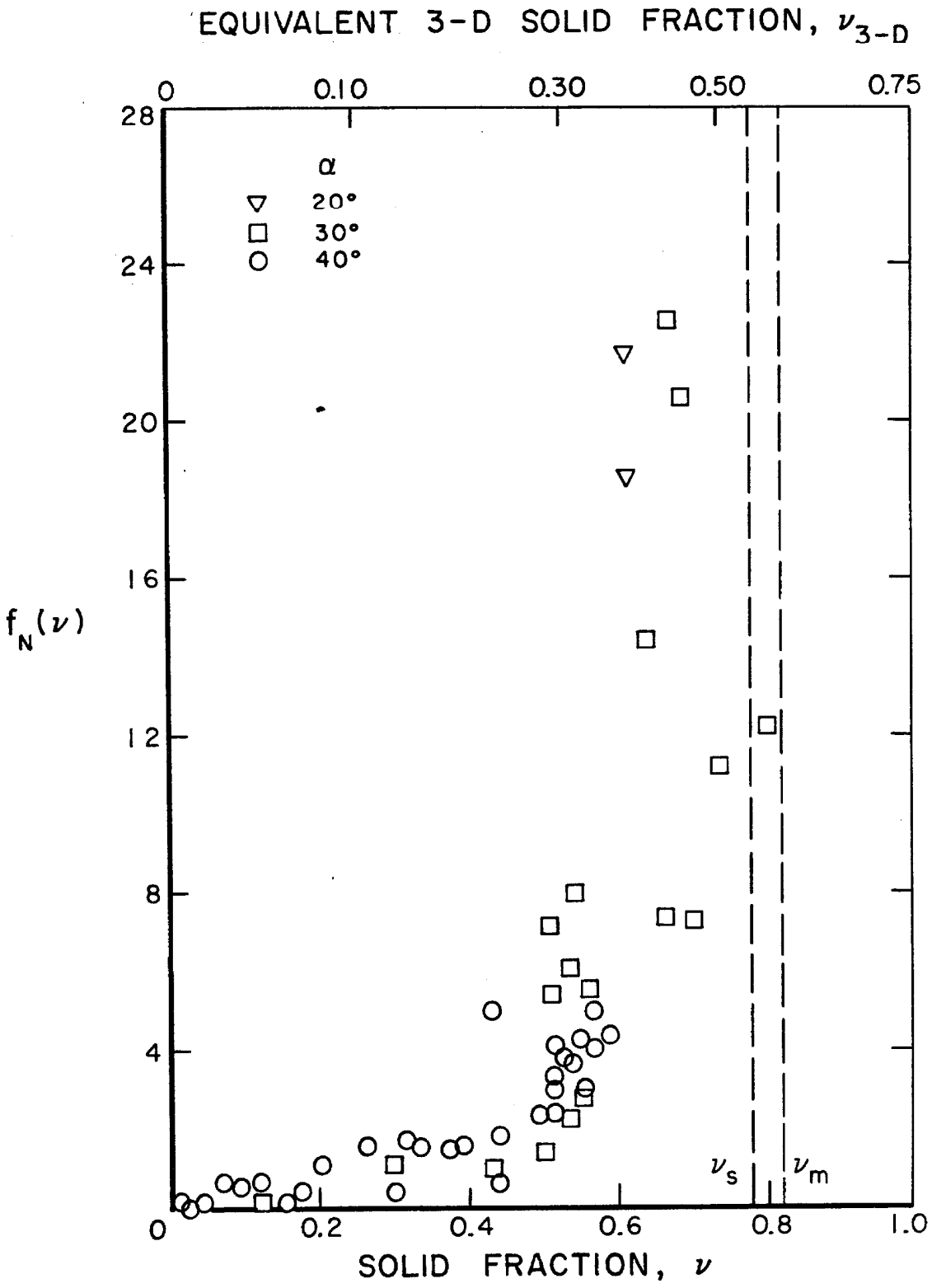

Figure 3.22 Normal stress density dependence of the Bagnold/Savage constitutive law, $f_N(\nu)$, $\varepsilon_w = 0.8$, $\varepsilon_p = 0.6$.

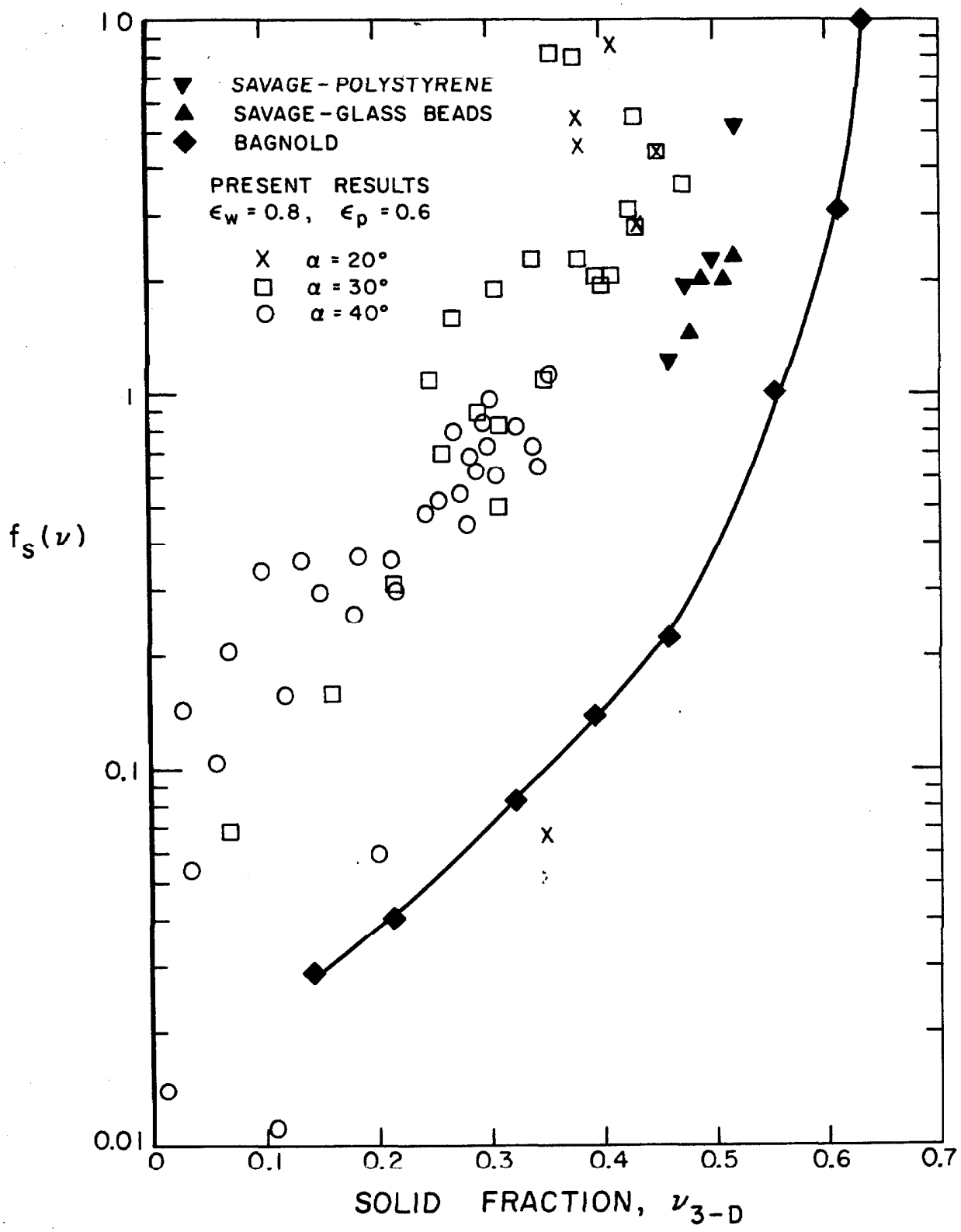

Figure 3.23 Comparison of experimentally determined values of $f_s(\nu)$, the shear stress dependence of the Bagnold/Savage constitutive law, with computed values, $\epsilon_w = 0.8$, $\epsilon_p = 0.6$.

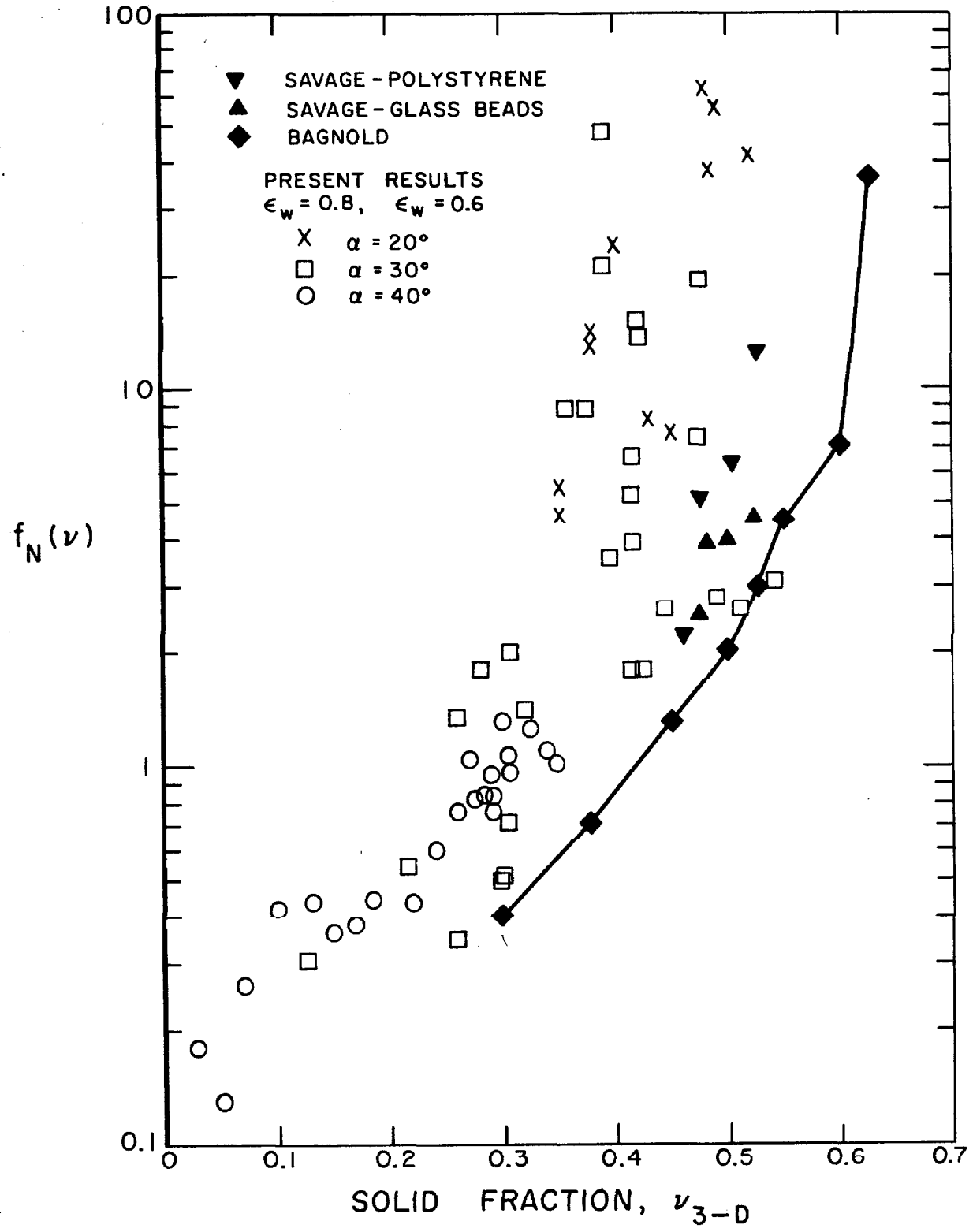

Figure 3.24 Comparison of experimentally determined values of $f_N(\nu)$, the normal stress dependence of the Bagnold/Savage constitutive law, with computed values, ($\epsilon_w = 0.8$, $\epsilon_p = 0.6$).

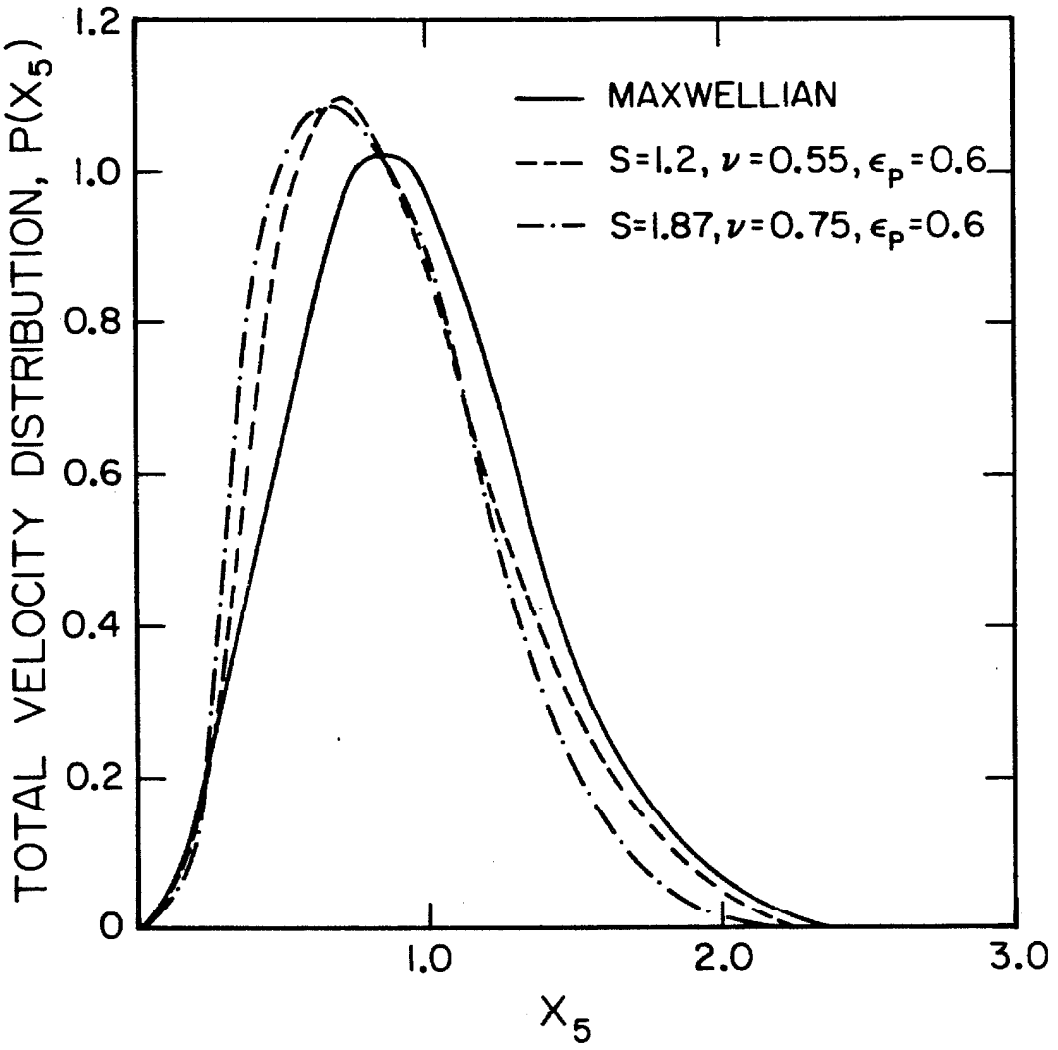

Figure 3.25 Total velocity distribution functions derived from the Couette flow simulation with the no-slip wall condition. Lines represent mean values of data points which are scattered within ±10%.

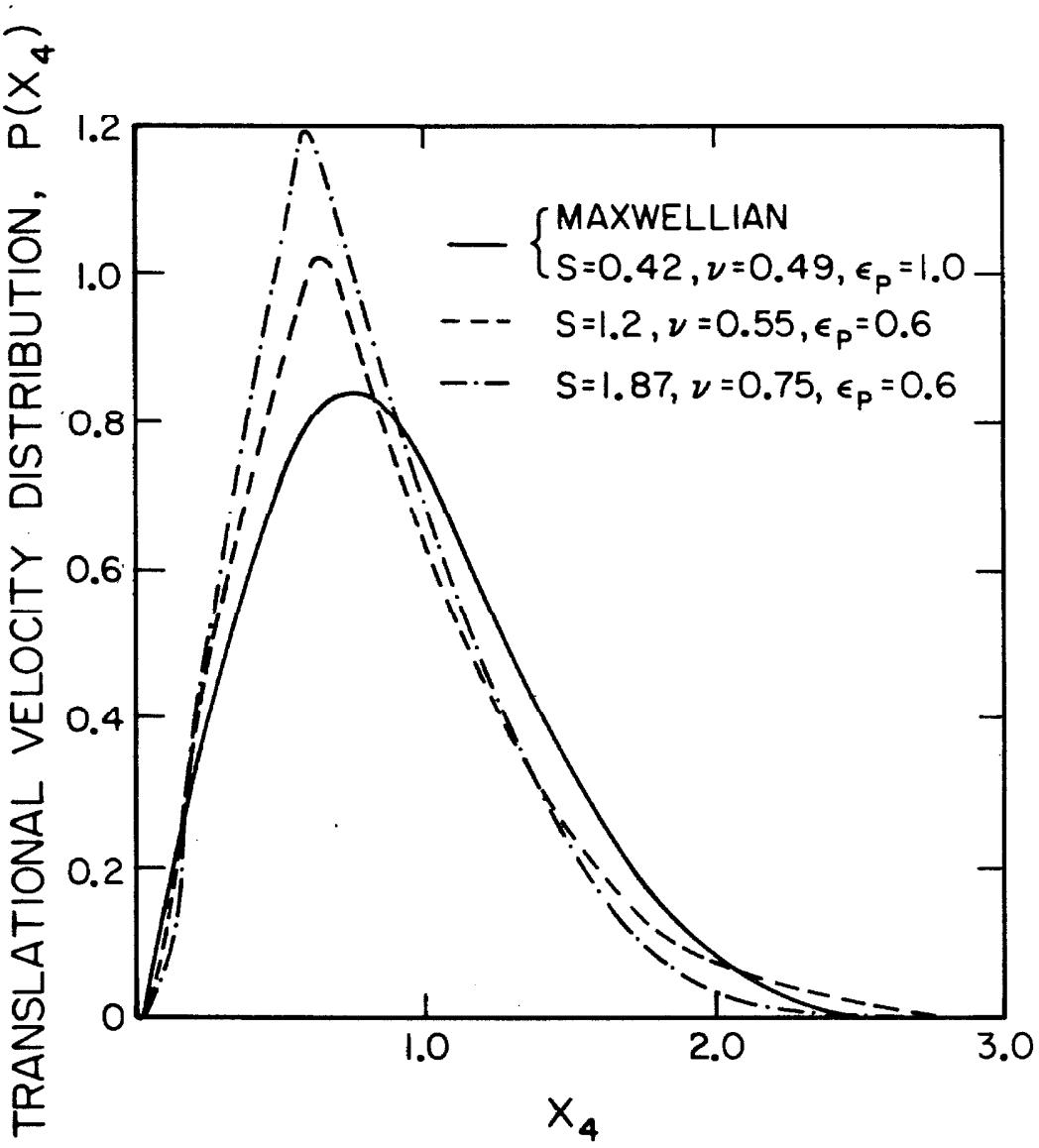

Figure 3.26 Translational velocity distribution functions derived from the Couette flow simulation with the no-slip wall condition. Lines represent mean values of data points which are scattered within ±10%.

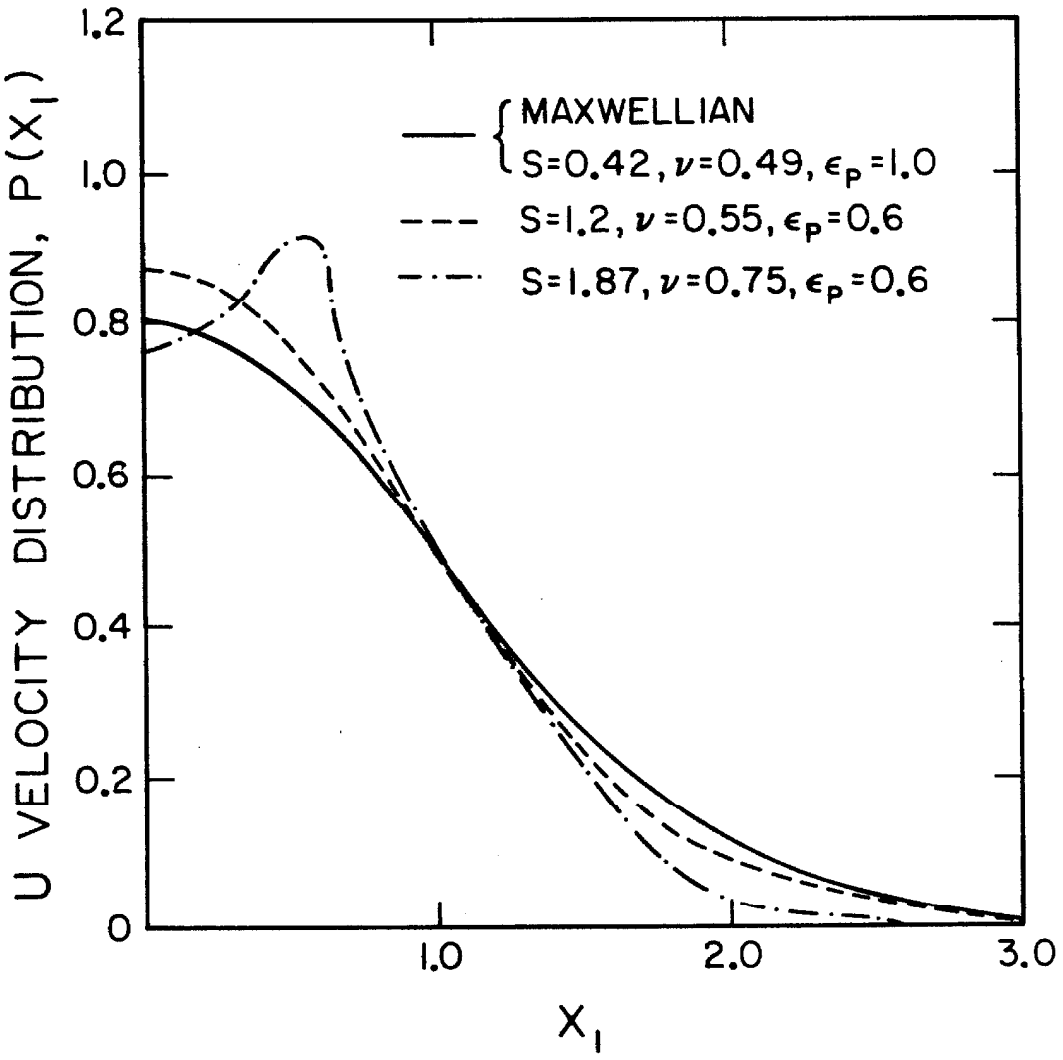

Figure 3.27 u - velocity distribution functions derived from the Couette flow simulation with the no-slip wall condition. Lines represent mean values of data points which are scattered within ±10%.

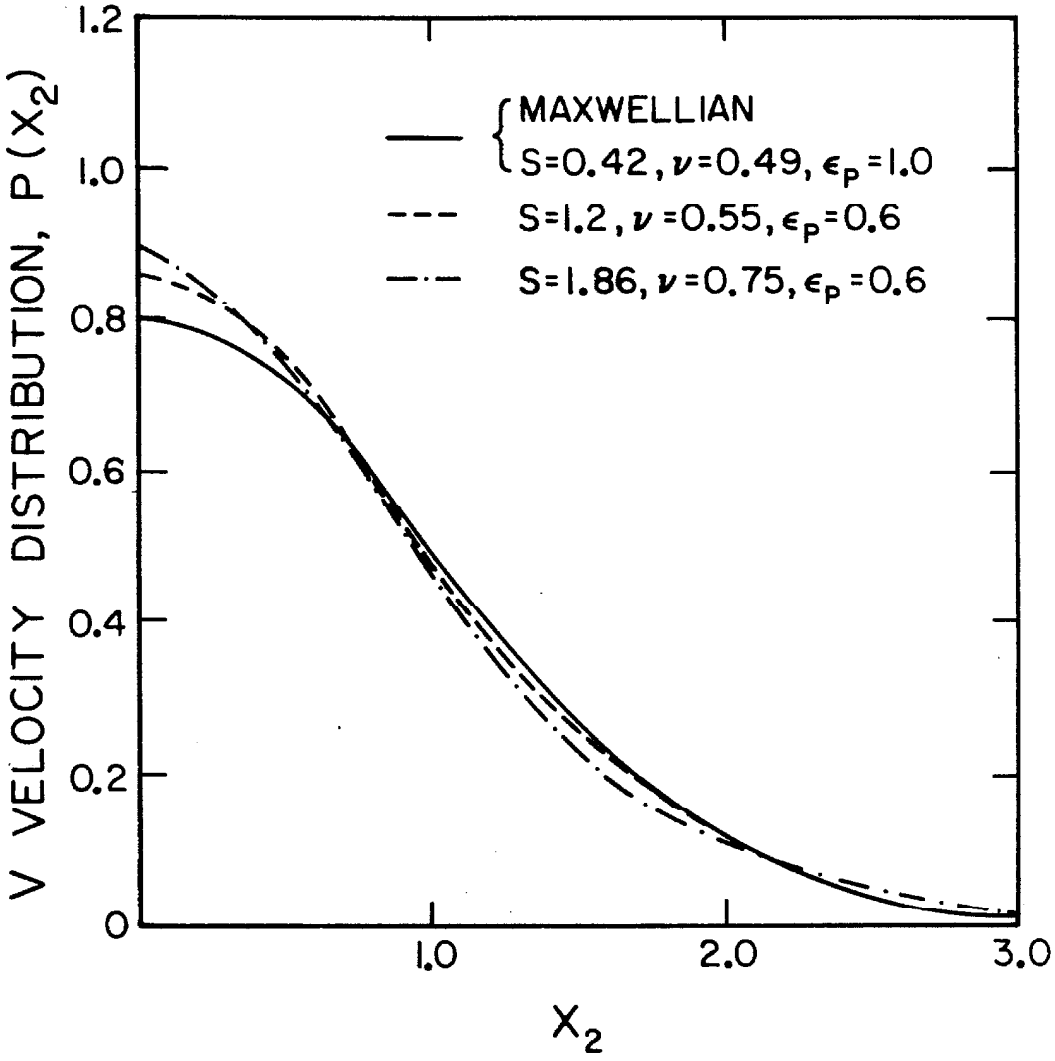

Figure 3.28 v - velocity distribution functions derived from the Couette flow simulation with the no-slip wall condition. Lines represent mean values of data points which are scattered within ±10%.

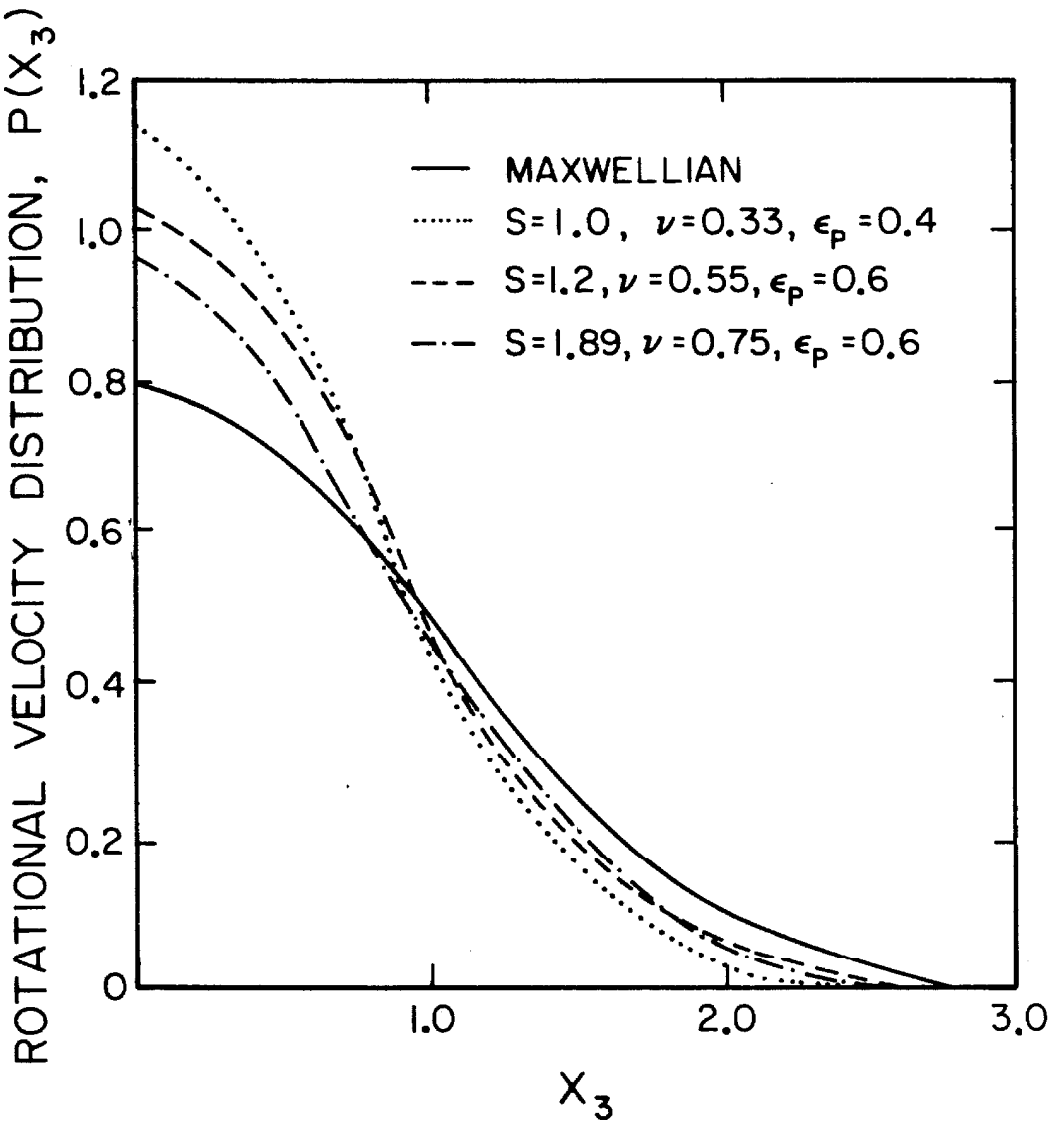

Figure 3.29 Rotational velocity distribution functions derived from the Couette flow simulation with the no-slip wall condition. Lines represent mean values of data points which are scattered within ±10%.

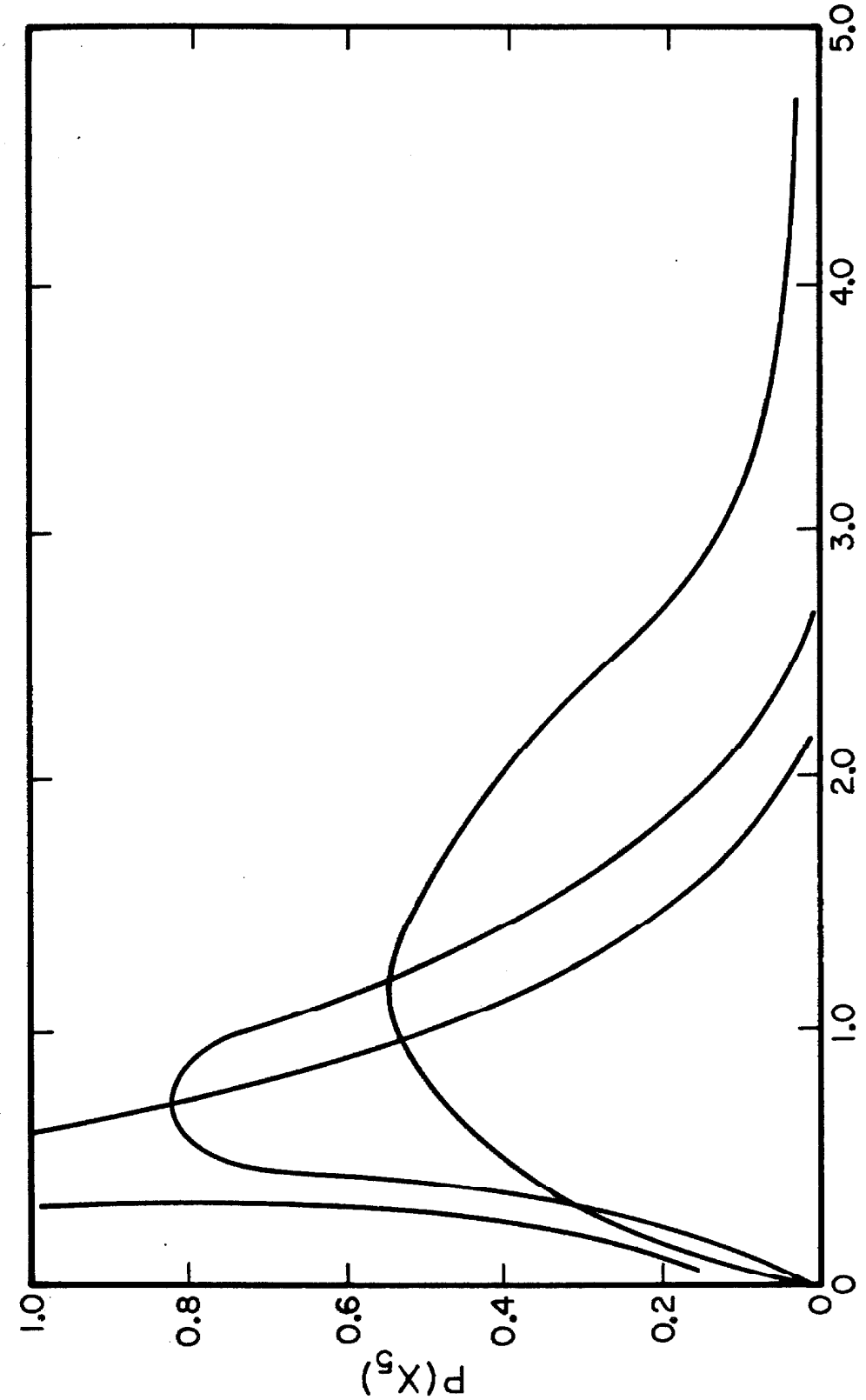

Figure 3.30 Representative total velocity distribution functions from the chute flow simulation.

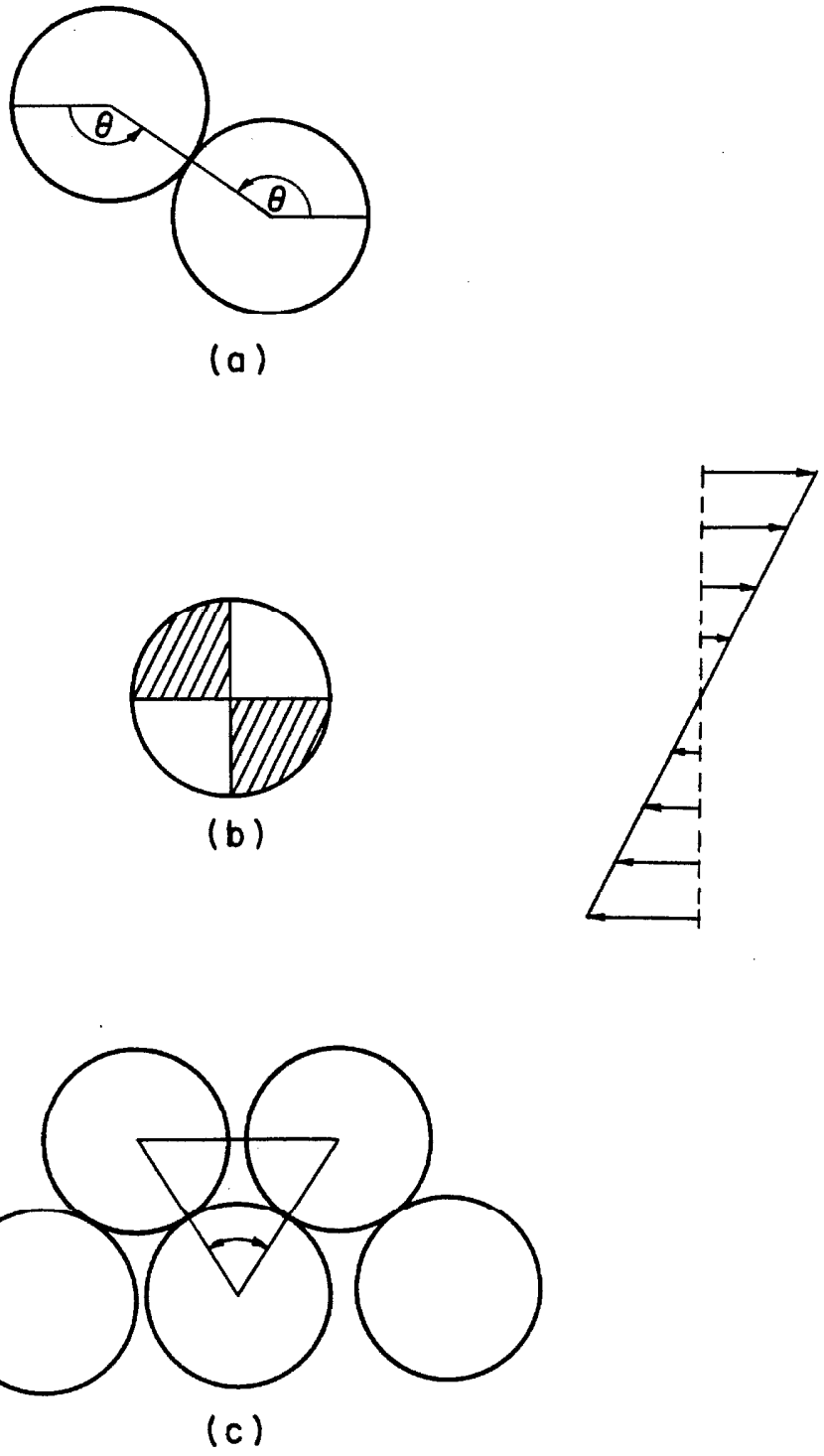

Figure 3.31 (a) definition of the collision angle θ. (b) collision anisotropy induced by a bulk shear motion. (c) Collision anisotropy induced by the formation of "layers" within the flow.

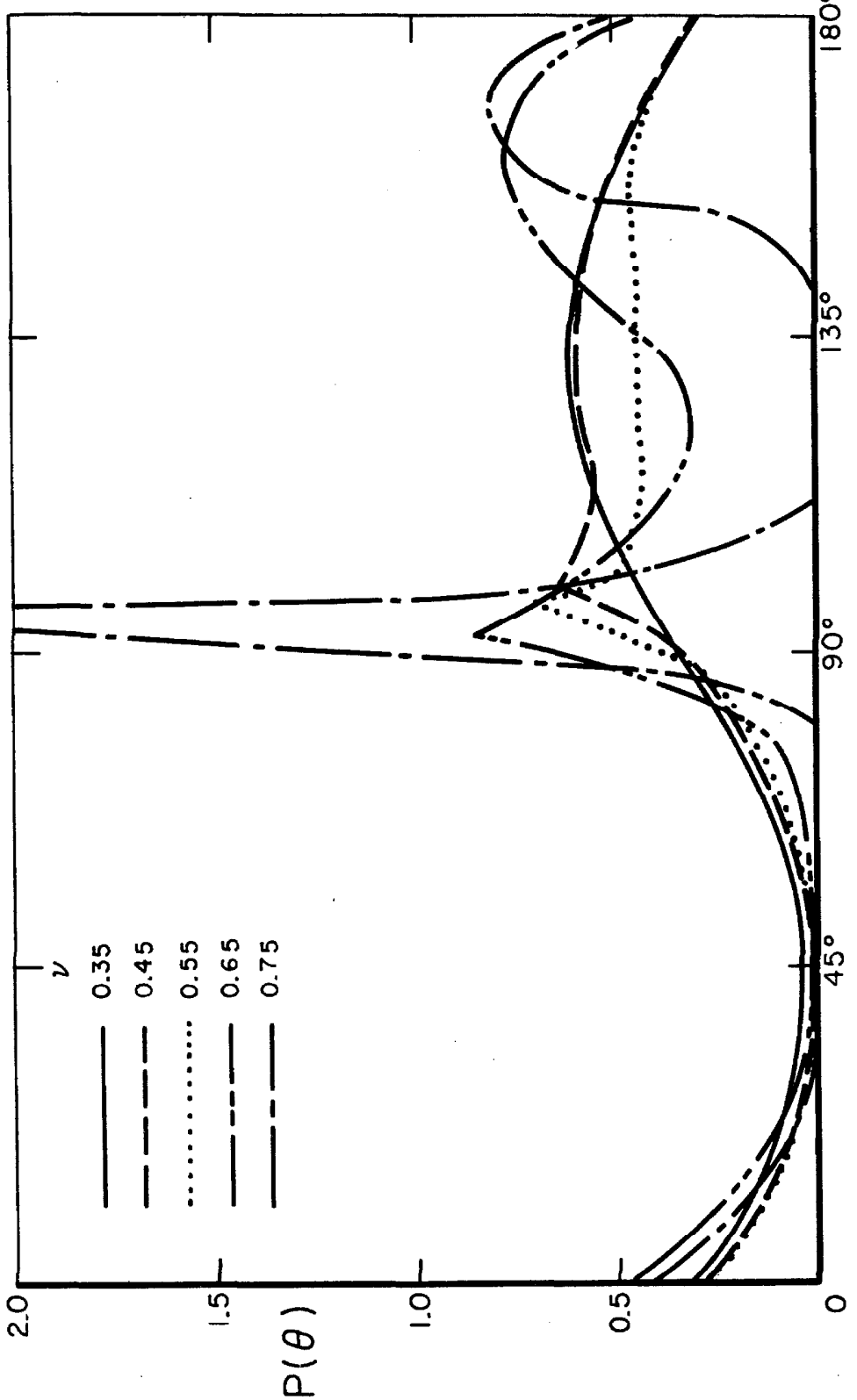

Figure 3.32 Collision angle distributions for various densities from the couette flow program with the no-slip wall condition.

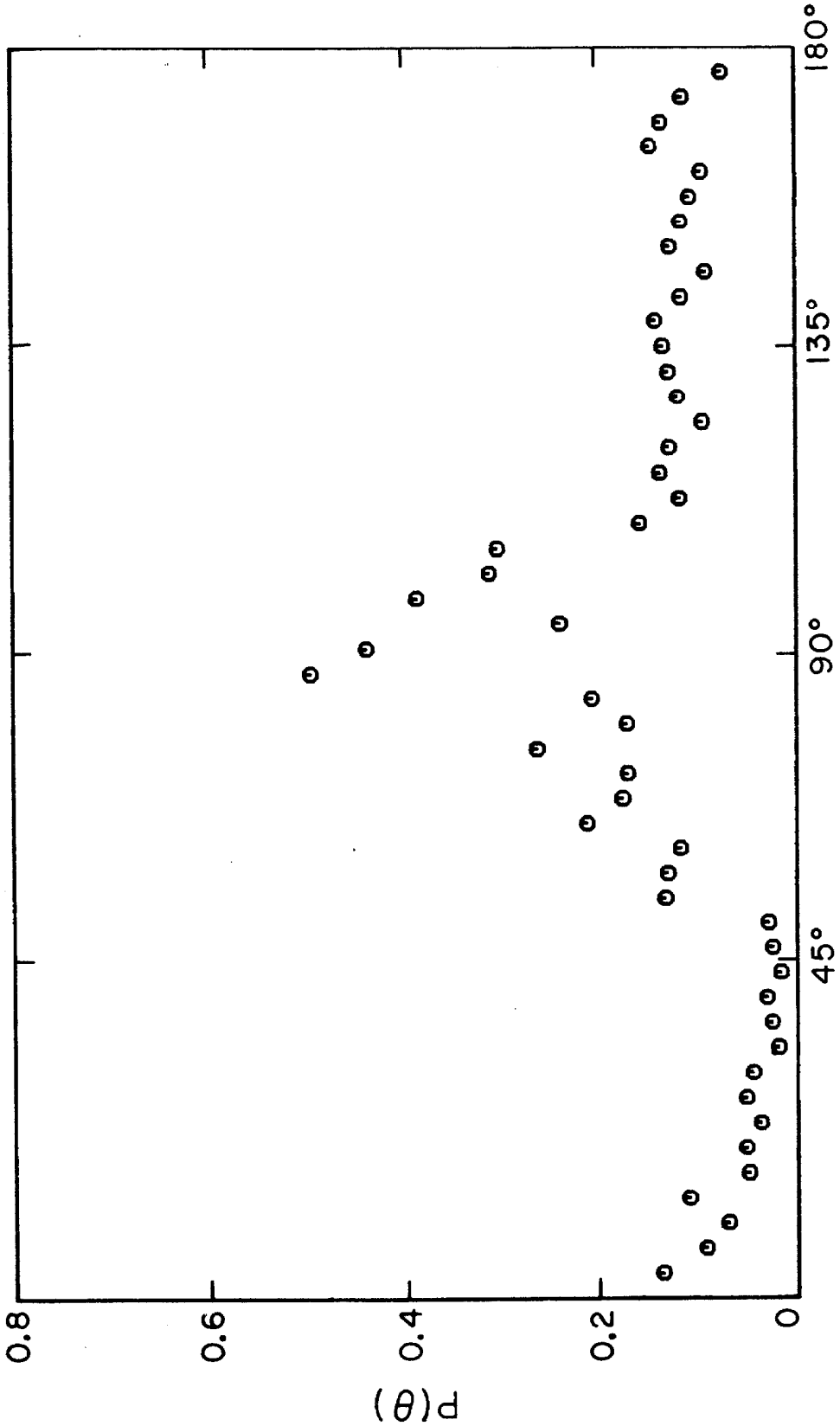

Figure 3.33 Representative collision angle distribution from the chute flow simulation. $\alpha = 40^{\circ}$, 10 x 4 particles, $\varepsilon_w = 0.8$, $\varepsilon_p = 0.6$.

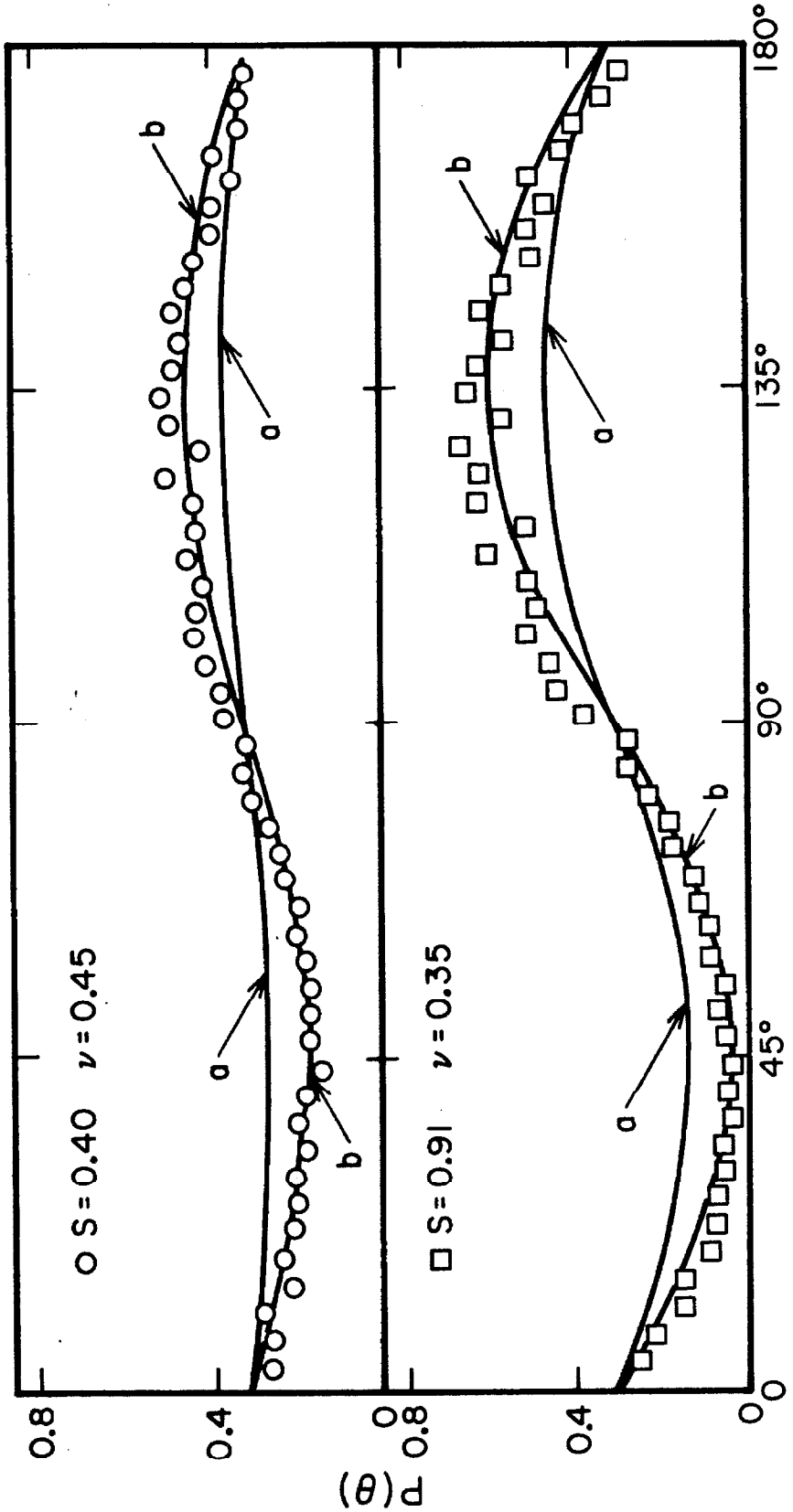

Figure 3.34 Low density collision angle distributions. (a) Predicted curve of Savage and Jeffrey [71], (b) corrected length scale. Top S = 0.40, ν = 0.45, ε_w = 1.0, ε_p = 1.0. Bottom S = 0.91, ν = 0.35, ε_w = 0.8 ε_p = 0.6.

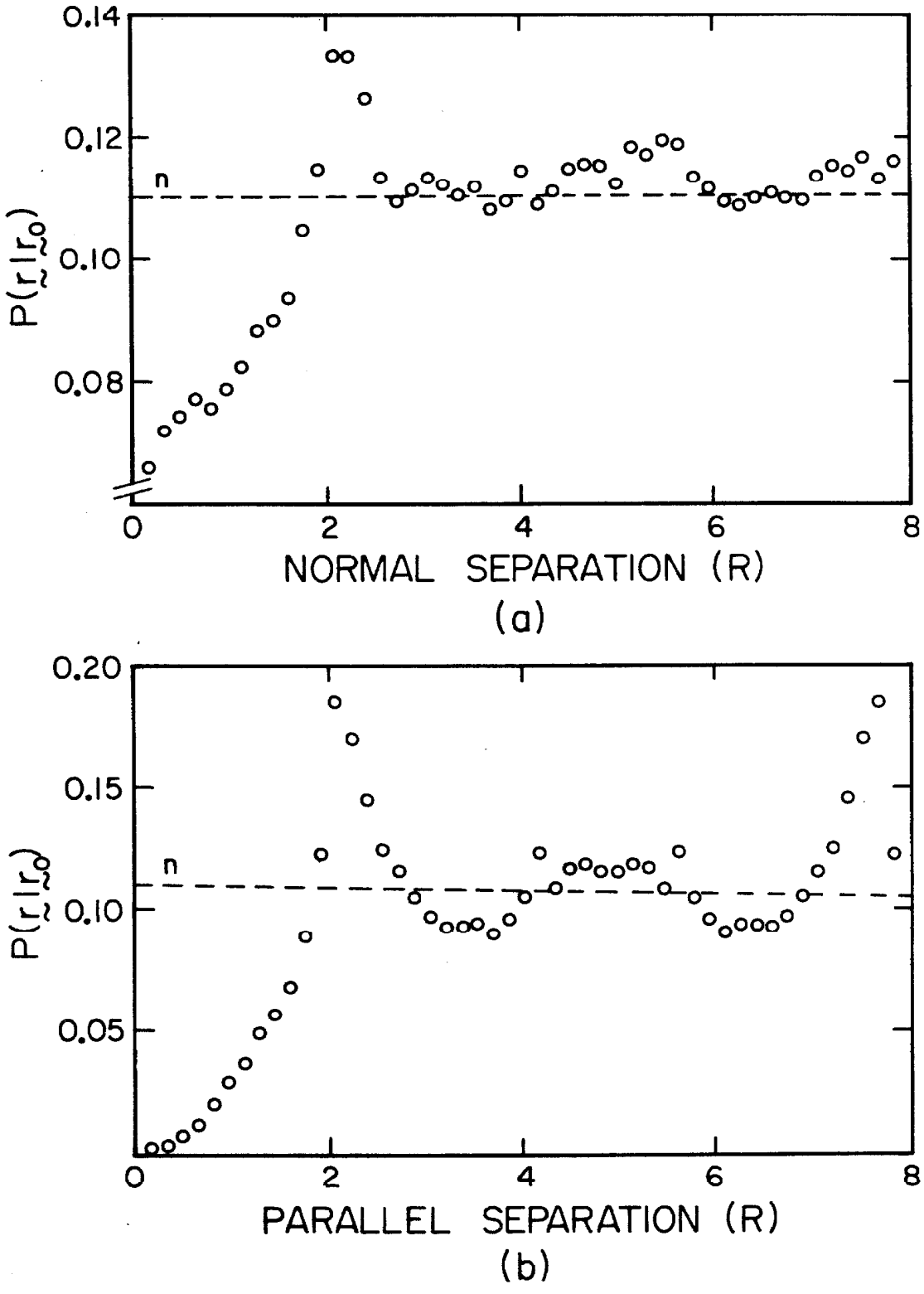

Figure 3.35 Structure within the Couette flow simulation with the no-slip wall condition. $\nu = 0.35$, $S = 0.91$, $\varepsilon_w = 0.8$, $\varepsilon_p = 0.6$. (a) normal distribution, (b) parallel distribution.

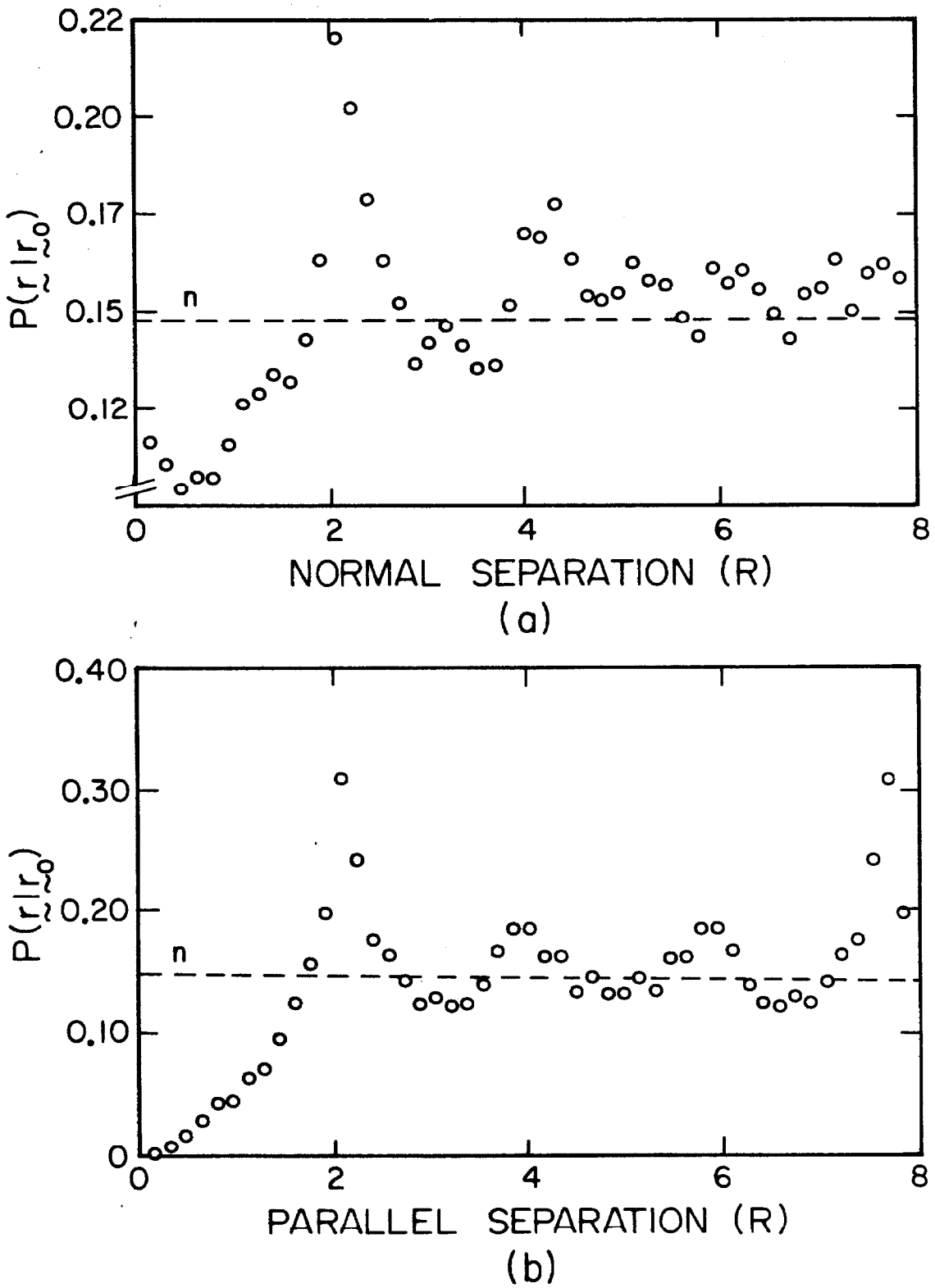

Figure 3.36 Structure within the Couette flow simulation with the no-slip wall condition. $\nu = 0.45$, $S = 1.10$, $\epsilon_w = 0.8$, $\epsilon_p = 0.6$. (a) normal distribution, (b) parallel distribution.

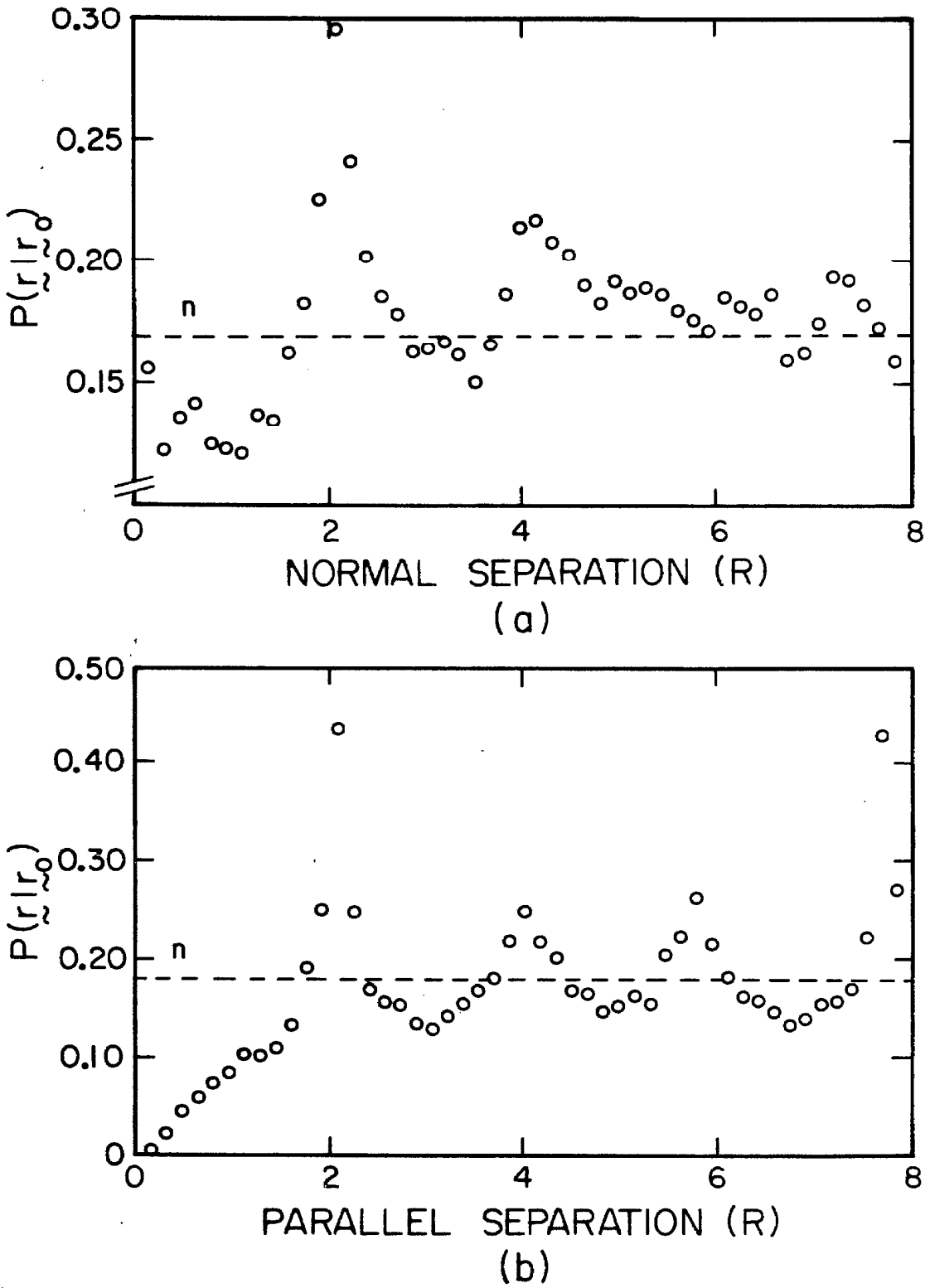

Figure 3.37 Structure within the Couette flow simulation with the no-slip wall condition. $\nu = 0.55$, $S = 1.33$, $\varepsilon_w = 0.8$, $\varepsilon_p = 0.6$, (a) normal distribution, (b) parallel distribution.

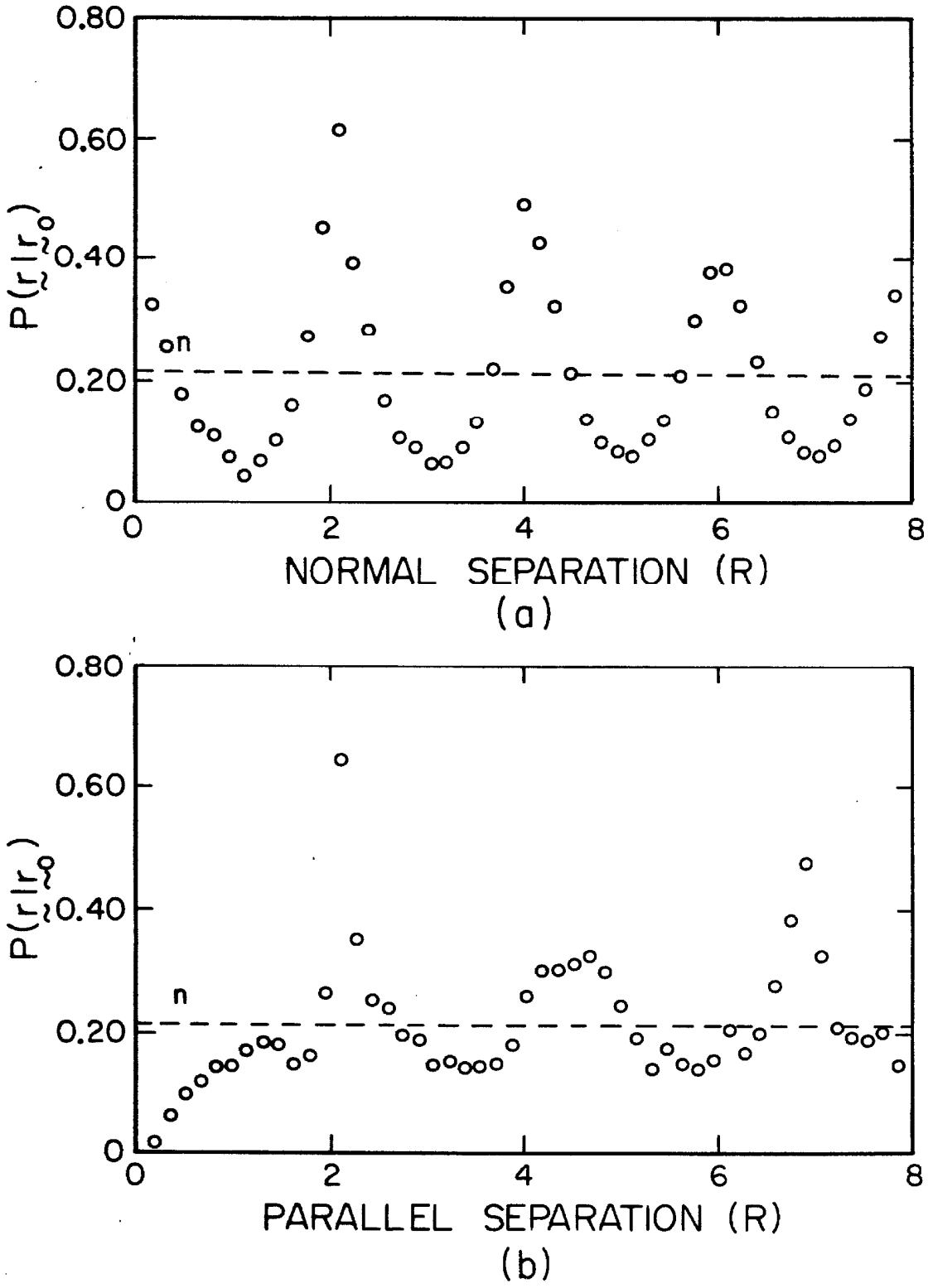

Figure 3.38 Structure within the Couette flow simulation with the no-slip wall condition. $\nu = 0.65$, $S = 1.30$, $\varepsilon_w = 0.8$, $\varepsilon_p = 0.6$. (a) normal distribution, (b) parallel distribution.

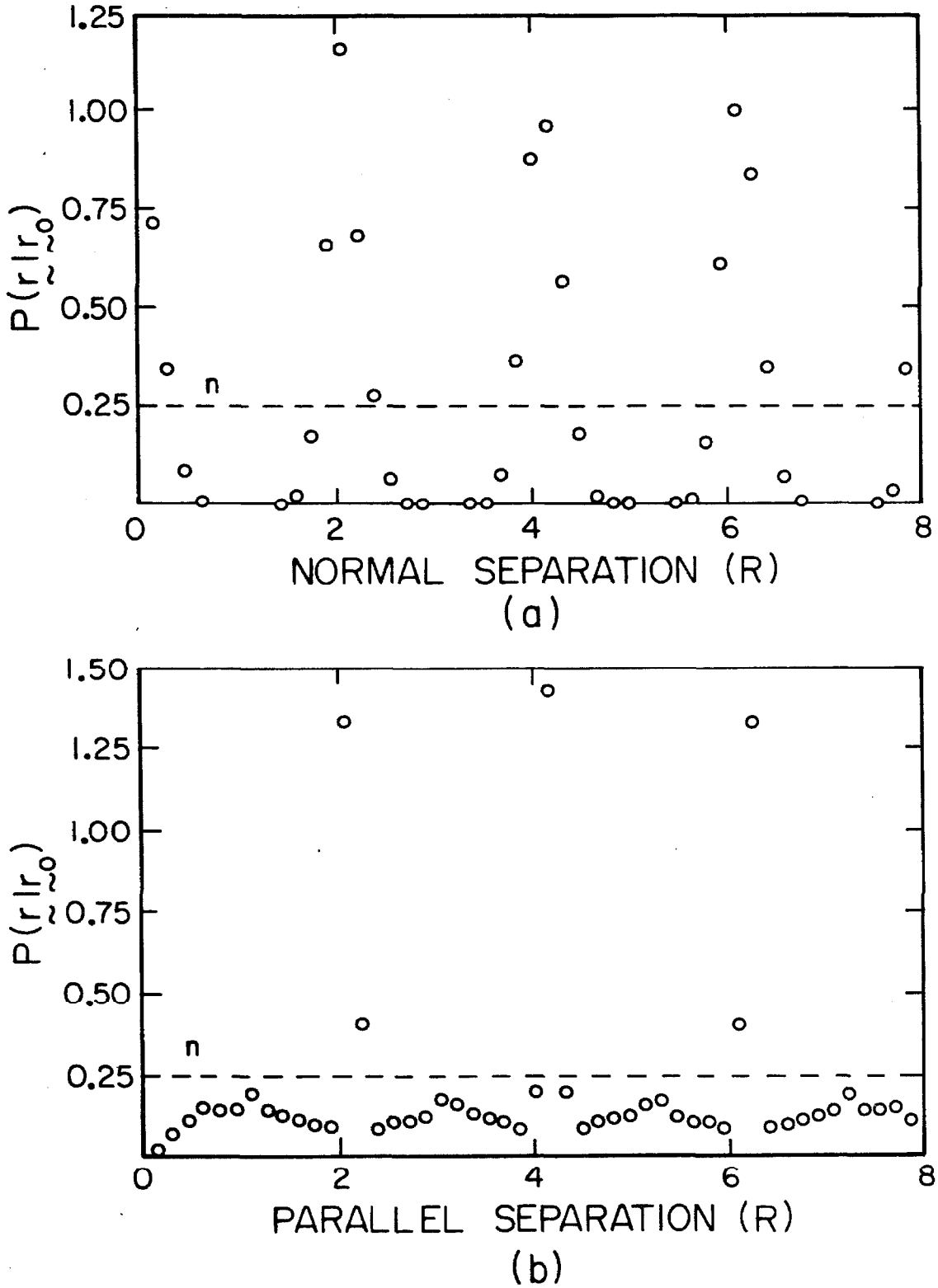

Figure 3.39 Structure within the Couette flow simulation with the no-slip wall condition. $\nu = 0.75$, $S = 1.70$, $\varepsilon_w = 0.8$, $\varepsilon_p = 0.6$. (a) normal distribution, (b) parallel distribution.

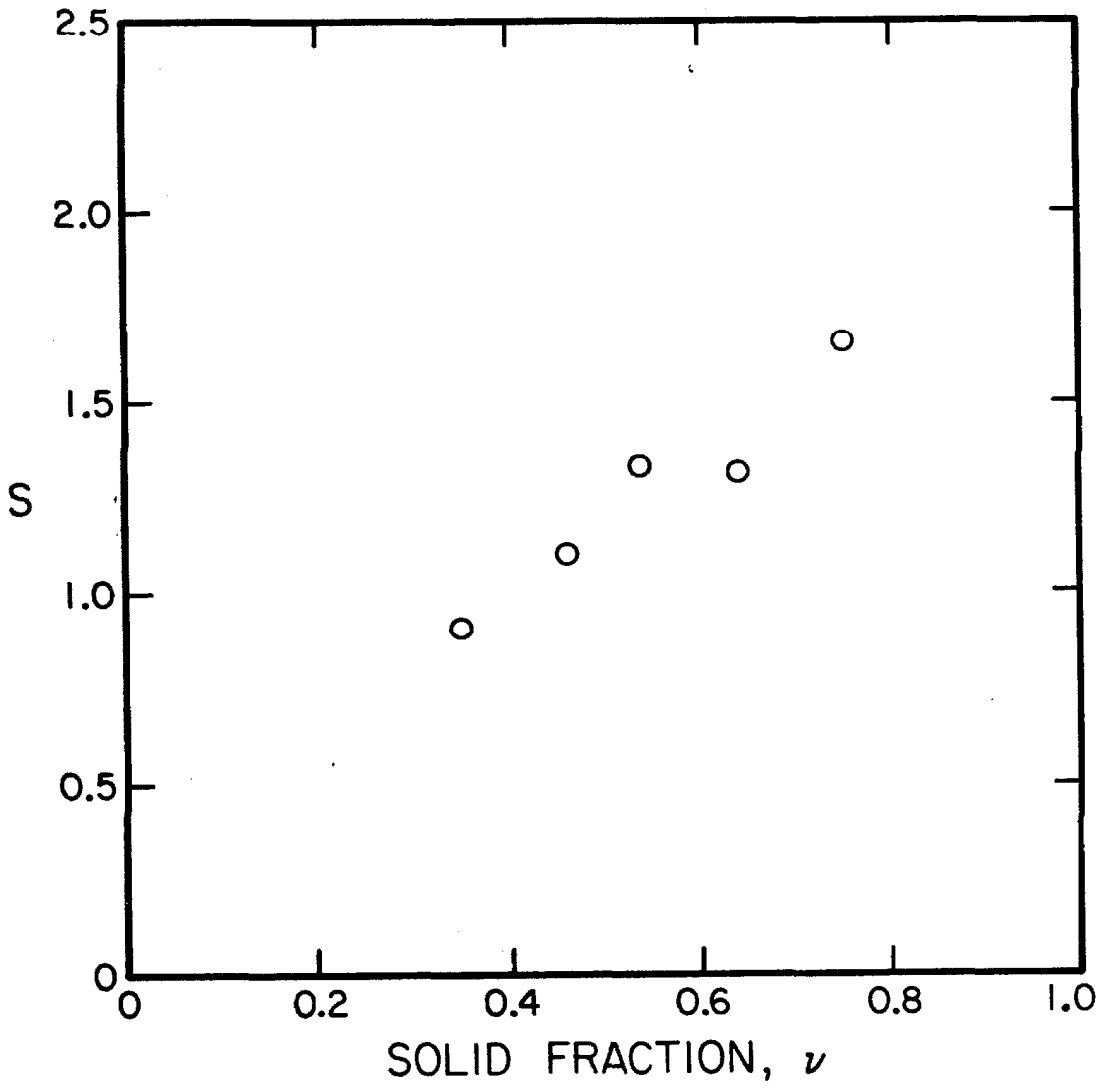

Figure 3.40 Variation of S with density in the Couette flow simulation with the no-slip wall condition. $\varepsilon_w = 0.8$, $\varepsilon_p = 0.6$.

Chapter 4

EXPERIMENTAL STUDY OF THE FLOW OF GRANULAR MATERIALS IN AN INCLINED CHUTE

4.1 Introduction

In the course of the present work a set of experiments was performed to determine some of the characteristics of granular flow in an inclined chute. A considerable amount of information has been obtained. The results do show a number of rather interesting features which may eventually be useful in formulating appropriate constitutive relations for such flows. Such conclusions have not yet been reached and the work is not considered complete. Nevertheless, it is hoped that it will form the basis for future studies and it is for this reason that some of the results available so far have been included here.

Hoppers and chutes are the two common gravity-driven devices used for transporting granular materials. Hoppers are generally used as a buffer to store materials as they arrive, and then deliver them to processing equipment on demand. It is essential that the material be able to discharge freely and, especially for perishable materials, that the material leave the hopper in more or less the same order in which it arrived. This requires that no stagnant zones or funnels should form inside the hopper, which may trap material until the hopper is emptied completely. In some large hoppers this may not happen for years.

Chutes are used to move material from one point, often a hopper's discharge, to another. An industrial chute will generally resemble a

circular pipe or duct, and not the rectangular open channel that will be examined later. It was noted by Choda and Willis [15] that when the duct fills completely with granular material, the flow will choke, causing a transition from what they called "fast flow" to "slow flow," and a corresponding drop in mass flow rate. The fast flow regime is clearly preferable. The material should not be allowed to fill the chute. Thus, despite its enclosing container, a chute flow is generally a free surface flow.

The performance requirements for a chute are roughly the same as for a hopper. It should allow free flow of material with no stagnant zones. Except in a few cases (for example, Wolf and von Hohenleighten [85]), these criteria present little difficulty to the chute designer. The flow in a chute is almost a unidirectional simple shear flow, much simpler than the converging flow inside a hopper. Consequently the problems are easy to solve; the solution generally requires a steepening of the chute angle, flaring the chute ends, or some "judicious pounding at points where stoppages occur" (Wolf and von Hohenleiten [85]).

The chute has not been an object of much pure engineering research, but because of its simple flow properties, it has been used as a model for analytical studies of granular material flow [26,42,48, 62,63,68] as well as for experimental research into their basic properties [1,2,22,62,63,68,82,83].

Takahasi [83] studied the flow of various granular materials down 150 cm long wooden chutes of various widths. The exit velocity was estimated by the trajectory of the particles as they left the

chute. He found that plots of exit velocity vs. chute angle showed a discontinuity in slope at a well-defined point. He thus defined two "modes" of granular flow which he likened to the laminar (for low chute angles) and the turbulent (for large angles) flow of liquids. (Choda and Willis [15] used the same analogy when describing their two regimes of granular flow.) The transition point was a function of the material and the chute width. In the laminar regime, the flow consisted of a thin layer of particles flowing over a bed of stagnant material, but the turbulent flow moved over the entire depth.

Roberts [62,63] developed a simple theory to explain the variations in depth and velocity along chutes and ducts of arbitrary shape. He had to assume, however, that the flow maintained a constant and uniform density, and that the friction could be accounted for by an equivalent friction coefficient that depended linearly on the flow depth. The theory compared well with his experiments on flowing millet seed in perspex chutes, but fared less well when Savage [68] tried to apply it to the flow of polystyrene beads in a rough-walled chute.

Augenstein and Hogg [2] measured the friction coefficient between thin layers of sand and both smooth and rough chute beds. They measured the exit velocity from chutes of various lengths by the same method as Takahasi. An acceleration was interpreted from the velocity differences between the different chute lengths and attributed to a balance of gravitational and frictional forces. The friction coefficients they determined depended only on the material, and were independent of chute angle, velocity, and depth.

Ridgway and Rupp [60] report a friction coefficient that varies with the inclination angle of the chute. Both Fowler and Chodziesner

[22] and Suzuki and Tanaka [82] assumed that the shear stresses on the wall always adjust to exactly balance the gravity force. This allows only uniform, non-accelerating flows, and assumes that the friction coefficient equals the tangent of the chute's inclination angle. This is not as poor an assumption as one might think. In the present study, flows at all angles appear to approach a state of uniform depth flow. This indicates that there is a dynamic component to the friction coefficient that may not have been apparent in the "thin" flows examined by Augenstein and Hogg [2].

4.2 Experimental Apparatus

The apparatus used in these experiments was modified from a chute with variable inclination angle, built as a summer project by John Pender, a senior undergraduate. A drawing and photograph of the modified chute are shown in Figures 4.1 and 4.2. The basic chute was constructed of plexiglass and supported on a frame of steel angle iron. It was 20 cm wide with 21.5 cm high walls, and a test section 2.9 m long. A hopper fed material to the top of the chute and the flow rate was controlled by a gate at the top of the test section. The material was collected in a second bin below the chute exit. This system had two major deficiencies. First, a considerable length of time was spent between runs to recycle the material from the collection bin to the upper hopper. Second, the data acquisition at the largest flow rates was very limited, sometimes as short as 10 seconds.

For the present experiments, a second movable wall was clamped on the chute to narrow the width. This reduced the mass flow rate, allowing more time to procure data, and allowed examination of the

effect of chute width.

Three chute widths were studied: 5.0 cm, 8.9 cm, 12.7 cm. With the movable wall in place, the length of the test section was reduced to 2.4 m in length. The initial depth of the flow was controlled by a second gate at the beginning of the test section. The upper gate was used only to start and stop the flow.

In the early experiments it was difficult to obtain repeatable results. This was due to an obvious accumulation of static charge on the particles as they rubbed against the plexiglass wall. After a run, particles could be seen sticking to the wall, or bouncing around as they exchanged charge, and a large charge built up on the collection bin. The problem was solved by first grounding all metal parts of the chute including the upper and lower bins, and then covering the bottom with a grounded aluminum sheet. Between runs the lucite walls were sprayed with an antistatic solution (MS-166 Enstat, Miller Stephenson Chemical Co., Inc.). After these precautions were taken it was possible to obtain repeatable results.

The basic quantities measured were the mass flow rate and the depth profile. Velocities were determined from the mass flow by assuming that the average density equals the measured critical density ρ_c. (Then $\overline{u} = \overline{m} / \rho_c bh$). The system always exhibited a starting transient. Data for a given run were collected after a steady state was reached. The flow was assumed to be steady when the depth profile stabilized.

The mass flow was determined by inserting a bucket into the flow and measuring the time it took to fill. The bucket, usually containing about 22 kgs of material, was then weighed on a scale with an

accuracy of ± 0.1 kg.

The depth profile along the chute was measured by movable point probes located for most of the experiments 0.75, 1.2, 1.65, and 2.1 m from the top of the test section. The probes consisted of brass rods, milled down to a point on one end, mounted on a vernier scale with an accuracy of 0.3 mm (about one particle diameter). Figure 4.3 is a photograph of one of the probes. In all of these experiments, despite the presence of a low density saltated layer, a distinct free surface was observed. For sufficiently small particles, a wake is formed in the surface by even the slightest insertion of the probe. The depth was determined as the point at which the wake disappears. So sensitive was the surface to the presence of the probe that it is felt its position could be determined to within one particle diameter.

To measure the surface velocity, a Bolex H16M movie camera with a 25 mm lens was mounted above the channel. During each run, colored beads were poured onto the free surface just above the frame area and photographed as they passed through the frame. The film was analyzed on a film reader to determine the surface velocity.

For most of the experiment the camera was placed so as to photograph the area beginning at and extending about six inches downstream of the second point probe from the top. When the chute was inclined at 18°, the camera had to be mounted further downstream so as not to interfere with a low false ceiling. Most of the films were recorded at 69 frames/sec, except at 18° where the flow was slow enough to allow exposure at 18 frames/sec.

The beads were colored with Kohinoor 3084-F Black Rapidraw Drafting film ink. Many methods of coloring beads were tried, but this was found to be best as it was a fast drying ink and did not leave a cohesive film on the particles.

4.3 Experimental Materials

Two sizes of spherical glass beads were used. The beads were manufactured under the brand name "Blast-O-Lite" by the Flexolite division of General Steel. They were originally intended for sandblasting purposes, but were found to have a greater uniformity of size and shape than most blasting beads. They will be referred to herein by Flexolite's designations, as BT4 and BT6, for the larger and smaller beads respectively.

The minimum error in a depth measurement will be on the order of a grain diameter. The apparent advantage of using small beads is somewhat offset by their greater susceptibility to the effects of static charge build-up.

Preliminary experiments were performed using sand and polystyrene beads. Both were found to be unacceptable materials. The sand tended to pulverize, resulting in an alteration of the material properties from experiment to experiment. The polystyrene beads were too large to give accurate depth measurements. Both materials were of non-uniform shape, would flow only at high inclination angles, and tended to form stagnant wedges on the chute bottom (see Section 4.5).

The properties of the test materials are shown in Table I. All properties were measured by the methods described in Pearce [55].

TABLE I

	BT4	BT6
Mean Particle Diameter (mm)	0.48	0.262
Standard Deviation (mm)	0.101	0.037
Particle Specific Gravity	2.5	2.5
Critical Specific Gravity	1.44	1.43
Critical Solid Fraction	0.58	0.57
Internal Friction Angle	25.8°	16.0°
Wall Friction Angle		
Smooth Aluminum	13.2°	15.95°
Rough Aluminum	18.2°	17.35°
Plexiglass	15.73°	18.6°
Angle of Repose	26.5°	24.0°

4.4 The Mass Flow Rate from Granular Chute Flows

Like a hopper, a chute is required to be able to deliver material at a given rate. Chutes are extremely efficient devices, and it is not difficult to build a chute that will meet any need. A chute will generally be fed from a hopper, and the flow rate from the chute-hopper system will, in most cases, be controlled by the hopper. Still, it is necessary for the designer to have some guidelines on how much material will be transported by a chute as a function of geometry and inclination angle, and to have some knowledge of the conditions under which the chute will limit the flow rate.

The mass flow from the chute used for the present experiments is controllable only by varying the gate opening and the inclination angle. Figure 4.4 shows the mass flow per unit width from the chute set at an angle of 22° for the three chute widths. In all three cases the mass flow follows a common curve until, at some opening peculiar to the chute geometry, the mass flow becomes a constant, independent of the gate opening. This point will be referred to hereafter as the "independence point."

The effect of chute inclination on mass flow rate for a single chute width is shown in Figure 4.5. Independence points can be observed for all angles less than and including 25°. Up until this point there is surprisingly little effect of the inclination angle on the mass flow rate.

By comparing the two pieces of information presented above, it may be concluded that the location of the independence point, which places a limit on the mass flow obtainable from a given chute, is a

function of chute geometry and inclination angle.

The independence point marks a transition in the flow conditions downstream from the gate. At that point the flow changes from what shall be called "supercritical flow" to "subcritical flow." More suggestive titles might be "upstream dominated" or "downstream dominated" flows. The flow type depends on the value of the Froude number:

$$Fr = \frac{\bar{u}}{\sqrt{gh}} = \frac{\dot{m}}{\rho_c b \sqrt{g}\, h^{3/2}}$$

If the Froude number is greater than some critical value, the flow is called supercritical and the flow rate is governed by upstream conditions, in this case the upper gate opening. If the Froude number is less than the critical value, the flow is called subcritical; the Froude number will increase along the chute to reach a critical value near the chute exit, and the flow rate will be governed by downstream conditions. These flow types will be discussed in detail in Section 4.5. They have been introduced here because of their effect on the mass flow rate. In the next two sections the flow rate in each regime will be discussed independently.

4.4.1 Supercritical Regime

As long as the flow within the chute remains supercritical, the mass flow rate will depend on the flow in the immediate vicinity of the gate. A diagram of that area is shown in Figure 4.6. Two stagnant zones are generally visible, one (A) directly behind the gate itself, and the other (B) on the chute bottom. The location of (B) and the size of both zones will depend on the gate opening and the flow rate.

Ignoring (B) for the moment, the flow pattern is reminiscent of that near the mouth of a half-hopper divided down the middle by the chute bottom, with walls perpendicular to the flow direction. It would be expected that the flow rate would be similar to that from a hopper with some correction for the chute inclination.

The mass flow rate may be characterized dimensionlessly in the form of a Froude number,

$$Fr = \frac{\bar{u}}{\sqrt{g\ell}}$$

where ℓ is some length scale. The mass flow rate may then be determined by the relation:

$$m = \rho_c b h \, Fr\sqrt{g\ell}$$

As the mass flow rate is expected to depend on the conditions at the gate, h is assumed to be the gate opening, h_g, and ℓ will be some length scale characteristic of gate conditions.

It was determined that the dependence of the Froude number on gate geometry may be characterized by choosing ℓ to be the hydraulic radius,

$$Hy = \frac{A}{P}$$

where A is the area, and P the perimeter of the gate opening. For the rectangular openings

$$Hy = \frac{h_g b}{2(h_g + b)}$$

The Froude number so defined at the gate, Fr_g, was found to fit the correlation

$$Fr_g = \frac{\bar{u}}{\sqrt{gHy}} = 2K \sin \alpha$$

where K is some constant characteristic of the material and has a value close to unity. This correlation is illustrated in Figures 4.7 and 4.8. Those results indicate $K_{BT6} \simeq 1.0$, $K_{BT4} \simeq 0.9$. The large scatter in the data may be attributed to the position of stagnant zone B shown in Figure 4.6, which approaches the gate at large openings (and may even extend through), effectively reducing the gate opening.

One would expect that this correlation bears some relationship to the flow in hoppers. Both Pearce [55] and Nguyen [47] have measured the flow rate from two-dimensional hoppers with various wall angles. They found that the Froude number, Fr_d, from a hopper with a 90° wall angle was

$$Fr_d = \frac{\bar{u}}{\sqrt{gd}} = 1$$

where d is the width of the hopper opening. The flow near the gate is reminiscent of that in a half-hopper, so it is logical to assume that

$$d \simeq 2\,hg$$

A two-dimensional hopper has effectively an infinite breadth. The appropriate value of the hydraulic radius is

$$\lim_{b \to \infty} Hy = \lim_{b \to \infty} \frac{h_g b}{2(h_g + b)} = \frac{h_g}{2} = \frac{d}{4}$$

From the predicted correlation,

$$Fr_d = \frac{\bar{u}}{\sqrt{gd}} = \frac{\bar{u}}{\sqrt{g\ 4\ Hy}} = \frac{1}{2}\ Frg = \left.\frac{2K \sin\alpha}{2}\right|_{\alpha=90°} = K \simeq 1$$

This agrees with the measured results of Pearce [55] and Nguyen [47], and confirms that the flow through the gate does indeed determine the flow rate in a manner similar to that of a 90° hopper.

4.4.2 Subcritical Regime

In the subcritical regime the mass flow rate becomes effectively constant. Increasing the gate opening no longer changes the flow rate. The mass flow is determined by conditions downstream of the gate. The effects of the chute bottom, side walls, and exit, control the flow. The flow rate may only be altered by changing the chute geometry. The maximum flow rate obtainable from a chute of fixed geometry is effectively the flow rate at the independence point.

The maximum mass flow rates obtained in these experiments are plotted in Figures 4.9, and 4.10 as a function of chute geometry and inclination angle.

The ratio of chute length to breadth (L/b) is chosen as an appropriate dimensionless quantity characterizing the chute geometry. Only the chute width was varied in these experiments, but the effect of chute length has been noted elsewhere: Subcritical flows appear at only extremely shallow angles in the short (0.9 m long, L/b = 12) chute used by Spelt [75,76]. Choda and Willis [15] noted that their fast flow/slow flow transition (which by their description appears to be similar to that observed in the present results) could be induced by attaching a length of straight chute to the end of their duct.

In these experiments, L/b was varied from 19 to 48. Takahasi [83] used chutes with values as high as L/b = 500.

It should be noted that L/b is used here only for convenience. It is not suggested that the maximum mass flow rate is a single-valued function of L/b. Comparing Figures 4.9 and 4.10, the maximum mass flow rate can be seen to be a function of the flowing material, and is probably also a function of the chute material and surface characteristics. More important, it is shown by Roberts [62,63] that the friction coefficient on the side walls is much smaller than that on the chute bottom. One might then expect that a long wide chute would have a smaller maximum mass flow than a short narrow chute with the same L/b. This has yet to be confirmed experimentally.

4.5 Supercritical and Subcritical Flows

Supercritical and subcritical conditions represent conjugate states of open channel flows of liquids. A given flow rate may have either a supercritical or subcritical Froude number, and may transition between the two. Such behavior in granular flow is evidenced in Figure 4.4, where for a small range of gate openings the flow rate can assume either a supercritical (gate dependent) or a subcritical (downstream dependent) value.

Fluid systems change from supercritical to subcritical flow via a hydraulic jump, and from subcritical to supercritical flow via an expansion wave. Both phenomena were observed for granular material flows during the present study. The profile of a granular hydraulic jump is much smoother and better defined than its fluid counterpart.

Hydraulic jumps in granular chute flows have been studied and analyzed by Brennen, Sieck, and Paslaski [11], Savage [68], and Morrison and Richmond [42].

The critical Froude number, Fr_c, relative to which a flow is classified as supercritical or subcritical, defines the propagation speed of small disturbances through the material. Consider an infinitesimal depth change dh of zero extent (dx = 0). Then the general equation for open channel flow derived in Appendix A becomes:

$$(\Gamma \cos \alpha - \gamma \, Fr^2) \, dh = 0$$

This defines the critical Froude number:

$$Fr_c = \left(\frac{\Gamma \cos \alpha}{\gamma}\right)^{1/2}$$

which has a corresponding critical velocity

$$V_c = Fr_c\sqrt{gh} = \left(\frac{\Gamma \cos \alpha}{\gamma}\right)^{1/2} \sqrt{gh}$$

which is the propagation speed of small disturbances. This must then be the speed at which an expansion wave will move into flow of depth h.

4.5.1 Subcritical Flow Control

At the exit, the chute bottom disappears with a corresponding dropoff in the surface of the flow. An expansion wave, propagating with the critical velocity, would try to communicate this information upstream. However, it cannot propagate into a flow moving with a velocity greater than or equal to the critical velocity. If the flow in a chute is to be subcritical at a point, then somewhere downstream,

before the chute exit, the flow must become critical. Generally this will occur slightly upstream of the chute exit.

In supercritical flows, critical conditions also occur at the gate. Otherwise, an expansion wave would travel up through the opening so that material will no longer be held behind it. Varying the gate opening while maintaining critical conditions at the gate controls the mass flow. From the correlation reported in Section 4.4.1, the critical Froude number at the gate is found to be:

$$Fr_c = \frac{\bar{u}}{\sqrt{g\, h_g}} = Fr \sqrt{\frac{b}{2(h_g + b)}} = 2K \sin\alpha \sqrt{\frac{b}{2(h_g + b)}}$$

It is expected that the downstream control of the mass flow rate for subcritical flows is also evidenced by critical conditions near the chute exit. Special experiments were performed to test this hypothesis. For these experiments, a point probe was placed 2cm from the chute. Knowing the mass flow and the depth at the exit, the Froude number is determined. Three more point probes were placed at 25cm intervals upstream of the exit so that the approach of quantities toward their exit values could be determined.

Figure 4.4 is a plot of the exit Froude numbers as a function of inclination angle and L/b. All of the flows represented were subcritical. These data were obtained from a wide range of gate openings. The relatively small scatter indicates that the flow is assuming a critical Froude number at the exit.

Controlling the Froude number at the exit is not sufficient to explain why the mass flow rate becomes independent of the gate opening. It only predicts a relationship between the mass flow and the exit depth or velocity:

$$\frac{m}{b} = \rho\, \bar{u}_e h_e = (\rho\, Fr_e\, g^{1/2})\, h_e^{3/2} = \left(\frac{\rho}{g\, Fr_e^2}\right) \bar{u}_e^3$$

Either h_e or u_e must be fixed, as well as Fr_e.

Plots of exit depths and velocities for various angles and chute geometries (again from subcritical flows) are shown in Figures 4.12 and 4.13. As expected, there is very little scatter in the individual points, even though the gate openings change by a factor of 3. These plots give an indication of just how complicated the exact flow mechanics may be. Both $u_e/\sqrt{gb}$ and h_e/b decrease with L/b for $\alpha = 22°$, remain fairly constant for $\alpha = 20°$, and increase for $\alpha = 18°$.

An intriguing aspect of this phenomenon is that critical depths and velocities, and the critical Froude numbers, are independent of their values directly upstream of the exit. Figures 4.14 and 4.15 are typical examples showing the approach of the depth and Froude numbers toward their critical values. In all cases, the curves approach the same limiting values but along unique paths.

At the moment, no explanation can be given for this phenomenon. However, future investigators may find the equation derived in Appendix A a helpful starting point:

$$(\Gamma \cos \alpha - \gamma Fr^2)\, dh = \left(\sin \alpha - \frac{\overline{\tau_w} P}{\rho_p \nu_c g\, bh}\right) dx$$

$$Fr_e^2 = \frac{\Gamma \cos \alpha}{\gamma}$$

at the chute exit. This expression may be used to determine back water curves for depth or Froude number. By measuring the depth profile and the friction term, a relationship between the profile parameters, Γ and γ, could be determined which may in turn yield some insights into the behavior of the flow.

4.5.2 General Features of Supercritical and Subcritical Flows

Supercritical flows are generally much faster and shallower than their subcritical counterparts. The phenomenological differences between supercritical and subcritical flows are clearly shown for $\alpha = 22°$ by the depth profile in Figure 4.19. A small increase in gate opening produces a four-fold increase in depth and the appearance of "breaking" (see Section 4.7). The free surface of a subcritical flow has a distinct structure. Except in the area immediately adjacent to the side walls (where the material shears in a direction parallel to the free surface), particles on the surface maintain the same relative positions. The material appears to move like a solid plug, sliding on a thin shearing layer next to the chute bottom. Near the gate the solid plug structure is also visible through the side walls. Further downstream the flow appears to shear all the way across its depth, but the surface far from the walls retains its distinct structure. On the basis of this last observation, the author is convinced that the shearing visible through the side wall is a peculiarity of the region next to the wall.

No distinct structure can be observed on the surface of supercritical flows. The surface always appears blurred, due to violent mixing in the interior.

4.5.3 Transition between the Flow Regimes

Immediately after the gate is opened, the flow is always supercritical. The leading edge sees no material downstream and cannot have any knowledge of the downstream conditions. The transition to subcritical flow is very gradual and may not even begin for as long as thirty seconds after the gate is opened. During the transition the depth of flow will oscillate as it approaches equilibrium, just as if small hydraulic jumps and expansion waves were carrying the downstream information to the rest of the flow. The distinct wavefront of a hydraulic jump, that is generated by placing a downstream obstruction in the chute was not observed although the expansion waves could be seen clearly. When both conjugate states are very close to the critical value, the system may experience relatively fast ($\sim$ 10 second period) oscillations between them.

The point of transition to subcritical flow was found to depend strongly on environmental conditions. Experiments performed in the summer were repeatable within a few days, but could not be repeated exactly in November, although similar phenomena were observed. Presumably this is the result of changes in humidity which indicate different dissipation rates for static electric charges.

The "laminar-turbulent" transition reported by Takahasi [83], and the "slow flow / fast flow" transition reported by Choda and Willis [15] for enclosed ducts are similar to the transition described here. None

of the authors report Froude number data, but their qualitative descriptions of their flow regimes agree with the present observations.

A transition between the flow types may be observed at any angle by placing a blockage in the channel which generates a hydraulic jump. The transition described earlier is found in unblocked chutes; the equivalent downstream disturbance is generated by the chute geometry (and was more likely in narrow chutes). Subcritical flows were not observed in our chute for inclination angles greater than 25°, but Takahasi observed transition in extremely narrow chutes at angles as high as 45°. A plot of Takahasi's data for transition angle versus chute geometry is included in Figure 4.16.

The flows in the present study had to be sufficiently deep before transition occurred. This makes comparison with Takahasi difficult because he made no attempt to control the depth of his flow. The depth was determined naturally by the feed supply to his chute system. He found a distinct inclination angle at which transition occurred for each chute geometry, while the present results indicate that both types of flow could be obtained at the same angle by varying the gate opening. In this light, Takahasi's transition point may be interpreted as the maximum inclination angle at which subcritical flows may be observed. For comparison purposes, some of the present data, extracted according to the above interpretation, is also plotted in Figure 4.16. Unlike Takahasi's, the chute angle in the present work was not continuously varied. The data shown in Figure 4.16 must be read as the largest of the angles studied (18°, 20°, 22°, 25°, 30°, 38°) at which subcritical flows were obtained. The transition for the glass beads

used in this study occurred at much smaller angles than Takahasi's. In fact, the transition occurred at angles where Takahasi's sand probably would not even flow.

The main difference between the present observations and Takahasi's is that his "laminar" regime is associated with the appearance of a stagnant wedge on the chute bottom. Stagnant wedges accompanying subcritical flows were also observed in these studies, but only at large gate openings. A stagnant wedge is essentially the continuation of stagnant zone B out through the gate and into the chute (see Figure 4.6). A wedge extending far into the chute is shown in Figure 4.17. The deeper the depth, the further down the chute the stagnant wedge would extend. In no case was the wedge allowed to extend as far as the first point probe location.

Subcritical flows occurred for a wide range of depths without any stagnant wedges. This is one of the benefits of using size-sorted glass beads as a test material as opposed to the various types of sand used by Takahasi. Sand tends to pulverize. The smaller particles fill the gaps between the larger, producing a bulk material that is difficult to shear. Sand flows wedge much more readily than glass beads.

The flow slows a great deal as it transitions to subcritical. The shear rate and the granular temperature (see Section 3.1.1) of the flow will proportionally drop. Thus stagnant regions and plug flows will be much more likely to develop. Hence it is the transition to subcritical flow that brings about the formation of the wedges, and not the other way around.

It is standard practice to prevent blockage by flaring the ends of industrial chutes (see Wolf and Van Hohenleighten [85]). This decreases the depth of the flow far downstream, increasing the Froude number above the critical value. Transition is thus avoided. Industry has once again provided a solution for a problem that had not yet been fully understood.

4.6 Depth Profiles

Figures 4.18 through 4.23 illustrate the variation in flow depth along the chute for various values of the gate opening and chute inclination. Almost all the profiles show the same general behavior. There is always the sharpest decrease in depth as the flow accelerates out of the gate. Even at large inclination angles, most of the depth change occurs between the gate and the first point probe. Even though the flow appears to approach a state of constant depth (uniform) flow, this is just the parabolic depth profile that characterizes a flow with more or less constant acceleration.

The exception to this rule can be seen in the depth profiles that correspond to subcritical flows. In many of these the flow appears to approach a uniform value, but will then "break" and undergo further acceleration, suffering a large depth change over a relatively short length of the chute. The break is visible through the chute side wall and has a well defined location.

It is possible that the break contributes to the downstream flow control. Subcritical flows are possible as long as the Froude number assumes a critical value somewhere downstream; it need not necessarily

be critical at the chute exit. The Froude number could be critical at the break. However, the experiments that examined the details of the flow near the chute exit (which were performed several months later) indicate that critical behavior does occur at the exit. It appears that the flow may assume critical behavior twice, once at the break point and once at the exit. This would explain why, in Figure 4.20, the flow depth after the break remains much deeper than the supercritical flows shown with roughly the same mass flow rate.

For constant mass flow rate

$$\bar{u} \propto \frac{1}{h}$$

$$Fr \propto \frac{1}{h^{3/2}}$$

The Froude number must then have a different value at the break than at the chute exit. However, the critical Froude number depends on the profile parameters Γ and γ, and can assume different values along the chute. It is then possible for the flow to become critical at both the break point and the exit. This implies that the ratio, Γ/γ undergoes relatively large changes.

4.7 Wall Friction Coefficients

The supercritical/subcritical flow transition, as well as the lack of dependence of the mass flow on the gate opening, depends on how downstream conditions affect the flow upstream. In the general equation for open channel flow derived in Appendix A, the downstream conditions are represented by the term:

$$\frac{\overline{\tau}_w P}{\rho_p \nu_c g b h} dx$$

This term looks much like a friction coefficient:

$$\mu = \left.\frac{\tau_s}{\tau_N}\right|_w \simeq \frac{\tau_w}{\rho_p \nu_c gh \cos \alpha}$$

The friction coefficient could be determined in much the same way as Augenstein and Hogg [2]. For a constant acceleration, a, starting from rest:

$$a = \frac{1}{2}\frac{u^2}{x}$$

where u is the velocity and x the position along the chute. Thus a is half the slope of the curve of u^2 versus x. By a simple force balance,

$$a = g(\sin\theta - \mu \cos \theta)$$

so

$$\mu = \tan \theta - \frac{1}{2}\frac{u^2}{gx}$$

$$= \tan \theta - \frac{1}{2}\frac{(u^2/gR)}{(x/R)}$$

A plot of u^2/gR versus x/R is shown in Figure 4.24. Several points are shown for each angle, corresponding to several gate openings. There is a great deal of scatter in the data, but it is still possible to draw a straight line that intersects most sets of points.

The friction coefficient corresponding to each line is also indicated on the graph. Contrary to the evidence presented by Augenstein and Hogg [2], there is clearly a large variation in μ with inclination

angle. (Augenstein and Hogg's results were for "thin" flows, although they do not state exactly what they mean.) The friction coefficient should reflect the velocity and density profiles, and depend on chute angle only indirectly through the angle's effect on the flow. It is likely that the scatter in the data is a result of depth and velocity changes. A more accurate method that could determine μ locally is needed to determine its functional dependence on depth and velocity.

After dividing by cos α, the general integral equation (A) becomes

$$\frac{\bar{\tau}_w P}{\rho_p \nu_c \, gb\, h \cos \alpha} = \tan \alpha + \frac{dh}{dx} \left(\gamma \frac{Fr^2}{\cos \alpha 2} - \Gamma \right)$$

If the side walls have a negligible contribution to the total shear stress, (if $\bar{\tau}_w \, P/b \cong \tau_w$) the left-hand side reduces to a friction coefficient and this equation may be used to determine the local value of μ.

The effect of the side walls is contained in the integral

$$\bar{\tau}_w P = \int_P \tau_w \, d\ell$$

In this simplest friction model the shear stress on a wall is proportional to the normal force, which is itself roughly proportional to the distance from the free surface. But due to the normal stress differences, the normal force on the side walls will be smaller than that which would be exerted at the same depth on a wall parallel to the bottom. Roberts [62,63] accounts for side wall effects by defining an effective friction coefficient μ_{eff} as if all the stress were applied on the chute bottom:

$$\mu_{eff} = \mu(1 + k \frac{h}{b})$$

where μ is the actual friction coefficient and k is twice the ratio of the side wall pressure to an equivalent bottom pressure. Roberts [62] measured k statically and found k = .3 for millet seed. Savage [68] repeated Roberts' experiment and found k = .453 for glass beads in a rough-walled chute. Savage and Jeffrey [71] found that the normal force in the direction perpendicular to both the flow direction and the velocity gradient was at most equal to the normal forces in the other directions. They predict that $k = 2$ as $S \to 0$, and decreases monotonically to $k = 2/3$ as $S \to \infty$.

Unfortunately, it would be difficult to measure k from the data taken during the present investigation. But for the 8.9 cm wide chute, the maximum depths at the point of measurement were about 3 cm. For k = .5 the correction due to side-wall effects would be about 16% of the total.

Ignoring side-wall effects, the equation for the friction coefficient is then:

$$\mu = \frac{\tau_w}{\rho g h \cos \alpha} = \tan \alpha + \frac{dh}{dx} \left(\gamma \frac{Fr^2}{\cos \alpha} - \Gamma\right)$$

where dh/dx is found from cubic spline fits through measured values of h.

The problem is now to approximate the profile parameters γ and Γ. Γ depends only on the density profile, which is not easily measured. In the absence of better information, Γ is assumed to be unity. The parameter γ may be approximated by assuming a linear profile based on the measured surface velocity u_s and the mean velocity interpreted from

the mass flow $\bar{u} = \frac{m}{\rho_p \nu_c bh}$. Then,

$$\gamma = \frac{1}{3}\left(\frac{u_s}{\bar{u}}\right)^2 - \frac{2}{3}\left(\frac{u_s}{\bar{u}}\right) + \frac{4}{3}$$

Typical computed values of μ are shown plotted against an appropriate dimensionless velocity $u_s/\sqrt{gR}$ is Figure 4.25. The dimensionless quantity is based on the surface velocity rather than the mean velocity. The velocity u_s was deemed more representative for shallow depths where the density may be lower than the critical value, distorting the value of $\bar{u}$ computed from the mass flow. It is expected that μ also varies with h/R, but no clear trend was apparent.

It is difficult to have a great deal of confidence in these results. In all cases, the flow is close to uniform and dh/dx is small. It would be expected from examination of the equation that μ would then vary as tan α with small velocity correction for large Fr^2. This is indeed the behavior seen in the data in Figure 4.25. There is no gentle transition from one angle to another. The data from each angle seems to follow its own curve. This would not be so troubling, except for the questionable validity of the assumptions used in deriving and using the equation, assumptions that are as yet unverified experimentally.

4.8 Conclusion

It has been shown that granular material flows in chutes may be

classified as supercritical or subcritical. The two flow types represent conjugate states of open channel flows. The classification of a flow depends on whether the Froude number $Fr = u/\sqrt{gh}$ is greater or smaller than some critical value $Fr_c = (\frac{\Gamma \cos \alpha}{\gamma})^{1/2}$. The quantities γ and Γ are profile parameters that reflect the shape of the local velocity and density profiles. The type of flow has been shown to have a strong effect on the mass flow rate.

The mass flow rate in a supercritical flow is choked at the inlet to the chute and is determined by the conditions there (i.e., gate opening). In such a case the chute behaves much like a hopper, and the mass flow follows the correlation:

$$Fr_g = 2K \sin \alpha$$

where $Fr_g = u/\sqrt{gH_y}$ is the Froude number based on the velocity and hydraulic radius:

$$H_y = \frac{A}{P} = \frac{h_g b}{2(h_g+b)}$$

at the gate. K is a material property and has a value close to one.

The mass flow rate in a subcritical flow is choked somewhere downstream and is independent of gate opening. The Froude number, velocity, and depth are all fixed at the chute exit, presumably at critical values. The critical values, however, depend on the inclination angle and the chute geometry. This occurrence was only phenomenologically described, and as yet no explanation presents itself.

An understanding of the supercritical/subcritical flow transition may have important engineering significance. Subcritical flows are generally undesirable because they are accompanied by slowing of the flow and the formation of stagnant wedges on the chute bottom. But more important, the maximum mass flow rate obtainable from a chute of fixed inclination angle is more or less limited to its transition value.

The depth profile in a supercritical granular chute flow follows the parabolic shape characteristic of a constantly accelerating flow, for all inclination angles. Subcritical flows may exhibit a phenomenon, termed "breaking," where the flow approaches a uniform depth and then breaks, accelerating for a short distance before approaching another uniform flow depth. It was hypothesized that the flow assumes critical values at the break point as well as at the chute exit.

The key to the subcritical flow behavior appears to depend on the frictional interaction between the material and the chute wall. Attempts to measure the friction coefficient produced inconclusive results, but indicated that the friction coefficient is not a constant material property. To characterize properly the frictional behavior requires direct measurement by load cells.

Finally, some mention should be made of the possible role of interstitial air effects in the experiments. Rough estimates of the Bagnold number (Section 1.2) yield values of the order of 10^3, suggesting that the experiments do lie in the granular material flow regime. Nevertheless the interstitial air may play a role in some parts of the flow, for example in the saltated layer.

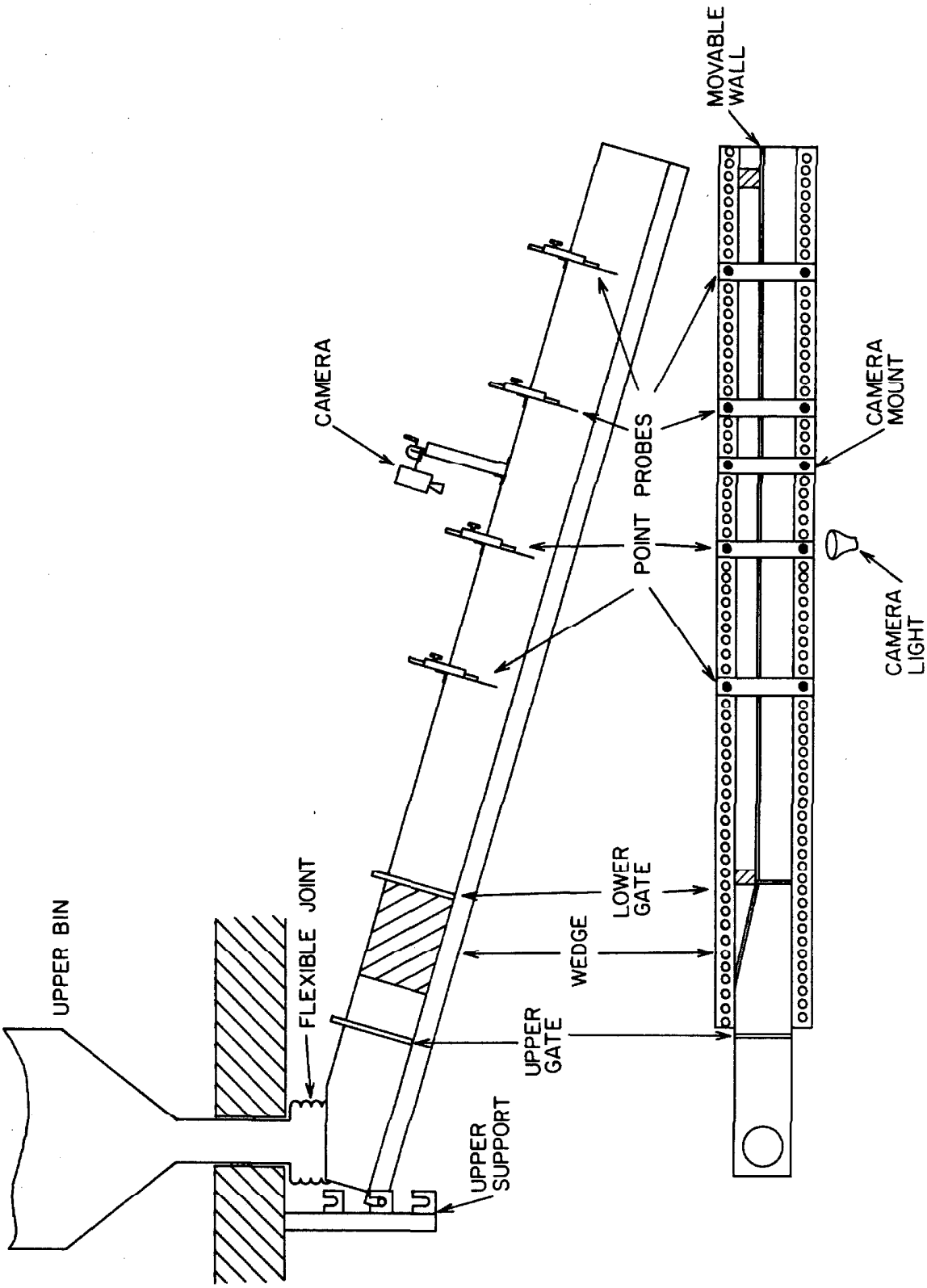

Figure 4.1 Diagram of the inclined chute apparatus.

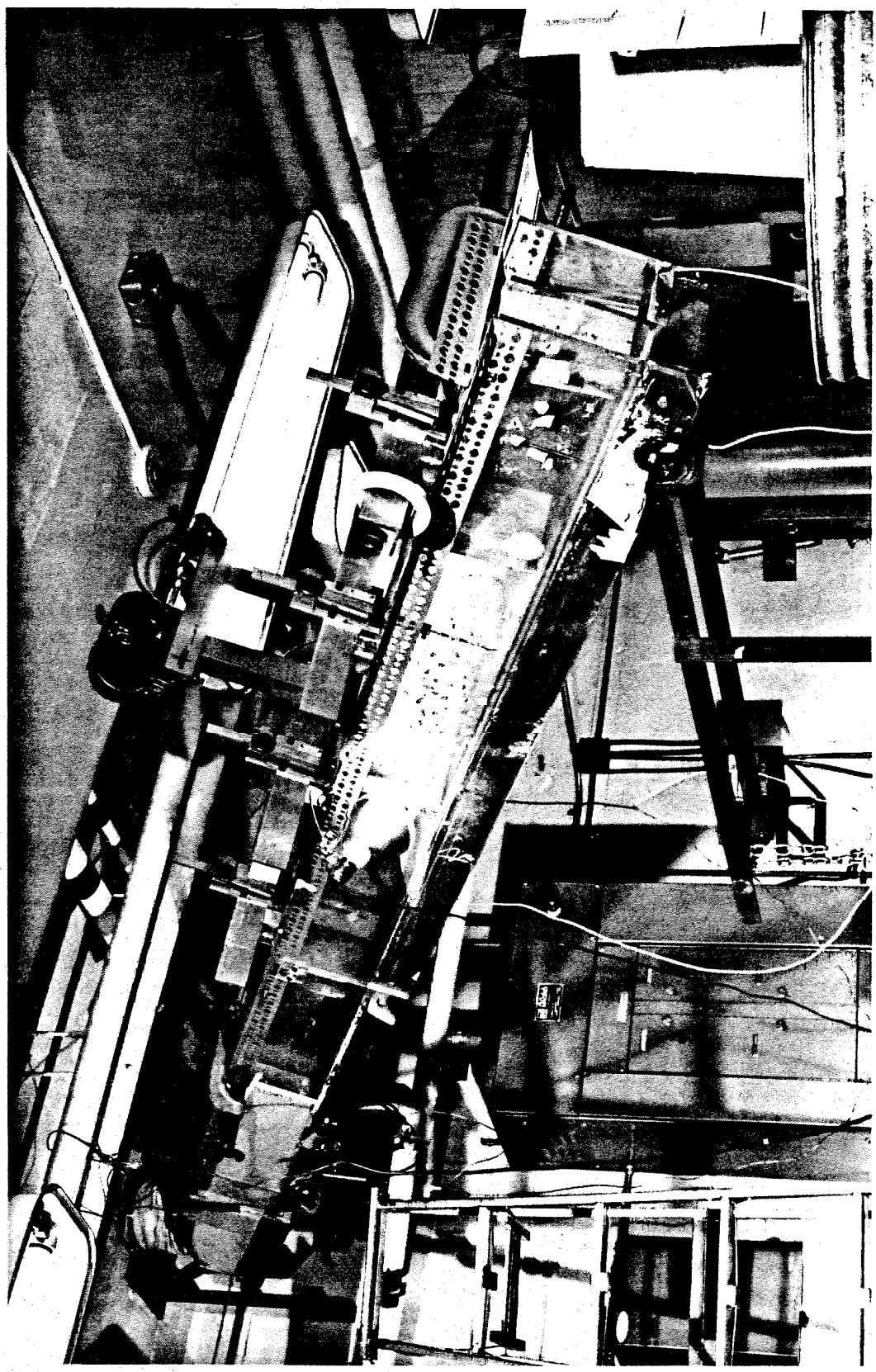

Figure 4.2 Photograph of the inclined chute apparatus.

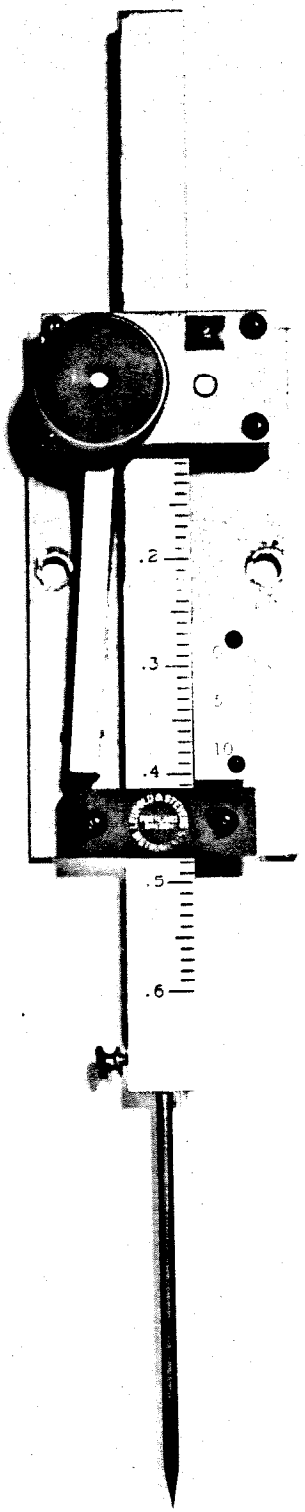

Figure 4.3 Photograph of a point probe used for flow depth measurements

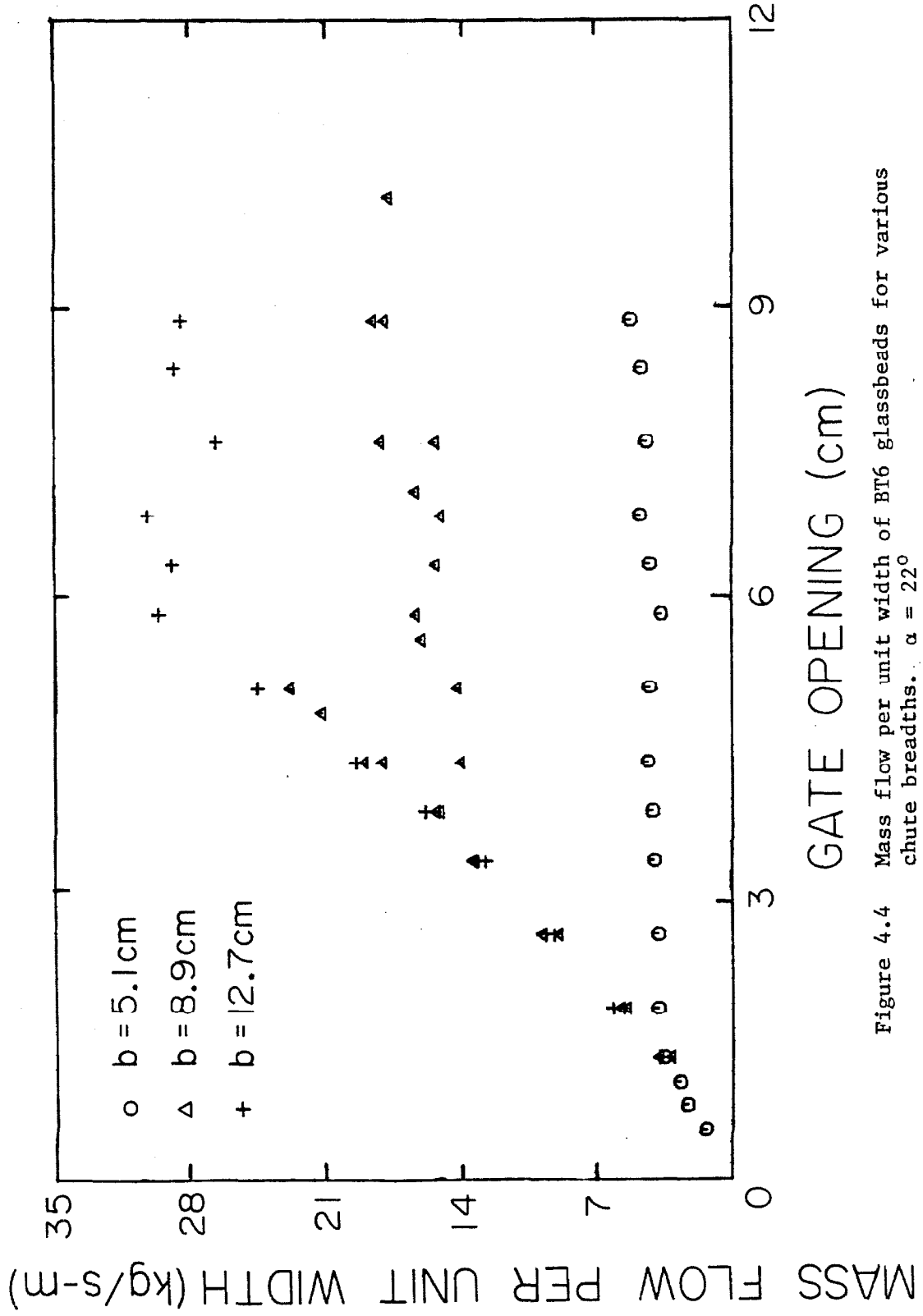

Figure 4.4 Mass flow per unit width of BT6 glassbeads for various chute breadths. $\alpha = 22^{\circ}$

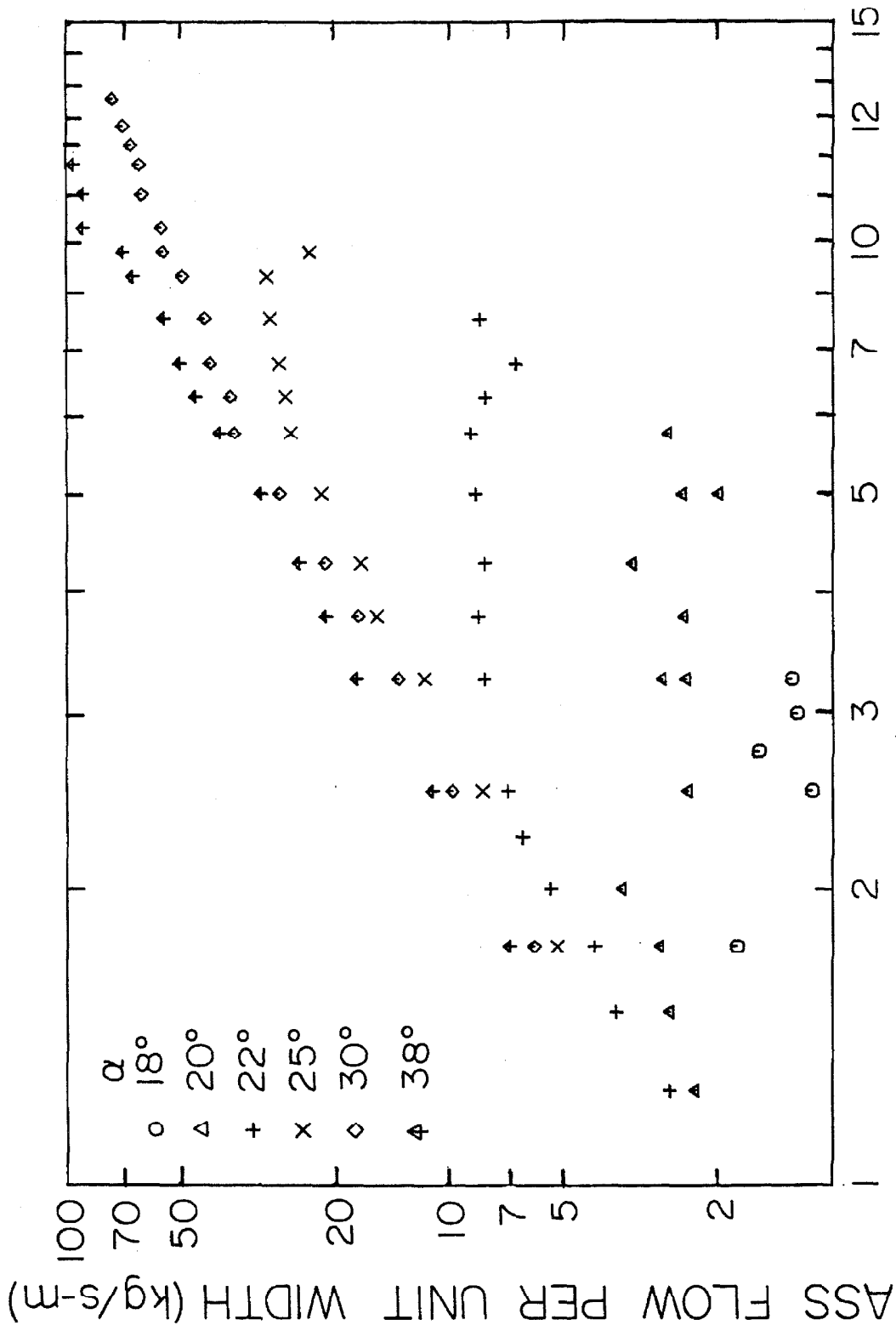

Figure 4.5 Mass flow per unit width of BT4 glassbeads for various chute inclinations. b = 8.9cm.

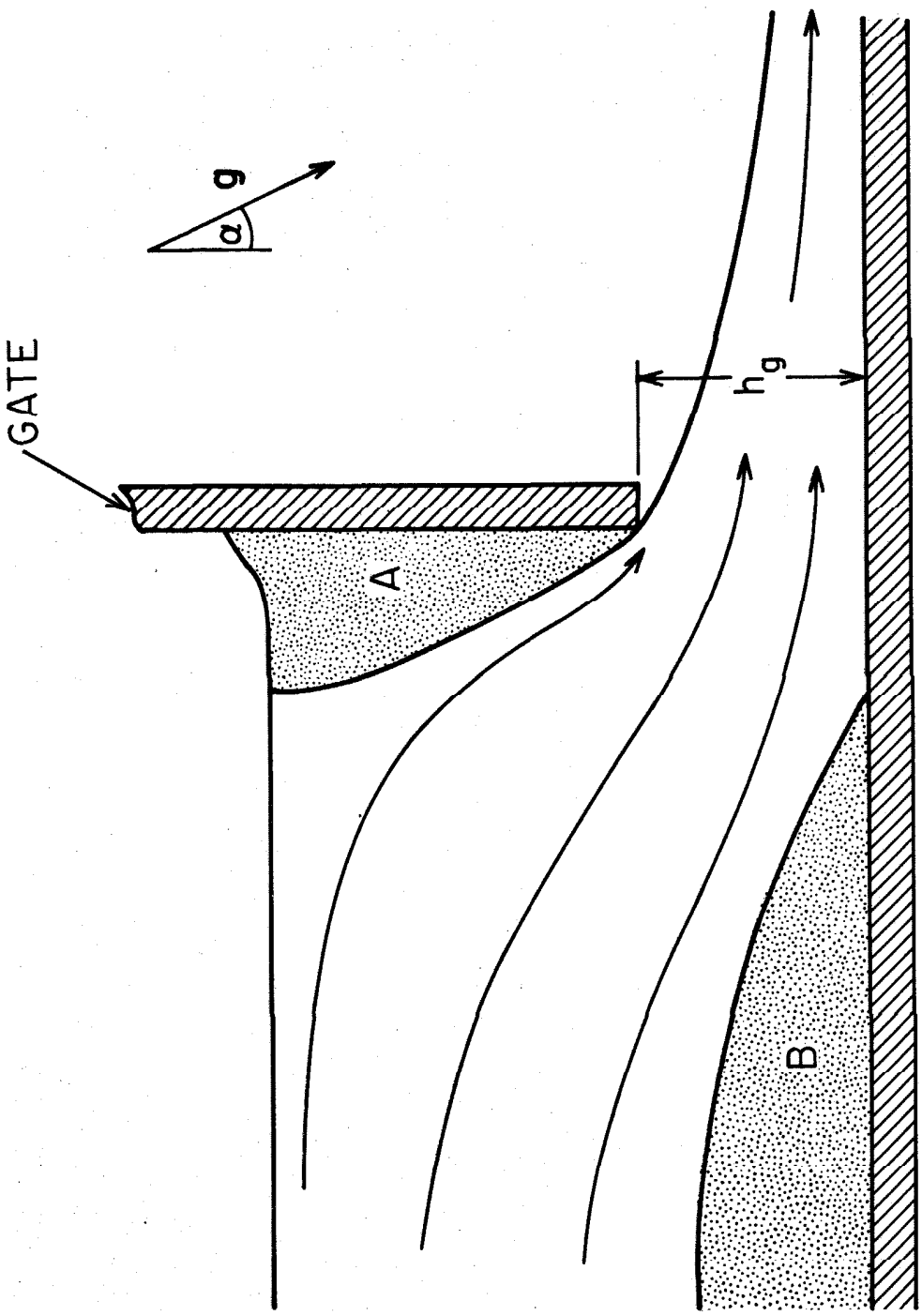

Figure 4.6 Detail of the flow pattern in the vicinity of the lower gate showing the two stagnant zones A, and B.

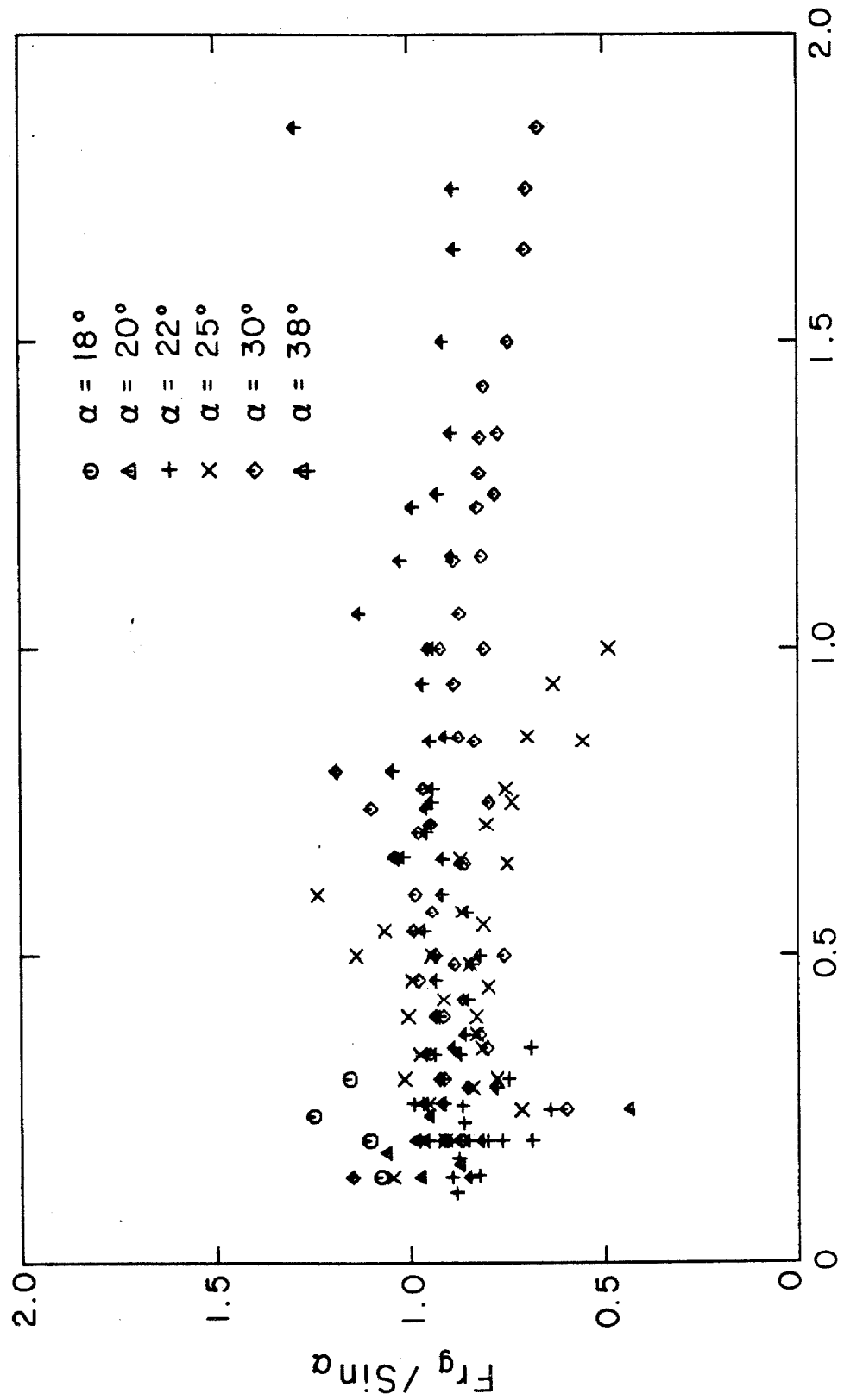

Figure 4.7 Gate Froude numbers for supercritical flows. BT4 glass-beads.

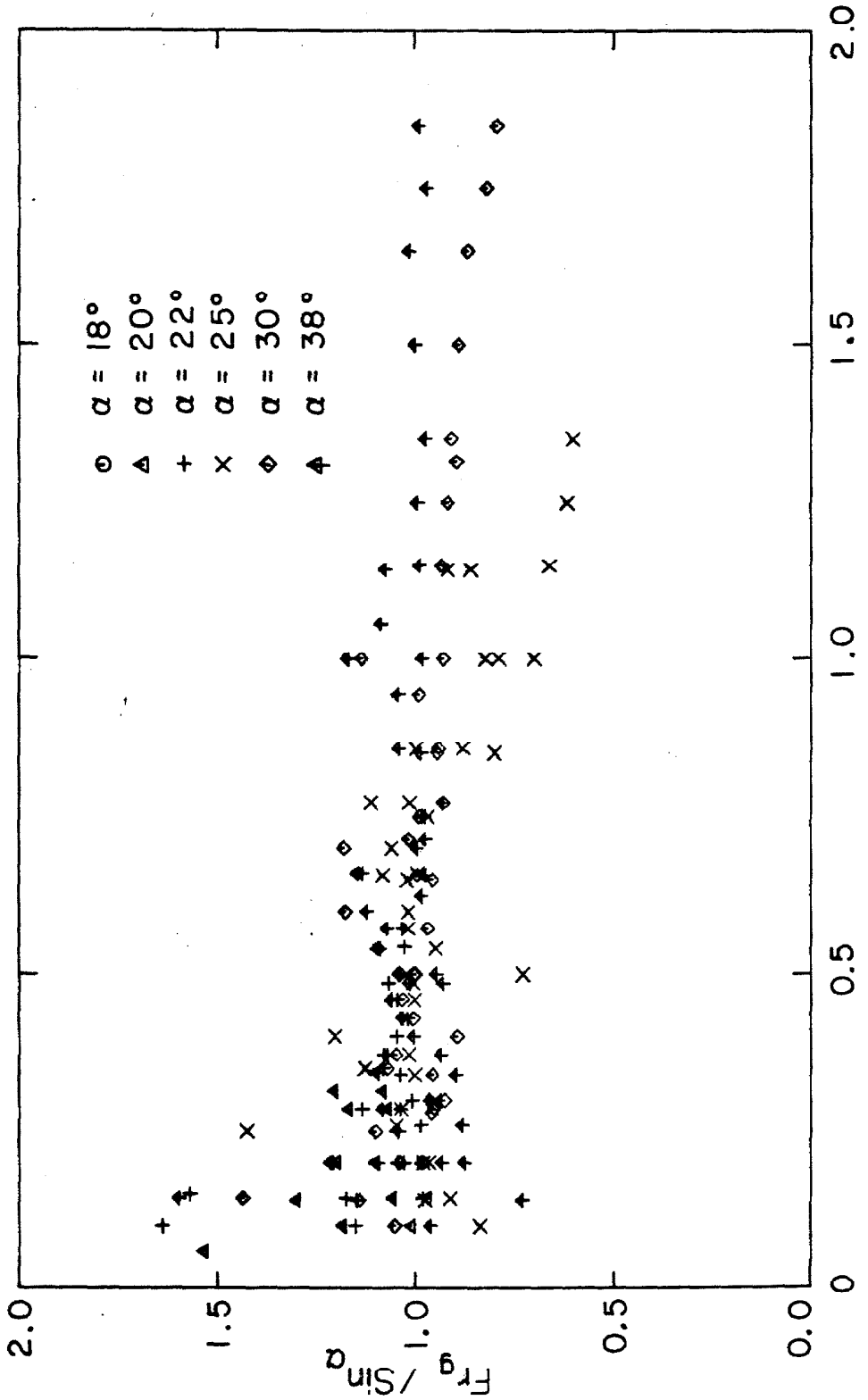

Figure 4.8 Gate Froude numbers for supercritical flows. BT6 glass-beads.

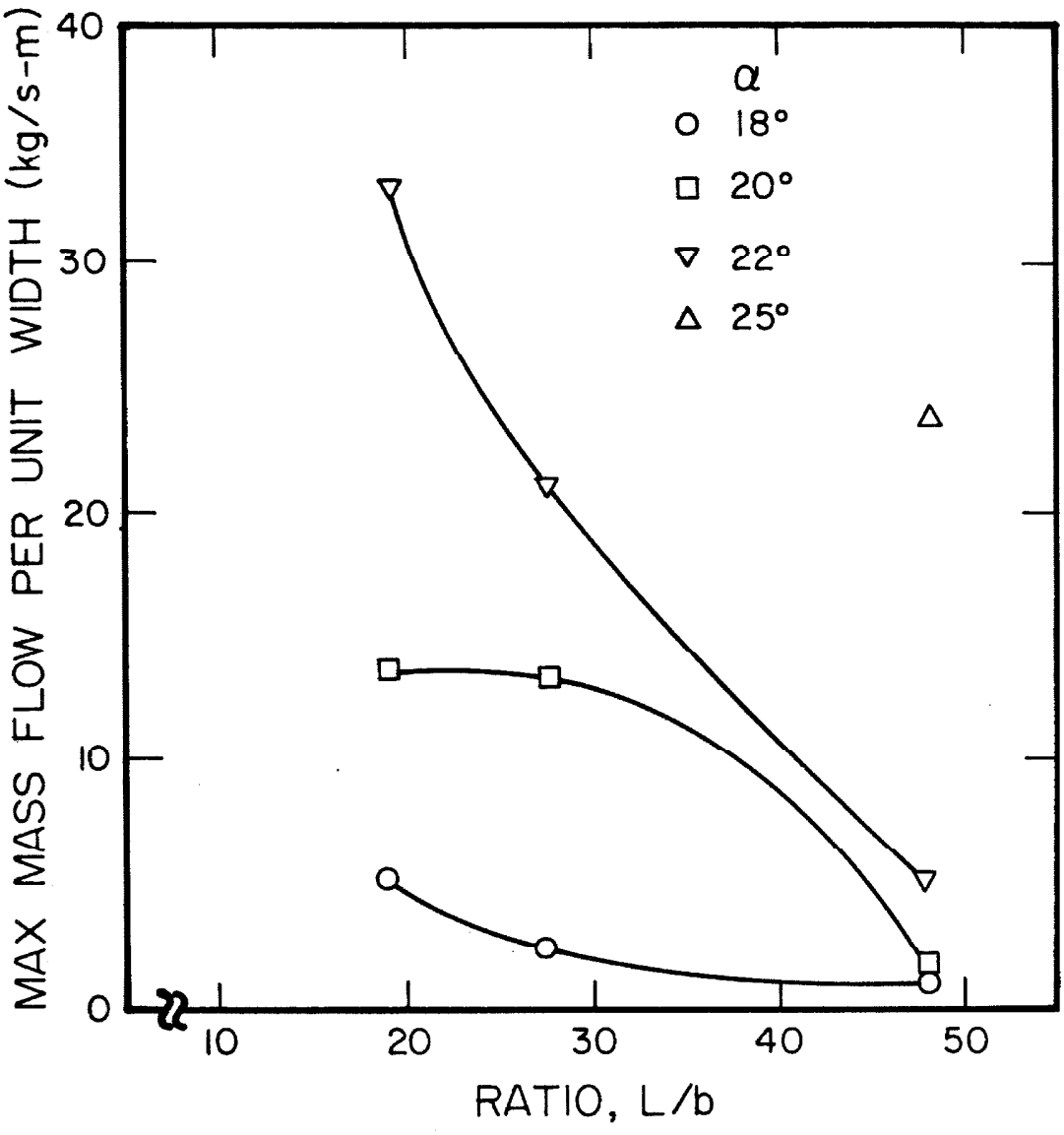

Figure 4.9 Maximum mass flow rates for subcritical flows as a function of chute geometry BT6 glassbeads.

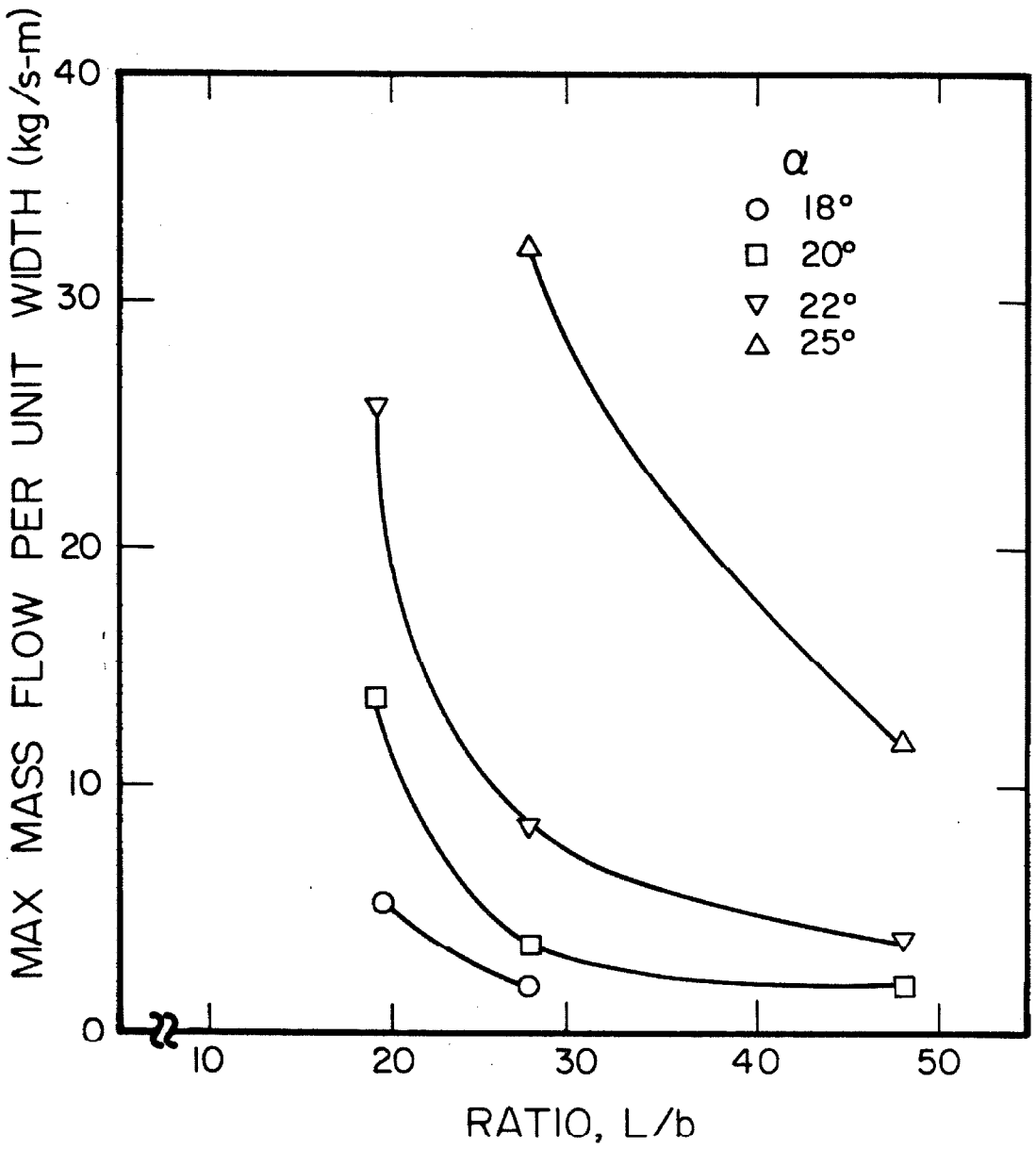

Figure 4.10 Maximum mass flow rates for subcritical flows as a function of chute geometry BT4 glassbeads.

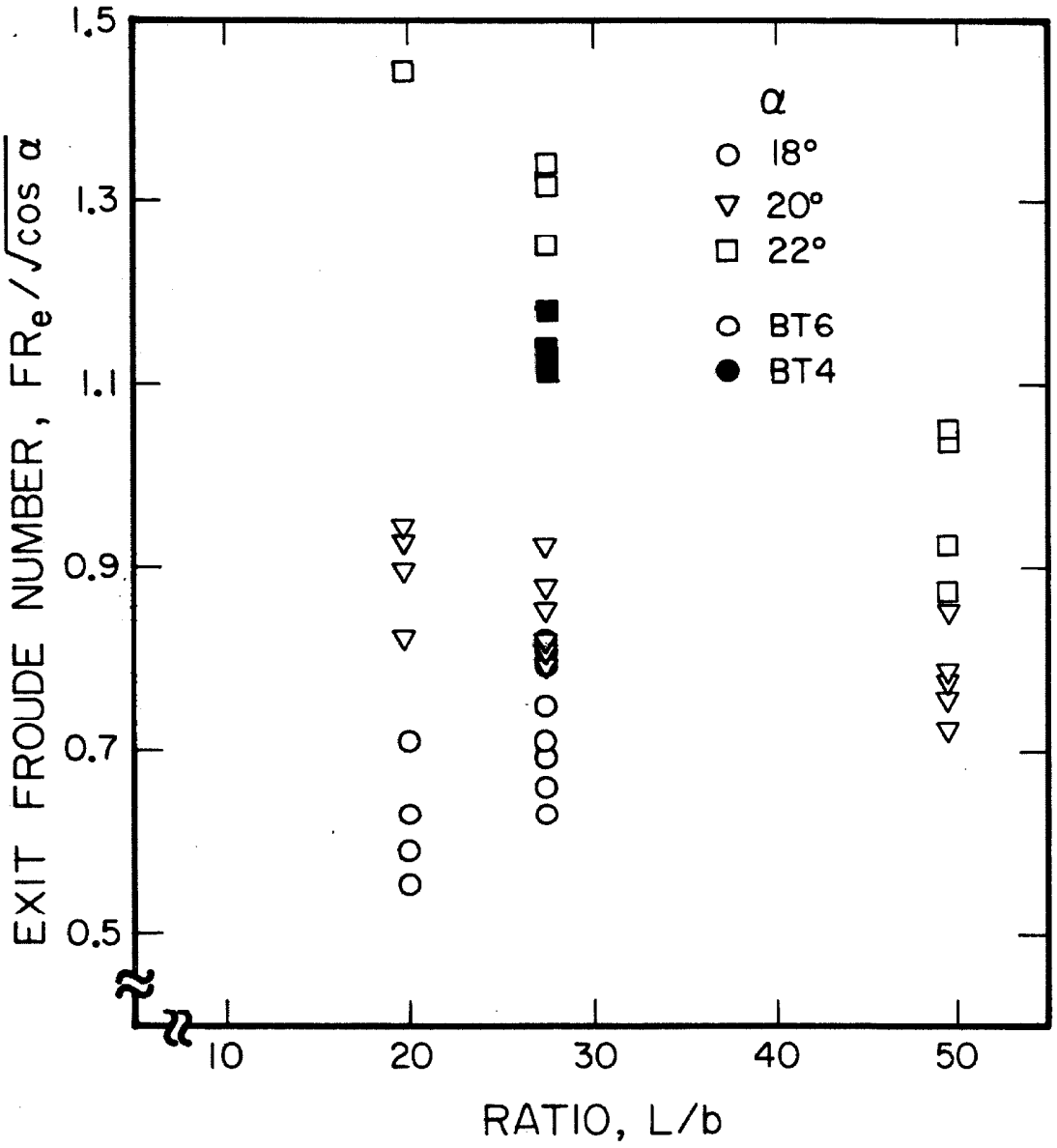

Figure 4.11 Exit (critical) Froude numbers, as a function of inclination angle and chute geometry.

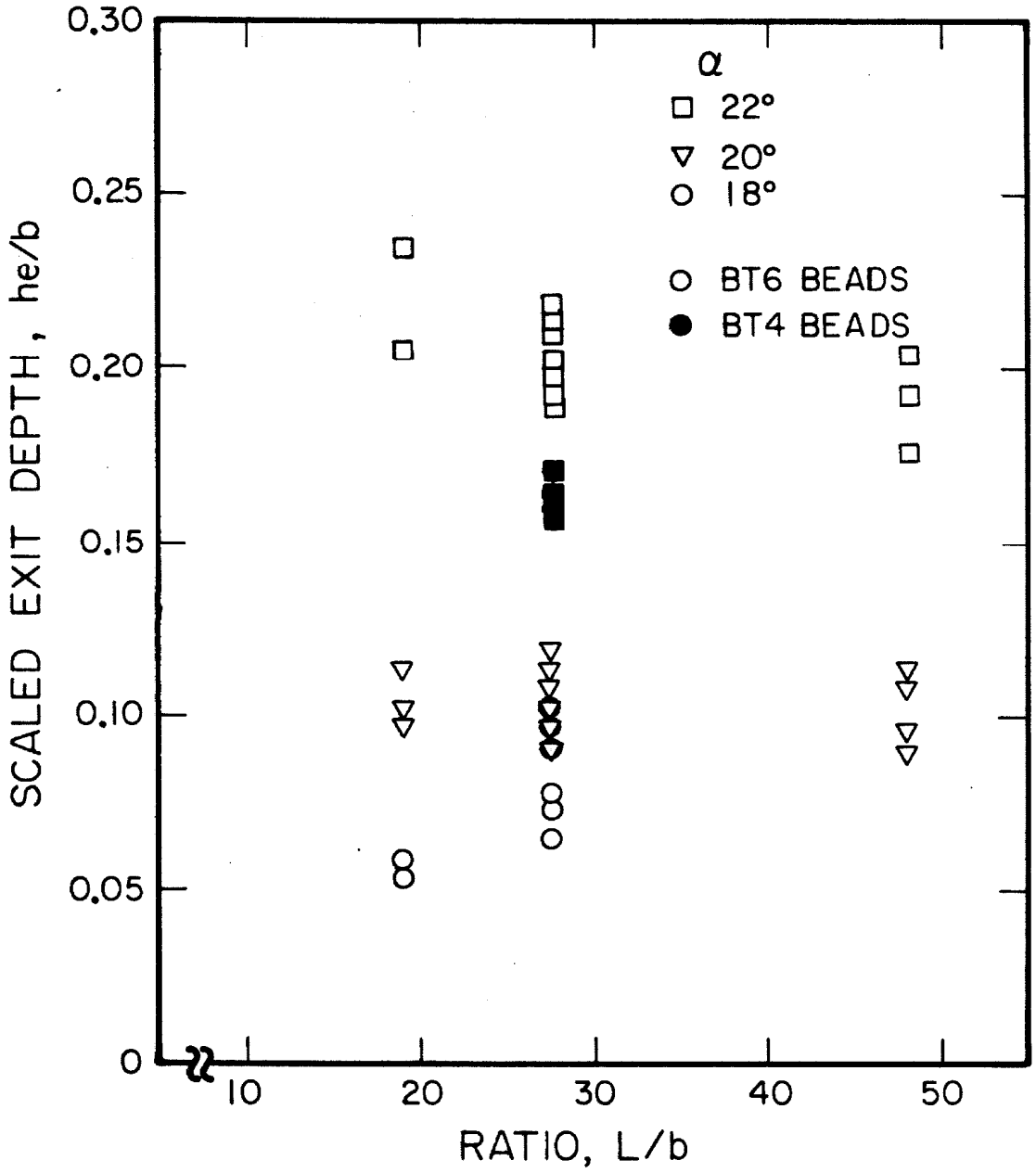

Figure 4.12 Exit (critical) depths as a function of inclination angle and chute geometry.

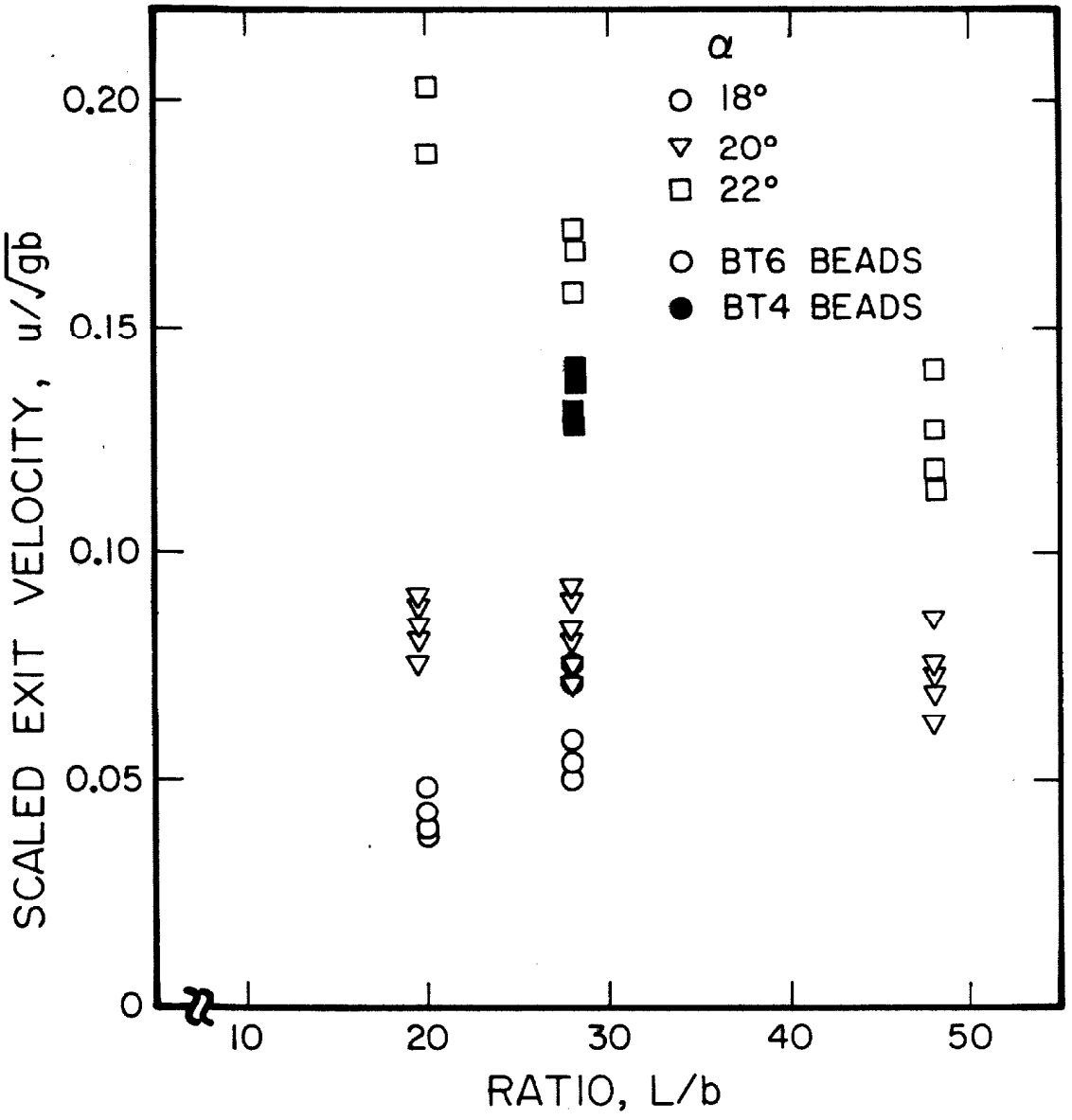

Figure 4.13 Exit (critical) velocities as a function of inclination angle and chute geometry.

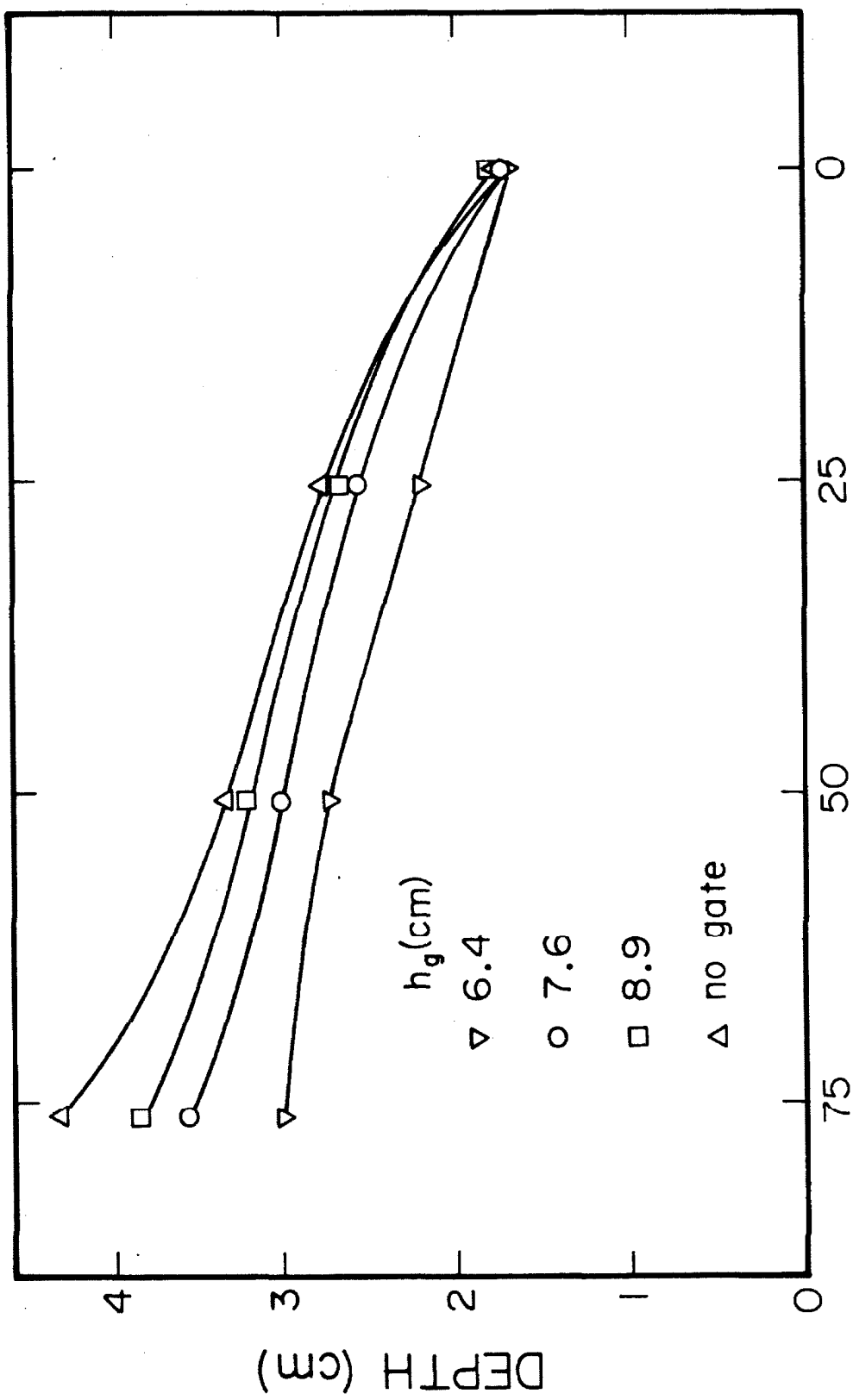

Figure 4.14 Approach at the flow depth toward its exit value. BT6 glassbeads, $\alpha = 22°$, 8.9cm.

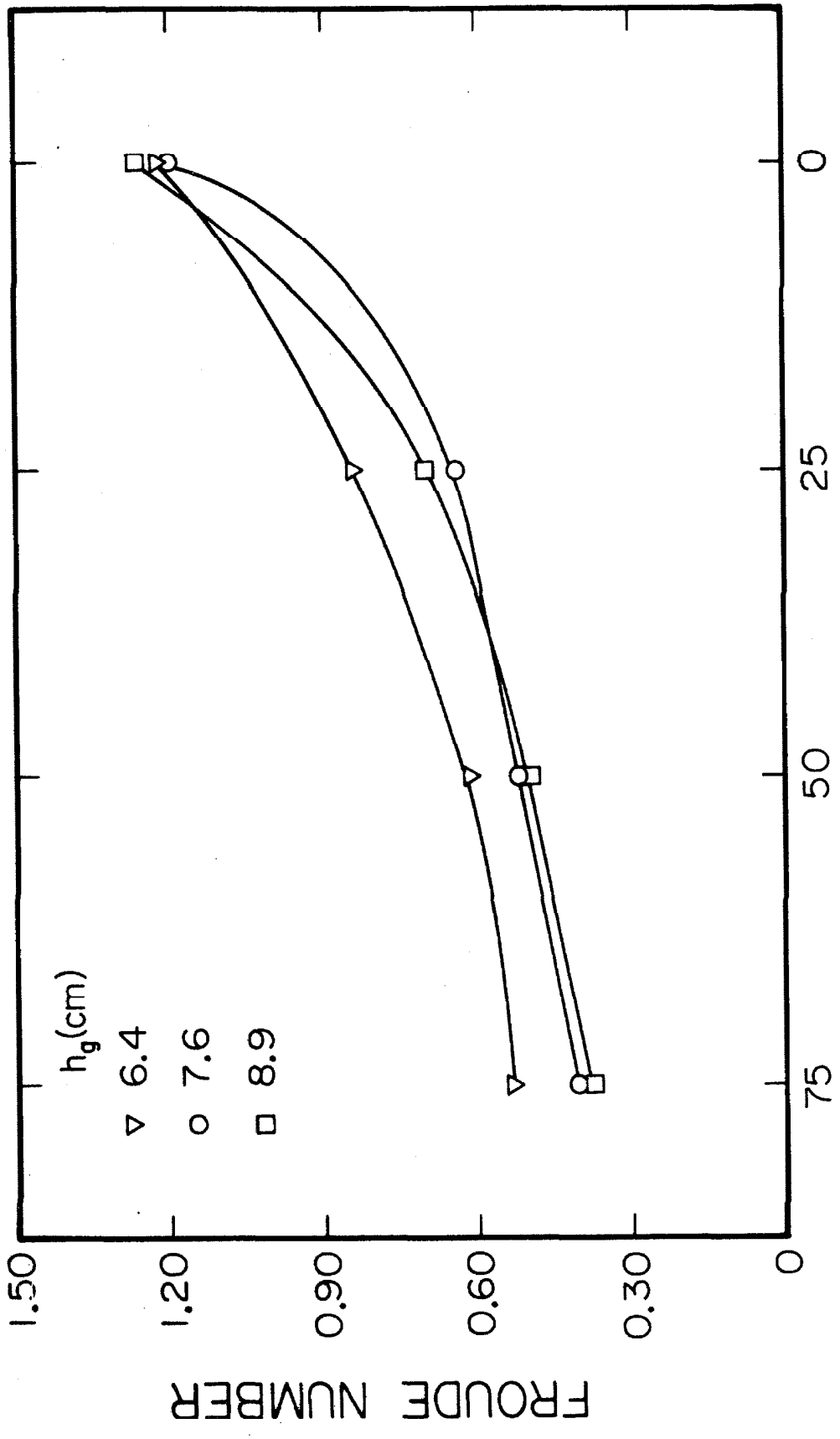

Figure 4.15 Approach of the Froude number toward its exit value. BT6 glassbeads. $\alpha = 22^{\circ}$, b = 8.9cm.

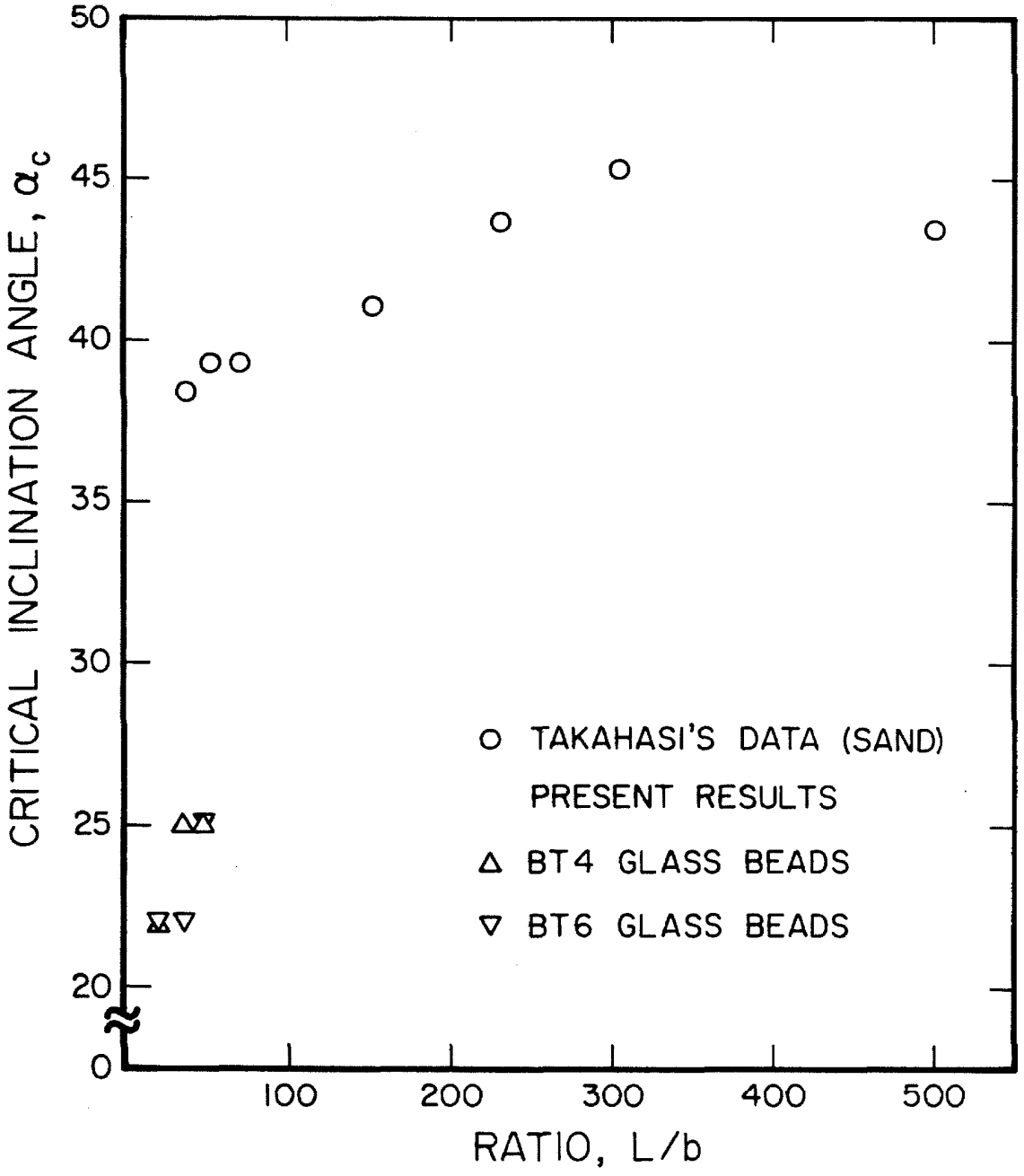

Figure 4.16 Transition angle as a function of chute geometry, showing the present data for glassbeads and Takahasi's data for sand.

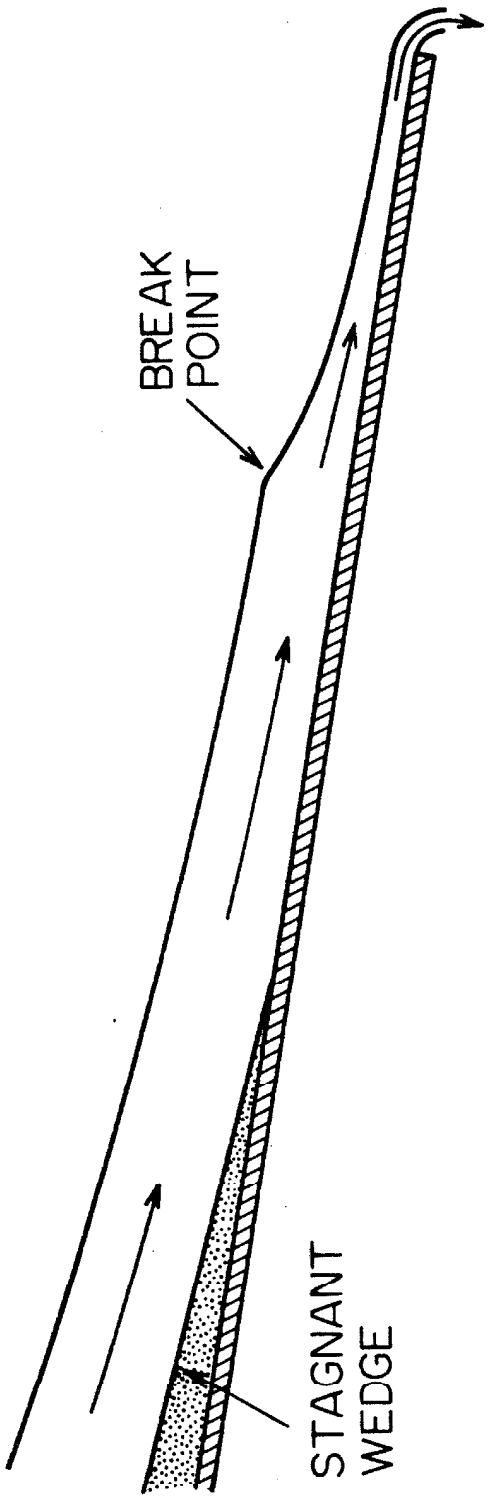

Figure 4.17 Diagram of subcritical chute flow showing, a stagnant wedge and "breaking" phenomena.

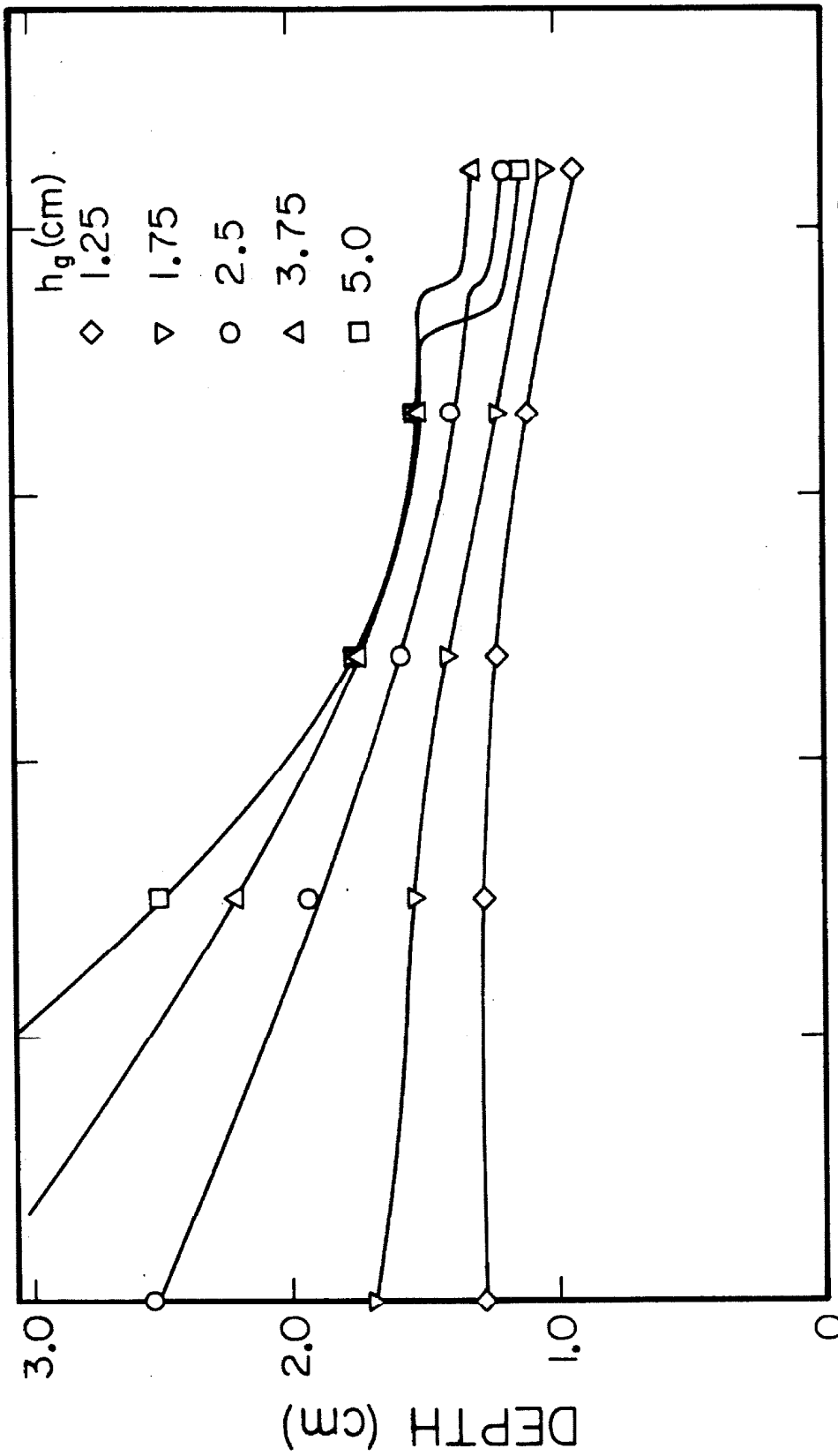

Figure 4.18 Depth profiles along the chute. BT6 glassbeads, $\alpha = 18^{o}$, b = 8.9cm.

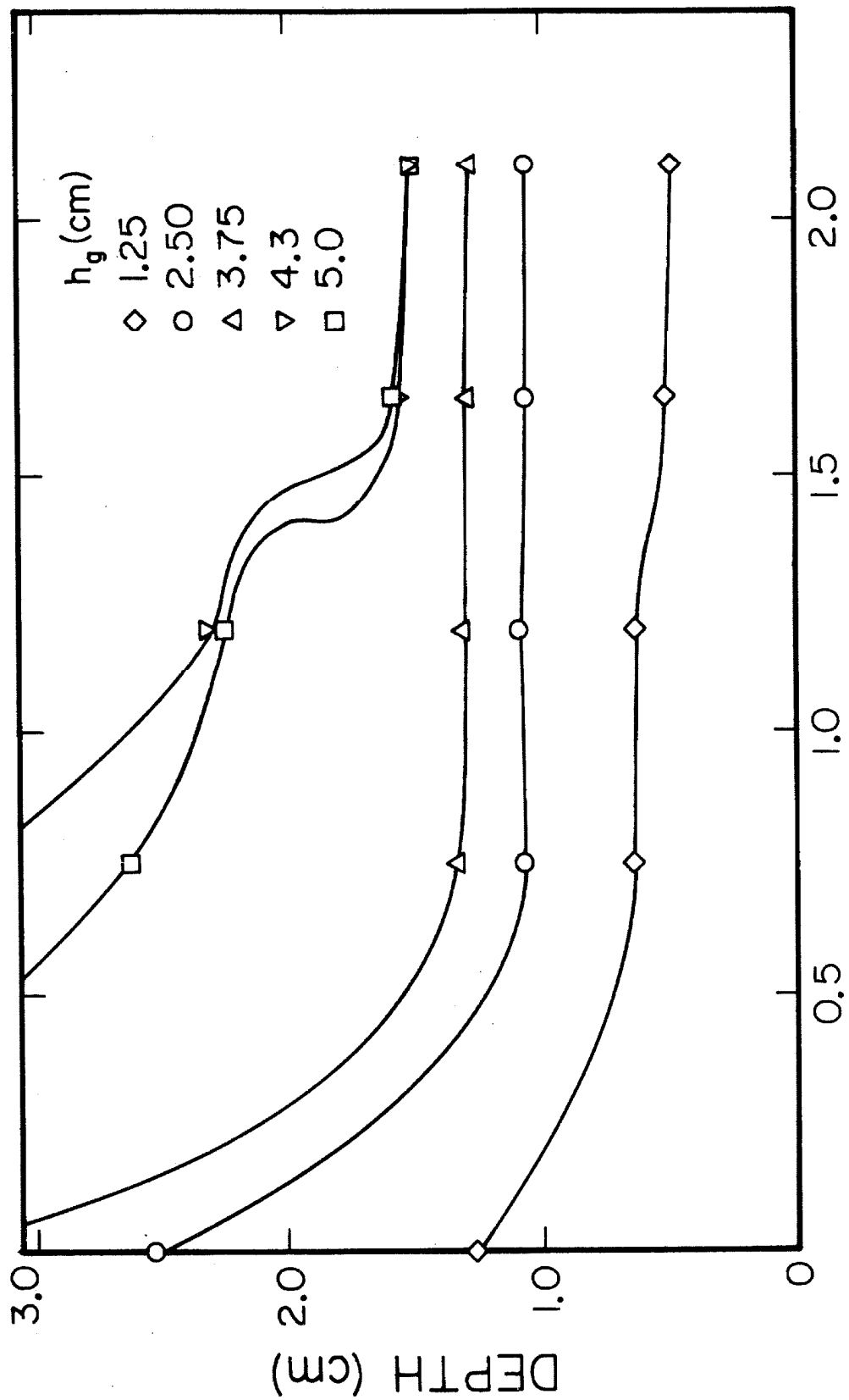

Figure 4.19 Depth profiles along the chute, BT6 glassbeads, $\alpha = 20^{o}$, b = 8.9cm.

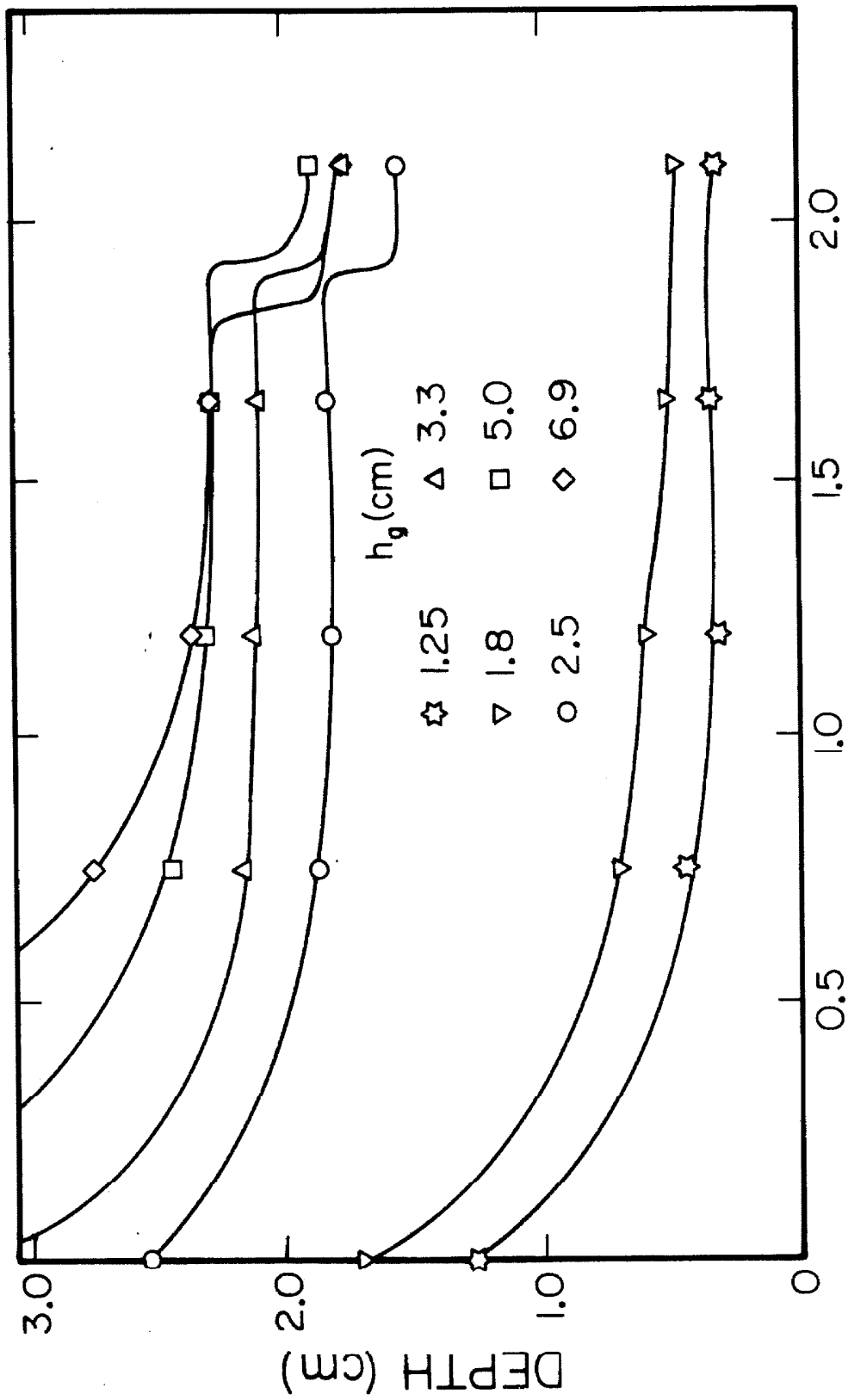

Figure 4.20 Depth profiles along the chute. BT6 glassbeads, $\alpha = 22^{o}$, b = 8.9cm.

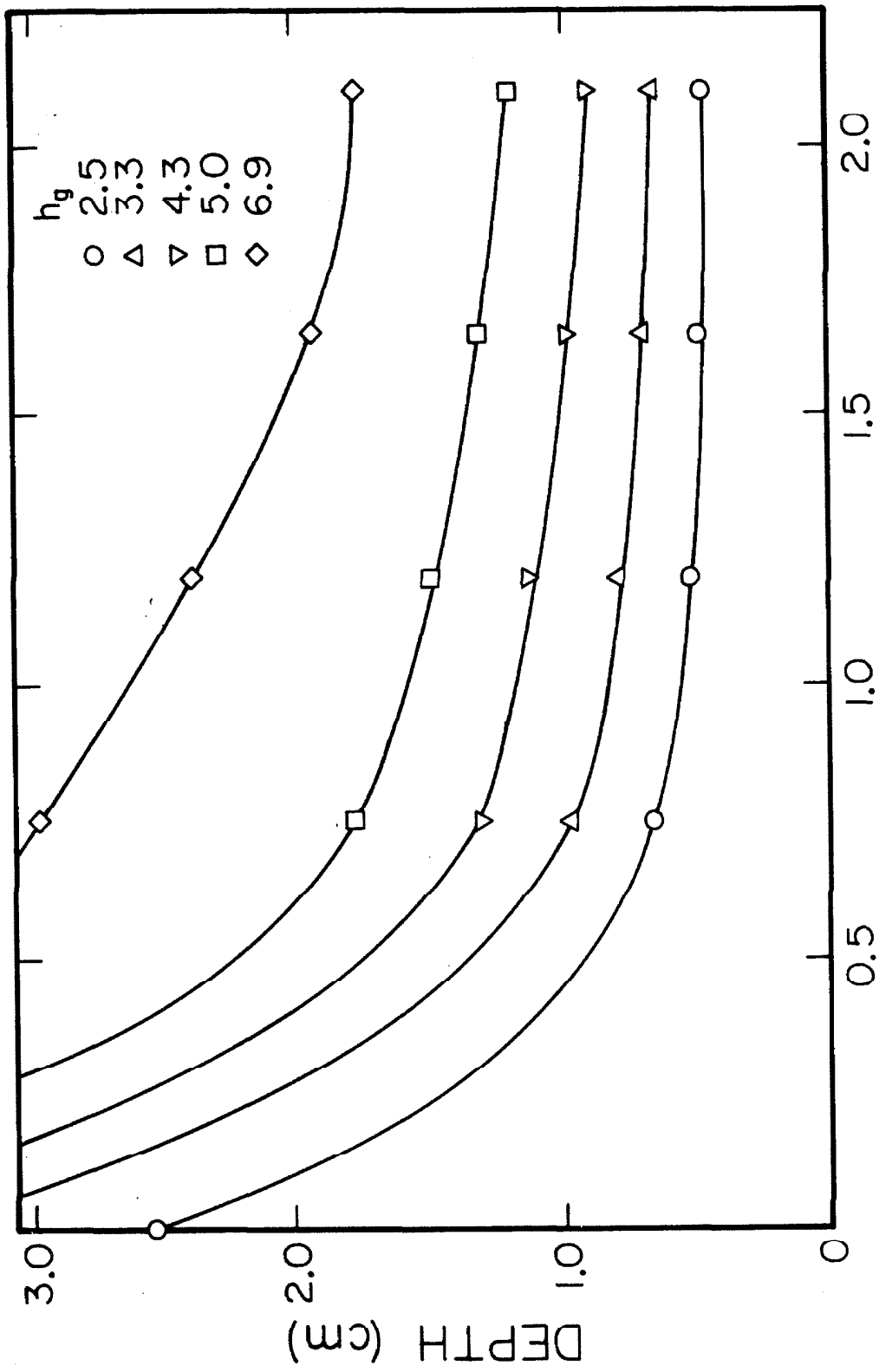

Figure 4.21 Depth profiles along the chute. BT6 glassbeads, $\alpha = 25^{\circ}$ b = 8.9cm.

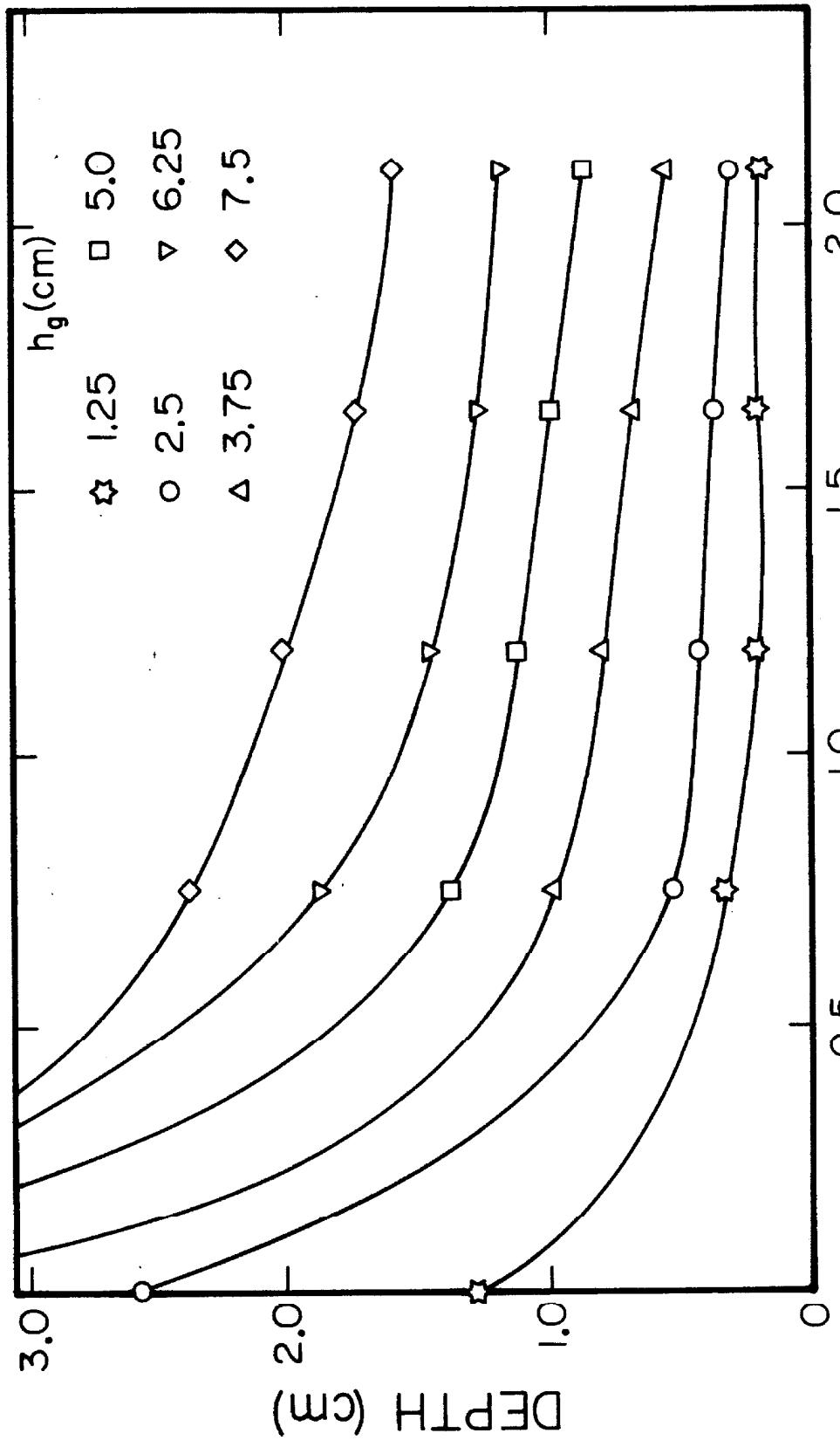

Figure 4.22 Depth profiles along the chute. BT6 glassbeads, $\alpha = 30^{\circ}$, $b = 8.9$cm.

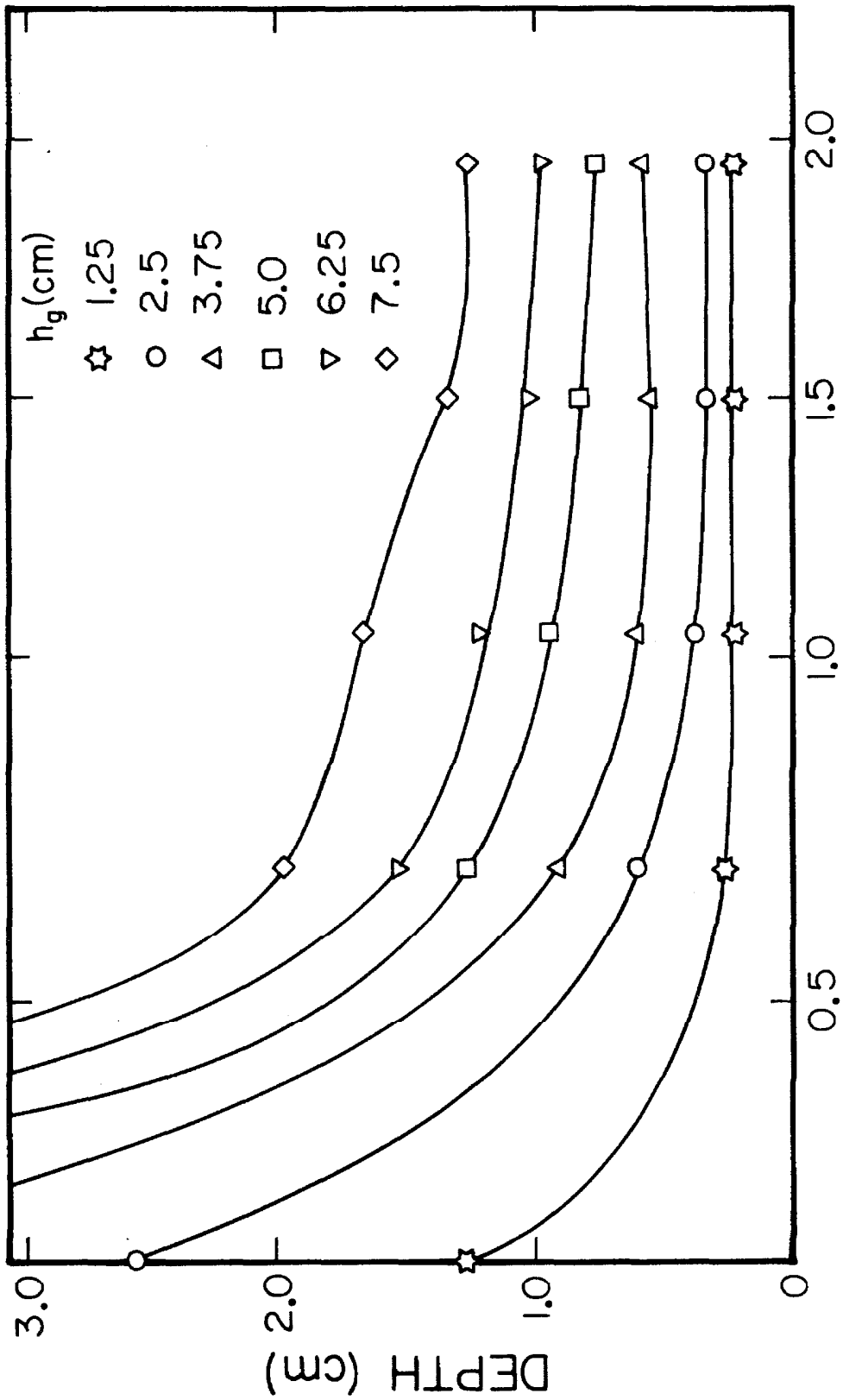

Figure 4.23 Depth profiles along the chute. BT6 glassbeads, $\alpha = 38^{\circ}$, $b = 8.9$cm.

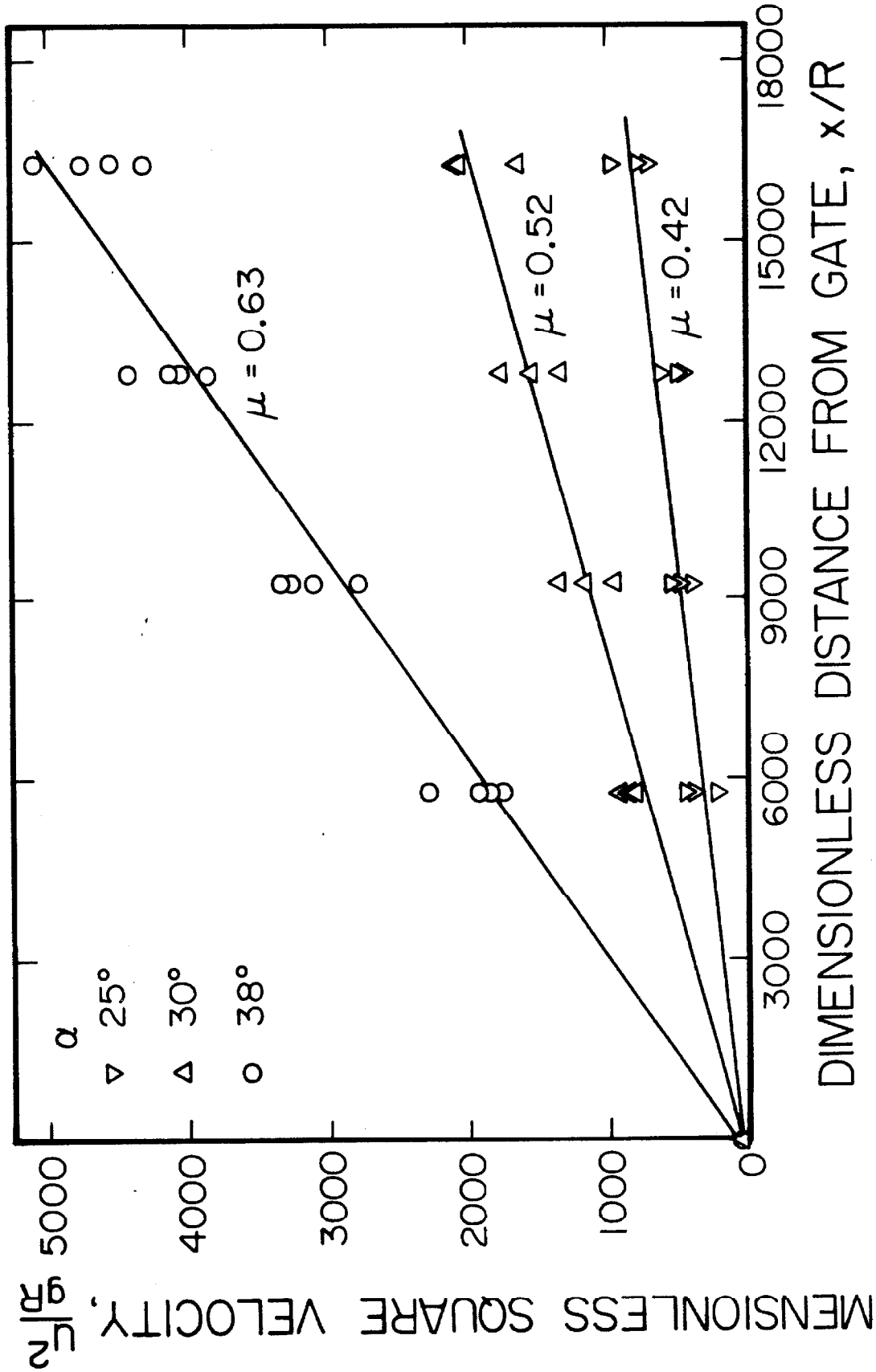

Figure 4.24 Acceleration of the flow along the chute showing the corresponding friction coefficient.

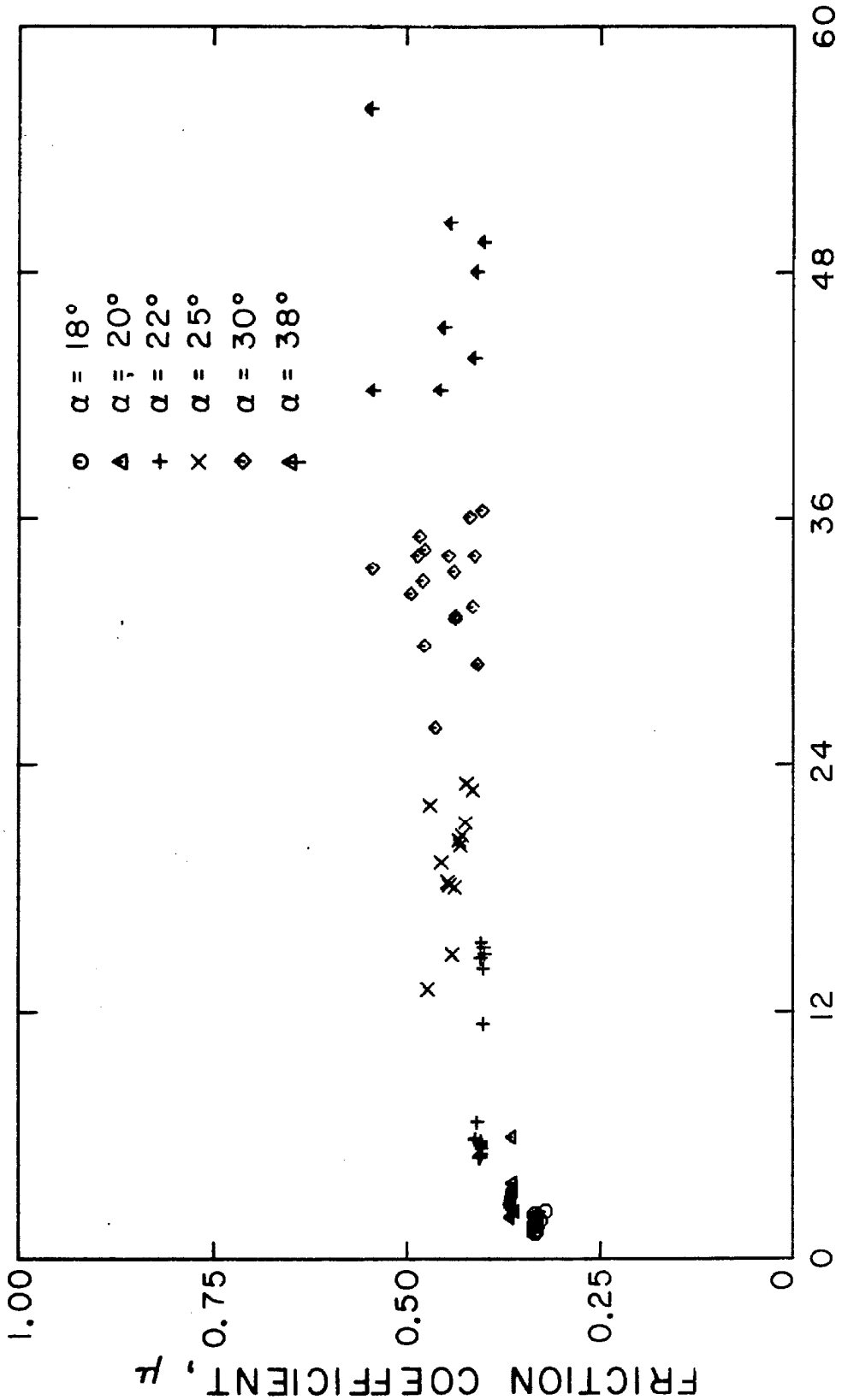

Figure 4.25 Friction coefficient as a function of velocity and inclination angle.

Appendix A

A GENERAL EQUATION DESCRIBING OPEN CHANNEL FLOWS

Consider a force balance on a control volume of width dx in a chute of breadth b, as shown in Figure A.1. The total momentum change within the control volume is

$$\rho_p b \left\{ \int_0^h \nu u^2 \, dy \Big|_2 - \int_0^h \nu u^2 \, dy \Big|_1 \right\}$$

This must be the result of a balance between a body force

$$\rho_p g b \, dx \sin \alpha \int_0^h \nu \, dy,$$

a pressure difference on the control volume walls,

$$\int_0^h p \, dy \Big|_1 - \int_0^b p \, dy \Big|_2$$

and the shear stress on the chute walls,

$$- \int_P \tau_w \, d\ell \, dx$$

where τ_w is the wall shear stress and is integrated around the wetted perimeter P of the system.

For the purposes of this analysis, we will assume that:

$$p(y) = \int_y^h \rho_p \nu g \cos \alpha \, dy'$$

It can be seen in Sundarum and Cowin [81] that the wall pressure varies in this manner near the free surface of static bins. Define

$$\gamma = \int_0^1 \frac{\nu}{\bar{\nu}} \left(\frac{u}{\bar{u}}\right)^2 \frac{dy}{h}$$

$$\Gamma = 2 \int_0^1 \int_{y/h}^1 \frac{\nu}{\bar{\nu}} \frac{dy'}{h} \frac{dy}{h}$$

$$\bar{\tau}_w = \frac{1}{P} \int_P \tau_w \, d\ell$$

where

$$\bar{\nu} = \frac{1}{h} \int_0^h \nu \, dy$$

$$\bar{u} = \frac{1}{h} \int_0^h u \, dy$$

Note that γ, Γ, $\bar{\tau}_w$, $\bar{\nu}$, h, and $\bar{u}$ are all functions of x. Γ and γ are characteristics of the profile shapes and probably change more slowly with x.

Then the force balance becomes

$$\rho_p b \, d(\bar{\nu} h \bar{u}^2 \gamma) = \rho_p g b \bar{\nu} h \sin\alpha \, dx - \rho_p g b \frac{1}{2} \cos\alpha \, d(\bar{\nu} h^2 \Gamma) - \bar{\tau}_w P \, dx$$

Mass conservation implies

$$\bar{\nu} h \bar{u} b = Q = \text{const.}$$

where Q is the volume flow rate and hence

$$\rho_p Q \frac{d}{dx} (\bar{u}\gamma) = \rho_p g b \bar{\nu} h \sin\alpha \, dx - \frac{1}{2} \rho_p g b \cos\alpha \, d(\bar{\nu} h^2 \beta) - \tau_w P \, dx$$

Up to this point the equation is exact. However, due to the lack of good instrumentation, $\bar{\nu}$, γ, and Γ cannot be determined experimentally. It was shown by Ridgway and Rupp [60] and in our computer simulation (see Section 3.1.1) that the density is constant over most of the depth even for relatively shallow flows. Hence, it seems a reasonable first approximation to assume that $\bar{\nu} = \nu_c = \text{const.}$ Γ and γ are functions only of the shape of the velocity and density profiles. It may be assumed that the profile parameters are adiabatic invariants, that they don't change very radically relative to other properties of the flow. (The evolving velocity and density profiles generated by the computer simulation appear to retain roughly the same shape. The profile parameters would not then vary a great deal.)

In particular:

$$dh >> d\Gamma$$

and

$$du >> d\gamma$$

While this assumption intuitively has physical validity, it is clearly subject to reevaluation once it becomes possible to determine Γ and γ experimentally.

The equation then may be written

$$-\rho_p \frac{Q^2}{b\nu_c h^2}\gamma\, dh = \rho_p \nu_c\, gb\, h \sin\alpha\, dx - \rho_p \nu_c\, gb\, h\, \Gamma\, dh - \bar{\tau}_w P\, dx$$

or, dividing by $\rho_p\, gb\, \nu_c h$,

$$-\frac{Q^2}{b^2 \nu_c^2\, gh^3}\gamma\, dh = \sin\alpha\, dx - \cos\alpha\, \Gamma\, dh - \frac{\bar{\tau}_w P\, dx}{\rho_p \nu_c\, gb\, h}$$

Note that

$$\frac{Q^2}{b^2 \nu_c^2 gh^3} = \frac{\bar{u}^2}{gh} = Fr^2$$

where $Fr = \bar{u} / \sqrt{gh}$ is the Froude number. Thus,

$$(\Gamma \cos\alpha - \gamma\ Fr^2)\, dh = (\sin\alpha - \frac{\bar{\tau}_w P}{\rho_p \nu_c gbh})\, dx$$

may be used to describe the flow in an open channel

Note that relative incompressibility is the only assumption made in deriving this equation. Thus it applies equally well or better to the flow of liquids. For liquid flow at high Reynolds number, it may be generally assumed that $\Gamma \equiv \gamma \equiv 1$. The inclination angles for fluid channels are generally very shallow, and it may be assumed that $\cos\alpha \simeq 1$. With these simplifications this equation takes on the general form of the open channel equation at motion generally used in hydraulic calculations (see, for example, Sabersky, Acosta, and Hauptmann [65].

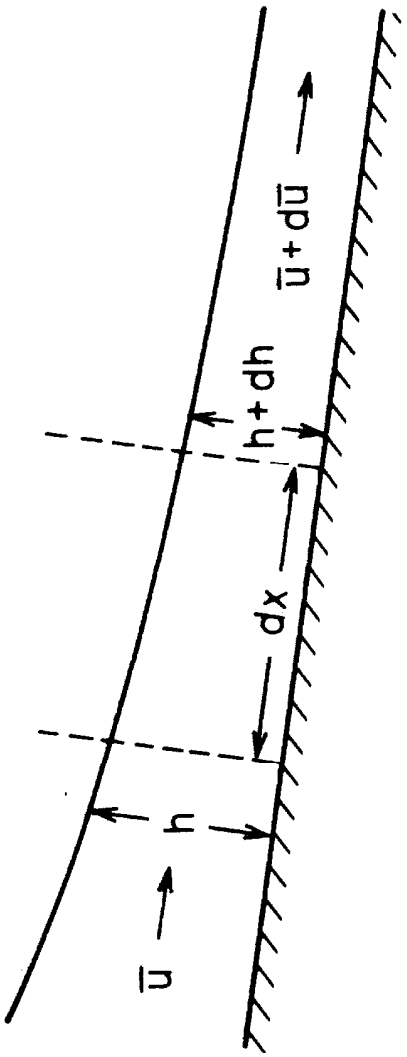

Figure A1 Diagram for the derivation of the open channel flow equation.

Appendix B

LISTINGS OF THE MAIN PROGRAMS

B.1 COL001: Main Program for the Inclined Chute Simulation

```
CCCCCCCCCCCCCCCCCCCCCCCCCCCCCCCCCCCCCCCCCCCCCCCCCCCCCCCCCCCCCCCCCCCCCCCCCCCCCCCCCCCCCCC
C                                                                               C
C    PROGRAM COL001                                                             C
C                                                                               C
C    THIS PROGRAM IS A SIMULATION OF THE FLOW OF TWO-DIMENSIONAL DISCS           C
C    IN AN INCLINED CHUTE                                                       C
C                                                                               C
C    THIS PROGRAM BELONGS TO CHARLES CAMPBELL, THOMAS 03, X4153                 C
C    THIS PROGRAM USES THE OUTPUT FROM COL007 AS INITIAL DATA.                  C
C    IT SUBSQUENTALLY GENERATES ITS OWN DATA SO THAT THE SIMULATION             C
C    MAY BE CONTINUED AFTER EXECUTION OF THIS RUN IS COMPLETE                   C
C                                                                               C
C    REQUIRED SUBPROGRAMS:                                                      C
C        COLLUP:   THE COLLISION ASSESSMENT ROUTINE                             C
C        PARTCL:   SOLVES THE COLLISION BETWEEN TWO PARTICLES                   C
C        WALLCL:   SOLVES THE COLLISION BETWEEN A PARTICLE AND A WALL           C
C        INIT   :  IS AN ENTRY INTO THE SUBPROGRAM INSRT THAT INITIALIZES       C
C                  THE COLLISION LIST                                           C
C        NEXT   :  IS AN ENTRY INTO THE SUBPROGRAM INSRT THAT YIELDS THE        C
C                  NEXT COLLISION TO OCCUR                                      C
C        REMOVE:   REMOVES FROM THE COLLISION LIST ALL COLLISIONS INVOLVING     C
C                  A SPECIFIED PARTICLE                                         C
C        PICTRE:   DRAWS A PICTURE OF THE CONTROL VOLUME                        C
C        SPLNE :   IS A CUBIC SPLINE FIT ROUTINE                                C
C        LSQUAR:   IS A LEAST-SQUARES FIT ROUTINE                               C
C        GRPLOT:   IS A PLOTTING ROUTINE                                        C
C        READNF, WRTNF, ENDMF, AND REWFF  ARE TAPE MANAGEMENT ROUTINES          C
C                                                                               C
CCCCCCCCCCCCCCCCCCCCCCCCCCCCCCCCCCCCCCCCCCCCCCCCCCCCCCCCCCCCCCCCCCCCCCCCCCCCCCCCCCCCCCC
      DIMENSION X(1000),Y(1000),U(1000),V(1000),W(1000),
     C MA(50),QM(50),QU(50),QV(50),QUV(50),QRH(50),QS3(50),
     C QD(50),QW(50),QN(50),IR(1000),DIST(1000),QT3(50),
     C DATA(3,20),DATA2(3,20),AV(10),AD(10),QE(1000),VMAP(50),
     C AN(10),QDP(50),QD2(50),DATA1(3,20),QUP(50),QVP(50),
     C MAP(80,84),DUY(50),DVY(50),DUY2(50),DVY2(50),DDY(50),
     C D2UY(50),D2VY(50),DIS(50),QS6(50),QR(50),NCOL(50),
     C QT6(50),QMF(50),QUVP(50),FY(300),QRXX(50),QRNS(50),
     C QRSS(50),QUDL(50),FNU(50),QMI(50),QNI(50),QFL(50),
     C QNUM(50),FNCOL(50),QS4(50),QT4(50),QU2(50),QV2(50),
     C QUV2(50),QM2(50),QN2(50),QW2(50),QWP(50),QRU(50),
     C QRV(50),COLDIS(50),QW1(50),QW3(50),RIMPLS(2),THETA(1000),
     C NAV(50),IFG(50),CON(100)
C
C    DO NOT USE WITH MORE THAN 80 PARTICLES WITHOUT CHANGING MAP DIMENSION
C
      DOUBLE PRECISION STOR(10,23),QT1(50),QS1(50),QT(50),QS(50),
     C QT2(50),QS2(50),QS3,QS4,QS5,QT3,QT4,QT5,TIM,TIME,DT,TIMEF
      LOGICAL XTEST,YTEST,LASTP,POINT,LINE,AXIS,TITLE,DASH,ORIGIN
     X  ,PDOC,SCX,SCY
        COMMON/A/IT,X,Y,U,V,W,SHEART,SHEARN,IR,AISS
        COMMON/B/ITA,ITB,ITC,ALS,ALC,ALT,ALCT,WL,WLS,WLC,AISN,AISC
        COMMON/D/DIS,ST,NCOL,RIMPLS
        COMMON/E/WDIS
       COMMON/PLDATA/XOFF,YOFF,XSZE,YSZE,NIX,NIY,XMIN,SCX,SCY,
      X              XMAX,YMIN,YMAX,XLPOS,YLPOS,ISYM,NDSH,ORIGIN,
      X              XTEST,YTEST,LASTP,POINT,LINE,AXIS,TITLE,DASH,
      X              FLD,XFMT(2),YFMT(2),NFX,NFY,PDOC
       COMMON/EXTRA/CSIZE
       COMMON/PARAMS/ EP,EW,NOC1,NOCL,SLVL,UMAX,ITPL,HM,ALPH
       DATA DFMT1/'(F7.'/,DFMT2/'4)  '/,DFMT3/'1)  '/,
      C     DFMT4/'0)  '/
CCCCCCCCCCCCCCCCCCCCCCCCCCCCCCCCCCCCCCCCCCCCCCCCCCCCCCCCCCCCCCCCCCCCCCCCCCCCCCCCCCCCCCC
C    INPUT VARIABLES:                                                           C
```

```
C       NOCD :  IS THE NUMBER OF COLLISIONS TO BE PERFORMED THIS RUN          C
C       NOCE :  IS THE NUMBER OF COLLISIONS FOR THE AVERAGING TIME            C
C       ST   :  IS THE AVERAGING STRIP WIDTH (IN PARTICLE RADII)              C
C       IPLT :  IS A FLAG:  IPLT= 0        NO PLOTS TO BE MADE THIS RUN       C
C                           IPLT NON-ZERO  PLOTS TO BE MADE                   C
C       ITAPE:  IS A FLAG INDICATING WETHER INTERMEDIATE SYSTEM STATES        C
C               ARE TO BE STORED ON A MAGNETIC TAPE                           C
C                           ITAPE= 0       NO STATES TO BE STORED             C
C                           ITAPE=N        STATES TO BE STORED AFTER          C
C                                          N COLLISIONS                       C
CCCCCCCCCCCCCCCCCCCCCCCCCCCCCCCCCCCCCCCCCCCCCCCCCCCCCCCCCCCCCCCCCCCCCCCCCCCCC
 2000  READ (5,502) NOCD,NOCE,ST,IPLT,ITAPE
  502 FORMAT(2I5,F10.0,2I10)
      IF (NOCD.EQ.0) STOP
       NOCI= NOCE
       NOCE= NOCD - NOCE
C   NOCE IS THE COLLISION AT WHICH AVERAGING IS TO BEGIN
       IF (NOCE.EQ.0) NOCE= 1
CCCCCCCCCCCCCCCCCCCCCCCCCCCCCCCCCCCCCCCCCCCCCCCCCCCCCCCCCCCCCCCCCCCCCCCCCCCCC
C   INPUT VARIABLES:                                                          C
C       TIME :  IS THE DIMENSIONLESS PROGRAM TIME AT THE START OF THE         C
C               CURRENT SIMULATION RUN                                        C
C       NOCI :  IS THE NUMBER OF COLLISIONS ALREADY RUN AT THE BEGINNING      C
C               OF THE CURRENT SIMULATION RUN                                 C
C       LAV3 :  IS THE NUMBER OF COLLISIONS ON THE TAPE THAT THE CURRENT      C
C               STATE OF THE SYSTEM IS TO BE ADDED TO THE END OF.             C
C       EW   :  IS THE CCEFFICENT OF RESTITUTION FOR WALL COLLISIONS          C
C       EP   :  IS THE COEFFICENT OF RESTITUTION FOR PARTICLE COLLISIONS      C
C       ALPH :  IS THE CHUTE INCLINATION IN DEGREES                           C
C       B    :  IS THE RATIO OF THE RADIUS OF GYRATION TO THE PARTICLE        C
C               RADIUS                                                        C
C       IT   :  IS THE NUMBER OF PARTICLES                                    C
C       WL   : IS THE CONTROL VOLUME WIDTH (IN PARTICLE RADII)                C
CCCCCCCCCCCCCCCCCCCCCCCCCCCCCCCCCCCCCCCCCCCCCCCCCCCCCCCCCCCCCCCCCCCCCCCCCCCCC
      READ (5,635) TIME,NOCI,LAV3
      READ (5,633) EW,EP,ALPH,B
      READ (5,634) IT, WL
       NOC1= NOCD + NOCI
      WRITE (6,600) EW,EP,ALPH,B,WL,IT,NOC1,NOCL,ST,
     C    ITAPE,IPLT
  600 FORMAT ( 26H  COEFF.OF RES.FOR WALL =  ,F12.3/
     C         26H  COEFF.OF RES.FOR PART.=  ,F12.3/
     C         26H  ALPHA                 =  ,F12.3/
     C         26H  B=K**2/R**2           =  ,F12.3/
     C         26H  WIDTH OF REGION       =  ,F12.3,/
     C         26H  NO. OF PARTICLES      =  ,I5,/
     C         26H  NO.OF COLLISIONS      =  ,I6/
     C         26H  SAMPLING TIME         =  ,I9/
     C         26H  SAMPLE INTERVAL       =  ,F12.3/
     C         26H  NEW  TAPE?               ,I9/
     C         26H  PLOTS THIS TIME?         ,I9///)
C
C   INITIALIZE VARIABLES
C
       ALF =0.0174532* ALPH
       ALS= SIN(ALF)
       ALC = COS(ALF)
       ITPL= IT
       ALT =ALS/ALC
       ALCT = ALC/ALS
       WLS =WL*ALS
       WLC = WL*ALC
       IEN= 0

 1000 IF (NDA.EQ.NDQ.AND.NDQ.GT.IT) GOTO 210
```

```
      AISN= ALS/(1 + B)
      AISS= AISN*ALS
      AISC= AISN*ALC
      TORQUE= ALS/(1.0 + 1.0/B)
      LAV= 0
      LAV2= 0
      TIME3= 0.0
      ST1= ST - 1.0
      ITA = IT+1
      ITB= IT+2
      ITC = IT+3
      IT1= IT - 1
      IDL= 0
      SHEARN= 0.0
      SHEART= 0.0
      QQAV= 0.0
      DAV= 0.0
      HM= 0.0
      FLMASS= 0.0
      MZ= 20
      APE=0.0
      AUE= 0.0
      AVE= 0.0
      AWE= 0.0
      ICRD= 7
     WRITE (6,637) TIME
  637 FORMAT(///24H ORIGINAL PARTICLE LIST   ,F15.5)
      UUAV= 0.0
CCCCCCCCCCCCCCCCCCCCCCCCCCCCCCCCCCCCCCCCCCCCCCCCCCCCCCCCCCCCCCCCCCCCCCCCCCCCCCC
C   INPUT THE INITIAL STATE OF THE SYSTEM.                                      C
C   THE INITIAL STATE OF THE SYSTEM IS DETERMINED BY THE INSTANTANEOUS          C
C   POSITIONS AND VELOCITIES OF THE PARTICLES.  THIS MAY BE THE TERMINAL        C
C   STATE OF A PREVICUS RUN OR MAY BE GENERATED BY THE PROGRAM COL007           C
C   AS AN INITIAL SYSTEM STATE                                                  C
C                                                                               C
C   INPUT VARIABLES:                                                            C
C       IR   :  IS A FLAG TO INDICATE WETHER A PARTICLE IS ROLLING              C
C                          IR(N)= 0      :   PARTICLE N IS NOT ROLLING          C
C                          IR(N) NON-ZERO:   PARTICLE N IS ROLLING              C
C       X    :  HORIZONTAL PARTICLE POSITION                                    C
C       Y    :  VERTICAL PARTICLE POSITION                                      C
C       U    :  HORIZONTAL PARTICLE VELOCITY                                    C
C       V    :  VERTICAL PARTICLE VELOCITY                                      C
C       W    :  ROTATIONAL PARTICLE VELOCITY                                    C
C                                                                               C
C   NOTE:  ALL PARTICLE POSITIONS AND VELOCITIES ARE REFERENCED WITH            C
C          THE GRAVITATIONAL BODY FORCE IN THE VERTICAL DIRECTION, AND          C
C          ARE NOT REFERENCED WITH RESPECT TO THE CHUTE BOTTOM.                 C
CCCCCCCCCCCCCCCCCCCCCCCCCCCCCCCCCCCCCCCCCCCCCCCCCCCCCCCCCCCCCCCCCCCCCCCCCCCCCCC
      DO 22 I= 1,IT
      READ (5,632) IR(I), X(I), Y(I), U(I), V(I), W(I)
       DS= X(I)*ALC - Y(I)*ALS
       DN= X(I)*ALS + Y(I)*ALC
       US= U(I)*ALC - V(I)*ALS
       UN= U(I)*ALS + V(I)*ALC
       UUAV= UUAV + US
   22 WRITE (6,631) I,DS,DN,US,UN,W(I),IR(I)
       WRITE (6,638)
  638 FORMAT(////////)
       UUAV= UUAV/FLOAT(IT)
       AVTM= 0.005*WL/UUAV
       UUAV= 0.0
      IF (ITAPE.NE.0) GOTO 23
```

```
      READ (20) NOCIF,TIMEF,EWF,EPF,ALPHF,BF,ITF,WLF
       FLAV3= FLOAT(LAV3)/1000.0
       NS= INT(FLAV3)
      IF (FLAV3-FLOAT(NS).GT.9.0E-4) THEN NS= NS+1
      READ(20,END=21)
   21 CALL READNF(20,NS)
C    CHECK TO SEE IF THIS IS THE PROPER TAPE
      IF (EWF.EQ.EW.AND.EPF.EQ.EP.AND.EWF.EQ.EW.AND.ALPHF.EQ.ALPH.
     C    AND.BF.EQ.B.AND.ITF.EQ.IT.AND.WLF.EQ.WL) GOTO 24
      WRITE(6,6231) NOCIF,TIMEF,EPF,EWF,ALPHF,BF,ITF,WLF,
     C              NOCIF,TIMEF,EPF,EWF,ALPHF,BF,ITF,WLF
 6231 FORMAT(I15,5F15.5,2I15/F15.5,5I15,2F15.5)
      WRITE (6,6003)
 6003 FORMAT('   WRONG TAPE MOUNTED')
      STOP
   23  NOC9= NOCI+ITAPE
      WRITE (20) NOC9,TIME,EW,EP,ALPH,B,IT,WL
      CALL WRTNF(20)
      LAV3= 0
C    COMPUTE INITIAL COLLISION LIST
   24 CALL INIT
       LAV5= LAV3
      DO 87 I= 1,IT
       LAT= I+1
   87 CALL COLLUP(I,LAT,0,TIME)

C    BEGIN MOTION
       NCA=0
       NDA=0
       NQA= 10
C    INITIALIZE ARRAYS THAT WILL CONTAIN AVERAGED QUANTITIES
      DO 162 LA=1,50
       QS(LA)= 0.0
       QT(LA)= 0.0
       QS2(LA)= 0.0
       IFG(LA)= 0
       NAV(LA)= 0
       QT2(LA)= 0.0
       QNUM(LA)= 0.0
       COLDIS(LA)= 0.0
  162  MA(LA)= 0
       DO 302 L=1, NOCD
C    COLLISION ASSESSMENT
 1100  NCA2= NCQ
       NDA2= NDQ
       NQA2= INT(DNQA)
       NCQ= NCA
       NDQ= NDA
       DNQA= FLOAT(NQA)
C    TAKE NEXT COLLISION FROM COLLISION LIST
C       NCA, NDA  ARE THE PARTICLES INVOLVED IN THE COLLISION
C       NQA       IS THE FRAME IN WHICH THE COLLISION IS TO OCCUR
C       TIM       IS THE PROGRAM TIME AT WHICH THE COLLISION IS TO OCCUR
      CALL NEXT(NCA,NDA,NQA,TIM)
C     WRITE (6,676) L,NCA,NDA,NQA,TIM,NCQ,NDQ,DNQA,IT
  676 FORMAT('  COLLISION  : ',4I7,F15.5,5X,2I5,F10.5,I5)
C    CHECK FOR CONTINUATION OF COLLISION PATTERNS THAT MAY BE INHIBITING
C       TIME ADVANCE. HERE WE CHECK TO SEE IF THERE IS A PATTERN OF
C       COLLISION OCCURENCE THAT IS DOMINATING COMPUTER TIME.  SUCH
C       A PATTERN IS INTERUPTED BY IGNORING A COLLISION
C       EVERY TEN PATTERN OCCURENCES TO ALLOW SOMETHING ELSE TO HAPPEN
      IF (TIM.EQ.TIME) GOTO 201
 1000 IF (NDA.EQ.NDQ.AND.NDQ.GT.IT) GOTO 210
```

```
      IF ((NCA.NE.NCA2.OR.NDA.NE.NDA2).AND.(NCA.NE.NDA2.OR.NDA.NE.NCA2))
     C GOTO 210
  201 IF (IDL.LT.10) GOTO 205
       IDL= 0
       IDL2= 1
      GOTO 1100
  205  IDL= IDL + 1
      GOTO 215
  210  IDL= 0
C    FIND TIME SINCE LAST COLLISION
  215  DT= TIM - TIME
C
C    TIME ADVANCE:    UPDATE PARTICLE POSITIONS AND VELOCITIES
C
      IF (L.EQ.NOCE) TIME1= TIME
  218  DTA= 0.5*DT*DT

       L5= L5 + 1
      DO 170 I=1,IT
       DD= U(I)*ALC - V(I)*ALS
       DS= U(I)*ALS + V(I)*ALC
C    COMPUTE INSTANTANEOUS ENERGY OF SYSTEM
       AUE= AUE + DD**2
       AVE= AVE + DS**2
       AWE= AWE + W(I)**2
       APE= APE + Y(I)
       UUAV= UUAV + DD
       IFR= 0

C    THIS SECTION COMPUTES THE TIME ADVANCE OF A ROLLING PARTICLE
       IF (IR(I).EQ.0) GOTO 107
        IFR= 1
        UISN= U(I)*ALC - V(I)*ALS
        DIST(I)= (X(I)*ALC - Y(I)*ALS) + UISN*DT + AISN*DTA
        X(I)= DIST(I)*ALC + 1.0*ALS
        Y(I)= 1.0*ALC - DIST(I)*ALS
        UISN= UISN + AISN*DT
        U(I)= UISN*ALC
        V(I)= -UISN*ALS
        W(I)= -UISN
       IF (L.LT.NOCE) GOTO 170
C    COMPUTE SHEAR STRESS APPLIED TO WALL BY ROLLING PARTICLE
        SHEART= SHEART - TORQUE*DT
        SHEARN= SHEARN + DT*ALC
       GOTO 170
C    UPDATE FOR NON-ROLLING PARTICLE
  107  Y(I) = Y(I) + DT*V(I) - DTA
       X(I) = X(I) + DT*U(I)
       V(I) = V(I) - DT
       DIST(I)= (X(I)*ALC) - (Y(I)*ALS)
  170 CONTINUE
  177 CONTINUE
C    PARTICLE-PARTICLE COLLISION SOLUTION
  220 IF (NDA.GT.IT) GOTO 131
       ISTRT= L - NOCE
       CALL PARTCL(NCA,NDA,NCA,B,EP,ISTRT)
       IR(NCA)= 0
       IR(NDA)= 0
       GOTO 132
C    PARTICLE-WALL COLLISION SOLUTION, INDICATED BY NDA= ITA= IT+1
  131 IF (NDA.GT.ITA) GOTO 133
       ISTRT = L - NOCE
      CALL WALLCL(NCA,B,EW,ISTRT)
```

```
      GOTO 132
C   THIS SECTION REMOVES PARTICLES THAT HAVE PASSED THE UPPER OR
C     LOWER BOUNDARIES
C
C   COLLISION WITH UPSTREAM PERIODIC BOUNDARY INDICATED BY NDA= ITB= IT+2
  133 IF (NDA.GT.ITB) GOTO 134
       Y(NCA)= Y(NCA) - WLS
       X(NCA)= X(NCA) + WLC
      GOTO 132
C   COLLISION WITH DOWNSTREAM PEIODIC BOUNDARY INDICATED BY NDA= ITC= IT+3
  134  Y(NCA)= Y(NCA) + WLS
       X(NCA)= X(NCA) - WLC

  132  TIME= TIM
       TIME2= TIME - TIME1
 6335  MAP(NCA,NDA)= MAP(NCA,NDA) + 1
       MAP(NDA,NCA)= MAP(NDA,NCA) + 1
C
C   ASSESS NEW COLLISIONS FOR THE TWO PARTICLES INVOLVED
C
      CALL COLLUP(NCA,1,NDA,TIME)
      IF (NDA.LE.IT) CALL COLLUP(NDA,1,NCA,TIME)
C
C   REASSESS NEW COLLISIONS FOR PARTICLES INVOLVED IN RECURRING PATTERN
C
      IF (IDL2.NE.1) GOTO 280
      CALL COLLUP(NCQ,1,0,TIME)
      IF (NDQ.LE.IT) CALL COLLUP(NDQ,1,NCQ,TIME)
       IDL2= 0
  280 IF (NDA.GT.ITA) GOTO 1100
C
C    WRITE STATE OF SYSTEM ONTO TAPE
C
      IF (DT.EQ.0.0.OR.L.LT.ITAPE) GOTO 157
       LAV3= LAV3+1
       NOC2= NOCI+L
      WRITE (20) TIME,NOC2,NCA,NDA,NQA,
     C    (X(I),Y(I),U(I),V(I),W(I), I= 1,IT)
      IF ((FLOAT(LAV3)/1000.0 - AINT(FLOAT(LAV3)/1000.0)).LT.1E-5)
     C  CALL WRTNF(20)
C   EVERY FIFTY COLLISIONS WRITE OUT THE SYSTEM ENERGY
  157 IF ((FLOAT(L)/50.0 - AINT(FLOAT(L)/50.0)).GT.0.00001) GOTO 142
 6340  AUE= AUE/FLOAT(2*IT*L5)
       AVE= AVE/FLOAT(2*IT*L5)
       AWE= B*AWE/FLOAT(2*IT*L5)
       UUAV= UUAV/FLOAT(L5*IT)
       AKE= AUE + AVE + AWE
       APE= APE/FLOAT(IT*L5)
       ATE= AKE + APE
       AUE= AUE - 0.5*UUAV**2
       UUAV= 0.0
       IEN= IEN+1
       QE(IEN)= ATE
       L5= 0
       L2= L - 50
      WRITE (6,650) L2,L,AKE,APE,ATE,TIME,AUE,AVE,AWE
  650 FORMAT(5X,I5,'-',I5,'  COLLISIONS,   AVERAGE KINETIC'
     C  ' POTENTIAL, AND TOTAL ENERGIES ARE: ',3F15.5/
     C  20X,'TIME,U,V,W,ENERGIES: ',4F15.5)
       AUE= 0.0
       AVE= 0.0
       AWE= 0.0
       APE= 0.0
```

```
CCCCCCCCCCCCCCCCCCCCCCCCCCCCCCCCCCCCCCCCCCCCCCCCCCCCCCCCCCCCCCCCCCCCCCCCCCC
C                                                                         C
C   AVERAGE THE PROPERTIES OF THE SYSTEM                                  C
C                                                                         C
CCCCCCCCCCCCCCCCCCCCCCCCCCCCCCCCCCCCCCCCCCCCCCCCCCCCCCCCCCCCCCCCCCCCCCCCCCC
  142 IF (L.LT.NOCE) GOTO 300
      IF (L.EQ.NOCE) LAV4= LAV3
      DO 1470 I= 1,MZ
 1470 IFG(I)= 0
      IF (NDA.GT.IT) GOTO 147
C
C   COLLISION ANGLE DISTRIBUTION ASSESSMENT, RESULT STORED IN ARRAY COLDIS
C
       LAV2= LAV2+1
       DNQA= FLOAT(NQA)
       DISY= Y(NDA) - (Y(NCA) + WLS*DNQA)
       DISX= X(NDA) + WLC*DNQA - X(NCA)
       DISC= SQRT(DISX*DISX + DISY*DISY)
       BS= DISY*ALC + DISX*ALS
       BC= DISX*ALC - DISY*ALS
      IF (BC.NE.0.0) GOTO 143
       NA= 25
      GOTO 144
  143  NA= 1+INT(-(ATAN(BS/BC) - 1.570196)/.062831861)
      IF (NA.GT.50.OR.NA.LT.0) GOTO 147
  144  COLDIS(NA)= COLDIS(NA) + 1.0
  147 IF (TIME-TIME3.LT.AVTM.AND.L.NE.NOCD) GOTO 300
       TIME3= TIME
C
C  DENSITY AND VELOCITY DISTRIBUTION ASSESSMENT
C
       LAV= LAV+1
      DO 500 I= 1,IT
       DC= Y(I)*ALC + X(I)*ALS
       DD= U(I)*ALC - V(I)*ALS
       DE= U(I)*ALS + V(I)*ALC
       M= 1 + INT(DC/ST)
      IF (M.GT.50) GOTO 500
  501  MZ= MAX0(MZ,M)
       HM= HM + DC
       FLMASS= FLMASS + DD
C
C   DETERMINE STRIP IN WHICH PARTICLE CENTER LIES
C   AND STRIP IN WHICH REST OF PARTICLE LIES
C
       S= DC - FLOAT(M-1)*ST
       A= 1.0
      IF (S.GE.1.0) GOTO 550
       M1= M-1
      IF (ABS(S).GT.1.0) GOTO 237
      GOTO 560
  550 IF (S.LE.ST1) GOTO 570
       S= ST - S
       M1= M+1
      IF (ABS(S).GT.1.0) GOTO 237
C   A AND A2 ARE THE PERCENTAGE OF EACH PARTICLE THAT LIE WITHIN EACH STRIP
  560  A= 1.0 + (S*SQRT(1.0 - S*S) - ARCOS(S))/3.14159
       A2= 1.0 - A
C
C   COMPUTE INSTANTANEOUS AVERAGE OF PROPERTIES WITHIN STRIP
C
  570  QD2(M)= QD2(M) + A
       MA(M)= MA(M) + 1
```

```
      QM2(M)= QM2(M) + A*DD
      QN2(M)= QN2(M) + A*DE
      QW1(M)= QW1(M) + A*W(I)
      QW3(M)= QW3(M) + A*W(I)**2
      QU2(M)= QU2(M) + A*DD**2
      QV2(M)= QV2(M) + A*DE**2
      QUV2(M)= QUV2(M) + A*DD*DE
     IF (IFG(M).NE.0) GOTO 5700
      NAV(M)= NAV(M)+1
      IFG(M)= 1
 5700 IF (L.NE.NOCE.AND.L.NE.NOCD) GOTO 575
      QS2(M)= QS2(M) + A*DD
      QT2(M)= QT2(M) + A*DE
  575 IF (A.EQ.1.0) GOTO 500
      QD2(M1)= QD2(M1) + A2
      QM2(M1)= QM2(M1) + A2*DD
      QN2(M1)= QN2(M1) + A2*DE
      QW1(M1)= QW1(M1) + A2*W(I)
      QW3(M1)= QW3(M1) + A*W(I)**2
      QU2(M1)= QU2(M1) + A2*DD**2
      QV2(M1)= QV2(M1) + A2*DE**2
      QUV2(M1)= QUV2(M1) + A2*DD*DE
     IF (IFG(M1).NE.0) GOTO 5701
      IFG(M1)= 1
      NAV(M1)= NAV(M1)+1
 5701 IF (L.NE.NOCE.AND.L.NE.NOCD) GOTO 500
C    QS AND QT ARE USED TO COMPUTE THE SHEAR AND NORMAL STRESSES RESPECTIVELY
      QS2(M1)= QS2(M1) + A2*DD
      QT2(M1)= QT2(M1) + A2*DE
  500 CONTINUE
     DO 580 I= 1,MZ
     IF (QD2(I).EQ.0.0) GOTO 580
C    AVERAGE INSTANTANEOUS SYSTEM STATE
      QD(I)= QD(I) + QD2(I)
      QDP(I)= QDP(I) + QD2(I)**2
      QM(I)= QM(I) + QM2(I)/QD2(I)
      QN(I)= QN(I) + QN2(I)/QD2(I)
      QU(I)= QU(I) + QU2(I)/QD2(I)
      QV(I)= QV(I) + QV2(I)/QD2(I)
      QW(I)= QW(I) + QW1(I)/QD2(I)
      QW2(I)= QW2(I) + QW3(I)/QD2(I)
      QUV(I)= QUV(I) + QUV2(I)/QD2(I)
      QRSS(I)= QRSS(I) + QUV2(I)
      QRNS(I)= QRNS(I) + QV2(I)
      QRXX(I)= QRXX(I) + QU2(I)
      QRU(I)= QRU(I) + QM2(I)
      QRV(I)= QRV(I) + QN2(I)
      QD2(I)= 0.0
      QM2(I)= 0.0
      QN2(I)= 0.0
      QU2(I)= 0.0
      QV2(I)= 0.0
      QUV2(I)= 0.0
      QW1(I)= 0.0
      QW3(I)= 0.0
     IF (L.NE.NOCE.AND.L.NE.NOCD) GOTO 580
      QS(I)= QS2(I) - QS(I)
      QT(I)= QT2(I) - QT(I)
      QS2(I)= 0.0
      QT2(I)= 0.0
  580 CONTINUE
  299 CONTINUE
C
```

```
C   IS RUN OVER?
C
  300 IF (LAV3.GE.15000) GOTO 301
  302 CONTINUE
C
C   IF SO WRITE RESULTS
C
  301  K1= 1
       K= MIN0(ITC,20)
  572 WRITE (6,603) (I,I= K1,K)
  603 FORMAT(////'     COLLISION MAP'//7X,20I5 /)
      DO 574 I= 1,IT
  574 WRITE (6,604) I,(MAP(I,I2), I2= K1,K)
  604 FORMAT(I7,20I5)
       K1= K+1
      IF (K.EQ.ITC) GOTO 573
       K= MIN0((K+20),ITC)
      GOTO 572
  573 IF (LAV.EQ.0) GOTO 237
       HM= HM/FLOAT(LAV*IT)
       MZ1= 1 + INT(2.0*HM/ST)
      IF (3.0*QD(MZ1).LT.QD(MZ1-1)) MZ1= MZ1 - 1
      WRITE(6,691)
  691 FORMAT('1'//40H   DENSITY AND VELOCITY DISTRIBUTIONS     /
     C /15X,15HSOLID FRACTION , 5X,1HU,14X,1HV,14X,1HW,13X,4HU**2,
     C 11X,4HV**2,12X,2HUV//)
       FLAV= FLOAT(LAV)
       UMAX= -1000.0
       NC= 0
      DO 130 M= 1,MZ
      IF (NAV(M).EQ.0) GOTO 130
       FNAV= FLOAT(NAV(M))
       QM(M)= QM(M)/FNAV
      IF (QM(M).GT.UMAX) UMAX=QM(M)
       QN(M)= QN(M)/FNAV
       QW(M)= QW(M)/FNAV
       QW2(M)= QW2(M)/FNAV
       QU(M)= QU(M)/FNAV
       QV(M)= QV(M)/FNAV
       QUV(M)= QUV(M)/FNAV
       QD(M)= 3.141593 * QD(M)/(ST*WL*FLAV)
  130 WRITE (6,690) M,MA(M),QD(M),QM(M),QN(M),QW(M),QU(M),QV(M),QUV(M)
     C ,M
  690 FORMAT(2I5,7E15.6,I5)

      WRITE (6,692)
  692 FORMAT(////16X,'W**2',16X,'D''',9X,'MASSFLOW ',
     C 7X,'U''**2',10X,'V''**2',10X,'W''**2',10X,'U''V'''//)
      DO 231 I= 1,MZ
       QDP1= (3.141593/(ST*WL))**2*QDP(I)/FLAV - QD(I)**2
       QUDL(I)= QM(I)/UMAX
       QMF(I)= QD(I)*QM(I)
       QUP(I)= QU(I) - QM(I)**2
       QVP(I)= QV(I) - QN(I)**2
       QWP(I)= QW2(I) - QW(I)**2
       QFL(I)= QUP(I) + QVP(I)
      IF (QUP(I)+QVP(I).GT.0.0) QQAV= QQAV + QD(I)*SQRT(QUP(I)+QVP(I))
       DAV= DAV + QD(I)
       QUVP(I)= QUV(I) - QM(I)*QN(I)
  231 WRITE(6,693) I,QW2(I),QDP1,QMF(I),QUP(I),QVP(I),QWP(I),
     C              QUVP(I),I
  693 FORMAT(I5,5X,7E15.5,I5)
  161 CONTINUE
```

```
C   REYNOLDS STRESS CALCULATION
      WRITE(6,694)
  694 FORMAT('1',' FLUCTUATING QUANTITIES'///
     C     14X,'NU*U**2',8X,'NU*V**2',9X,'NU*U*V',10X,'NU*U',
     C     11X,'NU*V',9X,'NU''*U''',9X,'NU''*V''')
      DO 232 I= 1,MZ
      IF (NAV(I).EQ.0) GOTO 232
       FNAV= FLOAT(NAV(I))
       QRSS(I)= 3.141593*QRSS(I)/(ST*WL*FNAV)
       QRNS(I)= 3.141593*QRNS(I)/(ST*WL*FNAV)
       QRXX(I)= 3.141593*QRXX(I)/(ST*WL*FNAV)
       QRUT= 3.141593*QRU(I)/(ST*WL*FNAV)
       QRVT= 3.141593*QRV(I)/(ST*WL*FNAV)
       QRU(I)= QRUT - QD(I)*QM(I)
       NC= NC + NCOL(I)
       QRV(I)= QRVT - QD(I)*QN(I)
  232 WRITE(6,693) I,QRXX(I),QRNS(I),QRSS(I),QRUT,QRVT,
     C     QRU(I),QRV(I),I
      WRITE (6,695)
  695 FORMAT(////35X,'REYNOLD''S STRESSES'//
     C     26X,'-NU*U''**2',6X,'-NU*V''**2',6X,'-NU*U''*V'''//)
      DO 233 I= 1,MZ
       QRSS(I)= -(QRSS(I) - (QRU(I)*QN(I) + QRV(I)*QM(I))
     C     - QD(I)*QM(I)*QN(I))
       QRXX(I)= -(QRXX(I) - 2*QRU(I)*QM(I) - QD(I)*QM(I)**2)
       QRNS(I)= -(QRNS(I) - 2*QRV(I)*QN(I) - QD(I)*QN(I)**2)
  233 WRITE(6,696) I,QRXX(I),QRNS(I),QRSS(I),I
  696 FORMAT(16X,I5,'  ',3E15.5,I7)
C   WALL STRESSES AND OTHER AVERAGE SYSTEM PROPERTIES
       SHERN= SHEARN/(TIME2*WL)
       SHERT= SHEART/(TIME2*WL)
       SHEARY= SHERN*ALC - SHERT*ALS
       SHEARX= SHERN*ALS + SHERT*ALC
       FRIC= ATAN(SHEART/SHEARN)/0.0174532
       FLMASS= FLMASS/FLAV
       QQAV= QQAV/DAV
       DAV= DAV/MZ
       AVVEL= FLMASS/FLOAT(IT)
       RIMPLS(1)= RIMPLS(1)/FLOAT(NC)
       RIMPLS(2)= RIMPLS(2)/FLOAT(NC)
       RIMANG= ATAN(RIMPLS(2)/RIMPLS(1))
      WRITE (6,640) SHERT,SHERN,SHEARY,SHEARX,FRIC,FLMASS,AVVEL,HM,
     C  QQAV,DAV,RIMPLS(1),RIMPLS(2),RIMANG
  640 FORMAT('1'////35X,24HWALL STRESS DISTRIBUTION,//
     C 25X,15HTANGENTIAL :   ,F15.5,/
     C 25X,15HNORMAL     :   ,F15.5,/
     C 25X,15HY-DIRECTION:   ,F15.5,/
     C 25X,15HX-DIRECTION:   ,F15.5,/
     C 25X,15HFRICTION ANGLE ,F15.5,//
     C 15X,19HMASS FLOW       :  ,F15.5,/
     C 15X,19HAVERAGE VELOCITY:  ,F15.5,/
     C 15X,19HMASS MEAN HEIGHT:  ,F15.5,/
     C 15X,19HAV. FLUC. VEL.  :  ,F15.5 /
     C 15X,19HAV DENSITY      :  ,F15.5,/
     C 15X,19HNORMAL IMPULSE  :  ,F15.5,/
     C 15X,19HTANGENTIAL IMP. :  ,F15.5,/
     C 15X,19HIMPULSE ANGLE   :  ,F15.5,///)
C   WRITE OUT THE FINAL STATE OF THE SYSTEM
  237 WRITE(6,620) TIME
  620 FORMAT('1'///19H NEW PARTICLE LIST    ,F15.5)
      DO 145 I= 1,IT
       DS= X(I)*ALC - Y(I)*ALS
       DN= X(I)*ALS + Y(I)*ALC
```

```
      US= U(I)*ALC - V(I)*ALS
      UN= U(I)*ALS + V(I)*ALC
  145 WRITE (6,631) I,DS,DN,US,UN,W(I),IR(I)
  631 FORMAT (I5,5F15.5,I5)
C   PUNCH STATE OF SYSTEM ONTO CARDS FOR LATER USE
      WRITE(7,635) TIME,NOC1,LAV3
      WRITE(7,633) EW,EP,ALPH,B
      WRITE(7,634) IT,WL
      DO 320 I=1,IT
      WRITE(12,632) IR(I), X(I), Y(I), U(I), V(I), W(I)
  320 WRITE(7,632) IR(I), X(I), Y(I), U(I), V(I), W(I)
  632 FORMAT(I5,5F10.5)
  633 FORMAT(4F10.4)
  634 FORMAT(I5,F10.4)
  635 FORMAT(F10.3,2I5)
C   DRAW PICTURE OF CONTROL VOLUME
      HM2= 2.0*HM
      CALL PICTRE(HM2)
C   MAKE LEAST SQUARES FITS TO VELOCITY AND DENSITY PROFILES
      DO 770 I= 1,MZ1
       DATA(1,I)= FLOAT(I-1)*ST + ST/2.0
       DATA(2,I)= QM(I)
       DATA(3,I)= 1.0
       DATA1(1,I)= FLOAT(I-1)*ST + ST/2.0
       DATA1(2,I)= QN(I)
       DATA1(3,I)= 1.0
       DATA2(1,I)= FLOAT(I-1)*ST + ST/2.0
       DATA2(2,I)= QD(I)
  770  DATA2(3,I)= 1.0
       CHISQ= 1.0
      CALL LSQUAR(DATA,MZ1,IORD,AV,CHISQ,STOR)
       CHISQ= 1.0
      CALL LSQUAR(DATA1,MZ1,IORD,AN,CHISQ,STOR)
       CHISQ= 1.0
      CALL LSQUAR(DATA2,MZ1,IORD,AD,CHISQ,STOR)
      WRITE (6,660) (AV(I), I= 1,IORD),(AN(I),I= 1,IORD)
  660 FORMAT(/////24H  VELOCITY COEFFICENTS:  //
     C 3X,5HU:     ,7D15.7/
     C 3X,5HV:     ,7D15.7)
      WRITE (6,675)  (AD(I), I= 1,IORD)
  675 FORMAT(///24H  DENSITY COEFFICENTS:   //8X,7D15.7//////)
C    COMPUTE AND WRITE OUT STRESS DISTRIBUTION
       QS6(MZ1+1)= 0
       QT6(MZ1+1)= 0
      WRITE (6,645)
  645 FORMAT(//35X,19HSTRESS DISTRIBUTION  ,//7X,3('TANGENTIAL',
     C 5X,'NORMAL',9X),'FRICTION ANGLE')
       DO 800 I2= 1,MZ1
        I= 1 + MZ1 - I2
        QS3(I)= -QS(I)/(TIME2*ST*WL*3.141593)
        QT3(I)= -QT(I)/(TIME2*ST*WL*3.141593)
        QS4(I)= QS3(I) + QD(I)*ALS/3.141593
        QT4(I)= QT3(I) - QD(I)*ALC/3.141593
        QS6(I)= QS6(I+1) + QS4(I)*ST
  800   QT6(I)= QT6(I+1) + QT4(I)*ST
       DO 801 I= 1,MZ1
        ANG= ATAN(QS6(I)/QT6(I))
  801 WRITE (6,647) I,QS3(I),QT3(I),QS4(I),QT4(I),QS6(I),
     C   QT6(I),ANG,I
  647 FORMAT(I5,7D15.6,I7)
C   WRITE OUT PROFILE OF ENERGY DISSIPATION BY SYSTEM
       WDIS= WDIS/TIME2
       TDIS= WDIS
```

```
      WRITE (6,610) WDIS
  610 FORMAT(////35X,'DISSIPATION DISTRIBUTION'/
     C  25X,'WALL DISSIPATION:   ',E15.6//)
      DO 423 I= 1, MZ1
       DIS(I)= DIS(I)/TIME2
       TDIS= TDIS + DIS(I)
  423 WRITE (6,615) I,DIS(I)
  615 FORMAT(36X,I5,5X,E15.6)
      WRITE (6,618) TDIS
  618 FORMAT(//25X,'TOTAL DISSIPATION:  ',E15.6)
      WRITE (6,648)
  648 FORMAT(/////)
C   COLLISION FREQUENCY AS A FUNCTION OF DENSITY
      WRITE (6,652)
  652 FORMAT('1',35X,'COLLISION FREQUENCY'//
     C       25X, ' LEVEL  NUMBER    PERCENTAGE        NU'//)
       NC=0
      DO 3499 I= 1,MZ
 3499  NC= NC + NCOL(I)
      DO 3500 I= 1,MZ
       FNCOL(I)= FLOAT(NCOL(I))/FLOAT(NC)
 3500 WRITE (6,653) I,NCOL(I),FNCOL(I),QD(I)
  653 FORMAT(25X,2I7,2F15.6)
C  CONDUCTIVITY EVALUATION, PRODUCED ERRONEOUS RESULTS
      WRITE (6,6472)
 6472 FORMAT(/////35X,'CONDUCTIVITY'/
     C             27X,'LEVEL  CONDUCTIVITY    SOLID FRACTION'/)
      DO 3510 I= 1,MZ
       TSM= QS6(I-1)
       TNM= QT6(I-1)
       TEM= ABS(QFL(I-1))
      IF (I.NE.1) GOTO 3505
       TSM= SHERT
       TNM= SHERN
       TEM= 0
 3505  CON(I)= QM(I)*(QS6(I+1)-TSM)+QN(I)*(QT6(I+1)-TNM)
     C        + U(I)*ALS - V(I)*ALC - ABS(DIS(I))
       IF (I.EQ.1) CON(I)= CON(I) - ABS(WDIS)
       CON(I)= CON(I)/(2*QFL(I)-(QFL(I+1)+TEM))
 3510 WRITE(6,6471) I,CON(I),QD(I)
 6471 FORMAT(27X,I5,2F15.5)
C   VELOCITY AND DENSITY GRADIENTS
      WRITE (6,677)
  677 FORMAT('1'///25X,22HDISTRIBUTION GRADIENTS   //
     C 12X,'DU/DY',6X,'(DU/DY)**2',8X,'D2U/DY2',9X,'DV/DY',
     C 6X,'(DV/DY)**2',8X,'D2V/DY2',8X,'DNU/DY'/)
       IOR1= IORD - 1
C
C   GRADIENTS ARE FOUND FROM A CUBIC SPLINE FIT TO THE DATA
C
      CALL SPLNE(MZ1,ST,QD,DDY,D2UY)
      CALL SPLNE(MZ1,ST,QM,DUY,D2UY)
      CALL SPLNE(MZ1,ST,QN,DVY,D2VY)
      DO 420 I= 1,MZ1
      IF (I.NE.1.AND.I.NE.MZ1) GOTO 401
C
C   ONLY THE GRADIENTS AT THE ENDPOINTS ARE COMPUTED BY THE LEAST
C   SQUARES FIT
C
      DO 400 I2= 2,IOR1
       D2MM= FLOAT(I2*(I2-1))*(FLOAT(I-1)*ST + ST/2.0)**(I2-2)
       D2UY(I)= D2UY(I) + AV(I2+1)*D2MM
  400  D2VY(I)= D2VY(I) + AN(I2+1)*D2MM
```

```
  401  DUY2(I)= DUY(I)**2
       DVY2(I)= DVY(I)**2
  420 WRITE(6,678) I,DUY(I),DUY2(I),D2UY(I),DVY(I),DVY2(I),
     C D2VY(I),DDY(I),I
  678 FORMAT(I5,7E15.6,I10)
C
C    MAKE THE APPROPRIATE PLOTS
C
       DO 3900 I= 1,MZ1
 3900   FY(I)= FLOAT(I)/FLOAT(MZ1)
       WRITE (6,6001)
 6001 FORMAT('1','  PLOTTED DATA'//
     C  20X,'FY',12X,'UNORM',8X,'MASS FLOW',8X,'F(NU)',
     C  12X,'R',12X,'S*R/2',8X,'TEMPERATURE')
       DO 5000 I= 1,MZ1
        FNU(I)= ABS(QS6(I))/DUY2(I)
        QMF(I)= QMF(I)/UMAX
        QR(I)= 2*SQRT(DUY2(I)/(QUP(I)+QVP(I)))
        QRH(I)= 0.5*QR(I)*SQRT(3.141593/QD(I))
 5000 WRITE (6,693) I,FY(I),QUDL(I),QMF(I),FNU(I),QR(I),QRH(I),
     C QFL(I),I
       CALL DFAULT
        SLVL= QM(1)
       CALL NEWPEN(3)
        YMAX= 1.10
       CALL GRPLOT(MZ1,QUDL,FY,'U/UMAX ',6,'Y/H ',3,
     C             'U/UMAX VS Y/H   ',13,'    ',0)
        XMAX= 1.0
       CALL GRPLOT(MZ1,QD,FY,'SOLID FRACTION  ',14,'Y/H ',3,
     C             'SOLID FRACTION  ',14,'    VS Y/H  ',10)
        XMAX= 0.6
       CALL GRPLOT(MZ1,QMF,FY,'NU*U/UMAX   ',9,'Y/H ',3,
     C             'DIMENSIONLESS   ',13,'MASS FLOW   ',9)
        XMAX= 1.0
        YSZE= 7.5
        NIY= 8
        YMAX=  2.0
       CALL GRPLOT(MZ1,QD,QR,'SOLID FRACTION  ',14,
     C       '2R*DUDY/V''  ',10,'R VS NU ',7,'    ',0)
        YMAX= 5.0
       CALL GRPLOT(MZ1,QD,QRH,'SOLID FRACTION  ',14,
     C       'R*S/2   ',5,'R*S VS NU ',9,'    ',0)
        YMAX= 4.0
       CALL GRPLOT(MZ1,QD,FNU,'SOLID FRACTION  ',14,
     C             'SHEAR/(DU/DY)2  ',14,
     C             'DENSITY DEPENDENCE  ',18,'OF SHEAR',8)
        YSZE= 5.0
        XSZE= 8.0
        NIX=  9
        NIY=  5
        YMAX= 1.1
        LASTP= .FALSE.
       DO 5101 I= 1,MZ1
        SHERT= ABS(QS6(I))
        SHRN=  ABS(QT6(I))
        SHERN= ABS(QRXX(I))
        SHRS=  ABS(QRSS(I))
        SHRT=  ABS(QRNS(I))
 5101   XMAX=  AMAX1(SHERT,SHERN,SHRT,SHRN,SHRS,XMAX)
        XMIN= -XMAX
        XFMT(1)= DFMT1
        XFMT(2)= DFMT2
        NFX= 7
```

```
      CALL GRPLOT(MZ1,QS6,FY,'DIM''LESS SHEAR  ',14,'Y/H ',3,
     C  'SHEAR VS Y/H',12,'    ',0)
       TITLE= .FALSE.
       PDOC= .FALSE.
       AXIS= .FALSE.
       ORIGIN= .FALSE.
       ISYM= 10
      CALL GRPLOT(MZ1,QT6,FY,'    ',0,'    ',0,'    ',0,'    ',0)
       ISYM= 2
      CALL GRPLOT(MZ1,QRSS,FY,'    ',0,'    ',0,'    ',0,'    ',0)
       ISYM= 3
      CALL GRPLOT(MZ1,QRNS,FY,'    ',0,'    ',0,'    ',0,'    ',0)
       ISYM= 6
       LASTP= .TRUE.
      CALL GRPLOT(MZ1,QRXX,FY,'    ',0,'    ',0,'    ',0,'    ',0)
      CALL ENDMF(20)
      DO 6051 I= 1,10
 6051 READ(20,END=6052)
 6052  TIME3= -AVTM
       NUMC= 0
C
C   REWIND TAPE TO COMPUTE VELOCITY DISTRIBUTIONS
C
       IRT=  INT(FLOAT(LAV5 + LAV3 - LAV4)/1000.0 + 0.00001)
      CALL READNF(20,IRT)
       LAV6= LAV3 - LAV4
      DO 6100 N= 1,LAV6
 6004 READ(20,END=6005) TIME,NOC2,NCA,NDA,NQA,
     C   (X(I),Y(I),U(I),V(I),W(I),I=1,IT)
      GOTO 6007
 6005 CALL READNF(20)
      GOTO 6004
 6007 IF (TIME-TIME3.LT.AVTM) GOTO 6100
       TIME3= TIME
      DO 6010 I= 1,IT
       DM= (X(I)*ALS + Y(I)*ALC)/ST
      IF (DM.EQ.0.0) WRITE(6,656) I,NOC2,IT,X(I),Y(I)
  656 FORMAT(' UNDER ',3I5,2F15.5)
       M= 1 + INT(DM)
      IF (QFL(M).LE.0.0) GOTO 6010
       DD= U(I)*ALC - V(I)*ALS
       DE= U(I)*ALS + V(I)*ALC
       MN= 1+INT(SQRT(((DD-QM(M))**2+(DE-QN(M))**2+B*(W(I)-QW(I))**2)
     C              /QFL(M))/.1)
      IF (MN.GT.50) GOTO 6010
       NUMC= NUMC+1
       QNUM(MN)= QNUM(MN) + 1.0
 6010 CONTINUE
 6100 CONTINUE
C   DISTRIBUTION OF COLLISION ANGLE
      WRITE (6,642)
  642 FORMAT('1'//15X,'COLLISION DISTRIBUTION',48X,
     C 'VELOCITY DISTRIBUTION'//
     C 10X,'ANGLE',10X,'NUMBER',7X,'PERCENTAGE',
     C 25X,'RANGE',10X,'NUMBER',7X,'PROBABILITY'//)
      DO 3700 I= 1,50
       DS= FLOAT(I)*0.1
       DD= FLOAT(I)*0.06283186
       PC= COLDIS(I)/(FLOAT(LAV2)*0.06283186)
       NOC= INT(COLDIS(I))
       PV= 10.0*QNUM(I)/NUMC
       NV= INT(QNUM(I))
 3700 WRITE (6,643) DD,NOC,PC,DS,NV,PV
```

```
 643 FORMAT(F15.5,I15,F15.5,20X,F15.1,I15,F15.5)
     DO 6000 I= 1,50
      FY(I)= FLOAT(I)*0.1
6000  QNUM(I)= QNUM(I)/FLOAT(NUMC)
      XMIN= 0.0
      XMAX= 5.0
      TITLE= .TRUE.
      AXIS= .TRUE.
      PDOC= .TRUE.
      ORIGIN=.TRUE.
      YMAX= 0.1
      ISYM= 1
     CALL GRPLOT(50,FY,QNUM,'(C-UAV)/V'' ',10,'N/NTOT ',
    C    6,'NUMBER DISTRIBUTION ',19,'    ',0)
     DO 6200 I= 1,50
      FY(I)= FLOAT(I)*0.0628318
6200  COLDIS(I)= COLDIS(I)/(FLOAT(LAV2)*0.0628318)
      YMAX= 1.0
      XMIN= 0.0
      XMAX= 3.141593
     CALL GRPLOT(50,FY,COLDIS,'ANGLE   ',5,'P(THETA)',8,
    C  'COLLISION ANGLE ',15,'DISTRIBUTION',12)

8003 DO 8004 I= 1,IEN
8004 FY(I)= FLOAT(I)*50.0
     CALL DFAULT
      XSZE= 8.0
      POINT= .FALSE.
      SCY=.TRUE.
      XFMT(1)= DFMT1
      XFMT(2)= DFMT4
      YFMT(1)= DFMT1
      YFMT(2)= DFMT4
      LINE= .TRUE.
C   WRITE OUT ENERGY HISTORY
      XMAX= FLOAT(IEN)*50.0
      SCY=.TRUE.
      ISYM= 1
     CALL GRPLOT(IEN,FY,QE,'COLLISIONS  ',10,
    C   'TOTAL ENERGY',12,'ENERGY HISTORY  ',14,'    ',0)
      STOP
      END
C THIS MARKS END OF MAIN PROGRAM
```

B.2 COL002: Main Program for the Couette Flow Simulation

```
CCCCCCCCCCCCCCCCCCCCCCCCCCCCCCCCCCCCCCCCCCCCCCCCCCCCCCCCCCCCCCCCCCCCCCCCCCCCCCC
C                                                                              C
C    PROGRAM COL002                                                            C
C                                                                              C
C    THIS PROGRAM IS A SIMULATION OF THE FLOW OF TWO-DIMENSIONAL DISCS          C
C    IN A COUETTE SHEAR CELL                                                   C
C                                                                              C
C    THIS PROGRAM BELONGS TO CHARLES CAMPBELL, THOMAS 03, X4153                C
C    THIS PROGRAM USES THE OUTPUT FROM COL006 AS INITIAL DATA.                 C
C    IT SUBSQUENTALLY GENERATES ITS OWN DATA SO THAT THE SIMULATION            C
C    MAY BE CONTINUED AFTER EXECUTION OF THIS RUN IS COMPLETE                  C
C                                                                              C
C    REQUIRED SUBPROGRAMS:                                                     C
C        COLLUP:   THE COLLISION ASSESSMENT ROUTINE                            C
C        PARTCL:   SOLVES THE COLLISION BETWEEN TWO PARTICLES                  C
C        WALLCL:   SOLVES THE COLLISION BETWEEN A PARTICLE AND A WALL          C
C        INIT  :   IS AN ENTRY INTO THE SUBPROGRAM INSRT THAT INITIALIZES      C
C                  THE COLLISION LIST                                          C
C        NEXT  :   IS AN ENTRY INTO THE SUBPROGRAM INSRT THAT YIELDS THE       C
C                  NEXT COLLISION TO OCCUR                                     C
C        REMOVE:   REMOVES FROM THE COLLISION LIST ALL COLLISIONS INVOLVING    C
C                  A SPECIFIED PARTICLE                                        C
C        PICTRE:   DRAWS A PICTURE OF THE CONTROL VOLUME                       C
C        SPLNE :   IS A CUBIC SPLINE FIT ROUTINE                               C
C        LSQUAR:   IS A LEAST-SQUARES FIT ROUTINE                              C
C        GRPLOT:   IS A PLOTTING ROUTINE                                       C
C        READMF, WRTMF, ENDMF, AND REWFF  ARE TAPE MANAGEMENT ROUTINES         C
C                                                                              C
CCCCCCCCCCCCCCCCCCCCCCCCCCCCCCCCCCCCCCCCCCCCCCCCCCCCCCCCCCCCCCCCCCCCCCCCCCCCCCC
C
C
      DIMENSION X(1000),Y(1000),U(1000),V(1000),W(1000),
     C MA(50),QM(50),QU(50),QV(50),QUV(50),QRH(50),
     C QD(50),QW(50),QN(50),IR(1000),DIST(1000),
     C DATA(3,20),DATA2(3,20),AV(10),AD(10),QR(50),QDI(50),
     C AN(10),QDP(50),QD2(50),DATA1(3,20),QUP(50),QVP(50),
     C MAP(50,54),DUY(50),DVY(50),DUY2(50),DVY2(50),DDY(50),
     C D2UY(50),D2VY(50),WDIS(2),DIS(50),VMAP(40,2),QS6(50),
     C QT6(50),QMF(50),QUVP(50),FY(400),QRXX(50),QRNS(50),QE(1000),
     C QRSS(50),QUDL(50),FNU(50),CMI(50),QNI(50),QFL(50),QNUM(50),
     C QETM(1000),QDPI(50),NCOL(50),FNCOL(50),COLDIS(50),QU2(50),
     C QV2(50),QUV2(50),QM2(50),QN2(50),QW2(50),QWP(50),QRU(50),
     C QRV(50),QW1(50),QW3(50),GCOL(50),RIMPLS(2),GCY(50),GCX(50),
     C QNUMU(50),QNUMV(50),QNUMW(50),FY2(50),IBN(50),VCOR(50),
     C UCOR(50),QFL1(50),QUP1(50),QVP1(50),QWP1(50),QTMP(50),
     C QNUM1(50),QFL2(50)
C
C    DO NOT USE WITH MORE THAN 50 PARTICLES WITHOUT CHANGING MAP DIMENSION
C
      DOUBLE PRECISION STOR(10,23),QS(50),QT(50),QS2(50),QT2(50),
     C   TIME,TIM,DT,TIMEF
      LOGICAL XTEST,YTEST,LASTP,PCINT,LINE,AXIS,TITLE,DASH,ORIGIN
     X  ,PDOC,SCX,SCY
      COMMON/A/IT,X,Y,U,V,W,SHEART,SHEARN,IR,AISS
      COMMON/B/ITA,ITB,ITC,ALS,ALC,ALT,ALCT,WL,WLS,WLC,AISN,AISC
      COMMON/D/DIS,SL,NCOL,RIMPLS
      COMMON/E/SHRT,SHRN,WDIS,VBOT,VTOP
      COMMON/PLDATA/XOFF,YOFF,XSZE,YSZE,NIX,NIY,XMIN,SCX,SCY,
     X              XMAX,YMIN,YMAX,XLPOS,YLPOS,ISYM,NDSH,ORIGIN,
     X              XTEST,YTEST,LASTP,PCINT,LINE,AXIS,TITLE,DASH,
     X              FLD,XFMT(2),YFMT(2),NFX,NFY,PDOC
      COMMON/EXTRA/CSIZE
      COMMON/PARAMS/ EP,EW,NOC1,NOCL,UW,UTOP,ITPL,HGT,ALF
```

```
      DATA DFMT1/'(F7.'/,DFMT2/'4)  '/,DFMT3/'1)  '/,
     C     DFMT4/'0)  '/

  639 FORMAT('1')
CCCCCCCCCCCCCCCCCCCCCCCCCCCCCCCCCCCCCCCCCCCCCCCCCCCCCCCCCCCCCCCCCCCCCCCCCCCCCCC
C    INPUT VARIABLES:                                                          C
C        NOCD :  IS THE NUMBER OF COLLISIONS TO BE PERFORMED THIS RUN          C
C        NOCE :  IS THE NUMBER OF COLLISIONS FOR THE AVERAGING TIME            C
C        ST   :  IS THE AVERAGING STRIP WIDTH (IN PARTICLE RADII)              C
C        UW   :  IS THE NORMAL STRESS APPLIED TO THE SOLID WALLS               C
C        IPLT :  IS A FLAG:  IPLT= 0        NO PLOTS TO BE MADE THIS RUN       C
C                            IPLT NON-ZERO  PLOTS TO BE MADE                   C
C        ITAPE:  IS A FLAG INDICATING WETHER INTERMEDIATE SYSTEM STATES        C
C                ARE TO BE STORED ON A MAGNETIC TAPE                           C
C                            ITAPE= 0       NO STATES TO BE STORED             C
C                            ITAPE=N        STATES TO BE STORED AFTER          C
C                                           N COLLISIONS                       C
C        IMOV :  A FLAG TO INDICATE WETHER THE SOLID WALLS BE ALLOWED TO       C
C                MOVE                                                          C
C        TIME :  IS THE DIMENSIONLESS PROGRAM TIME AT THE START OF THE         C
C                CURRENT SIMULATION RUN                                        C
C        NOCI :  IS THE NUMBER OF COLLISIONS ALREADY RUN AT THE BEGINNING      C
C                OF THE CURRENT SIMULATION RUN                                 C
C        LAV3 :  IS THE NUMBER OF COLLISIONS ON THE TAPE THAT THE CURRENT      C
C                STATE OF THE SYSTEM IS TO BE ADDED TO THE END OF.             C
C        EW   :  IS THE COEFFICENT OF RESTITUTION FOR WALL COLLISIONS          C
C        EP   :  IS THE COEFFICENT OF RESTITUTION FOR PARTICLE COLLISIONS      C
C        ALPH :  IS THE CHUTE DEGREES                                          C
C        B    :  IS THE RATIO OF THE RADIUS OF GYRATION TO THE PARTICLE        C
C                RADIUS                                                        C
C        UTOP :  IS THE TOP WALL VELOCITY                                      C
C        HGT  :  IS THE SOLID WALL SPACING                                     C
C        GEE  :  IS THE GRAVITATIONAL ACCELERATION                             C
C        IT   :  IS THE NUMBER OF PARTICLES                                    C
C        WL   :  IS THE CONTROL VOLUME WIDTH (IN PARTICLE RADII)               C
CCCCCCCCCCCCCCCCCCCCCCCCCCCCCCCCCCCCCCCCCCCCCCCCCCCCCCCCCCCCCCCCCCCCCCCCCCCCCCC
 2000 READ (5,502) NOCD,NOCE,ST,UW,IPLT,ITAPE,IMOV
  502 FORMAT(2I5,2F10.0,3I5)
      READ (5,635) TIME,NOCI,LAV3
      READ (5,633) EW,EP,ALPH,B
      READ (5,633) UTOP,HGT,GEE
      READ (5,634) IT, WL
       NOC1= NOCD + NOCI
      WRITE (6,600) EW,EP,ALPH,UTOP,GEE,HGT,UW,B,WL,IT,NOC1,NOCD,
     C NOCE,ST,IMOV,ITAPE,IPLT
  600 FORMAT('1',26H COEFF.OF RES.FOR WALL =  ,F12.3/
     C           26H  COEFF.OF RES.FOR PART.=  ,F12.3/
     C           26H  ALPHA                 =  ,F12.3/
     C           26H  WALL VELOCITY         =  ,F12.3/
     C           26H  GRAVITY               =  ,F12.3/
     C           26H  UPPER WALL HEIGHT     =  ,F12.3/
     C           26H  NORMAL STRESS         =  ,F12.3/
     C           26H  B=K**2/R**2           =  ,F12.3/
     C           26H  WIDTH OF REGION       =  ,F12.3,/
     C           26H  NO. OF PARTICLES      =  ,I9/
     C           26H  NO.OF COLLISIONS      =  ,I9/
     C           26H  COLLISIONS THIS RUN   =  ,I9/
     C           26H  SAMPLING TIME         =  ,I9/
     C           26H  SAMPLE INTERVAL       =  ,F12.3/
     C           26H  WALLS MOVING?            ,I9/
     C           26H  NEW TAPE?                ,I9/
     C           26H  PLOTS THIS TIME?         ,I9///)
C
```

```
C    INITIALIZE VARIABLES
C
       NOCL= NOCE
       NOCE= NOCD - NOCE
      IF (NOCE.EQ.0) NOCE= 1
       ALF= 0.0174532*ALPH
       ALS= SIN(ALF)
       ALC= COS(ALF)
      IF (ALC.NE.0.0) ALT=  ALS/ALC
      IF (ALS.NE.0.0) ALCT= ALC/ALS
       AVHGT= 0.0
       HGTO= HGT
       GR= UTOP/HGT
       WLS= WL*ALS
       WLC= WL*ALC
       IWL2= INT(WL/ST)
       WL2= AINT(WL)
       WL3= WL2-2.0
       SHAPE= WL/HGT
       TIMST= TIME
       AISN= GEE*ALS/(1+B)
       AISS= AISN*ALS
       AISC= AISN*ALC
       ITPL= IT
       IEN= 0
       LT= 3*IT
       FIT= FLOAT(IT)
       TORQUE= GEE*ALS/(1.0 + 1.0/B)
       FND= 1.0
       VTOP=  0.0
       VBOT= 0.0
       VSIDE= 0.0
       AVTOP= 0.0
       BWSH= 0.0
       ST1= ST - 1.0
       ITA = IT+1
       ITA1= IT+2
       ITB = IT+3
       ITC = IT+4
       IDL= 0
       QQAV= 0.0
       SHEARN= 0.0
       SHEART= 0.0
       HM= 0.0
       FLMASS= 0.0
       MZ= 0
       LAV= 0
       LAV2= 0
       LAV5= LAV3
       TIME3= -1000.0
       AKE=0.0
       APE=0.0
       AUE= 0.0
       AVE= 0.0
       AWE= 0.0
       NUMC= 0
       IORD= 4
      WRITE (6,637) TIME
  637 FORMAT(///24H ORIGINAL PARTICLE LIST   ,F15.5)
CCCCCCCCCCCCCCCCCCCCCCCCCCCCCCCCCCCCCCCCCCCCCCCCCCCCCCCCCCCCCCCCCCCCCCCCCCCCCCC
C    INPUT THE INITIAL STATE OF THE SYSTEM.                                   C
C    THE INITIAL STATE OF THE SYSTEM IS DETERMINED BY THE INSTANTANEOUS       C
C    POSITIONS AND VELOCITIES OF THE PARTICLES.  THIS MAY BE THE TERMINAL     C
```

```
C    STATE OF A PREVIOUS RUN OR MAY BE GENERATED BY THE PROGRAM COL006          C
C    AS AN INITIAL SYSTEM STATE                                                 C
C                                                                               C
C    INPUT VARIABLES:                                                           C
C        IR    :  IS A FLAG TO INDICATE WETHER A PARTICLE IS ROLLING            C
C                           IR(N)= 0       :   PARTICLE N IS NOT ROLLING        C
C                           IR(N)= 1       :   PARTICLE N IS ROLLING ON BOTTOM  C
C                                              WALL                             C
C                           IR(N)= 2       :   PARTICLE N IS ROLLING ON UPPER   C
C                                              WALL                             C
C        X     :  HORIZONTAL PARTICLE POSITION                                  C
C        Y     :  VERTICAL PARTICLE POSITION                                    C
C        U     :  HORIZONTAL PARTICLE VELOCITY                                  C
C        V     :  VERTICAL PARTICLE VELOCITY                                    C
C        W     :  ROTATIONAL PARTICLE VELOCITY                                  C
C                                                                               C
C    NOTE:  ALL PARTICLE POSITIONS AND VELOCITIES ARE REFERENCED WITH           C
C           THE GRAVITATIONAL BODY FORCE IN THE VERTICAL DIRECTION, AND         C
C           ARE NOT REFERENCED WITH RESPECT TO THE CHUTE BOTTOM.                C
C                                                                               C
C           BOTH THE UPPER AND LOWER SOLID WALLS ARE ALLOWED TO MOVE            C
C           ALL PARTICLE POSITIONS WILL BE REFERENCED WITH RESPECT TO THE       C
C           LOWER WALL POSITION                                                 C
CCCCCCCCCCCCCCCCCCCCCCCCCCCCCCCCCCCCCCCCCCCCCCCCCCCCCCCCCCCCCCCCCCCCCCCCCCCCCCC
       UUAV= 0.0
      DO 22 I= 1,IT
      READ (5,632) IR(I), X(I), Y(I), U(I), V(I), W(I)
       DS= X(I)*ALC - Y(I)*ALS
       DIST(I)= DS
       DN= X(I)*ALS + Y(I)*ALC
       US= U(I)*ALC - V(I)*ALS
       UN= U(I)*ALS + V(I)*ALC
   22 WRITE (6,631) I,DS,DN,US,UN,W(I),IR(I)
      WRITE (6,638)
  638 FORMAT(////////)
C    CHECK TAPE HEADER
      IF (ITAPE.NE.0) GOTO 23
      READ (20) NOCIF,TIMEF,EWF,EPF,ALPHF,BF,ITF,WLF,UTOPF,GEEF,UWF
       FLAV3= FLOAT(LAV3)/1000.0
       NS= INT(FLAV3)
      IF (FLAV3-FLOAT(NS).GT.9E-4) THEN NS= NS+1
      READ(20,END=21)
   21 CALL READNF(20,NS)
      IF (EWF.EQ.EW.AND.EPF.EQ.EP.AND.EWF.EQ.EW.AND.ALPHF.EQ.ALPH.
     C     AND.BF.EQ.B.AND.ITF.EQ.IT.AND.WLF.EQ.WL.AND.UTOPF.EQ.UTOP.
     C     AND.GEEF.EQ.GEE) GOTO 24
       WRITE(6,6231) NOCIF,TIMEF,EPF,EWF,ALPHF,BF,ITF,WLF,
     CNOCIF,TIMEF,EPF,EWF,ALPHF,BF,ITF,WLF
 6231 FORMAT(I15,5F15.5,2I15/F15.5,5I15,2F15.5)
      WRITE (6,6003)
 6003 FORMAT('   WRONG TAPE MOUNTED')
      STOP
   23 NOC9= NOCI+ITAPE
      WRITE (20) NOC9,TIME,EW,EP,ALPH,B,IT,WL,UTOP,GEE,UW
      CALL WRTNF(20)
      LAV3= 0

C    COMPUTE INITIAL COLLISION LIST
   24 CALL INIT
       LAV5= LAV3
      DO 87 I= 1,IT
       LAT= I+1
   87 CALL COLLUP(I,LAT,0,TIME,GEE,HGT,ITA1,VTOP,VBOT,VSIDE)
```

```
C : BEGIN MOTION
      NCA=0
      NDA=0
      NQA= 10
C    INITIALIZE AVERAGING ARRAYS
      DO 162 LA=1,50
       QDP(LA)= 0.0
       QUV(LA)= 0.0
       QW(LA)= 0.0
       QD2(LA)= 0.0
       QD(LA)= 0.0
       QV(LA)= 0.0
       QU(LA)= 0.0
       QM(LA)= 0.0
       QN(LA)= 0.0
       QS(LA)= 0.0
       QT(LA)= 0.0
       COLDIS(LA)= 0.0
       QNUM(LA)= 0.0
       QNUMU(LA)= 0.0
       QNUMV(LA)= 0.0
       QNUMW(LA)= 0.0
       GCOL(LA)= 0.0
       GCX(LA)= 0.0
       GCY(LA)= 0.0
       VCOR(LA)= 0.0
       UCOR(LA)= 0.0
       IBN(LA)= 0
  162  MA(LA)= 0
      DO 301 L=1, NOCD
C    COLLISION ASSESSMENT
C    CHECK FOR CONTINUATION OF COLLISION PATTERNS THAT MAY BE INHIBITING
C       TIME ADVANCE
 1100  NCA2= NCQ
       NDA2= NDQ
       NQA2= INT(DNQA)
       NCQ= NCA
       NDQ=NDA
       DNQA= FLOAT(NQA)
C    TAKE NEXT COLLISION FROM COLLISION LIST
C       NCA, NDA  ARE THE PARTICLES INVOLVED IN THE COLLISION
C       NQA       IS THE FRAME IN WHICH THE COLLISION IS TO OCCUR
C       TIM       IS THE PROGRAM TIME AT WHICH THE COLLISION IS TO OCCUR
      CALL NEXT(NCA,NDA,NQA,TIM)
      IF (L.EQ.NOCE) TIME1= TIME
 1000 IF (ITM.LT.5) GOTO 1002
       IDL2= 1
       ITM= 0
      GOTO 1100
 1002 IF ((NCA.NE.NCA2.OR.NDA.NE.NDA2).AND.(NCA.NE.NDA2.OR.NDA.NE.NCA2))
     CGOTO 210
      IF (IDL.LT.5) GOTO 205
       IDL= 0
       IDL2= 1
      GOTO 1100
  205  IDL= IDL + 1
      GOTO 215
  210  IDL= 0
C    FIND TIME SINCE LAST COLLISION
  215  DT= TIM - TIME
C       WRITE (6,676) L,NCA,NDA,NQA,TIM,AKE1
  676 FORMAT(' COLLISION  : ',4I7,4F15.5)
```

```
        AKE1= 0.0
       ITM= ITM+1
      IF (DT.GT.0.0) ITM= 0
       TIME= TIM
C
C   TIME ADVANCE:    UPDATE PARTICLE POSITIONS AND VELOCITIES
C
      IF (L.NE.NOCE) GOTO 218
       TIME1= TIME
       MZ= INT(HGT/ST)
       FND= FLOAT(MZ)
  218  DTA= 0.5*DT*DT
C   UPDATE SOLID WALL SPACING
       HGT= HGT + VTOP*DT
C   UPDATE PERIODIC WALL SPACING
       WL= WL + VSIDE*DT
       WLS= WL*ALS
       WLC= WL*ALC
C   UPDATE UPPER WALL VELOCITY TO KEEP VELOCITY GRADIENT CONSTANT
       UTOP= GR*HGT
C   COMPUTE INSTANTANEOUS ENERGY OF SYSTEM
      DO 170 I=1,IT
       AKE1= AKE1+U(I)**2+V(I)**2+B*W(I)**2
       DD= U(I)*ALC - V(I)*ALS
       DS= U(I)*ALS + V(I)*ALC
       AUE= AUE + DD**2
       AVE= AVE + DS**2
       AWE= AWE + W(I)**2
       APE= APE + Y(I)*GEE
       UUAV= UUAV + DD
      IF (DT.LE.0.0) GOTO 170

C   THIS SECTION COMPUTES THE TIME ADVANCE OF A ROLLING PARTICLE
      IF (IR(I).EQ.0) GOTO 107
       DN= FLOAT(IR(I) - 1)
       UISN= U(I)*ALC - V(I)*ALS
       DIST(I)= (X(I)*ALC - Y(I)*ALS) + UISN*DT + AISN*DTA
       X(I)= DIST(I)*ALC + ((HGT-2.00002)*DN + 1.00001)*ALS
       Y(I)= ((HGT - 2.00002)*DN +  1.00001)*ALC - DIST(I)*ALS
       UISN= UISN + AISN*DT
       U(I)= UISN*ALC
       V(I)= -UISN*ALS
       W(I)= (2*DN - 1)*UISN - DN*UTOP
      IF (L.LT.NOCE) GOTO 170
      IF (DN.NE.0.0) GOTO 169
C   COMPUTE WALL STRESS CONTRIBUTION OF ROLLING PARTICLES
       SHEART= SHEART - TORQUE*DT
       SHEARN= SHEARN + DT*ALC*GEE
      GOTO 170
  169  SHERT= SHERT + TORQUE*DT
      GOTO 170
C   UPDATE FREE FALLING PARTICLE POSITIONS AND VELOCITIES
  107  UISN= U(I)*ALC - V(I)*ALS
       VISN= U(I)*ALS + V(I)*ALC
       UI= UISN*ALC + (VISN-VBOT)*ALS
       IF (ALC.NE.0.0) VI= ((VISN - VBOT) - UI*ALS)/ALC
       IF (ALC.EQ.0.0) VI= U(I)
       Y(I) = Y(I) + DT*VI - DTA*GEE
       X(I) = X(I) + DT*UI
       V(I) = V(I) - DT*GEE
       DIST(I)= X(I)*ALC - Y(I)*ALS
  170 CONTINUE
  177 CONTINUE
```

```
  220 IF (NDA.GT.IT) GOTO 131
       ISTRT= L - NOCE
       SL= HGT/FND
C    PARTICLE-PARTICLE COLLISION SOLUTION
       CALL PARTCL (NCA,NDA,NOA,B,EP,ISTRT)
       IR(NCA)= 0
       IR(NDA)= 0
      GOTO 132
  131 IF (NDA.GT.ITA1) GOTO 133
       DN= 0.0
      IF (NDA.EQ.ITA1) DN= 1.0
       ISTRT = L - NOCE
C    PARTICLE-WALL COLLISION SOLUTION
C       LOWER WALL COLLISION INDICATED BY NDA= ITA= IT+1
C       UPPER WALL COLLISION INDICATED BY NDA= ITA1= IT+2
      CALL WALLCL(NCA,B,EW,ISTRT,DN,UTOP,HGT,GEE,UWSH,BWSH)
      GOTO 132
C    THIS SECTION REMOVES PARTICLES THAT HAVE PASSED THE UPPER OR
C    LOWER BOUNDERIES
C
C    COLLISION WITH UPSTREAM PERIODIC BOUNDARY INDICATED BY NDA= ITB= IT+2
  133 IF (NDA.GT.ITB) GOTO 134
       X(NCA)= X(NCA) + WLC
       Y(NCA)= Y(NCA) - WLS
      GOTO 132
C    COLLISION WITH DOWNSTREAM PEIODIC BOUNDARY INDICATED BY NDA= ITC= IT+3
  134  X(NCA)= X(NCA) - WLC
       Y(NCA)= Y(NCA) + WLS
  132  TIME2= TIME - TIME1
C       UPDATE COLLISION MAP
       MAP(NCA,NDA)= MAP(NCA,NDA) + 1
       MAP(NDA,NCA)= MAP(NDA,NCA) + 1
C
C    ASSESS NEW COLLISIONS FOR THE TWO PARTICLES INVOLVED
C
      CALL COLLUP(NCA,1,NDA,TIME,GEE,HGT,ITA1,VTOP,VBOT,VSIDE)
      IF (NDA.LE.IT) CALL COLLUP(NDA,1,NCA,TIME,GEE,HGT,ITA1,VTOP,
     C  VBOT,VSIDE)
       IF (IDL2.NE.1) GOTO 280
C
C    REASSESS NEW COLLISIONS FOR PARTICLES INVOLVED IN RECURRING PATTERN
C
      CALL COLLUP(NCQ,1,0,TIME,GEE,HGT,ITA1,VTOP,VBOT,VSIDE)
      IF (NDQ.LE.IT) CALL COLLUP(NDQ,1,NCQ,TIME,GEE,HGT,ITA1,VTOP,
     C  VBOT,VSIDE)
       IDL2= 0
  280 IF (L.EQ.LT.OR.IMOV.EQ.0) GOTO 1220
C
C    WALL VELOCITY CHANGES?  CHECK IMPULSE APPLIED TO WALL AGAINST
C                            REQUIRED STRESS AND PUT WALLS INTO
C                            APPROPRIATE MOTION
C
      IF ((L.LT.LT).AND.ABS(HGT-HGTO).LT.0.1) GOTO 1220
      WRITE (6,666) L,VTOP,UWSH,VBOT,BWSH,HGT
  666 FORMAT('   COLLISION, TOP VELOCITY, STRESS, AND HEIGHT  :',
     C  I10,5F12.6)
       HGTO= HGT
       LT= L+3*IT
       DTO= TIME - DTO
       IF (DTO.EQ.0.0) GOTO 1220
C    UWSH    CONTAINS THE TOTAL IMPULSE APPLIED BY PARTICLES TO THE UPPER WALL
C    BWSH    CONTAINS THE TOTAL IMPULSE APPLIED BY PARTICLES TO THE LOWER WALL
       BWSH= ABS(BWSH/(DTO*WL)) - (UW + GEE*FLOAT(IT)*DTO/WL)
```

```
        UWSH= ABS(UWSH/(DTO*WL)) - UW
        VBOT2= VBOT
        VBOT= 0.5*VBOT-SIGN(UW,BWSH)
       IF (ABS(BWSH).LT.UW) VBOT= 0.5*VBOT2-BWSH
        VTOP2= VTOP
        VTOP= 0.5*(VTOP+VBCT2) + SIGN(UW,UWSH) - VBOT
       IF (ABS(UWSH).LT.UW) VTOP= 0.5*(VTOP2+VBOT2) + UWSH - VBOT
        VSIDE= SHAPE*VTOP
C
C   IF VTOP OR VBOT MUST BE CHANGED RECOMPUTE THE ENTIRE COLLISION LIST
C
 1208  IF (VBOT.EQ.VBOT2.AND.VTOP.EQ.VTOP2) GOTO 1210
       CALL INIT
       DO 1200 I= 1,IT
        IR(I)= 0
        LAT= I+1
 1200 CALL COLLUP(I,LAT,0,TIME,GFE,HGT,ITA1,VTOP,VBOT,VSIDE)
 1210  DTO= TIME
        UWSH= 0.0
        BWSH= 0.0
 1220 IF (NDA.GT.ITA1) GOTO 1100
        L5= L5 + 1
C
C    WRITE STATE OF SYSTEM ONTO TAPE
C
       IF (DT.EQ.0.0.OR.L.LT.ITAPE) GOTO 1225
        LAV3= LAV3+1
        NOC2= NCCI+L
       WRITE (20) TIME,NOC2,NCA,ND4,NQA,HGT,
      C   (X(I),Y(I),U(I),V(I),W(I), I= 1,IT),WL,VTOP,VBOT
       IF ((FLOAT(LAV3)/1000.0 - AINT(FLOAT(LAV3)/1000.0)).LT.1E-5)
      C  CALL WRTNF(20)
C   EVERY 200 COLLISIONS WRITE OUT THE SYSTEM ENERGY
 1225 IF ((FLOAT(L)/200.0 - AINT(FLOAT(L)/200.0)).GT.0.00001.OR.
      C  L5.EQ.0) GOTO 142
        AUE= AUE/FLOAT(2*IT*L5)
        AVE= AVE/FLOAT(2*IT*L5)
        AWE= B*AWE/FLCAT(2*IT*L5)
        UUAV= UUAV/FLOAT(L5*IT)
        AKE= AUE + AVE + AWE
        APE= APE/FLOAT(IT*L5)
        ATE= AKE + APE +AWE
        AUE= AUE - 0.5*UUAV**2
        UUAV= 0.0
        IEN= IEN + 1
        QE(IEN)= ATE
        L5= 0
        L2= L - 200
       WRITE (6,650) L2,L,AKE,APE,ATE,TIME,AUE,AVE,AWE
  650 FORMAT(5X,I5,'-',I5,'  COLLISICNS,   AVERAGE KINETIC',
      C  ' POTENTIAL, AND TOTAL ENERGIES ARE: ',3F15.5/
      C  20X,'TIME,U,V,W,ENERGIES: ',4F15.5)
        AUE= 0.0
        AVE= 0.0
        AWE= 0.0
        APE= 0.0
CCCCCCCCCCCCCCCCCCCCCCCCCCCCCCCCCCCCCCCCCCCCCCCCCCCCCCCCCCCCCCCCCCCCCCCCCC
C                                                                        C
C   AVERAGE THE PROPERTIES OF THE SYSTEM                                 C
C                                                                        C
CCCCCCCCCCCCCCCCCCCCCCCCCCCCCCCCCCCCCCCCCCCCCCCCCCCCCCCCCCCCCCCCCCCCCCCCCCC
  142 IF (L.LT.NOCE) GOTO 299
       IF (L.NE.NOCE) GOTO 1420
```

```
      WL2= AINT(WL)
      WL3= WL2 - 2.0
C   AVTM IS THE AVERAGE TIME PASSED BETWEEN COLLISIONS BEFORE THE START
C     OF AVERAGING.  IT WILL BE REQUIRED THAT THIS TIME BE PASSED
C     BETWEEN SAMPLINGS OF THE SYSTEM PROPERTIES
      AVTM= 5*(TIME-TIMST)/NOCE
      TIME3= TIME - 1.1*AVTM
 1420 IFLG= 0
      IF (NDA.GT.IT.OR.DT.EQ.0.0) GOTO 147
      LAV2= LAV2+1
      DNOA= FLOAT(NOA)
C   COLLISION ANGLE DISTRIBUTION ASSESSMENT
      DISY= Y(NDA) - (Y(NCA) + WLS*DNCA)
      DISX= X(NDA) + WLC*DNOA - X(NCA)
      DISC= SQRT(DISX*DISX + DISY*DISY)
      BS= DISY*ALC + DISX*ALS
      BC= DISX*ALC - DISY*ALS
      IF (BC.NE.0.0) GOTO 143
      NA= 25
      GOTO 144
  143 NA= 1+INT(-(ATAN(BS/BC) - 1.570196)/.06283186)
      IF (NA.GT.50.OR.NA.LT.0) GOTO 147
  144 COLDIS(NA)= COLDIS(NA) + 1.0
  147 IF (TIME-TIME3.LT.AVTM.AND.L.NE.NOCD.AND.LAV3.NE.15000)
     C  GOTO 300
      TIME3= TIME
C   DENSITY AND VELOCITY DISTRIBUTION ASSESMENT
C
C   ADJUST STRIP WIDTH ACCORDING TO THE WALL SPACING
      ST= HGT/FND
      LAV= LAV + 1
      IF (L.NE.NOCE) AVHGT= AVHGT + ST
      IF (L.GE.NOCE) AVTOP= AVTOP + (VTOP - VBOT)
      DO 500 I= 1,IT
C
C   DETERMINE STRIP IN WHICH PARTICLE CENTER LIES
C   AND STRIP IN WHICH REST OF PARTICLE LIES
C
      DC= Y(I)*ALC + X(I)*ALS
      DD= U(I)*ALC - V(I)*ALS
      DE= U(I)*ALS + V(I)*ALC
      M= 1 + INT(DC/ST)
      IF (M.GT.50) GOTO 500
  501 HM= HM + DC
      FLMASS= FLMASS + DD
      S= DC - FLOAT(M-1)*ST
      A= 1.0
      A2= 0.0
      IF (S.GE.1.0) GOTO 550
      M1= M-1
      GOTO 560
  550 IF (S.LE.ST-1.0) GOTO 570
      S= ST - S
      M1= M+1
  560 A= 1.0 + (S*SQRT(1.0 - S*S) - ARCOS(S))/3.14159
      A2= 1.0 - A
C   A AND A2 ARE THE PERCENTAGE OF EACH PARTICLE THAT LIE WITHIN EACH STRIP
C
C   COMPUTE INSTANTANEOUS AVERAGE OF PROPERTIES WITHIN STRIP
C
  570 QD2(M)= QD2(M) + A
      MA(M)= MA(M) + 1
      QM2(M)= QM2(M) + A*DD
```

```
      QN2(M)= QN2(M) + A*DE
      QW1(M)= QW1(M) + A*W(I)
      QW3(M)= QW3(M) + A*W(I)**2
      QU2(M)= QU2(M) + A*DD**2
      QV2(M)= QV2(M) + A*DE**2
      QUV2(M)= QUV2(M) + A*DD*DE
     IF (L.NE.NOCE.AND.L.NE.NOCD) GOTO 575
      QS2(M)= QS2(M) + A*DD
      QT2(M)= QT2(M) + A*DE
  575 IF (A.EQ.1.0) GOTO 500
      QD2(M1)= QD2(M1) + A2
      QM2(M1)= QM2(M1) + A2*DC
      QN2(M1)= QN2(M1) + A2*DE
      QW1(M1)= QW1(M1) + A2*W(I)
      QW3(M1)= QW3(M1) + A*W(I)**2
      QU2(M1)= QU2(M1) + A2*DD**2
      QV2(M1)= QV2(M1) + A2*DE**2
      QUV2(M1)= QUV2(M1) + A2*DD*DE
     IF (L.NE.NOCE.AND.L.NE.NOCD) GOTO 500
      QS2(M1)= QS2(M1) + A2*DD
      QT2(M1)= QT2(M1) + A2*DE
  500 CONTINUE
C   AVERAGE INSTANTANEOUS SYSTEM STATE
      DO 580 I= 1,MZ
      IF (QD2(I).EQ.0.0) GOTO 580
      QD(I)= QD(I) + QD2(I)
      QDP(I)= QDP(I) + QD2(I)**2
      QM(I)= QM(I) + QM2(I)/QD2(I)
      QN(I)= QN(I) + QN2(I)/QD2(I)
      QU(I)= QU(I) + QU2(I)/QD2(I)
      QV(I)= QV(I) + QV2(I)/QD2(I)
      QW(I)= QW(I) + QW1(I)/QD2(I)
      QW2(I)= QW2(I) + QW3(I)/QD2(I)
      QUV(I)= QUV(I) + QUV2(I)/QD2(I)
      QRSS(I)= QRSS(I) + QUV2(I)
      QRNS(I)= QRNS(I) + QV2(I)
      QRXX(I)= QRXX(I) + QU2(I)
      QRU(I)= QRU(I) + QM2(I)
      QRV(I)= QRV(I) + QN2(I)
      QD2(I)= 0.0
      QM2(I)= 0.0
      QN2(I)= 0.0
      QU2(I)= 0.0
      QV2(I)= 0.0
      QUV2(I)= 0.0
      QW1(I)= 0.0
      QW3(I)= 0.0
     IF (L.NE.NOCE.AND.L.NE.NOCD) GOTO 580
C   QS AND QT ARE USED TO COMPUTE THE SHEAR AND NORMAL STRESS RESPECTIVELY
      QS(I)= QS2(I) - QS(I)
      QT(I)= QT2(I) - QT(I)
      QS2(I)= 0.0
      QT2(I)= 0.0
  580 CONTINUE
  299 CONTINUE
C
C   IS RUN OVER?
C
  300 IF (LAV3.GE.15000) GOTO 302
  301 CONTINUE
C
C   IF SO WRITE RESULTS
C
```

```
  302  K1 = 1
       K= MINO(ITC,20)
      WRITE (6,639)
  572 WRITE (6,603) (I,I= K1,K)
  603 FORMAT(////'     COLLISION MAP'//7X,20I5 /)
      DO 574 I= 1,IT
  574 WRITE (6,604) I,(MAP(I,I2), I2= K1,K)
  604 FORMAT(I7,20I5)
       K1= K+1
      IF (K.EQ.ITC) GOTO 573
       K= MINO((K+20),ITC)
      GOTO 572
  573  DAV= 0.0
       UAV= 0.0
       ST= AVHGT/FLOAT(LAV)
       AVHGT= ST
       MZ1= MZ
      WRITE(6,691)
  691 FORMAT('1'//40H   DENSITY AND VELOCITY DISTRIBUTIONS     /
     C /15X,15HSOLID FRACTION , 5X,1HU,14X,1HV,14X,1HW,13X,4HU**2,
     C 11X,4HV**2,12X,2HUV//)
       FLAV= FLOAT(LAV)
       UMAX= -1000.0
      DO 130 M= 1,MZ
       QM(M)= QM(M)/FLAV
      IF (QM(M).GT.UMAX) UMAX=QM(M)
       QN(M)= QN(M)/FLAV
       QW(M)= QW(M)/FLAV
       QW2(M)= QW2(M)/FLAV
       QU(M)= QU(M)/FLAV
       QV(M)= QV(M)/FLAV
       QUV(M)= QUV(M)/FLAV
       QD(M)= 3.141593 * QD(M)/(ST*WL*FLAV)
  130 WRITE (6,690) M,MA(M),QD(M),QM(M),QN(M),QW(M),QU(M),QV(M),QUV(M)
     C ,M
  690 FORMAT(2I5,7E15.6,I5)
      IF (UTOP.NE.0.0) UMAX= UTOP
       NC= 0
      WRITE (6,692)
  692 FORMAT(////16X,'W**2',16X,'D''',9X,'MASSFLOW ',
     C 7X,'U''**2',10X,'V''**2',10X,'W''**2',10X,'U''V'''//)
      DO 231 I= 1,MZ
       QDP1= (3.141593/(ST*WL))**2*QDP(I)/FLAV - QD(I)**2
       QUDL(I)= QM(I)/UMAX
       QMF(I)= QD(I)*QM(I)
       NC= NC + NCOL(I)
       QUP(I)= QU(I) - QM(I)**2
       QVP(I)= QV(I) - QN(I)**2
       QWP(I)= QW2(I) - QW(I)**2
       QFL(I)= QUP(I) + QVP(I) + B*QWP(I)
      IF (QUP(I)+QVP(I).GT.0.0) QQAV= QQAV + QD(I)*SQRT(QUP(I)+QVP(I))
       DAV= DAV + QD(I)
       QUVP(I)= QUV(I) - QM(I)*QN(I)
  231 WRITE(6,693) I,QW2(I),QDP1,QMF(I),QUP(I),QVP(I),QWP(I),
     C              QUVP(I),I
  693 FORMAT(I5,5X,7E15.5,I5)
  161 CONTINUE
C   REYNOLDS STRESS CALCULATION
      WRITE(6,694)
  694 FORMAT('1',' FLUCTUATING QUANTITIES'///
     C     14X,'NU*U**2',8X,'NU*V**2',9X,'NU*U*V',10X,'NU*U',
     C     11X,'NU*V',9X,'NU''*U''',9X,'NU''*V''')
      DO 232 I= 1,MZ
```

```
      QRSS(I)= 3.141593*QRSS(I)/(ST*WL*FLAV)
      QRNS(I)= 3.141593*QRNS(I)/(ST*WL*FLAV)
      QRXX(I)= 3.141593*QRXX(I)/(ST*WL*FLAV)
      QRUT= 3.141593*QRU(I)/(ST*WL*FLAV)
      QRVT= 3.141593*QRV(I)/(ST*WL*FLAV)
      QRU(I)= QRUT - QD(I)*QM(I)
      QRV(I)= QRVT - QD(I)*QN(I)
  232 WRITE(6,693) I,QRXX(I),QRNS(I),QRSS(I),QRUT,QRVT,
     C    QRU(I),QRV(I),I
      WRITE (6,695)
  695 FORMAT(////35X,'REYNOLD''S STRESSES'//
     C    26X,'-NU*U''**2',6X,'-NU*V''**2',6X,'-NU*U''*V'''//)
      DO 233 I= 1,MZ
      QRSS(I)= -(QRSS(I) - (QRU(I)*QN(I) + QRV(I)*QM(I))
     C    - QD(I)*QM(I)*QN(I))
      QRXX(I)= -(QRXX(I) - 2*QRU(I)*QM(I) - QD(I)*QM(I)**2)
      QRNS(I)= -(QRNS(I) - 2*QRV(I)*QN(I) - QD(I)*QN(I)**2)
  233 WRITE(6,696) I,QRXX(I),QRNS(I),QRSS(I),I
  696 FORMAT(16X,I5,'  ',3E15.5,I7)
      IF (TIME2.EQ.0.0) TIME2= TIME
C   WALL STRESSES AND OTHER AVERAGE SYSTEM PROPERTIES
      QQAV= QQAV/DAV
      DAV= DAV/MZ
      SHERN= SHEARN/(TIME2*WL)
      SHERT= SHEART/(TIME2*WL)
      SHEARY= SHERN*ALC - SHERT*ALS
      SHEARX= SHERN*ALS + SHERT*ALC
      SHRT= SHRT/(TIME2*WL)
      SHRN= SHRN/(TIME2*WL)
      SHRX= SHRN*ALS + SHRT*ALC
      SHRY= SHRN*ALC - SHRT*ALS
      FRIC= ATAN(SHEART/SHEARN)/0.0174532
      FRIC1= ATAN(SHRT/SHRN)/0.0174532
      HM= HM/FLOAT(LAV*IT)
      FLMASS= FLMASS/FLOAT(LAV)
      AVVEL= FLMASS/FLOAT(IT)
      DTL= TIME2*AVVEL
      AVTOP= AVTOP/(LAV)
      RIMPLS(1)= RIMPLS(1)/FLOAT(NC)
      RIMPLS(2)= RIMPLS(2)/FLOAT(NC)
      RIMANG= ATAN(RIMPLS(2)/RIMPLS(1))
     WRITE (6,640) SHERT,SHRT,SHERN,SHRN,SHEARY,SHRY,
     CSHEARX,SHRX,FRIC,FRIC1,FLMASS,AVVEL,HM,TIME2,DAV,DTL,QQAV,
     CAVTOP,AVHGT,HGT
  640 FORMAT('1'/////////35X,24HWALL STRESS DISTRIBUTION,/
     C 46X,' LOWER WALL',4X,' UPPER WALL'//
     C 25X,15HTANGENTIAL :   ,2F15.5,/
     C 25X,15HNORMAL     :   ,2F15.5,/
     C 25X,15HY-DIRECTION:   ,2F15.5,/
     C 25X,15HX-DIRECTION:   ,2F15.5,/
     C 25X,15HFRICTION ANGLE ,2F15.5,///
     C 15X,28HMASS FLOW                  :  ,F15.5,/
     C 15X,28HAVERAGE VELOCITY           :  ,F15.5,/
     C 15X,28HMASS MEAN HEIGHT           :  ,F15.5,/
     C 15X,28HAVERAGING TIME             :  ,F15.5,/
     C 15X,28HAVERAGE DENSITY            :  ,F15.5,/
     C 15X,28HAVERAGE FLUC. VELOCITY     :  ,F15.5 /
     C 15X,28HAVERAGE DISTANCE TRAVELED  :  ,F15.5 /
     C 15X,28HAV. VERT. TOP VELOCITY     :  ,F15.5 /
     C 15X,28HAV. SAMPLING INTERVAL      :  ,F15.5 /
     C 15X,28HFINAL HEIGHT               :  ,F15.5 )
      WRITE (6,641) UTOP,WL,RIMPLS(1),RIMPLS(2),RIMANG
  641 FORMAT(15X,28HFINAL WALL VELOCITY       :  ,F15.5 /
```

```
     C        15X,28HFINAL REGION WIDTH          :  ,F15.5 /
     C        15X,28HNORMAL IMPULSE              :  ,F15.5 /
     C        15X,28HTANGENTIAL IMPULSE          :  ,F15.5 /
     C        15X,28HIMPULSE ANGLE               :  ,F15.5 )
   237 WRITE(6,620) TIME
   620 FORMAT('1'////19H NEW PARTICLE LIST     ,F15.5)
       DO 145 I= 1,IT
       DS= X(I)*ALC - Y(I)*ALS
       DN= X(I)*ALS + Y(I)*ALC
       US= U(I)*ALC - V(I)*ALS
       UN= U(I)*ALS + V(I)*ALC
   145 WRITE (6,631) I,DS,DN,US,UN,W(I),IR(I)
   631 FORMAT (I5,5F15.5,I5)
C    RECORD FINAL STATE OF SYSTEM ONTO CARDS SC SIMULATION MAY BE CONTINUED
       WRITE (7,635) TIME,NOC1,LAV3
       WRITE (7,633) EW,EP,ALPH,B
       WRITE (7,633) UTOP,HGT,GEE
       WRITE (7,634) IT,WL
       DO 320 I=1,IT
       WRITE(12,632) IR(I), X(I), Y(I), U(I), V(I), W(I)
   320 WRITE(7,632) IR(I), X(I), Y(I), U(I), V(I), W(I)
   632 FORMAT(I5,5F10.5)
   633 FORMAT(4F10.4)
   634 FORMAT(I5,F10.4)
   635 FORMAT(F10.3,2I5)
C    DRAW A PICTURE OF THE SYSTEM
       CALL PICTRE(HGT)
        UTOP= UMAX
C    MAKE LEAST-SQUARES FITS TO VELOCITY AND DENSITY PROFILES
       DO 770 I= 1,MZ
        DATA(1,I)= FLOAT(I-1)*ST + ST/2.0
        DATA(2,I)= QM(I)
        DATA(3,I)= 1.0
        DATA1(1,I)= FLOAT(I-1)*ST + ST/2.0
        DATA1(2,I)= QN(I)
        DATA1(3,I)= 1.0
        DATA2(1,I)=  FLOAT(I-1)*ST + ST/2.0
        DATA2(2,I)= QD(I)
   770  DATA2(3,I)= 1.0
        CHISQ= 1.0
       CALL LSQUAR(DATA,MZ,IORD,AV,CHISQ,STOR)
        CHISQ= 1.0
       CALL LSQUAR(DATA1,MZ,IORD,AN,CHISQ,STOR)
        CHISQ= 1.0
       CALL LSQUAR(DATA2,MZ,IORD,AD,CHISQ,STOR)
       WRITE(6,638)
       WRITE (6,660) (AV(I), I= 1,IORD)
   660 FORMAT(////24H  VELOCITY COEFFICENTS:  //
      C 3X,5HU:     ,7D15.7/)
        WRITE (6,661) (AN(I),I= 1,IORD)
   661 FORMAT( 3X,5HV:     ,7D15.7)
       WRITE (6,675)  (AD(I), I= 1,IORD)
   675 FORMAT(///24H  DENSITY COEFFICENTS:   //8X,7D15.7/////)
       WRITE (6,677)
   677 FORMAT('1'///37X,22HDISTRIBUTION GRADIENTS   //
      C 14X,'DU/DY',6X,'(DU/DY)**2',8X,'D2U/DY2',9X,'DV/DY',
      C 6X,'(DV/DY)**2',8X,'D2V/DY2',8X,'DNU/DY'/)
       IOR1= IORD - 1
C
C    COMPUTE VELOCITY AND DENSITY GRADIENTS
C    GRADIENTS ARE FOUND FROM A CUBIC SPLINE FIT TO THE DATA
C
       CALL SPLNE(MZ1,ST,QD,DDY,D2UY)
```

```
      CALL SPLNE(MZ1,ST,QM,DUY,D2UY)
      CALL SPLNE(MZ1,ST,QN,DVY,D2VY)
      DO 420 I= 1,MZ1
      IF (I.NE.1.AND.I.NE.MZ1) GOTO 401
C
C   ONLY THE GRADIENTS AT THE ENDPOINTS ARE COMPUTED BY THE LEAST
C   SQUARES FIT
C
      DO 400 I2= 2,ICR1
       D2MM= FLOAT(I2*(I2-1))*(FLOAT(I-1)*ST + ST/2.0)**(I2-2)
       D2UY(I)= D2UY(I) + AV(I2+1)*D2MM
  400  D2VY(I)= D2VY(I) + AN(I2+1)*D2MM
  401  DUY2(I)= DUY(I)**2
       DVY2(I)= DVY(I)**2
  420 WRITE(6,678) I,DUY(I),DUY2(I),D2UY(I),DVY(I),DVY2(I),
     C D2VY(I),DDY(I),I
  678 FORMAT(I5,7E15.6,I10)
C   COMPUTE INTERNAL STRESSES BY A MOMENTUM BALANCE
      WRITE (6,645)
  645 FORMAT(//////35X,19HSTRESS DISTRIBUTION  ,//10X,
     C  3('TANGENTIAL',5X,'NORMAL',9X),'FRICTION ANGLE'/)
       QS5= SHERT
       QT5= SHERN
      DO 800 I= 1,MZ
       QS3= QS(I)/(TIME2*WL*ST*3.141593)
       QT3= QT(I)/(TIME2*WL*ST*3.141593)
       QS4= QS3 - QD(I)*GEE*ALS/3.141593
       QT4= QT3 + QD(I)*ALC*GEE/3.141593
       QS5= QS5 + QS4*ST
       QT5= QT5 + QT4*ST
       ANG= ATAN(QT5/QS5)
       QS6(I)= QS5
       QT6(I)= QT5
  800 WRITE (6,647) I,QS3,QT3,QS4,QT4,QS5,QT5,ANG
  647 FORMAT(2X,I5,7D15.6,I7)
C   COMPUTE DISTRIBUTION OF ENERGY DISTRIBUTION WITHIN SYSTEM
      DO 432 I= 1,2
      WDIS(I)= WDIS(I)/TIME2
  432 TDIS= TDIS + WDIS(I)
      WRITE (6,610) WDIS(1),WDIS(2)
  610 FORMAT(/////35X,'DISSIPATION DISTRIBUTION'//
     C 25X,'LOWER WALL:  ',E15.6/
     C 25X,'UPPER WALL:  ',E15.6//)
      DO 433 I= 1,MZ
       DIS(I)= DIS(I)/TIME2
       TDIS= TDIS + DIS(I)
  433 WRITE (6,615) I,DIS(I)
  615 FORMAT(33X,I5,E15.6)
      WRITE (6,618) TDIS
  618 FORMAT(///25X,'TOTAL DISSIPATION:  ',E15.6)
      WRITE (6,648)
  648 FORMAT(/////)
C   COLLISION FREQUENCY AS A FUNCTION OF DENSITY
      WRITE (6,652)
  652 FORMAT('1',35X,'COLLISION DISTRIBUTION'//
     C       25X, ' LEVEL  NUMBER    PERCENTAGE         NU'//)
      DO 3500 I= 1,MZ
       FNCOL(I)= FLOAT(NCOL(I))/FLOAT(LAV2)
 3500 WRITE (6,653) I,NCOL(I),FNCOL(I),QD(I)
  653 FORMAT(25X,2I7,2F15.6)
C   COLLISION ANGLE DISTRIBUTION
      WRITE (6,6421)
 6421 FORMAT('1'//40X,'COLLISION ANGLE DISTRIBUTION'/
```

```
     C 35X,'ANGLE',10X,'NUMBER',7X,'PROBABILITY')
       DO 3701 I= 1,50
        DD= FLOAT(I)*0.06283186
        PC= COLDIS(I)/(LAV2*0.062831861
        NCC= INT(COLDIS(I))
 3701 WRITE (6,6431) DD,NCC,PC
 6431 FORMAT(30X,F15.5,I15,F15.5)

C
C    MAKE THE APPROPRIATE PLOTS
C
       WRITE (6,6001)
 6001 FORMAT('1','  PLOTTED DATA'//
     C  20X,'FY',12X,'UNORM',8X,'MASS FLOW',8X,'F(NU)',
     C  12X,'R',12X,'S*R/2',8X,'TEMPERATURE')
        QRAV= 0.0
        GR2= (HGT/UTOP)**2
       DO 5000 I= 1,MZ
        FNU(I)= ABS(QS6(I))/DUY2(I)
        FY(I)= (FLOAT(I)-0.5)*ST/HGT
        QMF(I)= QMF(I)/UMAX
        QFL2(I)= QUP(I)+QVP(I)
        QR(I)= 2*SQRT(DUY2(I)/(QUP(I)+QVP(I)))
        QRAV= QRAV+QR(I)
        QFL1(I)= QFL(I)*GR2/3
        QUP1(I)= QUP(I)*GR2
        QVP1(I)= QVP(I)*GR2
        QWP1(I)= B*QWP(I)*GR2
        QTMP(I)= (QUP(I)+QVP(I))*GR2
       IF (QD(I).EQ.0.0) GOTO 5000
        QRH(I)= 0.5*QR(I)*SQRT(3.141593/QD(I))
 5000 WRITE (6,693) I,FY(I),QUDL(I),QMF(I),FNU(I),QR(I),QRH(I),
     C QFL(I),I
        QRAV= QRAV/MZ
       WRITE (6,6933) QRAV
 6933 FORMAT(///30X,' AVERAGE R= ',F15.5///////
     C           20X,'NORMALIZED TEMPERATURE DISTRIBUTION'//
     C           10X,'LEVEL',5X,'TOTAL TEMP','LINEAR TEMP    ',
     C           7X,'U''**2   ',7X,'V''**2   ',6X,'B*W''**2   LEVEL')
       DO 5001 I= 1,MZ
 5001 WRITE(6,6934) I,QFL1(I),QTMP(I),QUP1(I),QVP1(I),QWP1(I),I
 6934 FORMAT(10X,I5,5F15.5,I5)
       IF (IPLT.EQ.0) STOP
       CALL DFAULT
       CALL NEWPEN(3)
       CALL GRPLOT(MZ,QUDL,FY,'U/UTOP ',6,'Y/H ',3,
     C             'U/UTOP VS Y/H   ',13,'     ',0)
        XMAX= 1.0
       CALL GRPLOT(MZ,QD,FY,'SOLID FRACTION  ',14,'Y/H ',3,
     C             'SOLID FRACTION  ',14,'    VS Y/H  ',10)
        XMAX= 0.6
       CALL GRPLOT(MZ,QMF,FY,'NU*U/UTOP   ',9,'Y/H ',3,
     C             'DIMENSIONLESS   ',13,'MASS FLOW   ',9)
        XMAX= 3.0
        LASTP= .FALSE.
        NIX= 4
       CALL GRPLOT(MZ,QFL1,FY,'TEMP*HGT/UTOP   ',13,'Y/H ',3,
     C             'TEMPERATURE     ',11,'DISTRIBUTION',12)
        TITLE=.FALSE.
        AXIS=.FALSE.
        ORIGIN=.FALSE.
        ISYM= 2
       CALL GRPLOT(MZ,QUP1,FY,'TEMPERATURE ',11,'Y/H ',3,
```

```
     C              'TEMPERATURE     ',11,'DISTRIBUTION',12)
       ISYM= 3
      CALL GRPLOT(MZ,QVP1,FY,'TEMPERATURE ',11,'Y/H ',3,
     C              'TEMPERATURE     ',11,'DISTRIBUTION',12)
       ISYM= 4
      CALL GRPLOT(MZ,QWP1,FY,'TEMPERATURE ',11,'Y/H ',3,
     C              'TEMPERATURE     ',11,'DISTRIBUTION',12)
       ISYM= 5
       LASTP=.TRUE.
      CALL GRPLOT(MZ,QTMP,FY,'TEMPERATURE ',11,'Y/H ',3,
     C              'TEMPERATURE     ',11,'DISTRIBUTION',12)
       CALL DFAULT
       XMAX= 1.0
       YSZE= 7.5
       NIY= 7
       YMAX=  2.0
      DO 5002 I= 1,MZ
       FNU(I)= ABS(QS6(I))/DUY2(I)
 5002  QR(I)= 2*SQRT(DUY2(I)/(QUP(I)+QVP(I)))
      CALL GRPLOT(MZ,QD,QR,'SOLID FRACTION  ',14,
     C       '2R*DUDY/V''  ',10,'R VS NU ',7,'    ',0)
       YMAX= 4.0
      CALL GRPLOT(MZ,QD,FNU,'SOLID FRACTION  ',14,
     C              'SHEAR*(UTOP/DU/DY)2 ',19,
     C              'DENSITY DEPENDENCE  ',18,'OF SHEAR',8)
       YSZE= 5.0
       XSZE= 8.0
       NIX=  9
       NIY=  5
       YMAX= 1.0
       XMAX= 0.0
       LASTP= .FALSE.
      DO 5101 I= 1,MZ1
       SHERT= ABS(QS6(I))
       SHRN=  ABS(QT6(I))
       SHERN= ABS(QRXX(I))
       SHRS=  ABS(QRSS(I))
       SHRT=  ABS(QRNS(I))
 5101  XMAX=  AMAX1(SHERT,SHERN,SHRT,SHRN,SHRS,XMAX)
       XMIN= -XMAX
       XFMT(1)= DFMT1
       XFMT(2)= DFMT2
       NFX= 7
      CALL GRPLOT(MZ,QS6,FY,'DIM''LESS SHEAR  ',14,'Y/H ',3,
     C  'SHEAR VS Y/H',12,'    ',0)
       TITLE= .FALSE.
       PDOC= .FALSE.
       AXIS= .FALSE.
       ORIGIN= .FALSE.
       ISYM= 10
      CALL GRPLOT(MZ,QT6,FY,'    ',0,'    ',0,'    ',0,'    ',0)
       ISYM= 2
      CALL GRPLOT(MZ,QRSS,FY,'    ',0,'    ',0,'    ',0,'    ',0)
       ISYM= 3
      CALL GRPLOT(MZ,QRNS,FY,'    ',0,'    ',0,'    ',0,'    ',0)
       ISYM= 6
       LASTP= .TRUE.
      CALL GRPLOT(MZ,QRXX,FY,'    ',0,'    ',0,'    ',0,'    ',0)
      CALL DFAULT
       XSZE= 8.0
CCCCCCCCCCCCCCCCCCCCCCCCCCCCCCCCCCCCCCCCCCCCCCCCCCCCCCCCCCCCCCCCCCCCCCCC
C                                                                      C
C   VELOCITY DISTRIBUTION ASSESSMENT                                   C
```

```
C                                                                       C
C    REWIND TAPE AND COMPARE INSTANTANEOUS VELOCITIES TO THE AVERAGE VALUES   C
C                                                                       C
CCCCCCCCCCCCCCCCCCCCCCCCCCCCCCCCCCCCCCCCCCCCCCCCCCCCCCCCCCCCCCCCCCCCCCCCCCCCCC
      CALL ENDMF(20)
      DO 6051 I= 1,10
 6051 READ(20,END=6052)
 6052  TIME3= -AVTM
       NUMC= 0
       NUMU= 0.0
       NUMV= 0.0
       NUMW= 0.0
C      IRT=  INT(FLOAT(LAV5 + LAV3 - LAV4)/1000.0 + 0.0001)-1
C      IF (IRT.LT.0) IRT=0
      CALL READNF(20)
       LAV= 0
       LAV6= LAV3-1
       LAV1= 0
      DO 6100 N= 1,LAV6
 6004 READ(20,END=6005) TIME,NOC2,NCA,NDA,NQA,HGT,
     C   (X(I),Y(I),U(I),V(I),W(I),I=1,IT)
      GOTO 6006
 6005 CALL READNF(20)
      GOTO 6004
 6006 LAV= LAV+1
       HGT9= HGT/2
      DO 6010 I= 1,IT
       DM= (X(I)*ALS + Y(I)*ALC)
      IF (DM.EQ.0.0) GOTO 6101
       M= 1 + INT(DM/ST)
      GOTO 5010
      IF (ABS(DM-HGT9).LT.ST) GOTO 5010
C
C    PAIR CORRELATION FUNCTION ASSESSMENT
C
      DO 503 I2= 1,IT
      IF (I2.EQ.I) GOTO 503
C    RADIAL CORRELATION
       M2= 1+INT(50.0*(SQRT((X(I)-X(I2))**2+(Y(I)-Y(I2))**2)-2.0)
     C          /WL3)
      IF (M2.LE.50) GCOL(M2)= GCOL(M2)+1.0
       M2= 1+INT(50.0*(SQRT((X(I)-X(I2)-WLC)**2+(Y(I)-Y(I2)+WLS)**2)
     C        -2.0)/WL3)
      IF (M2.LE.50) GCOL(M2)= GCOL(M2)+1.0
       M2= 1+INT(50.0*(SQRT((X(I)-X(I2)+WLC)**2+(Y(I)-Y(I2)-WLS)**2)
     C        -2.0)/WL3)
      IF (M2.LE.50) GCOL(M2)= GCOL(M2)+1.0
C    NORMAL CORRELATION
       M2= 1+INT(50.0*ABS((X(I)-X(I2))*ALS+(Y(I)-Y(I2))*ALC)/WL2)
      IF (M2.LE.50) GCY(M2)= GCY(M2)+1.0
C    PARALLEL CORRELATION AND VELOCITY CORRELATIONS
      IF (INT(ABS(X(I2)*ALS+Y(I2)*ALC-DM)).LT.ST) GOTO 503
       M2= 1+INT(50.0*ABS((X(I)-X(I2))*ALC-(Y(I)-Y(I2))*ALS)/WL2)
      IF (M2.GT.50) GOTO 5030
       GCX(M2)= GCX(M2)+1.0
       UCOR(M2)= UCOR(M2) + (U(I)-QM(I))*(U(I2)-QM(I2))
       VCOR(M2)= VCOR(M2) + (V(I)-QN(I))*(V(I2)-QN(I2))
       IBN(M2)= IBN(M2)+1
 5030  M2= 1+INT(50.0*ABS((X(I)-X(I2)+WLC)*ALC-(Y(I)-Y(I2)-WLS)*ALS)
     C     /WL2)
      IF (M2.GT.50) GOTO 5031
       GCX(M2)= GCX(M2)+1.0
       UCOR(M2)= UCOR(M2) + (U(I)-QM(I))*(U(I2)-QM(I2))
```

```
      VCOR(M2)= VCOR(M2) + (V(I)-QN(I))*(V(I2)-QN(I2))
      IBN(M2)= IBN(M2)+1
 5031 M2= 1+INT(50.0*ABS((X(I)-X(I2)-WLC)*ALC-(Y(I)-Y(I2)+WLS)*ALS)
     C   /WL2)
      IF (M2.GT.50) GOTO 503
      GCX(M2)= GCX(M2)+1.0
      UCOR(M2)= UCOR(M2) + (U(I)-QM(I))*(U(I2)-QM(I2))
      VCOR(M2)= VCOR(M2) + (V(I)-QN(I))*(V(I2)-QN(I2))
      IBN(M2)= IBN(M2)+1
  503 CONTINUE
      LAV1= LAV1+1
C
C   VELOCITY DISTRIBUTIIONS
C
 5010 IF (TIME-TIME3.LT.AVTM) GOTO 6100
      TIME3= TIME
      IF (QFL(M).LE.0.0) GOTO 6010
      DD= U(I)*ALC - V(I)*ALS
      DE= U(I)*ALS + V(I)*ALC
      IF (QFL(M).NE.0.0)
     C MN= 1+INT(SQRT(((DD-QM(M))**2+(DE-QN(M))**2+B*(W(I)-QW(I))**2)
     C     /QFL(M))/0.1)
      IF (QFL2(M).NE.0.0)
     C MN1= 1+INT(SQRT(((DD-QM(M))**2+(DE-QN(M))**2)/QFL2(M))/0.1)
      IF (QUP(M).NE.0.0)
     C MNU= 1+INT(SQRT((DD-QM(M))**2/QUP(M))/0.1)
      IF (QVP(M).NE.0.0)
     C MNV= 1+INT(SQRT((DE-QN(M))**2/QVP(M))/0.1)
      IF (QWP(M).NE.0.0)
     C MNW= 1+INT(SQRT((W(I)-QW(M))**2/QWP(M))/0.1)
      IF (MN.GT.50)  GOTO 6007
      NUMC= NUMC + 1
      QNUM(MN)= QNUM(MN) + 1.0
 6007 IF (MNU.GT.50) GOTO 6069
      NUMU= NUMU + 1
      QNUMU(MNU)= QNUMU(MNU) + 1.0
 6069 IF (MN1.GT.50) GOTO 6008
      QNUM1(MN1)= QNUM1(MN1)+1
      NUM1= NUM1+1
 6008 IF (MNV.GT.50) GOTO 6009
      NUMV= NUMV + 1
      QNUMV(MNV)= QNUMV(MNV) + 1.0
 6009 IF (MNW.GT.50) GOTO 6010
      NUMW= NUMW + 1
      QNUMW(MNW)= QNUMW(MNW) + 1.0
 6010 CONTINUE
 6100 CONTINUE
 6101 WRITE (6,642)
  642 FORMAT('1'//,' VELOCITY DISTRIBUTION'//
     C 17X,'TOTAL DISTIBUTION',42X,'U DISTRIBUTION'/
     C ' SLOT',10X,'RANGE',10X,'NUMBER',7X,'PROBABILITY',
     C 10X,'RANGE',10X,'NUMBER',7X,'PROBABILITY'//)
      DO 3700 I= 1,50
      DS= FLOAT(I)*0.1
      NOT= INT(QNUM(I))
      NOU= INT(QNUMU(I))
      IF (NUMC.NE.0) QNUM(I)= 10*QNUM(I)/FLOAT(NUMC)
      IF (NUMU.NE.0) QNUMU(I)= 10*QNUMU(I)/FLOAT(NUMU)
 3700 WRITE (6,643) I,DS,NOT,QNUM(I),NOU,QNUMU(I)
  643 FORMAT(I5,F15.5,I15,F15.5,20X,I15,F15.5)
      WRITE (6,6423)
 6423 FORMAT('1'//,' VELOCITY DISTRIBUTION'//
     C 18X,'V DISTRIBUTION',43X,'W DISTRIBUTION'/
```

```
     C ' SLOT',10X,'RANGE',10X,'NUMBER',7X,'PROBABILITY',
     C 10X,'RANGE',10X,'NUMBER',7X,'PROBABILITY'//)
      DO 3711 I= 1,50
       DS= FLOAT(I)*0.1
       NOV= INT(QNUMV(I))
       NOW= INT(QNUMW(I))
       IF (NUMV.NE.0) QNUMV(I)= 10.0*QNUMV(I)/FLOAT(NUMV)
       IF (NUMW.NE.0) QNUMW(I)= 10.0*QNUMW(I)/FLOAT(NUMW)
3711  WRITE (6,643) I,DS,NOV,QNUMV(I),NOW,QNUMW(I)
      WRITE (6,6424)
6424  FORMAT('1'//,' VELOCITY DISTRIBUTION'//
     C 16X,'LINEAR DISTRIBUTION'/
     C ' SLOT',10X,'RANGE',10X,'NUMBER',7X,'PROBABILITY'//)
      DO 3712 I= 1,50
       DS= FLOAT(I)*0.1
       NO1= INT(QNUM1(I))
       IF (NUM1.NE.0) QNUM1(I)= 10*QNUM1(I)/NUM1
3712  WRITE (6,643) I,DS,NO1,QNUM1(I)
      DO 6000 I= 1,50
6000   FY(I)= FLOAT(I)*0.1
       XMIN= 0.0
       XMAX= 5.0
       TITLE= .TRUE.
       AXIS=  .TRUE.
       PDOC=  .TRUE.
       ORIGIN=.TRUE.
       NIY= 6
       YMAX= 1.2
       ISYM= 1
      CALL GRPLOT(50,FY,QNUM,'(C-UAV)/V''  ',10,'PROB(C) ',
     C     7,'NUMBER DISTRIBUTION ',19,'    ',0)
      CALL GRPLOT(50,FY,QNUM1,'(C-UAV)/V''  ',10,'PROB(C) ',
     C     7,'LINEAR DISTRIBUTION ',19,'    ',0)
      CALL GRPLOT(50,FY,QNUMU,'(C-UAV)/V''  ',10,'PROB(C) ',
     C     7,'U DISTRIBUTION  ',14,'    ',0)
      CALL GRPLOT(50,FY,QNUMV,'(C-UAV)/V''  ',10,'PROB(C) ',
     C     7,'V DISTRIBUTION  ',14,'    ',0)
      CALL GRPLOT(50,FY,QNUMW,'(C-UAV)/V''  ',10,'PROB(C) ',
     C     7,'W DISTRIBUTION  ',14,'    ',0)
      DO 6200 I= 1,50
       FY(I)= FLOAT(I)*0.0628316
6200   COLDIS(I)= COLDIS(I)/(LAV2*0.0628316)
      CALL DFAULT
       YMAX= 2.0
       XSZE= 8.0
       XMIN= 0.0
       XMAX= 3.141593
      CALL GRPLOT(50,FY,COLDIS,'ANGLE   ',5,'N/NCOL  ',6,
     C  'COLLISION ANGLE ',15,'DISTRIBUTION',12)
      SCY=.TRUE.

      DO 6300 I= 1,50
       FY2(I)= FLOAT(I)*WL2/50.0
6300   FY(I)= 2.0+FLOAT(I)*WL3/50.0
      WRITE(6,6610)
6610  FORMAT('1',35X,'PAIR CORRELATION FUNCTION'//
     C       10X,'SLOT',9X,'DISTANCE',5X,'NUM. COUNTED',3X,
     C       'DISTANCE',6X,
     C       'PERCENTAGE',2X,'VERTICAL NUM',1X,'PERCENTAGE',
     C       1X,'HORIZONTAL NUM','PERCENTAGE'//)
      DO 6630 I= 1,50
       NAB= GCOL(I)
```

```
      DIS2= 2.0 + FLOAT(I)*WL3/50.0
      DIS3= FLOAT(I)*WL2/50.0
      GCOL(I)= 25.0*GCOL(I)*3.141593/(LAV6*DIS2*WL3*DAV**2)
      NAY= GCY(I)
      GCY(I)= 25.0*GCY(I)/(LAV6*WL2*WL)
      NAX= GCX(I)
     IF (LAV1.NE.0.0) GCX(I)= 25.0*GCX(I)/(LAV1*WL2*ST)
6630 WRITE(6,6620) I,DIS2,NAB,GCOL(I),DIS3,NAY,GCY(I),NAX,GCX(I)
6620 FORMAT(10X,I5,F15.6,I10,F15.6,F15.6,I10,F15.6,I10,F15.6)
     WRITE(6,6625)
6625 FORMAT('1'/'   VELOCTIY CORRELATIONS'//
    C 10X,' SLOT',6X,'DISTANCE ',10X,'U-  CORRELATION',
    C 10X,'V-  CORRELATION')
      DO 6626 I= 1,50
      DIS3= FLOAT(I)*WL2/50.0
      IF (IBN(I).EQ.0) GOTO 6626
      UCOR(I)= 50.0*UCOR(I)/(IBN(I)*QU(IWL2)*WL2)
      VCOR(I)= 50.0*VCOR(I)/(IBN(I)*QV(IWL2)*WL2)
6626 WRITE(6,6627) I,DIS3,UCOR(I),VCOR(I)
6627 FORMAT(10X,I5,F15.5,10X,E15.5,10X,E15.5)
      XMIN= 2.0
      XMAX= WL2
      SCY=.TRUE.
     CALL GRPLOT(50,FY,GCOL,'SEPARATION  ',10,'G FUNCTION  ',10,
    C            'PAIR CORRELATION',16,'    ',0)
     XMIN= 0.0
     CALL GRPLOT(50,FY2,GCY,'SEPARATION  ',10,'PROBABILITY ',11,
    C            'VERT CORRELATION',16,'    ',0)
     CALL GRPLOT(50,FY2,GCX,'SEPARATION  ',10,'PROBABILITY ',11,
    C            'HORZ CORRELATION',16,'    ',0)
     CALL GRPLOT(50,FY2,UCOR,'SEPARATION  ',10,'CORRELATION ',11,
    C            'U-VELOCITY  ',16,'CORRELATION ',11)
     CALL GRPLOT(50,FY2,VCOR,'SEPARATION  ',10,'CORRELATION ',11,
    C            'V-VELOCITY  ',16,'CORRELATION ',11)
C   SYSTEM ENERGY HISTORY
8003 DO 8004 I= 1,IEN
8004 FY(I)= FLOAT(I)*50.0
     CALL DFAULT
      XSZE= 8.0
      XMAX= FLOAT(NOCD)
      SCY=.TRUE.
      LINE= .TRUE.
      POINT= .FALSE.
      XFMT(1)= DFMT1
      XFMT(2)= DFMT4
C     CALL GRPLOT(IEN,FY,QE,'COLLISIONS  ',10,
C    C   'TOTAL ENERGY',12,'ENERGY HISTORY  ',14,
C    C   'COLLISION PLOT  ',14)
      XFMT(2)= DFMT3
      XMIN= TIMST
      XMAX= TIME
      STOP
      END
C THIS MARKS END OF MAIN PROGRAM
```

Appendix C

LISTING OF THE INITIAL STATE CREATION ROUTINES

C.1 COL007: Initial State Creation for the Inclined Chute Simulation

```
CCCCCCCCCCCCCCCCCCCCCCCCCCCCCCCCCCCCCCCCCCCCCCCCCCCCCCCCCCCCCCCCCCCCCCCCCCCCCCCCCC
C                                                                               C
C   PROGRAM COL007                                                              C
C                                                                               C
C   THIS PROGRAM GENERATES INITIAL SYSTEM CONFIGURATIONS FOR THE                C
C   INCLINED CHUTE SIMULATION                                                   C
C                                                                               C
C   THIS PROGRAM BELONGS TO CHARLES CAMPBELL, THOMAS 03, X4153                  C
C                                                                               C
C   REQUIRES SUBPROGRAM NRAND, INTEGER RANDOM NUMBER GENERATOR                  C
C                                                                               C
CCCCCCCCCCCCCCCCCCCCCCCCCCCCCCCCCCCCCCCCCCCCCCCCCCCCCCCCCCCCCCCCCCCCCCCCCCCCCCCCCC
      DIMENSION X(1000),Y(1000),U(1000),V(1000),W(1000),D(5),
     C IR(1000)
C   GENERATE INITIAL VELOCITY ACCORDING TO SEVENTH ORDER LEAST SQUARES
C   FIT TO A VELOCITY PROFILE
      F(Z)= A8*Z**7+A7*Z**6+A6*Z**5+A5*Z**4+
     C      A4*Z**3+A3*Z*Z+A2*Z+A1
      DATA A1/0.2018029/,A2/3.5299215/,A3/-15.2262754/,A4/47.4364204/,
     C    A5/-88.1786499/,A6/93.5828476/,A7/-51.8336868/,A8/11.4877520/
CCCCCCCCCCCCCCCCCCCCCCCCCCCCCCCCCCCCCCCCCCCCCCCCCCCCCCCCCCCCCCCCCCCCCCCCCCCCCCCCCC
C                                                                               C
C   INPUT VARIABLES                                                             C
C       EW   :  WALL COEFFICENT OF RESTITUTION                                  C
C       EP   :  PARTICLE COEFFICENT OF RESTITUTION                              C
C       ALPH :  CHUTE INCLINATION ANGLE (IN DEGREES)                            C
C       B    :  RATIO OF THE RADIUS OF GYRATION TO THE PARTICLE RADIUS          C
C       NPL  :  NUMBER OF PARTICLES VERTICALLY                                  C
C       NPH  :  NUMBER OF PARTICLES HORIZONTALLY                                C
C       SPI  :  HALF MEAN PARTICLE SPACING                                      C
C       UMAX :  MAXIMUM VELOCITY                                                C
C       QPI  :  SCALE OF ALLOWED RANDOMNESS                                     C
C                                                                               C
CCCCCCCCCCCCCCCCCCCCCCCCCCCCCCCCCCCCCCCCCCCCCCCCCCCCCCCCCCCCCCCCCCCCCCCCCCCCCCCCCC
      READ (5,633) EW,EP,ALPH,B
      READ (5,501) NPL,NPH,SPI,UMAX,QPI
  501 FORMAT(2I5,4F10.0)
      WRITE (6,600) EW,EP,ALPH,B,NPL,NPH,SPI,UMAX
  600 FORMAT (  26H  COEFF.OF RES.FOR WALL =  ,F12.3/
     C          26H  COEFF.OF RES.FOR PART.=  ,F12.3/
     C          26H  ALPHA                 =  ,F12.3/
     C          26H  B=K**2/R**2           =  ,F12.3/
     C          26H  NO.VERTICALLY         =  ,I5/
     C          26H  NO.HORIZONTALLY       =  ,I5/
     C          26H  SPACING               =  ,F12.3/
     C          26H  MAXIMUM VELOCITY      =  ,F12.3/)
C   INITIALIZE VARIABLES
      ALF =0.0174532* ALPH
      ALS= SIN(ALF)
      ALC = COS(ALF)
      ALT =ALS/ALC
      ALCT = ALC/ALS
      DO 25 I= 1,IT
   25 IR(I)= 0
      WL = 2.0*SPI*FLOAT(NPH)
      WLS =WL*ALS
      WLC = WL*ALC
      WH = 2.0*SPI*FLOAT(NPL)-SPI
      IT = NPL*NPH
      NOCD= 0

      WRITE (6,601) QPI,WL,WH
  601 FORMAT ( 26H  INITIAL OSC.VEL.%     =  ,F12.3/
```

```
     C          26H  LENGTH                =  ,F12.3/
     C          26H  HEIGHT                =  ,F12.3/)

C    INITIAL RANDOM X,Y,U,V,W  SETUP
       NRAN = 12345
       DO 200 J= 1,NPL
       DO 200 K= 1,NPH
       DO 201 L= 1,4
       NRAN = NRAND(NRAN)
  201  D(L) = 2.0 * FLOAT(NRAN) / 0.2147484E10  -1.0
       N=  K+ NPH*(J-1)
       DS= SPI + 2.0*SPI*FLOAT(K-1) + D(1)*(SPI-1.0)
       DN= 2.0*SPI*FLOAT(J) - SPI+D(2)*(SPI-1.0)
       UY= F(DN/WH)*UMAX
       X(N)=  DS*ALC + DN*ALS
       Y(N)=  DN*ALC - DS*ALS
       U(N)=  UY*ALC + D(3)*QPI*UY
       V(N)= -UY*ALS + D(4)*QPI*UY
  200  W(N)=  0.0
C    WRITE OUT ORIGINAL SETUP
       TIME = 0.0
      WRITE (6,637) TIME
  637 FORMAT(///24H ORIGINAL PARTICLE LIST   ,F15.5)
       DO 22 I= 1,IT
       DS= X(I)*ALC - Y(I)*ALS
       DN= X(I)*ALS + Y(I)*ALC
       US= U(I)*ALC - V(I)*ALS
       UN= U(I)*ALS + V(I)*ALC
   22 WRITE (6,631) I,DS,DN,US,UN,W(I),IR(I)
  631 FORMAT(I5,5F15.5,I5)
C    WRITE INITIAL RESULTS ONTO CARDS
       WRITE(7,635) TIME,NOCD
       WRITE(7,633)EW,EP,ALPH,B
       WRITE(7,634)IT,WL
       DO 320 I=1,IT
  320 WRITE(7,632) IR(I), X(I), Y(I), U(I), V(I), W(I)
 632  FORMAT(I5,5F10.5)
 633  FORMAT(4F10.4)
 634  FORMAT(I5,F10.4)
  635 FORMAT(F10.3,I5)
       STOP
       END
C THIS MARKS END OF MAIN PROGRAM
```

C.2 COL006: Initial State Creation for the Couette Flow Simulation

```
CCCCCCCCCCCCCCCCCCCCCCCCCCCCCCCCCCCCCCCCCCCCCCCCCCCCCCCCCCCCCCCCCCCCCCCCCCCCCC
C                                                                             C
C   PROGRAM COL006                                                            C
C                                                                             C
C   THIS PROGRAM GENERATES INITIAL SYSTEM CONFIGURATIONS FOR THE              C
C   COUETTE SHEAR CELL SIMULATION                                             C
C                                                                             C
C   THIS PROGRAM BELONGS TO CHARLES CAMPBELL, THOMAS 03, X4153                C
C                                                                             C
C   REQUIRES SUBPROGRAM NRAND, INTEGER RANDOM NUMBER GENERATOR                C
C                                                                             C
CCCCCCCCCCCCCCCCCCCCCCCCCCCCCCCCCCCCCCCCCCCCCCCCCCCCCCCCCCCCCCCCCCCCCCCCCCCCCC
      DIMENSION X(1000),Y(1000),U(1000),V(1000),W(1000),D(5),
     C IR(1000)
CCCCCCCCCCCCCCCCCCCCCCCCCCCCCCCCCCCCCCCCCCCCCCCCCCCCCCCCCCCCCCCCCCCCCCCCCCCCCC
C                                                                             C
C   INPUT VARIABLES                                                           C
C       EW   :  WALL COEFFICENT OF RESTITUTION                                C
C       EP   :  PARTICLE COEFFICENT OF RESTITUTION                            C
C       ALPH :  CHUTE INCLINATION ANGLE (IN DEGREES)                          C
C       B    :  RATIO OF THE RADIUS OF GYRATION TO THE PARTICLE RADIUS        C
C       NPL  :  NUMBER OF PARTICLES VERTICALLY                                C
C       NPH  :  NUMBER OF PARTICLES HORIZONTALLY                              C
C       SPI  :  HALF MEAN PARTICLE SPACING                                    C
C       UTOP :  UPPER WALL VELOCITY                                           C
C       QPI  :  SCALE OF ALLOWED RANDOMNESS                                   C
C                                                                             C
CCCCCCCCCCCCCCCCCCCCCCCCCCCCCCCCCCCCCCCCCCCCCCCCCCCCCCCCCCCCCCCCCCCCCCCCCCCCCC
      READ (5,633) EW,EP,ALPH,B,GEE
      READ (5,501) NPL,NPH,SPI,UTOP,QPI
  501 FORMAT(2I5,3F10.5)
      WRITE (6,600) EW,EP,ALPH,B,NPL,NPH,SPI,GEE,UTOP
  600 FORMAT ( 26H  COEFF.OF RES.FOR WALL =  ,F12.3/
     C           26H  COEFF.OF RES.FOR PART.=  ,F12.3/
     C           26H  ALPHA                 =  ,F12.3/
     C           26H  B=K**2/R**2           =  ,F12.3/
     C           26H  NO.VERTICALLY         =  ,I12/
     C           26H  NO.HORIZONTALLY       =  ,I12/
     C           26H  SPACING               =  ,F12.3/
     C           26H  GRAVITY               =  ,F12.3/
     C           26H  TOP PLATE VELOCITY    =  ,F12.3/)

       ALF =0.0174532* ALPH
       ALS= SIN(ALF)
       ALC= COS(ALF)
       ALT= ALS/ALC
       ALCT= ALC/ALS
      DO 25 I= 1,IT
   25  IR(I)= 0
       WL = 2.0*SPI*FLOAT(NPH)
       WLS =WL*ALS
       WLC = WL*ALC
       WH = 2.0*SPI*FLOAT(NPL)
       IT = NPL*NPH
       NOCD= 0

      WRITE (6,601) QPI,WL,WH
  601 FORMAT ( 26H  INITIAL OSC.VEL.%    =  ,F12.3/
     C           26H  LENGTH             =  ,F12.3/
     C           26H  HEIGHT             =  ,F12.3/)
C   INITIAL RANDOM X,Y,U,V,W  SETUP
       NRAN = 12345
      DO 200 J=1, NPL
```

```
      DO 200 K=1, NPH
      DO 201 L= 1,4
       NRAN = NRAND(NRAN)
  201  D(L) = 2.0 * FLOAT(NRAN) / 0.2147484E10  -1.0
       N = K+ NPH*(J-1)
       DS = SPI + 2.0*SPI*FLOAT(K-1) + D(1)*(SPI-1.0)
       DN = 2.0*SPI*FLOAT(J)-SPI+D(2)*(SPI-1.0)
       X(N) = DS*ALC + DN*ALS
       Y(N) = DN*ALC- DS*ALS
       U(N)= (ALC+D(3)*QPI)*(0.2+0.6*DN)*UTOP/WH
       V(N)=(-ALS+D(4)*QPI)*(0.2+0.6*DN)*UTOP/WH
  200  W(N) =0.0
C    WRITE OUT INITIAL STATE OF SYSTEM
       TIME = 0.0
      WRITE (6,637) TIME
  637 FORMAT(///24H ORIGINAL PARTICLE LIST   ,F15.5)
      DO 22 I= 1,IT
       DS= X(I)*ALC - Y(I)*ALS
       DN= X(I)*ALS + Y(I)*ALC
       US= U(I)*ALC - V(I)*ALS
       UN= U(I)*ALS + V(I)*ALC
   22 WRITE (6,631) I,DS,DN,US,UN,W(I),IR(I)
  631 FORMAT(I5,5F15.5,I5)
C    RECORD INITIAL STATE ON CARDS
      WRITE(7,635) TIME,NOCD
      WRITE(7,633)EW,EP,ALPH,B
      WRITE(7,633)UTOP,WH,GEE
      WRITE(7,634)IT,WL
      DO 320 I=1,IT
  320 WRITE(7,632) IR(I), X(I), Y(I), U(I), V(I), W(I)
  632 FORMAT(I5,5F10.5)
  633 FORMAT(5F10.4)
  634 FORMAT(I5,F10.4)
  635 FORMAT(F10.3,I5)

       STOP
       END
C THIS MARKS END OF MAIN PROGRAM
```

Appendix D

LISTINGS OF THE COLLISION ASSESSMENT ROUTINES: COLLUP

D.1 Collision Assessment for the Inclined Chute Simulation

```
      SUBROUTINE COLLUP(N,LAT,JA,TIME)
CCCCCCCCCCCCCCCCCCCCCCCCCCCCCCCCCCCCCCCCCCCCCCCCCCCCCCCCCCCCCCCCCCCCCCCCCCCCCCC
C                                                                              C
C   SUBROUTINE COLLUP                                                          C
C                                                                              C
C   COLLISION ASSESSMENT ROUTINE FOR THE INCLINED CHUTE SIMULATION             C
C                                                                              C
C   ASSESSES ALL COLLISION LIST ENTRIES FOR THE PARTICLE N.  THE TARGET        C
C       PARTICLE AND THE TIME OF THE COLLISION IS STORED IN THE COLLISION      C
C       LIST VIA THE ROUTINE INSRT                                             C
C                                                                              C
C       A TARGET NEX= ITA DENOTES A LOWER WALL COLLISION                       C
C                NEX= ITA1 DENOTES AN UPPER WALL COLLISION                     C
C                NEX = ITB DENOTES A DISAPPEARANCE UPSTREAM                    C
C                NEX = ITC A DISAPPEARANCE DOWNSTREAM.                         C
C                                                                              C
C   ONE PARTICLE CAN BE EXCLUDED AS A TARGET BY INCLUDING IT AS JA. THIS       C
C    IS ADVISABLE IF N HAS JUST COMPLETED A COLLISON WITH JA AND THEY ARE      C
C    PRESENTLY TOUCHING                                                        C
C                                                                              C
C   LAT IS THE FIRST PARTICLE IN NUMERICAL SEQUENCE THAT IS TO BE CONSIDERED   C
C    AS A TARGET PARTICLE                                                      C
C                                                                              C
C   OCCASIONALLY A PARTICLE IN THE MAIN FIELD OF VIEW MAY HAVE ITS PRIMARY     C
C    COLLISON WITH A PARTICLE IN THE REPEATED FRAME EITHER UPSTREAM OR          C
C    DOWNSTREAM OF THE MAIN FRAME . THE CASE IN WHICH THE N PARTICLE COLLIDESC
C    WITH A PARTICLE IN THE UPSTREAM REPEATED FRAME IS DENOTED BY NQA=-1 ;     C
C    FOR A COLLISION WITH THE DOWNSTREAM REPEATED FRAME NQA=+1. OTHERWISE      C
C    NQA=0                                                                     C
CCCCCCCCCCCCCCCCCCCCCCCCCCCCCCCCCCCCCCCCCCCCCCCCCCCCCCCCCCCCCCCCCCCCCCCCCCCCCCC
      DIMENSION X(1000),Y(1000),U(1000),V(1000),W(1000),
     C          IR(1000)
      REAL IL,JL
      DOUBLE PRECISION TIME,TIM,DA,DB,DC,DTA,DTB,DTN,DX,DY,DU,DV,DD,
     C                 DE,A1,A2,A3,A4,A5,H,FA,FB,H2,DT83,FD,DT82,
     C                 CH,F,FPRI,R
      COMMON/A/IT,X,Y,U,V,W,SHEART,SHEARN,IR,AISS
      COMMON/B/ITA,ITB,ITC,ALS,ALC,ALT,ALCT,WL,WLS,WLC,AISN,AISC
      F(R)= R**4 + A1*R**3 + A2*R*R + A3*R + A4
      FPRI(R)= 4.0D0*R**3 + 3.0*A1*R*R + 2.0*A2*R + A3
      DTN = 1.0D+6
      IF (IR(N).EQ.1) GOTO 930
C   ASSESS SOLID WALL COLLISION
      DB = DBLE(-V(N))- DBLE(ALT*U(N))
      DC = -2.0*(DBLE(Y(N)) + DBLE(X(N)*ALT) - 1.0D0/ALC)
C   CHECK FOR OVERLAP
      IF (DC.LE.0.0.OR.DB.LT.0.0) GOTO 920
      CALL INSRT(N,10,ITA,TIME,IT)
      RETURN
  920 DD= DB**2 - DC
      IF (DD.LT.0.0) DD= 0.0
      DD= DSQRT(DD)
      DTN= (-DB) - DD
      IF (DTN.LT.0.0) DTN= -(DB) + DD
      NEX= ITA
      NQA= 10
C   ASSESS UPSTREAM PERIODIC BOUNDARY COLLISION
  930 DB= DBLE(U(N)*ALCT) - DBLE(V(N))
      IF (IR(N).EQ.1) DB= DB*ALS/AISN
      DC= 2.0*(DBLE(X(N)*ALCT) - DBLE(Y(N)))
      IF (IR(N).EQ.1) DC= DC*ALS/AISN
      IF (JA.EQ.ITC) GOTO 940
C   CHECK FOR OVERLAP
```

```
      IF (DC.GE.0.0.OR.DB.GT.0.0) GOTO 935
      CALL INSRT(N,4,ITB,TIME,IT)
      RETURN
  935  DD= DB*DB - DC
      IF (DD.LT.0.0) GOTO 940
       DD= DSQRT(DD)
       DTB= -(DB + DD)
      IF (DTB.LE.0.0) DTB= (-DB) + DD
      IF (DTB.LT.0.0.OR.DTB.GT.DTN) GOTO 940
       NEX= ITB
       NQA= 4
C   ASSESS DOWNSTREAM PERIODIC BOUNDARY COLLISION
  940  DC= DC - 2.0*DBLE(WL/ALS)
      IF (IR(N).EQ.1) DC= DC + 2.0*WL*(1.0/ALS - 1.0/AISN)
C   CHECK FOR OVERLAP
      IF (DC.LT.0.0.OR.DB.LT.0.0.OR.JA.EQ.ITB) GOTO 945
      CALL INSRT(N,6,ITC,TIME,IT)
      RETURN
  945  DD= DB*DB - DC
      IF (DD.LT.0.0) DD= 0.0
       DD= DSQRT(DD)
       DTB= (-DB) - DD
      IF (DTB.LT.0.0) DTB= (-DB) + DD
      IF (DTB.GT.DTN) GOTO 950
       DTN= DTB
       NEX= ITC
       NQA= 6
  950  TIM= TIME + DTN
      IF (DTN.GT.100.0) STOP
      CALL INSRT(N,NQA,NEX,TIM,IT)
C   ASSESS PARTICLE-PARTICLE COLLISIONS
      IF (LAT.GT.IT) RETURN
      DO 100 I=1,3
      DO 100 J= LAT, IT
      IF (J.EQ.N) GOTO 100
       DX = DBLE(X(J)) - DBLE(X(N)) + DBLE(WLC*FLOAT(I-2))
       DY = DBLE(Y(J)) - DBLE(Y(N)) - DBLE(WLS*FLOAT(I-2))
       DU = DBLE(U(J)) - DBLE(U(N))
       DV = DBLE(V(J)) - DBLE(V(N))
       DA = DV**2 + DU**2
       DB = DV*DY+ DU*DX
       DC = DX**2 + DY**2-4.0D0
      IF (J.EQ.JA) GOTO 200
C   CHECK FOR OVERLAPS
      IF (DC.GE.0.0) GOTO 200
       NEX= J
       NQA= I-2
      CALL INSRT(N,NQA,J,TIME,IT)
      RETURN
  200 IF ((DU*DU + DV*DV).LT.0.00001) GOTO 100
      IF ((IR(N) + IR(J)).EQ.1) GOTO 300
      IF (J.EQ.JA) GOTO 100
       DD = DB**2 - DA*DC
      IF (DD.LT.0.0) GOTO 100
       DE = DSQRT(DD)
       DTA = (DE-DB)/DA
       DTB = -(DB+DE)/DA
      IF (DTB.LT.0.0) DTB= DTA
      IF (DTB.LT.0.0) GOTO 100
      IF (DTB.GT.DTN) GOTO 100
       NEX = J
       NQA=I-2
       TIM= TIME + DTB
```

```
      CALL INSRT(N,NQA,NEX,TIM,IT)
      GOTO 100

C   COLLISION ASSESSMENT BETWEEN A ROLLING AND A NON-ROLLING PARTICLE
  300  DG= FLOAT(IR(N) - IR(J))
       A5= 0.25*(DBLE(AISN*AISN) - DBLE(2.0*AISS) + 1.0D+0)
       A4= DC/A5
       A3= 2.0*DB/A5
       A2= (DA + DG*((AISS - 1.0)*DY - AISC*DX))/A5
       A1= DG*(DV*(AISS - 1.0) - DU*AISC)/A5
C    CHECK IF SOLUTION TO QUARTIC EXISTS
       H= A2 - A1*A1
       IL= A4 - 4.0*A1*A3 + 3.0*A2*A2
       G= A3 - 3.0*A1*A2 + 2.0*A1**3
       JL= H*IL - G*G - 4.0*H**3
       DD1= IL**3 - 27.0*JL*JL
       DD2= 3.0*JL - 2.0*H*IL
      IF (DD1.GT.0.0.AND.((H.GT.0.0).OR.(DD2.LT.0.0))) GOTO 100
C    NARROW DOWN THE LOCATION OF THE TIME BY A BISECTION METHOD
       NPATH= 1
       DTB= 0.0D0
       H= -0.25*DSQRT(DC+4.0)/DB
       IF (H.LT.0.0) H= .0675
       FA= A4
      IF  (DABS(FA).LT.1.0E-25) GOTO 910
  900  FB= F(DTB+H)
      IF (FA*FB) 907, 905, 905
  905  DTB= DTB+H
  906 IF (DTB.GT.DTN) GOTO 100
       FA= FB
      GOTO (900,907), NPATH
  907  H2= H
       H= H/2.0
      IF (H.LT.1.0D-8) GOTO 910
       NPATH= 2
      IF (H.GT.0.01) GOTO 900
C    WHEN CLOSE ENOUGH USE A NEWTONS METHOD TO FIND COLLISION TIME
       ICON= 0
       DTB3= DTB
       FD= FA
       DTB2= DTB
  909  ICON= ICON+1
       CH= FD/FPRI(DTB2)
      IF(DABS(CH).LT.1.0D-8) GOTO 908
       DTB2= DTB2 - CH
      IF (DABS(DTB2-DTB3).GT.H2.OR.ICON.GT.200) GOTO 900
       FD= F(DTB2)
      IF (DABS(FD).GT.1.0E-25) GOTO 909
  908  DTB= DTB2
  910  NEX = J
       NQA= I-2
       TIM= TIME + DTB
      CALL INSRT(N,NQA,NEX,TIM,IT)
  100 CONTINUE

  110 RETURN
      END
```

D.2 Collision Assessment for the Couette Flow Simulation

```
      SUBROUTINE COLLUP(N,LAT,JA,TIME,GEE,HGT,ITA1,VTOP,VBOT,VSIDE)
CCCCCCCCCCCCCCCCCCCCCCCCCCCCCCCCCCCCCCCCCCCCCCCCCCCCCCCCCCCCCCCCCCCCCCCCCC
C                                                                       C
C   SUBROUTINE COLLUP                                                   C
C                                                                       C
C   COLLISION ASSESSMENT ROUTINE FOR THE COUETTE FLOW SIMULATION        C
C                                                                       C
C   ASSESSES ALL COLLISION LIST ENTRIES FOR THE PARTICLE N.  THE TARGET C
C       IS STORED IN THE COLLISION LIST VIA THE ROUTINE INSRT.          C
C       A TARGET NEX= ITA DENOTES A LOWER WALL COLLISION                C
C                 NEX= ITA1 DENOTES AN UPPER WALL COLLISION             C
C                 NEX = ITB DENOTES A DISAPPEARANCE UPSTREAM            C
C                 NEX = ITC A DISAPPEARANCE DOWNSTREAM.                 C
C                                                                       C
C   VTOP, VBOT, AND VSIDE ARE THE VELLOCITES  OF THE UPPER, LOWER AND   C
C         PERIODIC BOUNDARIES RESPECTIVELY                              C
C                                                                       C
C   ONE PARTICLE CAN BE EXCLUDED AS A TARGET BY INCLUDING IT AS JA. THIS C
C    IS ADVISABLE IF N HAS JUST COMPLETED A COLLISON WITH JA AND THEY ARE C
C    PRESENTLY TOUCHING                                                 C
C                                                                       C
C   LAT IS THE FIRST PARTICLE IN NUMERICAL SEQUENCE THAT IS TO BE CONSIDERED C
C    AS A TARGET PARTICLE                                               C
C                                                                       C
C   OCCASIONALLY A PARTICLE IN THE MAIN FIELD OF VIEW MAY HAVE ITS PRIMARY C
C    COLLISON WITH A PARTICLE IN THE REPEATED FRAME EITHER UPSTREAM OR   C
C    DOWNSTREAM OF THE MAIN FRAME . THE CASE IN WHICH THE N PARTICLE COLLIDESC
C    WITH A PARTICLE IN THE UPSTREAM REPEATED FRAME IS DENOTED BY NQA=-1 ; C
C    FOR A COLLISION WITH THE DOWNSTREAM REPEATED FRAME NQA=+1. OTHERWISE C
C    NQA= 0.                                                            C
C                                                                       C
CCCCCCCCCCCCCCCCCCCCCCCCCCCCCCCCCCCCCCCCCCCCCCCCCCCCCCCCCCCCCCCCCCCCCCCCCC
      DIMENSION X(1000),Y(1000),U(1000),V(1000),W(1000),
     C IR(1000)
      REAL IL,JL
      DOUBLE PRECISION TIME,TIM,DA,DB,DC,DTA,DTB,DTN,DX,DY,DU,DV,DD,
     C                 DE,A1,A2,A3,A4,A5,H,FA,FB,H2,DTB3,FD,DTB2,
     C                 CH,F,FPRI,R,DHGT,DVT,DVB,DVSC,DVSS
      COMMON/A/IT,X,Y,U,V,W,SHEART,SHEARN,IR,AISS
      COMMON/B/ITA,ITB,ITC,ALS,ALC,ALT,ALCT,WL,WLS,WLC,AISN,AISC
      F(R)= R**4 + A1*R**3 + A2*R*R + A3*R + A4
      FPRI(R)= 4.0*R**3 + 3.0*A1*R*R + 2.0*A2*R + A3
       DHGT= DBLE(HGT)
       DVT=  DBLE(VTOP)
       DVB=  DBLE(VBOT)
       DVS= DBLE(VSIDE)
       DVSC= DVS*ALC
       DVSS= DVS*ALS
       DTN = 1.0D+6
       NQA= 0
C     IF THERE IS NO GRAVITY OR THE SYSTEM IS VERTICAL THE
C       EQUATIONS ARE LINEAR
      IF (GEE.NE.0.0.AND.ALC.NE.0.0) GOTO 1000
      IF (IR(N).NE.0) GOTO 1030
C     LOWER WALL COLLISIONS
       DB= DBLE(U(N)*ALS) + DBLE(V(N)*ALC) - DVB
       DC= DBLE(X(N)*ALS) + DBLE(Y(N)*ALC)  - 1.0D0
      IF (DC.GE.0.0.OR.JA.EQ.ITA.OR.DB.GT.0.0) GOTO 1010
      CALL INSRT(N,0,ITA,TIME,IT)
      RETURN
 1010 IF (DB.EQ.0.0) GOTO 1015
       DTB= -DC/DB
      IF (DTB.LT.0.0) GOTO 1015
```

```
       DTN= DTB
       NEX= ITA
C     UPPER WALL COLLISIONS
 1015  DC= DC + 2.0D0 - DHGT
       DB= DB  - DVT
      IF (DC.LE.0.0.OR.JA.EQ.ITA1.OR.DB.LT.0.0) GOTO 1020
      CALL INSRT(N,0,ITA1,TIME,IT)
      RETURN
 1020 IF (DB.EQ.0.0) GOTO 1030
       DTB= -DC/DB
      IF (DTB.LT.0.0.OR.DTB.GT.DTN) GOTO 1030
       DTN= DTB
       NEX= ITA1
C    UPPER BOUNDARY COLLISIONS FOR ZERO G OR ZERO ANGLE
 1030 IF (GEE.NE.0.0.AND.ALS.NE.0.0) GOTO 930
 1035  DB= DBLE(U(N)*ALC) - DBLE(V(N)*ALS)
      IF (DB.EQ.0.0) GOTO 950
       DC= DBLE(X(N)*ALC) - DBLE(Y(N)*ALS)
      IF (JA.EQ.ITC) GOTO 1040
      IF (DC.GE.0.0.OR.DB.GT.0.0) GOTO 1038
      CALL INSRT(N,0,ITB,TIME,IT)
      RETURN
 1038  DTB= -DC/DB
      IF (DTB.LT.0.0.OR.DTB.GT.DTN) GOTO 1040
       DTN= DTB
       NEX= ITB
C    LOWER BOUNDARY COLLISIONS
 1040 IF (JA.EQ.ITB) GOTO 950
       DC= DC - DBLE(WL)
       DB= DB - DVS
      IF (DC.LT.0.0.OR.DB.LT.0.0) GOTO 1045
      CALL INSRT(N,0,ITC,TIME,IT)
      RETURN
 1045  DTB= -DC/DB
      IF (DTB.LT.0.0.OR.DTB.GT.DTN) GOTO 950
       DTN= DTB
       NEX= ITC
      GOTO 950
C     QUADRATIC EQUATION SOLTION FOR NON-ZERO G
 1000 IF (IR(N).NE.0) GOTO 930
       DB = -(DBLE(V(N)) +  DBLE(ALT*U(N)))
       DC = -2.0*(DBLE(Y(N)) + DBLE(X(N)*ALT) - 1.0D0/ALC)
      IF (DC.LE.0.0) GOTO 920
      CALL INSRT(N,0,ITA,TIME,IT)
      RETURN
  920  DD= DB**2 - DC
      IF (DD.LT.0.0) DD= 0.0
       DD= DSQRT(DD)
       DTN= -DB + DD
       NEX= ITA
       DC= DC + (2.0D0/ALC - DHGT/ALC)
       DB= DB - DVT
      IF (DC.LE.0.0) GOTO 925
      CALL INSRT(N,0,ITA1,TIME,IT)
      RETURN
  925  DD= DB*DB - DC
      IF (DD.LT.0.0) GOTO 930
       DD= DSQRT(DD)
       DTB= -(DB + DD)
      IF (DTB.LT.0.0) DTB= -DB + DD
      IF (DTB.LT.0.0.OR.DTB.GT.DTN) GOTO 930
       DTN= DTB
       NEX= ITA1
```

```
C
C   WALL AND PERIODIC BOUNDARY COLLISIONS IF GRAVITY IS PRESENT
C   NOTE:  SIMULATIONS OF THIS TYPE WERE NEVER RUN AND THE ACCURACY
C          OF THIS SECTION IS UNKNOWN
C
  930 IF (ALS.EQ.0.0) GOTO 1035
      DB= DBLE(U(N)*ALCT) - DBLE(V(N))
      IF (IR(N).NE.0) DB=DB*ALS/AISN
      DC= 2.0*(DBLE(X(N)*ALCT) - DBLE(Y(N)))
      IF (IR(N).NE.0) DC= DC*ALS/AISN
      IF (JA.EQ.ITC) GOTO 940
      IF (DC.GE.0.0.OR.DB.GT.0.0) GOTO 935
      CALL INSRT(N,0,ITB,TIME,IT)
      RETURN
  935 DD= DB*DB - DC
      IF (DD.LT.0.0) GOTO 940
      DD= DSQRT(DD)
      DTB= -(DB + DD)
      IF (DTB.LT.0.0) DTB= (-DB) + DD
      IF (DTB.LT.0.0.OR.DTB.GT.DTN) GOTO 940
      NEX= ITB
  940 DC= DC - 2.0D0*WL/ALS
      DB= DB - 2.0*DVS/ALS
      IF (IR(N).NE.0) DC= DC + 2.0*WL*(1.0D0/ALS - 1.0D0/AISN)
      IF (DC.LT.0.0.OR.DB.LT.0.0.OR.JA.EQ.ITB) GOTO 945
      CALL INSRT(N,0,ITC,TIME,IT)
      RETURN
  945 DD= DB*DB - DC
      IF (DD.LT.0.0) DD= 0.0
      DD= DSQRT(DD)
      DTB= (-DB) - DD
      IF (DTB.LT.0.0) DTB= (-DB) + DD
      IF (DTB.GT.DTN) GOTO 950
      DTN= DTB
      NEX= ITC
C   STORE SHORTEST SOLID BOUNDARY COLLISION IN COLLISION LIST
  950 TIM= TIME + DTN
      CALL INSRT(N,0,NEX,TIM,IT)
C
C   PARTICLE-PARTICLE COLLISIONS
C
      IF (LAT.GT.IT) RETURN
      DO 100 I=1,3
      IFR= I-2
      DO 100 J= LAT, IT
      IF (J.EQ.N) GOTO 100
      DX = DBLE(X(J)) - DBLE(X(N)) + DBLE(WLC)*IFR
      DY = DBLE(Y(J)) - DBLE(Y(N)) - DBLE(WLS)*IFR
      DU = DBLE(U(J)) - DBLE(U(N)) + DVSC*IFR
      DV = DBLE(V(J)) - DBLE(V(N)) - DVSS*IFR
      DA = DV**2 + DU**2
      DB = DV*DY+ DU*DX
      DC = DX**2 + DY**2 - 4.0D0
      IF (DC.GE.0.0.OR.J.EQ.JA) GOTO 200
      NQA= IFR
      CALL INSRT(N,NQA,J,TIME,IT)
      RETURN
  200 IF ((DU*DU + DV*DV).LT.1.0D-06) GOTO 100
      IF (((IR(N).EQ.0.AND.IR(J).NE.0).OR.(IR(N).NE.0.AND.IR(J)
     C            .EQ.0)).AND.GEE.NE.0.0) GOTO 300
      IF(J.EQ.JA)GOTO 100
      DD = DB**2 - DA*DC
      IF (DD.LT.0.0) GOTO 100
```

```
      DE = DSQRT(DD)
      DTA = (DE-DB)/DA
      DTB = (-DB-DE)/DA
     IF (DTB.LT.0.0) DTB= DTA
     IF (DTB.LT.0.0) GOTO 100
     IF (DTB.GT.DTN) GOTO 100
      NQA=I-2
      TIM= TIME + DTB
     CALL INSRT(N,NQA,J,TIM,IT)
     GOTO 100

C    COLLISION ASSESMENT BETWEEN A ROLLING AND A NON-ROLLING PARTICLE
C    NOTE: THE EQUATIONS ARE ONLY DIFFERENT FROM THE FREE FALLING PARTICLE
C          CASE IF GRAVITY IS PRESENT.  AGAIN THIS SECTION HAS NEVER
C          BEEN TESTED.
  300  DG= FLOAT(ISIGN(1,IR(N) - IR(J)))
C    CHECK THESE TWO STATEMENTS IF YOU RUN INTO TROUBLE
      DU = DBLE(U(J)) - DBLE(U(N)) - DG*(1-DN)*DVB*ALS
      DV = DBLE(V(J)) - DBLE(V(N)) - DG*(1-DN)*DVB*ALC
      DA = DV**2 + DU**2
      DB = DV*DY+ DU*DX
      A5= 0.25*(DBLE(AISN*AISN) - 2.0D0*AISS + DBLE(GEE*GEE))
      A4= DC/A5
      A3= 2*DB/A5
      A2= (DA + DG*((AISS - GEE)*DY - AISC*DX))/A5
      A1= DG*(DV*(AISS - GEE) - DU*AISC)/A5

      H= A2 - A1*A1
      IL= A4 - 4.0*A1*A3 + 3.0*A2*A2
      G= A3 - 3.0*A1*A2 + 2.0*A1**3
      JL= H*IL - G*G - 4.0*H**3
      DD1= IL**3 - 27.0*JL*JL
      DD2= 3.0*JL - 2.0*H*IL
     IF (DD1.GT.0.0.AND.((H.GT.0.0).OR.(DD2.LT.0.0))) GOTO 100
      NPATH= 1
      DTB= 0.0
      H= 0.75*DSQRT(DC+4.0)/DB
      IF (H.LT.0.0) H= H/3.0
      FA= A4
     IF  (DABS(FA).LT.1.0E-25) GOTO 910
  900  FB= F(DTB+H)
     IF (FA*FB) 907, 905, 905
  905  DTB= DTB+H
  906 IF (DTB.GT.DTN) GOTO 100
      FA= FB
     GOTO (900,907), NPATH
  907  H2= H
      H= H/2.0
     IF (H.LT.1.0D-8) GOTO 910
      NPATH= 2
     IF (H.GT.0.01) GOTO 900
      ICON= 0
      DTB3= DTB
      FD= FA
      DTB2= DTB
  909  ICON= ICON+1
      CH= FD/FPRI(DTB2)
     IF(DABS(CH).LT.1.0D-8) GOTO 908
      DTB2= DTB2 - CH
     IF (DABS(DTB2-DTB3).GT.H2.OR.ICON.GT.200) GOTO 900
      FD= F(DTB2)
     IF (DABS(FD).GT.1.0E-25) GOTO 909
  908  DTB= DTB2
```

```
910  NFX = J
     NQA= I-2
     TIM= TIME + DTB
    CALL INSRT(N,NQA,NEX,TIM,IT)
100 CONTINUE

110 RETURN
    END
```

Appendix E

LISTING OF THE PARTICLE COLLISION SOLUTION ROUTINE: PARTCL

```
      SUBROUTINE PARTCL(NA,NB,NQA,B,EP,IST)
CCCCCCCCCCCCCCCCCCCCCCCCCCCCCCCCCCCCCCCCCCCCCCCCCCCCCCCCCCCCCCCCCCCCCCCCCCCC
C                                                                          C
C  SUBROUTINE PARTCL                                                       C
C                                                                          C
C  THIS ROUTINE SOLVES THE ZERO DEPARTURE CONTACT SURFACE RELATIVE         C
C     VELOCITY COLLISION BETWEEN PARTICLES NA AND NB WITH A RADIUS OF      C
C     GYRATION RATIO OF B AND A COEFFICIENT OF RESTITUTION OF EP.          C
C                                                                          C
CCCCCCCCCCCCCCCCCCCCCCCCCCCCCCCCCCCCCCCCCCCCCCCCCCCCCCCCCCCCCCCCCCCCCCCCCCCC
     DIMENSION X(1000),Y(1000),U(1000),V(1000),W(1000),
    C IR(1000),QS(50),QN(50),DIS(50),NCOL(50),RIMPLS(2)
      COMMON/A/IT,X,Y,U,V,W,SHEART,SHEARN,IR,AISS
      COMMON/B/ITA,ITB,ITC,ALS,ALC,ALT,ALCT,WL,WLS,WLC,AISN,AISC
      COMMON/D/DIS,ST,NCOL,RIMPLS
      BB = 1.0+ 1.0/B
C   INSURE THAT PARTICLES DO NOT OVERLAP
      DNQA= FLOAT(NQA)
      DISY= Y(NB) - (Y(NA) + WLS*DNQA)
      DISX= X(NB) + WLC*DNQA - X(NA)
      DISC= SQRT(DISX*DISX + DISY*DISY)
     IF (DISC.GT.2.1) RETURN
      BS = DISY/DISC
      BC= DISX/DISC
      X(NB)= X(NA) + 2.00001*BC - DNQA*WLC
      Y(NB)= Y(NA) + 2.00001*BS + DNCA*WLS
C   COMPUTE INITIAL ENERGY OF PARTICLES
      ENER= 0.5*(U(NA)**2 + U(NB)**2 + V(NA)**2 + V(NB)**2
    C  +  B*(W(NA)**2 + W(NB)**2))
C   COMPUTE COLLISION IMPULSE AND USE TO UPDATE PARTICLE VELOCITIES
      DA = U(NB) - U(NA)
      DB = V(NB) - V(NA)
     IF (DISX*DA + DISY*DB.GT.0.0) RETURN
      DC= 0.5*(DA*BS - DB*BC + W(NA) +W(NB))/BB
      DF=0.5*(1.0+EP)*(-DA*BC-DB*BS)
      DG = DC/B
      DH = DF*BC - BS*DC
      DI = BS*DF + BC*DC
      W(NB) = W(NB) - DG
      W(NA) = W(NA) - DG
      U(NB) = U(NB) + DH
      U(NA) = U(NA) - DH
      V(NB) = V(NB) + DI
      V(NA) = V(NA) - DI
C   AVERAGE MAGNITUDE AND DIRECTION OF IMPULSE
     IF (IST.LT.0.0) GOTO 100
      IC= 1+INT(((X(NA)+X(NB))*ALS+(Y(NA)+Y(NB))*ALC)/(2.0*ST))
      RIMPLS(1)= RIMPLS(1) + ABS(DF)
      RIMPLS(2)= RIMPLS(2) + ABS(DC)
C   COMPUTE COLLISION FREQUENCY
      NCOL(IC)= NCOL(IC) + 1
C   COMPUTE ENERGY DISSIPATED IN COLLISION
      DIS(IC)= DIS(IC) + ENER - 0.5*(U(NA)**2 + U(NB)**2 +
    C  V(NA)**2 + V(NB)**2 + B*(W(NA)**2 + W(NB)**2))
  100 RETURN
      END
```

Appendix F

LISTINGS OF THE WALL COLLISION SOLUTION ROUTINES: WALLCL

F.1 Wall Collision Solution for the Inclined Chute Simulation

```
      SUBROUTINE WALLCL( NA,B,EW,IST)
CCCCCCCCCCCCCCCCCCCCCCCCCCCCCCCCCCCCCCCCCCCCCCCCCCCCCCCCCCCCCCCCCCCCCCCCCC
C                                                                        C
C   SUBRCUTINE WALLCL                                                    C
C                                                                        C
C      THIS ROUTINE SOLVES THE ZERO DEPARTURE CONTACT SURFACE RELATIVE    C
C       VELOCITY COLLISICN BETWEEN THE PARTICLE NA AND THE WALL WITH A   C
C       RADIUS OF GYRATION RATIO OF B AND A CCEFFICIENT OF RESTITUTION OF EW C
C       FOR THE CHUTE FLOW SIMULATION.                                   C
C                                                                        C
CCCCCCCCCCCCCCCCCCCCCCCCCCCCCCCCCCCCCCCCCCCCCCCCCCCCCCCCCCCCCCCCCCCCCCCCCC
      DIMENSION X(1000), Y(1000), U(1000), V(1000), W(1000),
     C IR(1000)
      COMMON/A/IT,X,Y,U,V,W,SHEART,SHEARN,IR,AISS
      COMMON/B/ITA,ITB,ITC,ALS,ALC,ALT,ALCT,WL,WLS,WLC,AISN,AISC
      COMMON/E/WDIS
      BB= 1.0 +1.0/B
C   COMPUTE NORMAL AND TANGENTIAL COLLISION IMPULSES
      DA = (V(NA)*ALS-U(NA)*ALC-W(NA))/BB
      DD=-(1.0+EW)*(U(NA)*ALS+V(NA)*ALC)
      UI= U(NA)
      VI= V(NA)
      WI= W(NA)
C   UPDATE PARTICLE VELOCITIES
      U(NA) = U(NA) + DA*ALC + DD*ALS
      V(NA) = V(NA) + DD*ALC-DA*ALS
      W(NA) = W(NA) + DA/B
C   INSURE THAT PARTICLE DOES NOT OVERLAP WALL
      DIST= X(NA)*ALC - Y(NA)*ALS
      X(NA)= DIST*ALC + 1.00001*ALS
      Y(NA)= 1.00001*ALC - DIST*ALS
C   IF SYSTEM IS BEING AVERAGED COMPUTE IMPULSE APPLIED TO WALL
      IF (IST.LT.0) GOTO 100
      SHEART= SHEART + DA
      SHEARN= SHEARN + DD
      WDIS= WDIS - 0.5*(U(NA)**2 - UI**2 + V(NA)**2 - VI**2
     C + B*(W(NA)**2 - WI**2))
  100 VISN= U(NA)*ALS+V(NA)*ALC
C   IF THE VELOCITY NORMAL TO WALL IS SMALL ENOUGH, LABEL PARTICLE
C     AS ROLLING
      IF (ABS(VISN).GT.0.0001) GOTO 1000
      UISN= U(NA)*ALC - V(NA)*ALS
      U(NA)= UISN*ALC
      V(NA)= -UISN*ALS
      IR(NA)= 1
C      WRITE (6,600) NA
  600 FORMAT(/15H     PARTICLE  ,I5, 10H   ROLLING/)
 1000 RETURN
      END
```

F.2 Wall Collision Solution for the Couette Flow Simulation with the Rough Particle/Wall Surface Condition

```
      SUBROUTINE WALLCL(NA,B,EW,IST,DN,UTOP,HGT,GEE,UWSH,BWSH)
CCCCCCCCCCCCCCCCCCCCCCCCCCCCCCCCCCCCCCCCCCCCCCCCCCCCCCCCCCCCCCCCCCCCCCCCC
C                                                                       C
C   SUBROUTINE WALLCL                                                   C
C                                                                       C
C      THIS ROUTINE SOLVES THE ZERO DEPARTURE CONTACT SURFACE RELATIVE  C
C       VELOCITY COLLISION BETWEEN THE PARTICLE NA AND THE WALL WITH A  C
C       RADIUS OF GYRATION RATIO OF B AND A CCEFFICIENT OF RESTITUTION OF EW C
C       FOR THE COUETTE FLOW SIMULATION.                                C
C      DN=0 INDICATES A LOWER WALL COLLISION                            C
C      DN= 1 INDICATES AN UPPER WALL COLLISION                          C
C                                                                       C
CCCCCCCCCCCCCCCCCCCCCCCCCCCCCCCCCCCCCCCCCCCCCCCCCCCCCCCCCCCCCCCCCCCCCCCCC
      DIMENSION X(1000),Y(1000),U(1000),V(1000),W(1000),
     C  IR(1000),WDIS(2)
      COMMON/A/IT,X,Y,U,V,W,SHEART,SHEARN,IR,AISS
      COMMON/B/ITA,ITB,ITC,ALS,ALC,ALT,ALCT,WL,WLS,WLC,AISN,AISC
      COMMON/E/SHRT,SHRN,WDIS,VBOT,VTOP
      BB= 1.0 +1.0/B
      DN2= 1.0 - DN
      DN3= 1.0 - 2.0*DN
      VB= DN2*VBOT - DN*(VTOP+VBOT)
      DA = (V(NA)*ALS+UTOP*DN-(U(NA)*ALC+DN3*W(NA)))/BB
      VISN= U(NA)*ALS + V(NA)*ALC
      VW= ABS(DN2*VBOT + DN*(VTOP+VBOT))
C   INSURE THAT PARTICLE DOES NOT OVERLAP WALL
      DIST= X(NA)*ALC - Y(NA)*ALS
      X(NA)= DIST*ALC + ((HGT - 2.00002)*DN + 1.00001)*ALS
      Y(NA)= ((HGT - 2.00002)*DN + 1.00001)*ALC - DIST*ALS
      UI= U(NA)
      VI= V(NA)
      WI= W(NA)
     IF (ABS(VISN)-VW.LT.0.0001.AND.VB.GT.0.0) GOTO 100
     IF (DN3*VISN.GT.0.0) GOTO 290
C    COLLISION SOLUTION
      DD=-(1.0+EW)*(VISN+VW)
      U(NA) = U(NA) + DA*ALC + DD*ALS
      V(NA) = V(NA) + DD*ALC - DA*ALS
      W(NA) = W(NA) + DN3*DA/B
     GOTO 300
 100  UISN= U(NA)*ALC - V(NA)*ALS
      U(NA)= UISN*ALC
      V(NA)= -UISN*ALS
      W(NA)= -(DN3*UISN + DN*UTOP)
      DA= B*(W(NA)-WI)*DN3
     IF (GEE*DN.NE.0.0) GOTO 290
      IR(NA)= 1 + INT(DN)
 290  DD= DN3*ABS(VISN)
C   COMPUTE WALL SHEAR STRESS FOR NORMAL STRESS COMPARISOM
 300  UWSH= UWSH + DN*DD
      BWSH= BWSH + DN2*DD
     IF (IST.LT.0) GOTO 1000
C   COMPUTE DISSIPATION AT WALL
      WDIS(DN+1)= WDIS(DN+1) - 0.5*(U(NA)**2 - UI**2 + V(NA)**2
     C    - VI**2 + B*(W(NA)**2 - WI**2))
     IF (DN.NE.0.0) GOTO 90
C   COMPUTE WALL STRESSES
      SHEART= SHEART + DA
      SHEARN= SHEARN + DD
     GOTO 1000
  90  SHRT= SHRT + DA
      SHRN= SHRN + DD
1000 RETURN
      END
```

F.3 Wall Collsion Solution for the Couette Flow Simulation with the No-Slip Wall Condition

```
      SUBROUTINE WALLCL(NA,B,EW,IST,DN,UTOP,HGT,GEE,UWSH,BWSH)
CCCCCCCCCCCCCCCCCCCCCCCCCCCCCCCCCCCCCCCCCCCCCCCCCCCCCCCCCCCCCCCCCCCCCCCC
C                                                                      C
C   SUBROUTINE WALLCL                                                  C
C                                                                      C
C      THIS ROUTINE SOLVES THE ZERO DEPARTURE  RELATIVE (NO-SLIP)      C
C       VELOCITY COLLISION BETWEEN THE PARTICLE NA AND THE WALL WITH A C
C       RADIUS OF GYRATION RATIO OF B AND A CCEFFICIENT OF RESTITUTION OF EW C
C       FOR THE COUETTE FLOW SIMULATION.                               C
C      DN=0 INDICATES A LOWER WALL COLLISION                           C
C      DN= 1 INDICATES AN UPPER WALL COLLISION                         C
C                                                                      C
CCCCCCCCCCCCCCCCCCCCCCCCCCCCCCCCCCCCCCCCCCCCCCCCCCCCCCCCCCCCCCCCCCCCCCCC
      DIMENSION X(1000),Y(1000),U(1000),V(1000),W(1000),
     C IR(1000),WDIS(2)
      COMMON/A/IT,X,Y,U,V,W,SHEART,SHEARN,IR,AISS
      COMMON/B/ITA,ITB,ITC,ALS,ALC,ALT,ALCT,WL,WLS,WLC,AISN,AISC
      COMMON/E/SHRT,SHRN,WDIS,VBOT,VTOP
      BB= 1.0 +1.0/B
      DN2= 1.0 - DN
      DN3= 1.0 - 2.0*DN
      VB= DN2*VBOT - DN*(VTOP+VBOT)
      DA = UTOP*DN - (U(I)*ALC - V(I)*ALS)
      VISN= U(NA)*ALS + V(NA)*ALC
      VW= ABS(DN2*VBOT + DN*(VTCP+VBOT)) + 0.0001
C   INSURE THAT PARTICLE DOES NOT OVERLAP WALL
      DIST= X(NA)*ALC - Y(NA)*ALS
      X(NA)= DIST*ALC + ((HGT - 2.00002)*DN + 1.00001)*ALS
      Y(NA)= ((HGT - 2.00002)*DN + 1.00001)*ALC - DIST*ALS
      UI= U(NA)
      VI= V(NA)
      WI= W(NA)
     IF (ABS(VISN).LT.VW.AND.VB.GT.0.0) GOTO 100
     IF (DN3*VISN.GT.0.0) GOTO 290
C   WALL COLLISION SOLUTION
      DD=-(1.0+EW)*VISN
      U(NA) = DN*UTOP
      V(NA) = -EW*V(NA)
     GOTO 300
C   IS PARTICLE TO BE TAGGED AS ROLLING?
  100 U(NA)= UTOP*DN
      V(NA)= 0.0
      W(NA)= 0.0
      DA= B*(W(NA)-WI)*DN3 + U(NA)-UI
     IF (GEE*DN.NE.0.0) GOTO 290
      IR(NA)= 1 + INT(DN)
  290 DD= DN3*ABS(VISN)
C   COMPUTE INSTANTANEOUS STRESS AT WALL
  300 UWSH= UWSH + DN*DD
      BWSH= BWSH + DN2*DD
C   COMPUTE DISIPATION AT WALL
     IF.(IST.LT.0) GOTO 1000
      WDIS(DN+1)= WDIS(DN+1) - 0.5*(U(NA)**2 - UI**2 + V(NA)**2
    C   - VI**2 + B*(W(NA)**2 - WI**2))
C   COMPUTE WALL SHEAR  STRESS
     IF (DN.NE.0.0) GOTO 90
      SHEART= SHEART + DA
      SHEARN= SHEARN + DD
     GOTO 1000
   90 SHRT= SHRT + DA
      SHRN= SHRN + DD
 1000 RETURN
      END
```

Appendix G

LISTINGS OF THE COLLISION LIST MANAGEMENT ROUTINES

G.1 INSRT: General Collision List Manager

```
      SUBROUTINE INSRT(N,NQA,NEX,TIM,IT)
CCCCCCCCCCCCCCCCCCCCCCCCCCCCCCCCCCCCCCCCCCCCCCCCCCCCCCCCCCCCCCCCCCCCCCCCCCCCCCC
C                                                                              C
C     SUBROUTINE INSRT                                                         C
C                                                                              C
C   THIS SUBPROGRAM MAINTAINS A COLLISION LIST                                 C
C                                                                              C
C      ENTRY INSRT INSERTS COLLISIONS INTO THE LIST                            C
C            INIT  INITIALIZES THE COLLISION LIST                              C
C            NEXT  TAKES NEXT COLLISICN FROM THE COLLISION LIST                C
C                                                                              C
C   THIS SUBPROGRAM REUIRES THE AUXILLARY SUBROGRAM REMOVE WHICH               C
C            REMOVES ALL COLLISIONS INVOLVING A GIVEN PARTICLE FROM            C
C            THE LIST                                                          C
C                                                                              C
C   THE COLLISION INFORMATION IS STORED IN THE ARRAY ICOLL                     C
C                                                                              C
C   IFREE POINTS TO THE NEXT FREE LINE IN ICOLL IN WHICH A  COLLISION          C
C      MAY BE INSERTED                                                         C
C      THE LIST IS CONTINUED IN COLUMN 9 OF ICOLL                              C
C   ISHORT POINTS TO THE LINE IN ICOLL WHICH CONTAINS THE NEXT COLLISION       C
C   ILONG  POINTS TO THE LAST COLLISION IN ICCLL                               C
C   NPOINT(N) POINTS TO A LIFO LIST CONTAINED IN ICOLL COLUMNS 6,7,8,9         C
C      CONNECTING ALL THE COLLISIONS FOR THE PARTICLE N.                       C
C      IF NPOINT(N)= I THEN THE  NEXT ELEMENT IN THE LIST CAN BE FOUND         C
C         IN COLUMNS 6,7 OF LINE I IN ICOLL                                    C
C      IF NPOINT(N) HAS THE FORMAT  NPOINT(N)= 200000+I THEN THE NEXT          C
C         ELEMENT IN THE LIST CAN BE FOUND IN COLUMNS 8,9 IN ICOLL LINE I      C
C   TIME(I) IS THE REAL VALUED ARRAY CONTAINING THE TIME AT WHICH THE          C
C      COLLISIONS DESCRIBED IN ICCLL LINE I WILL OCCUR                         C
C                                                                              C
CCCCCCCCCCCCCCCCCCCCCCCCCCCCCCCCCCCCCCCCCCCCCCCCCCCCCCCCCCCCCCCCCCCCCCCCCCCCCCC
      INTEGER ICOLL(1000,9),NPOINT(1000)
      DOUBLE PRECISION TIME(1000),TIM
CCCCCCCCCCCCCCCCCCCCCCCCCCCCCCCCCCCCCCCCCCCCCCCCCCCCCCCCCCCCCCCCCCCCCCCCCCCCCCC
C   ICOLL IS ORGANIZED AS FOLLOWS:                                             C
C       ICOLL(I,1) CONTAINS A PARTICLE NUMBER                                  C
C       ICOLL(I,2) CONTAINS ITS TARGET NUMBER                                  C
C       ICOLL(I,3) CONTAINS NQA, THE COLLISION FRAME IN WHICH THE              C
C              COLLISION WILL OCCUR                                            C
C       ICOLL(I,4) POINTS TO THE COLLISION LINE THAT IS TO OCCUR JUST BEFORE   C
C              THIS ONE                                                        C
C       ICCLL(I,5) PCINTS TO THE NEXT COLLISICN TO OCCUR.                      C
C       ICOLL(I,6) IS A BACKWARD POINTER IN THE LIFO LIST OF ALL THE           C
C              COLLISIONS FOR THE PARTICLE ICOLL(I,1)                          C
C       ICOLL(I,7) IS THE FORWARD POINTER IN THE LIFO LIST FOR PARTICLE        C
C              ICOLL(I,1)                                                      C
C       ICOLL(I,8) IS THE BACKWARD POINTER IN THE LIFO LIST FOR PARTICLE       C
C              ICOLL(I,2)                                                      C
C       ICOLL(I,9) IS THE FORWARD POINTER IN THE LIST FOR PARTICLE ICOLL(I,2)  C
C                                                                              C
C   A ZERO IN A POINTER POSITION INDICATES THE END OF THE LIST                 C
C                                                                              C
CCCCCCCCCCCCCCCCCCCCCCCCCCCCCCCCCCCCCCCCCCCCCCCCCCCCCCCCCCCCCCCCCCCCCCCCCCCCCCC
      COMMON/C/TIME,NPOINT,ICOLL,IFREE,ISHORT,ILONG
       NT= IFREE
       TIME(NT)= TIM
       ICOLL(NT,1)= N
       ICOLL(NT,2)= NEX
       ICOLL(NT,3)= NQA
       ICOLL(NT,7)= NPOINT(N)
       ICOLL(NT,6)= 0
       ICOLL(NT,8)= 0
```

```
      IFREE= ICOLL(NT,9)
      IF (IFREE.EQ.0) STOP
     IF (NPOINT(N).NE.0) GOTO 80
      NPOINT(N)= NT
     GOTO 90
   80  NP2= NPOINT(N)/100000
      NP= NPOINT(N) - NP2*100000
      NPOINT(N)= NT
      ICOLL(NP,6+NP2)= NT
   90  IF (NEX.LE.IT) GOTO 97
      ICOLL(NT,9)= 0
     GOTO 100
   97 IF (NPOINT(NEX).NE.0) GOTO  95
      NPOINT(NEX)= NT + 200000
      ICOLL(NT,9)= 0
     GOTO 100
   95  NP2= NPOINT(NEX)/100000
      NP= NPOINT(NEX) - NP2*100000
      ICOLL(NP,6+NP2)= NT + 200000
      ICOLL(NT,9)= NPOINT(NEX)
      NPOINT(NEX)= NT + 200000
C    SORT FOR POSITION IN ORDER OF OCCURENCE LIST
C
C    IS THIS COLLISION TO BE THE FIRST IN THE LIST
   100 IF (TIME(NT).GT.TIME(ISHORT)) GOTO 110
      ICOLL(ISHORT,4)= NT
      ICOLL(NT,4)= 0
      ICOLL(NT,5)= ISHORT
      ISHORT= NT
     RETURN

C    IS THIS COLLISION TO BE THE LAST IN THE LIST
   110 IF (TIME(NT).LT.TIME(ILONG)) GOTO 120
      ICOLL(NT,4)= ILONG
      ICOLL(ILONG,5)= NT
      ICOLL(NT,5)= 0
      ILONG= NT
     RETURN

C    START THE SEARCH FOR THE POSITION IN THE COLLISION QUEUE WITH THE
C       LAST ENTRY IN THE LIST
   120  ILAST= ILONG
   130 IF(TIME(NT).GE.TIME(ICOLL(ILAST,4)).OR.ILAST.EQ.0) GOTO 140
      ILAST= ICOLL(ILAST,4)
     GOTO 130

   140  ICOLL(NT,4)= ICOLL(ILAST,4)
      ICOLL(ICOLL(ILAST,4),5)= NT
      ICOLL(NT,5)= ILAST
      ICOLL(ILAST,4)= NT
     RETURN
       --
       -
     ENTRY INIT
C
C    THIS ENTRY INITIALIZES THE COLLISION LIST
C
     DO 25 I= 1,1000
     DO 20 I2= 1,8
    20  ICOLL(I,I2)= 0
      ICOLL(I,9)= I+1
      TIME(I)= 0.0
    25  NPOINT(I)= 0
```

```
      ICOLL(1000,9)=0
      IFREE= 1
      ISHORT= 1
      ILONG= 1
      TIME(1)= 1000000000.0
      RETURN

      ENTRY NEXT(N,NEX,NQA,TIM)

C     THIS ENTRY POINT YIELDS THE NEXT COLLISION IN THE LIST

      N= ICOLL(ISHORT,1)
      NEX= ICOLL(ISHORT,2)
      NQA= ICOLL(ISHORT,3)
      TIM= TIME(ISHORT)
      ISHORT= ICOLL(ISHORT,5)
      ICOLL(ISHORT,4)= 0
      CALL REMOVE(N)
      IF (NEX.LE.IT) CALL REMOVE(NEX)
      RETURN
      END
```

G.2 REMOVE: Routine to Remove All Collisions from the List Involving a Given Particle

```
      SUBROUTINE REMOVE(N)
CCCCCCCCCCCCCCCCCCCCCCCCCCCCCCCCCCCCCCCCCCCCCCCCCCCCCCCCCCCCCCCCCCCCCCCCCCC
C                                                                         C
C   SUBROUTINE REMOVE                                                     C
C                                                                         C
C   THIS SUBROUTINE REMOVES ALL THE ENTRIES IN THE COLLISION LIST ICOLL   C
C        INVOLVING PARTICLE N.                                            C
C                                                                         C
CCCCCCCCCCCCCCCCCCCCCCCCCCCCCCCCCCCCCCCCCCCCCCCCCCCCCCCCCCCCCCCCCCCCCCCCCCC
      INTEGER  ICOLL(1000,9), NPOINT(1000)
      DOUBLE PRECISION TIME(1000)
      COMMON/C/ TIME,NPOINT,ICOLL,IFREE,ISHORT,ILONG
C   START WITH FIRST PARTICLE IN LIST
       NP2= NPOINT(N)/100000
       NP= NPOINT(N) - NP2*100000
       NPOINT(N)= 0

C   END OF LIST?
 1000 IF (NP.EQ.0) RETURN
C   RECONNECT UNAFFECTED LISTS
       NEXT= ICOLL(NP,9-NP2)
       LAST= ICOLL(NP,8-NP2)
      IF (NEXT.EQ.0) GOTO 100
       NEX2= NEXT/100000
       NEX= NEXT - NEX2*100000
       ICOLL(NEX,6+NEX2)= LAST
  100 IF (LAST.EQ.0) GOTO 105
       LAS2= LAST/100000
       LAS= LAST - LAS2*100000
       ICOLL(LAS,7+LAS2)= NEXT
      GOTO 110
  105  NPOINT(ICOLL(NP,2-NP2/2))= NEXT
  110  NT= ICOLL(NP,7+NP2)
       ICOLL(ICOLL(NP,5),4)= ICOLL(NP,4)
       ICOLL(ICOLL(NP,4),5)= ICOLL(NP,5)
C   ATTACH FREED ELEMENT TO LIST OF FREE SPACES
       ICOLL(NP,9)= IFREE
       IFREE= NP
      IF (NP.NE.ILONG) GOTO 200
       ILONG= ICOLL(NP,4)
       ICOLL(ILONG,5)= 0
  200 IF (NP.NE.ISHORT) GOTO 250
       ISHORT= ICOLL(NP,5)
       ICOLL(ISHORT,4)= 0
  250  NP2= NT/100000
       NP= NT - 100000*NP2
      GOTO 1000
      END
```

REFERENCES

1. Augenstein, D. A., and Hogg, R., "An Experimental Study of the Flow of Dry Powders on Inclined Surfaces", Powder Technology, 19, 205, 1978.

2. Augenstein, D. A., and Hogg, R., "Friction Factors for Powder Flow", Powder Technology, 10, 43, 1974.

3. Bagnold, R. A., "Experiments on a Gravity Free Dispersion of Large Solid Spheres in a Newtonian Fluid", Proc. Roy. Soc., 225, 49, 1954.

4. Bagnold, R. A., "The Shearing and Dilation of Dry Sand and the 'Singing' Mechanism", Proc. Roy. Soc. A., 295, 219, 1966.

5. Barker, J. A., and Henderson, D., "What is Liquid? Understanding the States of Matter", Reviews of Modern Physics, 48, 587, 1976.

6. Barnes, George, "Study of Collisions Part I: A Survey of the Periodical Literature", Am. J. Phys., 26, 5, 1958. Part II: "Survey of the Textbooks", Am. J. Phys.26, 9, 1958.

7. Batchelor, G. K., An Introduction to Fluid Dynamics , Cambridge University Press, 1967.

8. Bird, G. A., Molecular Gas Dynamics , Clarendon Press Oxford, 1976.

9. Blair-Fish, P. M., and Bransby, R. L., "Flow Patterns and Wall Stresses in a Mass Flow Bunker", J. Eng. for Ind., 95, 17, 1973.

10. Brennen, C. E., and Pearce J. C., "Granular Material Flow in Two-Dimensional Hoppers", J. App. Mech., 100, 43, 1978.

11. Brennen, C. E., Sieck, K., and Paslaski, J., "Hydraulic Jumps in Granular Material Flows", to be submitted to Powder Technology.

12. Campbell, C. S., "Lubrication Mechanism for Long Runout or Sheeted Landslides", in preparation.

13. Carnahan, N. F. and Starling, K. E., "Equations of State for Non-Attracting Rigid Spheres", J. Chem. Phys., 51, 635, 1969.

14. Chapman, S., and Cowling, T.G., The Mathematical Theory of Non-Uniform Gases", Cambridge University Press, third edition, 1970.

15. Choda, A., and Willis, A.H., "Flow Regimes of Grains in Inclined Ducts", Trans. Amer. Soc. Aggr. Eng., 10, 136, 1967.

16. Connelly, L.M., "Wall Pressure and Material-Velocity Measurements for the Flow of Granular Material Under Plane Strain Conditions", from Mechanics Applied to the Transport of Bulk Solids, ASME AMD, 31, 35, 1979.

17. Cowin, S.C., "A Theory for the Flow of Granular Materials", Powder Technology, 9, 61, 1974.

18. Cowin, S.C., and Goodman, M.A., "A Variational Principal for Granular Materials", ZAMM, 56, 281, 1976.

19. Cundall, P.A., and Strack, O.D.L., "A Discrete Numerical Model for Granular Assemblies", Geotechnique, 29, 47-65, 1979. See also: Cundall, P.A. "A Computer Model for Rock-Mass Behavior using Interactive Graphics for the Input and Output of Geometrical Data". Technical Report MRD-2-74, Missouri River Division, U.S. Army Corps of Engineers.

20. de Coulomb, C. A., "Essai sur un Application de Règles de Maximis et Minimis à quelques Problèmes de Statique, Relatifs à L'Architecture", Mem. de Math. et de Phys. Acd. Roy. des Sci. Paris, 7, 343, 1773.

21. Ferziger, J. H., and Kaper, H. G., Mathematical Theory of Transport Processes in Gases , North Holland Pub., 1972.

22. Fowler, R. T., and Chodziesner, W. B., "The Influence of Variables Upon the Angle of Friction of Granular Materials", Chem. Eng. Sci., 10, 157, 1959.

23. Goldsmith, W., Impact, the Theory and Physical Behavior of Colliding Solids , Edward Arnold Pub., 1960.

24. Goldsmith, W., "The Coefficient of Restitution", Bull. Mech. Div. Amer. Soc. Eng. Ed., 2, 10, 1952.

25. Goodman, M. A., and Cowin, S. C., "A Continuum Theory for Granular Materials", Arch. Rat. Mech. and Anal., 44, 249, 1972.

26. Goodman, M. A., and Cowin, S. C., "Two Problems in the Gravity Flow of Granular Materials", J. Fluid Mech., 45, 321, 1971.

27. Ishida, M., and Shirai, T., J. Chem. Eng. Japan, 12, 46, 1979.

28. Ishida, M., Shirai, J., and Nisiwaki, A., "Measurement of the Velocity and Direction of Flow of Solid Particles in a Fluidized Bed", Powder Technology, 27, 1, 1980.

29. Ishida, M, Hatano, H., and Shirai, T., "The Flow of Solid Particles in an Aerated Inclined Channel", Powder Technology, 27, 7, 1980.

30. Jenike, A. W., and Shield, R. T., "On the Plastic Flow of Coulomb Solids Beyond Original Failure", Jour. App. Mech., 26, 599, 1959.

31. Jenike, A. W., "Steady Gravity Flow of Frictional Cohesive Solids in Converging Channels", Jour. App. Mech., 31, 5,1964.

32. Jenkins, J. T., "Static Equilibrium of Granular Materials", Jour. App. Mech., 42, 603, 1975.

33. Jenkins, J. T., and Cowin, S. C., "Theories for Flowing Granular Materials", from Mechanics Applied to the Transport of Bulk Solids, ASME, AMD 31, 79, 1979.

34. Johanson, J. R., "Stress and Velocity Field in the Gravity Flow of Bulk Solids", Jour. App. Mech., 31, 499, 1964.

35. Kahatani, Ken-Ichi, "A Micropolar Continuum Theory for the Flow of Granular Materials", Int. J. Eng. Sci., 17, 419, 1979.

36. Landau, L. D., and Lifshitz, E. M., Statistical Physics , Pergammon Press, 1958.

37. Lee, J., Cowin, S. C., and Templeton, J. S., "An Experimental Study of the Kinematics of Flow through Hoppers", Trans. Soc. Rheology, 18: 2, 247, 1974.

38. Litwiniszyn,J.,"Colmatage Considered as a Certain Stochastic Process", Bull. de L'Acad. Pol. des Sci., 9, 81, 1963.

39. Marble, F. E., "Mechanism of Particle Collision in the One-Dimensional Dynamics of Gas - Particle Mixtures", Physics of Fluids, 7, 1270, 1964.

40. McTigue, D. F., "A Model for the Stresses in the Shear Flow of a Granular Material", Presented at the NSF Conference, "Continuum Mechanical and Statistical Approaches in the Flow of Granular Materials", Sendai, Japan, June 5-8, 1978.

41. Metropolis, N., Rosenbluth, A., Rosenbluth, M., Teller, A., and Teller, E., "Equation of State Calculations by Fast Computing Machines", J. Chem. Phys., 21, 1087, 1953.

42. Morrison, H. L., and Richmond, O., "Application of Spencer's Ideal Soil Model to Granular Material Flows", Jour. App. Mech., 43, 49, 1976.

43. Mullins, W. W., "Experimental Evidence for the Stochastic Theory of Particle Flow", Powder Technology, 9, 29, 1974.

44. Nedderman, R. M., and Tuzun, V., "A Kinematic Model for the Flow of Granular Materials", Powder Technology, 22, 243, 1979.

45. Nedderman, R. M., Davies, S. T., and Horton, D. J., "The Flow of Granular Materials Round Obstacles", Powder Technology, 25, 215, 1980.

46. Nguyen, T., Brennen, C., and Sabersky, R. H., "Gravity Flow of Granular Materials in Conical Hoppers", Jour. App. Mech., 46, 529, 1979.

47. Nguyen, T., Studies in the Flow of Granular Materials , Ph.D Thesis , California Institute of Technology, 1979.

48. Nunziato,J. W., Passman, S. L., and Thomas, J. P., "Gravitational Flows of Granular Materials with Incompressible Grains", Jour. Rheology, 24, 395, 1980.

49. Nunziato, J. W., Personal Communication.

50. Ogawa, S., "Multi-Temperature Theory of Granular Materials", Presented at the NSF Conference", "Continuum Mechanical and Statistical Approaches in the Mechanics of Granular Materials", Sandai,Japan, June 5-8, 1978.

51. Ogawa, S., Umemura, A., and Oshima, N., "On the Equations of Fully Fluidized Granular Materials", ZAMP, 31, 483, 1980.

52. Oki, K., Walawender, W., Fan , L. T., "The Measurement of the Local Velocity of Solid Particles", Powder Technology, 18, 171, 1977.

53. Passman, S. L., Nunziato, J. W., Baily, P. B., and Thomas, J. P., "Shearing Flows of Granular Materials", Trans. ASCE, Jour. Eng. Mech. Div., 106, 773, 1980.

54. Passman, S. L., "Mixtures of Granular Materials", Int. J. Eng. Sci., 15, 117, 1977.

55. Pearce, J. C., "Mechanics of Flowing Granular Materials", Ph.D Thesis , California Institute of Technology.

56. Powell, M. J., "Computer Simulated Random Packings of Spheres", Powder Technology, 25, 45, 1980.

57. Raman, C. V., "The Photographic Study of Impact at Minimal Velocities", Physical Review, 12, 442, 1918.

58. Reynolds, Osborne, "On the Dilatancy of Media Composed of Rigid Particles in Contact", Phil. Mag., 20, 1885.

59. Reynolds , Osborne, "Experiments Showing Dilutency, A Property of Granular Materials Possibly Connected with Gravitation", Proc. Roy. Inst. Great Brit., 11, 354, 1887.

60. Ridgway, K., and Rupp, R., "Flow of Granular Materials down Chutes", Chem. Proc. Eng., 51, 82, 1970.

61. Ridgway, K., and Rupp, R., "The Mixing of Particle Layers on a Chute: The Effect of Particle Size and Shape", Powder Technology, 4, 195, 1971.

62. Roberts, A. W., "The Dynamics of Granular Material Flow Through Curved Chutes", Mech. and Chem. Eng. Trans., Inst. of Eng., Australia, MC3, 216, 1967.

63. Roberts, A. W., "An Investigation of the Gravity Flow of Non-Cohesive Granular Materials", J. Eng. for Ind. Trans. ASME, 91, 373, 1969.

64. Rogers, R. S. C., and Gardner, R. P., "A Monte-Carlo Method for Simulating Dispersion and Transport Through Horizontal Rotating Cylinders", Powder Technology, 23, 159, 1979.

65. Sabersky, R. H., Acosta, A. J., and Hauptmann, E.G., Fluid Flow: A First Course in Fluid Mechanics , 2nd ed. Macmillan Pub., 1971.

66. Savage, S. B., "Gravity Flow of a Cohesionless Bulk Solid in a Converging Channel", Int. J. Mech. Sci., 9, 651, 1967.

67. Savage, S. B., "Experiments on Shear Flows of Cohesionless Granular Material", Presented at the NSF Conference", "Continuum Mechanical and Statistical Approaches in the Mechanics of Granular Materials", Sendai,Japan, June 5-8, 1978.

68. Savage, S. B., "Gravity Flow of Cohesionless Granular Materials in Chutes and Channels", JFM, 92, 53, 1979.

69. Savage, S. B., Personal Communication.

70. Savage, S., and Sayed, M., "Experiments on Dry Cohesionless Materials in an Annular Shear Cell at High Strain Rates", Presented at Euromech, 133, Statics and Dynamics of Granular Materials, Oxford University, 1980.

71. Savage, S. B., and Jeffrey, D. J., "The Stress Tensor in Granular Flow at High Shear Rates", to be published in JFM.

72. Savage, S. B., and Sayed, M., "Stresses Developed by Dry Cohesionless Granular Materials Sheared in an Annular Shear Cell", to be submitted to JFM.

73. Scott, R. F., Principles of Soil Mechanics , McGraw Hill, 1963.

74. Shield, R. T., "On Coulombs Law of Failure in Soils", J. of Mech. and Phys. of Solids, 4, 10, 1955.

75. Spelt, J. K., An Experimental Study of Heat Transfer to Flowing Granular Materials , Thesis, California Institute of Technology, 1981.

76. Spelt, J. K., and Sabersky, R. H., "Heat Transfer to Flowing Granular Material", to be published in Int. J. Heat. Mass Transfer.

77. Spencer, A. J. M., "A Theory of the Kinematics of Ideal Soils under Plane Strain Conditions", J. Mech. Phys. Solids, 12, 337, 1964.

78. Spencer, A. J. M., and Kingston, M. R., "Plane Mechanics and Kinematics of Compressible Ideal Granular Materials", Rheological Acta, 12, 194, 1973.

79. Sullivan, W. N., Heat Transfer to Flowing Granular Materials , Ph.D Thesis, California Institute of Technology, 1973.

80. Sullivan, W. N. and Sabersky, R. H., "Heat Transfer to Flowing Granular Media", Int. J. of Heat Transfer, 18, 97, 1975.

81. Sundarum, V., and Cowin, S. C., "A Reassessment of Static Bin Pressure Experiments", Powder Technology, 22, 23, 1979.

82. Suzuki, A., and Tanaka, T., "Measurement of Flow Properties of Powders along an Inclined Plane", Ind. Eng. Chem. Fund., 10, 84, 1971.

83. Takahasi, K., "On the Dynamical Properties of Granular Mass", Geophysical Mag., 11, 165, 1937.

84. Wieghardt, K., "Experiments in Granular Flow", Annual Review of Fluid Mechanics, 7, 89, 1975.

85. Wolf, E. F., and von Hohenleighten, H. L., "Experimental Study of the Flow of Coal in Chutes at Riverside Generating Station", J. App. Mech., 67, 585, 1945.

86. Wood, W. W., "Computer Studies on Fluid Systems of Hard-Core Particles", in Fundamental Problems of Statistical Mechanics, Vol. 3, E.D.G. Cohen Ed., No. Holland, Pub., 1975.

87. Yoshida, H., Mashuda, H., and Inoya, K., "Model Simulation of Particle Motion in Turbulent Gas-Solid Pipe Flow", Powder Technology, 26, 217, 1980.